THE GREEN SIDE OF THE WATER CYCLE: NEW ADVANCES IN THE STUDY OF PLANT WATER DYNAMICS

EDITED BY: Juan Pedro Ferrio, Maren Dubbert and Cristina Maria Máguas

PUBLISHED IN: Frontiers in Plant Science

frontiers Research Topics

frontiers

ISSN 1664-8714
ISBN 978-2-88966-114-5
DOI 10.3389/978-2-88966-114-5

About Frontiers

Frontiers is more than just an open-access publisher of scholarly articles: it is a pioneering approach to the world of academia, radically improving the way scholarly research is managed. The grand vision of Frontiers is a world where all people have an equal opportunity to seek, share and generate knowledge. Frontiers provides immediate and permanent online open access to all its publications, but this alone is not enough to realize our grand goals.

Frontiers Journal Series

The Frontiers Journal Series is a multi-tier and interdisciplinary set of open-access, online journals, promising a paradigm shift from the current review, selection and dissemination processes in academic publishing. All Frontiers journals are driven by researchers for researchers; therefore, they constitute a service to the scholarly community. At the same time, the Frontiers Journal Series operates on a revolutionary invention, the tiered publishing system, initially addressing specific communities of scholars, and gradually climbing up to broader public understanding, thus serving the interests of the lay society, too.

Dedication to Quality

Each Frontiers article is a landmark of the highest quality, thanks to genuinely collaborative interactions between authors and review editors, who include some of the world's best academicians. Research must be certified by peers before entering a stream of knowledge that may eventually reach the public - and shape society; therefore, Frontiers only applies the most rigorous and unbiased reviews.
Frontiers revolutionizes research publishing by freely delivering the most outstanding research, evaluated with no bias from both the academic and social point of view. By applying the most advanced information technologies, Frontiers is catapulting scholarly publishing into a new generation.

What are Frontiers Research Topics?

Frontiers Research Topics are very popular trademarks of the Frontiers Journals Series: they are collections of at least ten articles, all centered on a particular subject. With their unique mix of varied contributions from Original Research to Review Articles, Frontiers Research Topics unify the most influential researchers, the latest key findings and historical advances in a hot research area! Find out more on how to host your own Frontiers Research Topic or contribute to one as an author by contacting the Frontiers Editorial Office: researchtopics@frontiersin.org

THE GREEN SIDE OF THE WATER CYCLE: NEW ADVANCES IN THE STUDY OF PLANT WATER DYNAMICS

Topic Editors:
Juan Pedro Ferrio, Fundacion Agencia Aragonesa para la Investigacion y el Desarrollo, Spain
Maren Dubbert, University of Freiburg, Germany
Cristina Maria Máguas, University of Lisbon, Portugal

Citation: Ferrio, J. P., Dubbert, M., Máguas, C. M., eds. (2020). The Green Side of the Water Cycle: New Advances in the Study of Plant Water Dynamics. Lausanne: Frontiers Media SA. doi: 10.3389/978-2-88966-114-5

Table of Contents

frontiers in Plant Science

EDITORIAL
published: 02 September 2020
doi: 10.3389/fpls.2020.582846

Editorial: The Green Side of the Water Cycle: New Advances in the Study of Plant Water Dynamics

Juan Pedro Ferrio[1,2*], *Maren Dubbert*[3,4] *and Cristina Máguas*[5]

[1] Aragon Agency for Research and Development (ARAID), Zaragoza, Spain, [2] Department of Forest Resources, Agrifood Research and Technology Centre of Aragon (CITA), Zaragoza, Spain, [3] Ecosystem Physiology, University of Freiburg, Freiburg, Germany, [4] Landscape Ecohydrology, IGB Berlin, Berlin, Germany, [5] Centre for Ecology, Evolution and Environmental Changes (cE3c), Faculdade de Ciências da Universidade de Lisboa, Lisboa, Portugal

Keywords: water uptake, water transport, hydrological tracers, water status, stable isotopes, noninvasive techniques, plant-fungi interactions, water footprint

Editorial on the Research Topic

The Green Side of the Water Cycle: New Advances in the Study of Plant Water Dynamics

Dynamics within the water cycle is a crucial topic under current climate change conditions. To understand terrestrial ecosystems and their role in the water cycle, we need to characterize the uptake, storage and transport of water along the soil-plant-atmosphere continuum. Assessing these processes is still challenging due to the trade-off between the uncertainty of upscaling approaches and the complexity of *in situ* direct measurements. In this Research Topic, we integrated the information available from multiple disciplines, from plant hydraulics to economy, going through material science and biomolecular techniques, covering a wide range of temporal and spatial scales.

Stable isotope analysis is a long-used powerful tool to study plant water relations. However, the temporal resolution of stable isotope analysis based on classical destructive sampling techniques is limited, precluding the characterization of highly dynamic hydrological processes. Here, two articles focused on methods for continuous monitoring of the isotopic signature of water, either in the soil (Kübert et al.) or in the tree stem (Marshall et al.). Kübert et al. assessed the use of a gas-permeable membrane to monitor soil water vapor by isotope ratio infrared spectrometry (IRIS). Compared to standard methods, in-situ soil water isotopic monitoring showed similar results, and tracked fast changes in soil water, although it might be affected by spatial heterogeneity, and the alteration of soil structure during installation. Marshall et al. tested a method in which air flows through a borehole in the tree trunk, measuring water vapor (equilibrated with stem water) by IRIS. The article shows that the method detects fast changes in source water, but faces some potential limitations, e.g., in species with narrow active sapwood, or small stems.

Also aimed at in-field continuous monitoring, Scalisi et al. and Scalisi et al. shifted the usual focus on leaves and stems toward the assessment of fruits. Changes in fruit (nectarine and olive) diameter and leaf pressure were monitored together with standard methods for determining plant water status. In a study on nectarine under deficit irrigation, Scalisi et al. showed how nocturnal fruit growth peaked at intermediate water potentials (*ca.* -1.5 MPa), but declined rapidly under lower water potentials, highlighting the suitability of the method to determine optimal irrigation regimes. In the case of olive trees, Scalisi et al. found that different cultivars may prioritize either leaf or fruit water status, suggesting that the comparison of one single compartment may lead to wrong conclusions regarding tree water status.

Edited and reviewed by:
Maria Paz Diago,
Institute of Vine and Wine Sciences (ICVV), Spain

****Correspondence:***
Juan Pedro Ferrio
jpferrio@cita-aragon.es

Specialty section:
This article was submitted to Technical Advances in Plant Science, a section of the journal Frontiers in Plant Science

Received: *13 July 2020*
Accepted: *19 August 2020*
Published: *02 September 2020*

Citation:
Ferrio JP, Dubbert M and Máguas C (2020) Editorial: The Green Side of the Water Cycle: New Advances in the Study of Plant Water Dynamics. Front. Plant Sci. 11:582846. doi: 10.3389/fpls.2020.582846

At the leaf level, Gomez Alvarez-Arenas et al. presented a contactless method, based on ultrasonic resonance, which provides information on different leaf properties, such as thickness and density. In this work, the method allowed to determine the surface density of the palisade and spongy mesophyll in three species (*Ligustrum lucidum*, *Vitis vinifera*, and *Viburnum tinus*). The technique showed, in a non-invasive way, the relative contribution of palisade and spongy mesophylls to leaf thickness, as well as the differential responses of these two layers to leaf water loss.

Two articles focused on the regulation of plant water transport. In an experimental study with maize, Hayat et al. tracked the changes in transpiration and water potential during soil drying, in order to assess whether stomata are downregulated to minimize losses in hydraulic conductance. Comparing root-pressurized and non-pressurized plants, they concluded that losses in soil-plant hydraulic conductance drove stomatal closure in maize. At the other extreme of the soil-plant-atmosphere continuum, Du et al. assessed the acclimation to high vapor pressure deficit (VPD) of two tomato cultivars. The cultivar Jinpeng showed an anisohydric behavior, with high VPD inducing an increase in whole-plant hydraulic conductance, keeping high stomatal conductance and transpiration rates. Conversely, the cultivar Zhongza displayed a more conservative, isohydric strategy, showing a coordinated decline in stomatal and hydraulic conductance. Interestingly, the contrasting acclimation strategies involved differential changes in anatomical traits.

In connection with the study of water transport, Xu and Zwiazek presented in a *Perspectives* paper a theoretical framework on the regulation of plant water status through the aquaporins of ectomycorrhizal fungi, discussing existing evidence and future challenges. Although a moderate increase in fungal aquaporin expression may enhance root hydraulic conductivity, under adverse conditions it may cause opposite effects. In this context, the authors highlighted the need to assess the coordination between plant and fungal aquaporins under water stress.

Finally, the *Opinion* paper by Cazcarro and Bielsa addressed, from an economic viewpoint, current issues in the quantification of water footprints at regional scales. Firstly, they highlighted the lack of consensus regarding what should be considered as anthropogenic water footprint, exemplified by the case of forestry. They also discussed the challenges in upscaling transpiration and evaporation to regional scales, concluding with some recommendations on how to improve the interaction between natural and social sciences in the valorization of water resources.

Although far from a comprehensive compilation of methods, we gathered new conceptual approaches and applications, with a particular focus on continuous-monitoring methods. Bearing in mind the highly dynamic nature of soil-plant-atmosphere interactions, the techniques presented here are likely to foster our knowledge on the mechanism and regulation of plant water use. Besides the application to plant ecophysiology and precision agriculture, online sensing of the "green side" of the water cycle is needed to fine-tune ecohydrological models, e.g., to anticipate plant responses to climate change, and their implications for land water resources.

AUTHOR CONTRIBUTIONS

JF prepared the first draft of this editorial. MD and CM revised the editorial. All authors contributed to the article and approved the submitted version.

FUNDING

JF was supported by Reference Group H09_20R (Gobierno de Aragón, Spain) and the project PID2019-106701RR-I00/AEI/10.13039/501100011033. CM acknowledges financial support from Fundação para a Ciência e Tecnologia (FCT), through the strategic project UIDB/00329/2020 granted to the Centre for Ecology, Evolution and Environmental Changes, cE3c, Faculdade de Ciências, Universidade de Lisboa. MD was supported by the German Science Foundation (DFG; DU1688/1-1, DU1688/4-1).

ACKNOWLEDGMENTS

The editors would like to thank all reviewers and associate editors who evaluated manuscripts for this Topic.

Conflict of Interest: The authors declare that the research was conducted in the absence of any commercial or financial relationships that could be construed as a potential conflict of interest.

frontiers in Plant Science

ORIGINAL RESEARCH
published: 03 July 2019
doi: 10.3389/fpls.2019.00805

Fruit and Leaf Sensing for Continuous Detection of Nectarine Water Status

Alessio Scalisi[1,2], Mark Glenn O'Connell[2], Dario Stefanelli[2] and Riccardo Lo Bianco[1]*

[1]Department of Agricultural, Food and Forest Sciences (SAAF), University of Palermo, Palermo, Italy, [2]Department of Jobs, Precincts and Regions, Agriculture Victoria, Tatura, VIC, Australia

Continuous assessment of plant water status indicators provides the most precise information for irrigation management and automation, as plants represent an interface between soil and atmosphere. This study investigated the relationship of plant water status to continuous fruit diameter (FD) and inverse leaf turgor pressure rates (p_p) in nectarine trees [*Prunus persica* (L.) Batsch] throughout fruit development. The influence of deficit irrigation treatments on stem (Ψ_{stem}) and leaf water potential, leaf relative water content, leaf stomatal conductance, and fruit growth was studied across the stages of double-sigmoidal fruit development in 'September Bright' nectarines. Fruit relative growth rate (RGR) and leaf relative pressure change rate (RPCR) were derived from FD and p_p to represent rates of water in- and outflows in the organs, respectively. Continuous RGR and RPCR dynamics were independently and jointly related to plant water status and environmental variables. The independent use of RGR and RPCR yielded significant associations with midday Ψ_{stem}, the most representative index of tree water status in anisohydric species. However, a combination of nocturnal fruit and leaf parameters unveiled an even more significant relationship with Ψ_{stem}, suggesting a changing behavior of fruit and leaf water flows in response to pronounced water deficit. In conclusion, we highlight the suitability of a dual-organ sensing approach for improved prediction of tree water status.

Keywords: drought, fruit growth, irrigation, *Prunus persica* (L.) Batsch, turgor pressure, water potential

OPEN ACCESS

Edited by:
Juan Pedro Ferrio, Fundacion Agencia Aragonesa para la Investigacion y el Desarrollo, Spain

Reviewed by:
Nathalie Wuyts, Julich Research Centre, Germany
Wenceslao Conejero, Spanish National Research Council (CSIC), Spain

****Correspondence:***
Alessio Scalisi
alessio.scalisi@ecodev.vic.gov.au

Specialty section:
This article was submitted to Technical Advances in Plant Science, a section of the journal Frontiers in Plant Science

Received: *10 April 2019*
Accepted: *04 June 2019*
Published: *03 July 2019*

Citation:
Scalisi A, O'Connell MG, Stefanelli D and Lo Bianco R (2019) Fruit and Leaf Sensing for Continuous Detection of Nectarine Water Status. Front. Plant Sci. 10:805. doi: 10.3389/fpls.2019.00805

INTRODUCTION

Precision irrigation is becoming a crucial management approach for environmentally and economically sustainable fruit tree production. The vast majority of fruit crops need irrigation supply as rainfall does not match crop water requirements (Stöckle et al., 2011; Snyder, 2017). In most cases of fruit crops cultivated in dry areas, rainfed agriculture is not sustainable and deficit irrigation (DI) is a reasonable strategy to improve water use efficiency. Fereres and Soriano (2007) highlighted the benefits of regulated DI as a strategy to reduce agricultural water use. The main purpose of regulated DI is to reduce irrigation at specific developmental stages of the crop with no or limited effects on yield. The use of DI in different phenological stages of fruit crops started in the 1980s by Chalmers et al. (1981, 1986). Today, water supply for DI treatments is often calculated as a fraction of crop evapotranspiration (ET_c) (Naor, 2006;

Paço et al., 2006) or weather-based modeling crop water requirements. Additional approaches rely on soil- or plant-based sensing. Irrigation management in nectarine was recently studied with regard to soil water content (Vera et al., 2019).

Plant physiological indicators of water deficit are predominantly subjected to changes in tissue water content and status rather than to soil water dynamics (Jones, 2004; Steppe et al., 2008). Moreover, to adequately represent soil spatial variability and wetted and non-wetted zones in irrigated crops, soil-based sensing requires the use of many sensors, making this approach costly and difficult. Therefore, a continuous assessment of plant water status indicators might provide the most precise information for irrigation management and automation. The advantage of plant-based methods over soil-based techniques resides in the fact that plants are an interface between soil and atmosphere (Fernández, 2017), being in the middle of the soil-plant-atmosphere continuum (SPAC). Therefore, precise automated irrigation management, in terms of the quantity and timing of water effectively required by plants, is likely to be highly associated to direct or indirect measurements of plant physiological indicators.

Midday stem water potential (Ψ_{stem}) is one of the most widely used indicators of plant water status for irrigation scheduling in anisohydric plants (McCutchan and Shackel, 1992; Shackel et al., 1997; Naor, 2000). Conversely, Blanco-Cipollone et al. (2017) suggested the adoption of pre-dawn leaf water potential (Ψ_{leaf}) as a suitable parameter for irrigation scheduling in isohydric species such as grapevine. Leaf relative water content (RWC) can also be used as a water deficit indicator (Lo Bianco and Scalisi, 2017; Mossad et al., 2018), although differently from water potential it does not give an indication of water energy status (Jones, 2007). Indicators of leaf water status may not be very useful in the early detection of plant water deficit in isohydric species (Jones, 2004), as their preventive stomatal closure preserves leaf turgor and leaf RWC.

A completely automated model for irrigation management in fruit crops is difficult to achieve, as responses to water deficit not only depend on environmental variables and soil water availability, but also on fruit tree phenology. In stone fruits (e.g., peach, nectarines, plums), tree water status and sink-source relationships differ in the three stages of the typical double sigmoidal fruit growth model (Connors, 1919; Chalmers and van den Ende, 1975), as shown in peach by DeJong and Goudriaan (1989). Consequently, DI applied at each of the stages of peach fruit growth affects vegetative and fruit growth differently, causing changes in final fruit size and composition (Li et al., 1989a). Fruit water exchanges follow skin transpiration, phloem and xylem streams, with different mechanisms linked to fruit growth stages (i.e., cell division, pit hardening, and cell enlargement), such as increasing transpiration and xylem inflow toward harvest (Marsal and Girona, 1997; Morandi et al., 2007a, 2010a). In peach, drought in early stages induces a relatively lower reduction of fruit development, compared to final stages, when cell enlargement occurs (Li et al., 1989a; Génard and Huguet, 1996).

A field direct, error-free, and continuous estimation of Ψ_{stem}, Ψ_{leaf}, or leaf RWC is not feasible yet in fruit tree crops, although stem psychrometers are currently being revived (Tran et al., 2015). The use of further plant-based technologies might represent a viable solution for the estimation of tree water status indicators. Trunk-based sensing such as sap-flow methods and dendrometry have been used for irrigation scheduling in peach and several other fruit crops (Fernández, 2017). Li et al. (1989b), Simonneau et al. (1993), and Goldhamer et al. (1999) successfully associated peach tree water status to stem diameter fluctuations obtained by dendrometers built on linear variable displacement transducers (LVDTs). In addition, Conejero et al. (2007) studied peach maximum trunk daily shrinkage and sap-flow signals for irrigation scheduling, suggesting that the former represents a more sensitive indicator of plant water deficit. Nevertheless, the use of stem/trunk diameter variations and sap flow for irrigation scheduling is questionable. Trunk diameter fluctuations are affected by plant age and size, crop load, environmental variables, and growth patterns (Fernández, 2017), whereas sap flow rates reflect transpiration dynamics, which are not only dependent on stomatal closure and aperture, but also on environmental variables (Jones, 2004).

The use of fruit- and leaf-based sensors to study tree water relations has also been reviewed in the literature (Jones, 2004; Fernández, 2017; Scalisi et al., 2017). Combined information obtained from fruit and leaf water continuous sensing may represent an innovative approach to determine sensitive indicators to water deficit. Changes in peach fruit water content in response to drought may be assessed with a model developed by Génard and Huguet (1996). The most common type of fruit-based sensor used to determine when trees enter water deficit conditions is based on LVDT technologies. Lang (1990) used LVDT sensors on apple fruit to emphasize the role of phloem, xylem, and transpiration on diameter changes over time. Similar sensors were used by Morandi et al. to study vascular flows in peach (Morandi et al., 2007a, 2010a), kiwifruit (Morandi et al., 2010b), and pear (Morandi et al., 2014). Fruit growth dynamics are a good indirect indicator of fruit water status (Fernandes et al., 2018), as dry matter accumulation is negligible on a daily scale (Blanke and Lenz, 1989). Fruit growth dynamics however can be influenced by growth stage and crop load. In peach, fruit water dynamics vary across the season, with maximum transpiration at fruit cell enlargement (Morandi et al., 2010a). Consequently, the use of fruit gauges alone may not be a reliable indicator of water deficit in trees.

Leaf-based sensing technologies mainly adopt leaf thickness sensors and pressure probes. The continuous outputs of the former were related to leaf RWC (Burquez, 1987), although their long-term use is not feasible as they commonly injure leaves after short time (Zimmermann et al., 2008). Therefore, recently, a less invasive leaf pressure probe for the continuous determination of leaf water status (Zimmermann et al., 2008) has entered the market. These so-called leaf patch clamp pressure (LPCP) probes can be used to assess water stress for irrigation scheduling, as they respond to leaf turgor pressure, which has an important role in Ψ_{leaf}. Most of the initial studies with LPCP probes were carried out on olive (Fernández et al., 2011; Ehrenberger et al., 2012; Rodriguez-Dominguez et al., 2012; Padilla-Díaz et al., 2016) because the thick leaves of this species better suit the prolonged use of sensors. Olive is cultivated

in dry or semi-dry regions with limited or no irrigation water supply. LPCP probes were also related to plant water status indicators in other fruit crops, such as banana (Zimmermann et al., 2010), grapevine (Rüger et al., 2010), clementine (Ballester et al., 2017), and persimmon (Ballester et al., 2017; Martínez-Gimeno et al., 2017). However, as for fruit sensors, the use of LPCP probes alone can only give partial information on whole plant water status, unless many sensors are used on a tree. This is particularly due to different leaf initial conditions depending on age (especially in evergreen species) and exposure to light within the canopy. Even accepting the quality of the data, a further need to test LPCP probes on species with thinner leaves (e.g., stone fruits) arises, as their prolonged use might damage leaf cuticle and alter measurements (Scalisi et al., 2017). As mentioned above, the use of a single type of sensors can only provide partial information on tree water status. Most of C3 fruit trees exchange water with the surrounding atmosphere by means of transpiring fruit and leaves.

This study aimed to investigate the relationship of Ψ_{stem} and other plant water status indicators to continuous fruit size and leaf turgor pressure dynamics in nectarine trees [*Prunus persica* (L.) Batsch] subjected to DI at each of the individual stages of fruit growth. The main hypothesis was that the combined information from fruit and leaves (i.e., the transpiring organs) provides more powerful information than individual indicators to determine plant water status on a continuous basis for adoption of precision irrigation management.

MATERIALS AND METHODS

Experimental Design

The experiment was carried out in summer 2017/18 on late ripening 'September Bright' nectarine trees grafted on "Elberta" rootstock at the research station of Agriculture Victoria, Tatura, Australia (36°26′7.2″ S and 145°16′8.4″ E, 113 m a.s.l.). Within the experimental site, 144 4-year-old trees trained to an open Tatura system with 4.5 m × 1 m spacing (i.e., 2,222 trees/ha) were selected. Trees were disposed along N-to-S oriented rows. The soil was a clay-loam and trees were regularly fertigated according to conventional protocols. Fruit thinning and summer pruning were carried out at 43 and 125 days after full bloom (DAFB), respectively.

The typical double-sigmoidal fruit growth pattern was characterized by measurements of fruit diameter in control trees at weekly intervals from shuck fall to harvest. Growth stages were divided as follows: a cell division stage (I), a pit hardening stage (II), and a cell expansion stage (III) further subdivided into two equal phases of about a month each (previous year observations), with the first (IIIa) starting when fruit cells re-establish a strong sink power after stage II, and the second being the final period of sugar accumulation and chlorophyll degradation (stage IIIb). Four different DI levels, namely 100% of crop evapotranspiration (ET_c, control), 40% of ET_c (DI-40), 20% of ET_c (DI-20), and 0% of ET_c (DI-0) were applied from the beginning to the end of each fruit growth stage, using a drip irrigation system. At stage I, an initial fertigation resulted in additional 13 mm of water added to the DI-0 treatment. The experimental design included six replications in a randomized complete block design, each with two tree orientations (East and West) per treatment and fruit growth stage; measurement trees were separated by buffer trees and rows. At stage IIIb, the DI-40 treatment was not considered, due to limited number of trees available. Canopy orientation was also considered in the design, including West- and East-oriented trees of the open Tatura system. This was particularly helpful to explain different responses among trees due to light interception at different times of the day.

Meteorological data were collected using a weather station located in the experimental field. Solar radiation was measured using a silicon pyranometer (SK01D, Carter-Scott Design, Brunswick, Australia). Relative humidity (RH) and temperature (T) measurement were based on the combination of a capacitive thin film polymer sensor HUMICAP®180 and resistive platinum sensors (HMP 45A-T, Vaisala, Finland). Rainfall was measured using a TB3A rain gauge (Hydrological Services PL, Warwick Farm, Australia). Wind speed was measured with a wind transmitter (Model No. 4.3519.00.000, Thies Clima, Göttingen, Germany). Measurements were stored at 10-min intervals in a 6004C-21 STARLOG data logger (Unidata, O'Connor, Australia).

Reference evapotranspiration (ET_0) and vapor pressure deficit (VPD) were calculated using the methods described by Allen et al. (1998). Cumulative average daily VPD (Σ_{VPD}) and cumulative ET_0 (Σ_{ET0}) were obtained by the summation of average daily VPD and total daily ET_0, respectively, for each fruit growth stage. Average daily vapor pressure deficit (μ_{VPD}) and average daily reference evapotranspiration (μ_{ET0}) were obtained by dividing respectively Σ_{VPD} and Σ_{ET0}, by the number of days in each fruit development stage. Crop evapotranspiration (ET_c) was estimated based on Equation 1.

$$ET_c = \left(K_{cb} \times ET_0\right) + \left(K_e \times ET_0\right) \quad (1)$$

where K_{cb} is the crop basal coefficient, calculated as 1.05 × EAS (effective area of shade) (Goodwin et al., 2006), and K_e is a soil evaporation coefficient of 0.1 in accordance with Bonachela et al. (2001).

Fruit Size and Tree Water Relations

Fruit Size

Fruit diameters were measured at weekly intervals in the morning of stages I, II, IIIa, and IIIb, using a Calibit digital caliper (HK Horticultural Knowledge srl, Bologna, Italy). Measurements were carried out on three fruits per tree for each irrigation treatment and canopy orientation, for a total of 36 fruits on 12 trees (two in each of the six blocks) for each irrigation treatment. Data from differently oriented trees, i.e., East and West, were pooled together as fruit diameters were not significantly different at any of the stages considered.

Water Potential

A pressure chamber (3000 Scholander Plant Water Status Consol, ICT International, Armidale, Australia) was used for the

measurements of Ψ_{stem} and Ψ_{leaf} according to Turner (1988). Mature, fully expanded leaves were covered with foil-laminate bags 2 h prior to each Ψ_{stem} measurement, except for pre-dawn. Midday Ψ_{stem} was determined at weekly intervals in all the stages of fruit growth on three leaves of the two trees (East- and West-oriented) per treatment in one of the six blocks. The block was randomly selected at the beginning of the experiment and used throughout the experimental period for water potential and other water status indicators. Daily curves from pre-dawn to 19:00 h were plotted using Ψ_{stem} and Ψ_{leaf} data collected at three-hour intervals. Measurements for daily curve characterization were carried out on a single day for each growth stage (I at 50 DAFB, II at 92 DAFB, IIIa at 132 DAFB and IIIb at 155 DAFB) for Ψ_{stem} and only in stage IIIa (132 DAFB) and IIIb (155 DAFB) for Ψ_{leaf}.

Leaf Relative Water Content

Leaf RWC was obtained using the method described by Barrs and Weatherley (1962). Mature, fully expanded leaves were collected, sealed in plastic bags, and transported to the laboratory for fresh weight (FW) determination. Turgid weight (TW) was obtained after immersing leaves in deionized water for 24 h at 4°C. Subsequently, leaves were dried in an oven at 60°C until constant weight (2–3 days) to estimate dry weight (DW). Leaf RWC was calculated as shown in Equation 2.

$$\mathrm{RWC} = \left(\mathrm{FW} - \mathrm{DW}\right) / \left(\mathrm{TW} - \mathrm{DW}\right) \times 100 \quad (2)$$

Leaf RWC was determined at 3-hour intervals on the same days and trees as Ψ_{stem} and Ψ_{leaf}.

Leaf Stomatal Conductance

A Delta-T AP4 dynamic porometer (Delta-T Devices LTD, Cambridge, UK) was used to determine leaf stomatal conductance (g_s). Mid-morning (10–11 am) measurements of g_s were undertaken at weekly intervals in all the stages of fruit growth on four leaves of the two trees (East- and West-oriented) for each treatment, and in the same block selected for water potential measurements. Stage-related g_s daily curves were obtained from three leaves on the same days and trees as Ψ_{stem} and Ψ_{leaf} determination.

Fruit Diameter and Leaf Turgor Pressure Continuous Sensing

Fruit diameter (FD) was determined continuously with the LVDT-based fruit gauges described by Morandi et al. (2007b) connected to CR-1000 data loggers (Campbell scientific, Inc., Logan, US). Concurrently, leaf-mounted LPCP probes (Yara International, Oslo, NO) were used to track leaf turgor pressure dynamics using the attenuated pressure of leaf patches (p_p), an index which is inversely related to leaf cell turgor pressure (p_c), as described by Zimmermann et al. (2008). Data from both sensors were recorded at 15-min intervals for a week at each of the growth stages (starting at 48, 86, 127, and 155 DAFB for stage I, II, IIIa, and IIIb, respectively) in one of the blocks within the experimental orchard. The block selected was the same used for g_s, Ψ_{stem}, Ψ_{leaf}, and leaf RWC measurements. Two fruit gauges and LPCP probes were mounted on each West- and East-oriented tree under all irrigation treatments, at mid-canopy height and in nearby positions. Before the actual week of measurements, a preliminary 3-day comparison test between East- and West-oriented trees was carried out to verify if canopy orientation had an effect on sensors' outputs. Data from East- and West-oriented trees were compared using daily relative standard deviations (RSD), mean, sum, max, and min.

Raw data obtained from fruit gauges and LPCP probes were smoothed using a 15-point convoluted spline function (Savitzky and Golay, 1964). Subsequently, FD and p_p values were standardized by using z-scores [i.e., $z = (x - \mathrm{mean})/\mathrm{standard\ deviation}$] to enable the comparison among fruits or leaves, respectively, which had different characteristics when the sensors were attached (i.e., fruit diameter and leaf turgor pressure). Resulting z-scores show positive and negative values as they are calculated assuming a distribution with a mean of 0 and a standard deviation of 1, in the specific time interval used for the calculation. Once FD and p_p were standardized, it was possible to average more sensors' output on the same tree and compare different treatments. Furthermore, the second derivatives of fruit diameter and p_p were calculated to determine fruit relative growth rate (RGR) and leaf relative pressure change rate (RPCR), as shown in Equations 3 and 4, respectively. Second derivatives were not standardized as they are calculated based on the previous FD and p_p, allowing possible comparisons among outputs from different sensors.

$$\mathrm{RGR} = \left[\ln\left(\mathrm{FD}_2\right) - \ln\left(\mathrm{FD}_1\right)\right] / t_2 - t_1 \quad (3)$$

$$\mathrm{RPCR} = \left[\ln\left(p_{p2}\right) - \ln\left(p_{p1}\right)\right] / t_2 - t_1 \quad (4)$$

where FD_2 and FD_1 correspond to FD at time 2 (t_2) and 1 (t_1), and p_{p2} and p_{p1} correspond to p_p at time 2 (t_2) and 1 (t_1), respectively. The time interval between t_2 and t_1 was 15 min.

Diel, diurnal, and nocturnal variance of sensors' outputs was expressed as relative standard deviation (RSD = standard deviation/|mean|), to allow comparison among variances of different units (i.e., FD/p_p and RGR/RPCR). In addition, also diel, diurnal, and nocturnal statistical parameters from data series were calculated for the variables considered (i.e., maximum, minimum, and sum values) in order to find the best predictor of midday Ψ_{stem}.

A small portion of data (<5%) from sensors that either caused damage to leaves or fruit or that were displaced by strong wind was not considered in the analysis.

Statistical Analysis

Statistical analysis was carried out using SYSTAT procedures (Systat software Inc., Chicago, USA). Analysis of variance was performed based on the randomized block design, using irrigation treatments, canopy orientation, and time as factors, and, when appropriate, means were compared by Tukey's multiple range test and honestly significant difference (HSD). Canopy orientation often did not influence results or interact with other factors. Main interactions were found when using irrigation treatments

and time as factors. Sigmaplot procedures (Systat software Inc., Chicago, USA) were used for linear and multiple linear regression analyses in order to associate continuous sensors' output to plant water status indicators.

RESULTS AND DISCUSSION

Fruit Developmental Stages, Weather Conditions, and Crop Water Supply

The typical double sigmoidal fruit development pattern was observed in control fruit, and stages I, II, IIIa, and IIIb lasted 36, 50, 29, and 31 days, respectively (**Table 1**).

Temperature (T), relative humidity (RH), ET_0, and VPD recorded from 27 to 173 days DAFB are shown in **Figure 1**. The gap in the data from 106 to 110 DAFB was due to a battery discharge. In stage II, frequent and abundant precipitations (**Table 1**) led to relatively low T (**Figure 1B**) and high RH (**Figure 1C**) (i.e., from 78 to 89 DAFB). Maximum ET_0 occurred at stage IIIa (**Figure 1A, Table 1**), driven by a combination of high T and low RH which caused a rise in VPD (**Figure 1D**). Precipitations progressively decreased toward the end of stage IIIb (**Table 1**). Trees received more water in stage II, due to more rainfall and a longer duration compared to other fruit growth stages (**Table 1**). Overall, the crop water supply (irrigation + rainfall) during fruit development stages for control trees was equal to 558 mm (**Table 1**). The highest Σ_{VPD} and Σ_{ET0} occurred in stage II (**Table 1**), due to the relatively higher duration of this stage compared to others and to the abundant crop water supply. Indeed, when the latter were weighed on the number of days (μ_{VPD} and μ_{ET0}) the highest values were found in stage IIIa (**Table 1**).

Fruit Size and Tree Water Relations

Fruit Size

No significant difference in fruit size determined with digital caliper measurements was found between East- and West-oriented trees (data not shown), thus data from the two sides were pooled together. At stage I, fruit diameter was significantly reduced by DI at 55 DAFB, with DI-20 and DI-40 inducing similar reductions and intermediate between the control and DI-0 (**Figure 2A**). At stage II, during pit hardening, fruit diameter was only slightly affected by DI treatments, and significant differences only emerged at the end of the stage between control and DI-0 trees (**Figure 2B**). At stage IIIa, DI induced fruit diameter reductions similar to those at stage I, with all DI treatments showing similar reductions compared to the control (**Figure 2C**). Finally, DI caused the highest reduction of fruit growth at stage IIIb (**Figure 2D**). Results from DI in stages I, II, IIIa, and IIIb are in line with findings in peach from Li et al. (1989a) and Génard and Huguet (1996), and in nectarines from Naor et al. (1999, 2001).

Water Potential

When water potentials from East- and West-oriented trees were compared, no statistically significant differences were found, thus data from the two sides were pooled together. Daily curves of Ψ_{stem} highlighted a relevant and gradual separation among irrigation treatments at solar noon measurements, except for stage II (**Figure 3**), a further evidence of the suitability of midday Ψ_{stem} as an indicator of plant water deficit, as previously shown by Naor et al. (1999). The lack of an effect of DI on Ψ_{stem} at stage II might be related to the abundant precipitations which occurred during this phase (**Table 1**).

Similarly, when weekly midday Ψ_{stem} was considered, the effect of DI treatments increased gradually with fruit growth, reaching the most marked reductions at the end of stage IIIb (**Figure 4**). Overall, Ψ_{stem} decreased in all treatments along the fruit development period, suggesting a likely higher tree water consumption in the latest stages of high assimilate demand (Chalmers and Wilson, 1978). Even in this case, minor or no effects were found at stage II, although in the second half, decreasing precipitations (data not shown) unveiled a drop of midday Ψ_{stem} in DI-0 trees (**Figure 4B**). A steeper decrease of midday Ψ_{stem} at stage II was also found by Fereres and Soriano (2007) in peach.

Daily measurements of Ψ_{leaf} carried out only in stage IIIa and IIIb (**Figures 5A,B**), and concomitantly with Ψ_{stem}, showed typical patterns with lowest values around solar noon. As expected, Ψ_{leaf} resulted in slightly lower values than Ψ_{stem}, in accordance with the water potential gradient along the SPAC. DI-0 trees reached the lowest Ψ_{leaf} of −3.82 and −3.75 MPa in stages IIIa and IIIb, respectively (**Figure 5**).

TABLE 1 | Total rainfall, average daily vapor pressure deficit (μ_{VPD}), cumulative average daily vapor pressure deficit (Σ_{VPD}), average daily reference evapotranspiration (μ_{ET0}), cumulative reference evapotranspiration (Σ_{ET0}), and irrigation volumes for trees irrigated to 100% (control), 40% (DI-40), 20% (DI-20), and 0% (DI-0) of crop evapotranspiration at each of the fruit growth stages.

Fruit growth stage	Duration (days)	Rainfall (mm)	μ_{VPD} (kPa)	Σ_{VPD} (kPa)	μ_{ET0} (mm)	Σ_{ET0} (mm)	Irrigation volume (mm)			
							Control	DI-40	DI-20	DI-0
I	36	27	0.75	27.2	4.92	177	63	28	16	13[y]
II	50	141	1.14	50.1	6.18	309	78	27	15	0
IIIa	29	35	1.48	42.8	7.28	211	75	32	16	0
IIIb	31	3	1.26	40.4	6.13	190	83	n.a.[z]	19	0
Total	146	243	1.16	160.5	6.15	848	315	91	54	13

[y]*Fertigation.* [z]*Not applicable.*

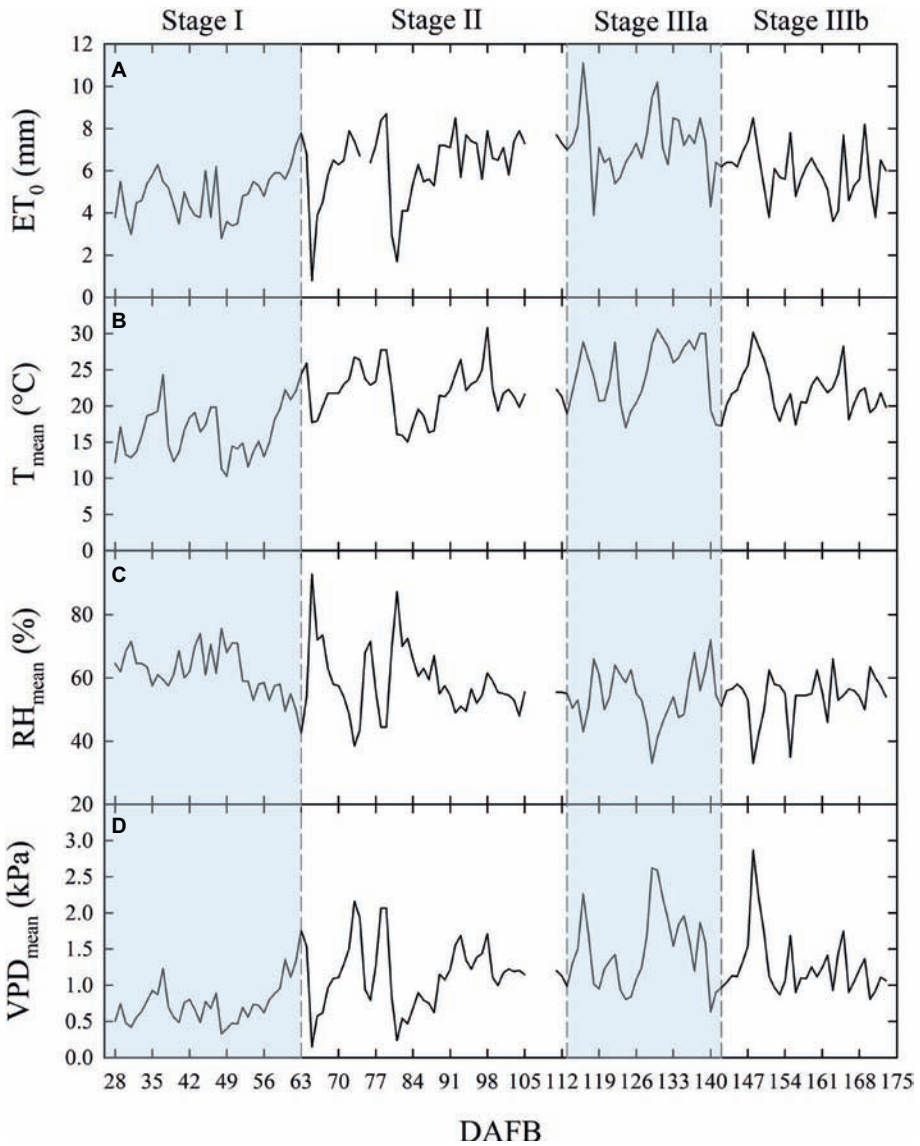

FIGURE 1 | Daily total reference evapotranspiration [ET_0 **(A)**], mean temperature [T_{mean} **(B)**], mean relative humidity [RH_{mean} **(C)**], and mean vapor pressure deficit [VPD_{mean} **(D)**] along the considered four stages of fruit growth in days after full bloom (DAFB). Missing data from 106 to 110 DAFB.

Leaf Relative Water Content

Daily curves of leaf RWC obtained from measurements carried out at all the fruit development stages and on all the irrigation treatments did not highlight differences among West- and East-oriented trees (data not shown), thus data from the two sides were pooled together. At stage I, leaf RWC varied greatly, showing erratic effects of DI (**Figure 6A**). At stage II, irrigation treatment and time of day had no significant effect on leaf RWC (**Figure 6B**). However, leaf RWC was found gradually lower along the irrigation treatment gradient at stage IIIa (**Figure 6C**), where the maximum differences between the two extreme treatments, control and DI-0, occurred at mid-morning and mid-afternoon. Ultimately, at stage IIIb, differences among treatments were once again nonsignificant, except for the measurement at 19:00 h (**Figure 6D**). Therefore, leaf RWC cannot be considered as sensitive as Ψ_{stem} and Ψ_{leaf} for nectarine water status determination, mainly because the variability of RWC among leaves is high and results in nonsignificant effects of DI (i.e., HSD in **Figure 6**). This variability is determined by intrinsic leaf characteristics such as age and competition with other leaves on the same shoot. In addition, when trees cope with high water deficit, stomata tend to close (as suggested by our g_s results shown in the next paragraph) and leaf RWC is readjusted in accordance with osmotic gradients. This explains why, despite daily Ψ_{stem} and Ψ_{leaf} being similar in DI-0 trees in stages IIIa and IIIb (**Figures 3C,D, 5A,B**), average daily leaf RWC in the same trees was slightly higher in stage IIIb (76.5% ± 0.49) than in stage IIIa (73.4% ± 0.73), with the former not showing significant changes from 7:00 to 19:00 h (**Figure 6D**).

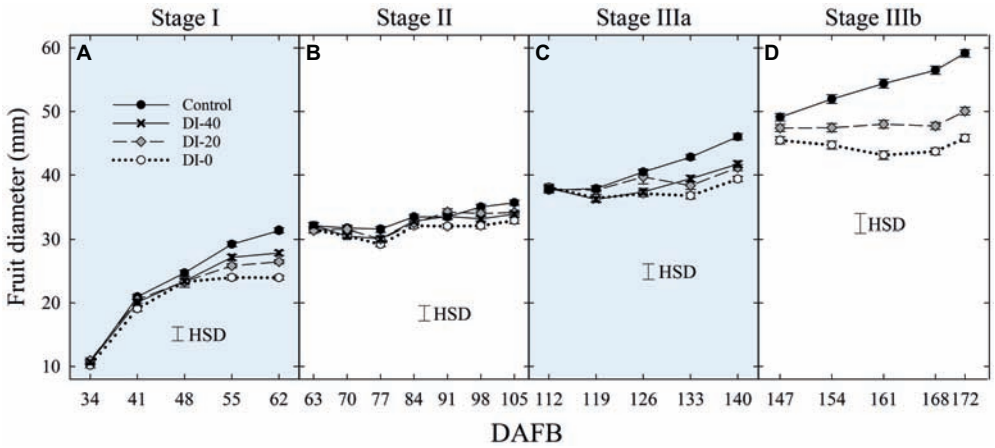

FIGURE 2 | Fruit diameter at stage I **(A)**, II **(B)**, IIIa **(C)**, and IIIb **(D)** of 'September Bright' nectarine fruit growth. Measurements done with a fruit caliper on trees irrigated to 100% (control), 40% (DI-40), 20% (DI-20), and 0% (DI-0) of crop evapotranspiration. Timeline expressed in days after full bloom (DAFB). Error bars represent standard errors of means (n = 36). Significant differences determined with analysis of variance and Tukey's honestly significant difference (HSD, $p < 0.05$).

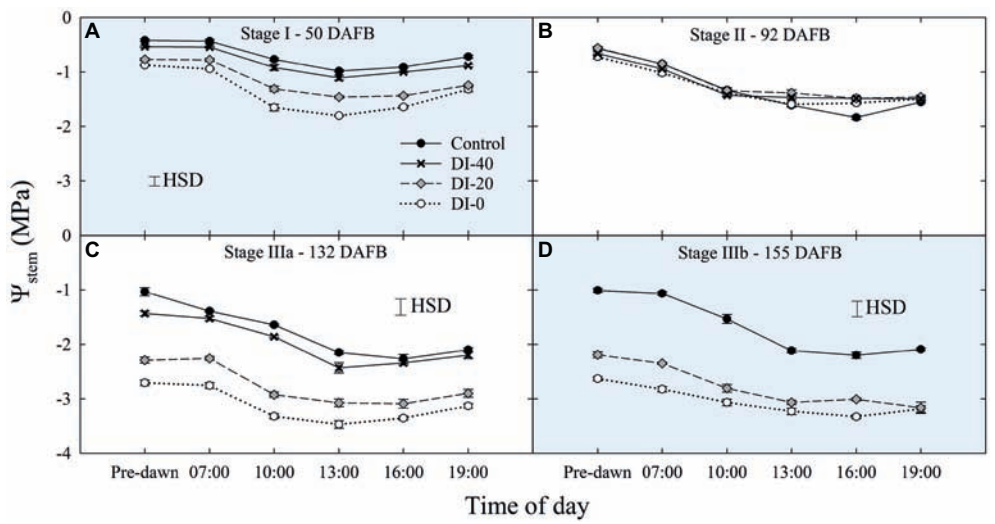

FIGURE 3 | Daily curves of stem water potential (Ψ_{stem}) at stages I **(A)**, II **(B)**, IIIa **(C)**, and IIIb **(D)** of 'September Bright' nectarine fruit growth. Trees irrigated to 100% (control), 40% (DI-40), 20% (DI-20), and 0% (DI-0) of crop evapotranspiration. Error bars represent standard errors of means (n = 6). Significant differences determined with analysis of variance and Tukey's honestly significant difference (HSD, $p < 0.05$).

Leaf Stomatal Conductance

Data of g_s are available since stage II of fruit development due to instrument malfunctioning. At stage II, no significant differences in daily g_s were found among irrigation treatments (**Figure 7A**). When maximum stomatal aperture occurred (mid-morning), there was a significant influence of canopy orientation, resulting in higher g_s in leaves of West-oriented trees (**Figure 7B**), as they intercepted greater PAR than East trees. After noon, an overall partial closure of stomata induced a consequential reduction of g_s in all the treatments. At stage IIIa, control irrigated trees expressed a g_s higher than 300 mmol m^{-2} s^{-1} in the morning, whereas DI-0 trees barely opened their stomata (about 10 mmol m^{-2} s^{-1}) in response to high water deficit conditions (**Figure 7C**). Differently from stage II, no differences were found between West- and East-oriented trees, because measurements were done on a cloudy day (**Figure 7D**). At stage IIIb, leaves of control trees had higher g_s compared to DI-20 and DI-0 trees, which instead showed similar g_s levels (**Figure 7E**). In addition, even in the case of stage IIIb daily curve, a cloudy morning concealed the effect of canopy orientation, and the increase of photosynthetic photon flux density (PPFD) caused by the disappearance of clouds after solar noon was not sufficient to show differences between West- and East-oriented trees (**Figure 7F**).

When measured at weekly intervals, g_s showed no differences among irrigation treatments at stage II (**Figure 8A**), whereas DI treatments reduced mid-morning stomatal aperture in the second half of stage IIIa (**Figure 8B**). Only at stage IIIb, leaves

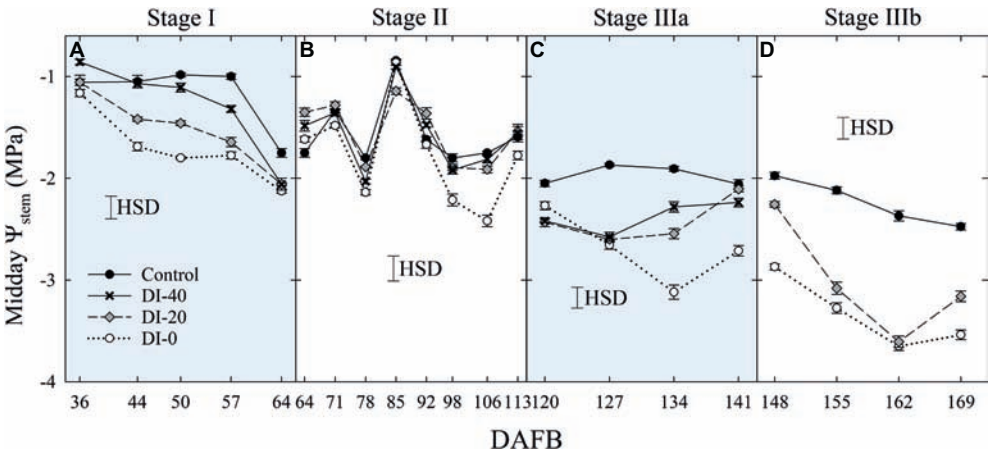

FIGURE 4 | Midday stem water potential (Ψ_{stem}) at stages I **(A)**, II **(B)**, IIIa **(C)**, and IIIb **(D)** of 'September Bright' nectarine fruit growth. Trees irrigated to 100% (control), 40% (DI-40), 20% (DI-20), and 0% (DI-0) of crop evapotranspiration. Timeline expressed in days after full bloom (DAFB). Error bars represent standard errors of means (n = 6). Significant differences determined with analysis of variance and Tukey's honestly significant difference (HSD, $p < 0.05$).

from control trees consistently kept their g_s higher than leaves from DI-20 and DI-0 trees (**Figure 8C**). At this stage, after reaching a severe water deficit, DI-0 and DI-20 trees limited their gas exchanges to minimal levels, and likely DI induced a reduction of phloem flows toward fruit, or increasing xylem backflow, following water potential gradients along the vascular path. To confirm this hypothesis, studies on isolated xylem and phloem contribution to 'September Bright' fruit growth might be carried out on girdled and detached fruit, as explained by Lang (1990). Therefore, a reduction of leaf gas exchanges might partially explain the poor, nonsignificant increase of fruit size observed in DI-0 (**Figure 2D**). Overall, g_s data at mid-morning were found to be a representative indicator of plant water deficit, as that is the time of highest leaf transpiration and maximum evidence of partial stomatal closure in response to water deficit.

The Interdependency of Plant Water Status Indicators

Among the others, Ψ_{stem} can be considered as the most sensitive indicator of plant water status in nectarines, and it is strictly related to other water status indices along the SPAC (e.g., Ψ_{leaf} and external VPD) and to the regulation of stomatal opening, expressed in terms of g_s. Leaf RWC has also been linked to Ψ_{stem} as shown by Koide et al. (1989), although results of this study were not always in line. Indeed, leaf RWC was not found to be a sensitive measurement to highlight differences among irrigation treatments, especially at stages I, II, and IIIb of fruit development (**Figures 6A,B,D**). In our case, the strongest association between leaf RWC and Ψ_{stem} occurred at pre-dawn, when water potential and water content were in equilibrium (data not shown).

The combined interdependency of VPD, Ψ_{leaf}, g_s, and leaf RWC with Ψ_{stem} was tested analyzing data extrapolated from daily curves from all the fruit growth stages. Data were pooled together and associated to Ψ_{stem} through a multiple linear regression model. Stomatal aperture and closure dynamics are known to be regulated by leaf RWC and Ψ_{leaf} among other factors, which in turn are influenced by VPD and strictly related to Ψ_{stem}. Leaf RWC is adjusted responding to Ψ_{stem} and VPD gradients. More water can flow toward leaves in order to maintain higher Ψ_{leaf}, stomatal aperture, and photosynthetic activity. Therefore, we expected to find the strongest association of Ψ_{stem} with Ψ_{leaf}, followed by decreasingly tight associations with g_s, VPD, and leaf RWC, respectively. However, leaf RWC resulted to be nonsignificant in a first backward stepwise regression model (p = 0.98), and it was excluded from the final outcome. Minor leaf RWC changes on a daily scale (**Figure 6**) may explain the absence of a relationship with Ψ_{stem}. In the obtained multiple linear regression model, Ψ_{stem} was predicted from a linear combination of Ψ_{leaf}, g_s, and VPD (R^2 = 0.867, $p < 0.001$, S.E. = 0.240), as shown in Equation 5.

$$\Psi_{stem} = -0.311 + (0.882 \times \Psi_{leaf}) + (0.004 \times g_s) + (0.077 \times VPD) \quad (5)$$

Our results are in line with findings in nectarines and other woody species (Naor, 1998), where Ψ_{stem} was found to be related to leaf stomatal conductance (g_s) and Ψ_{leaf}.

Fruit Diameter and Leaf Turgor Pressure Continuous Sensing

The preliminary trial on FD, p_p, RGR, and RPCR responses of East- and West-oriented trees did not show any significant effect of canopy orientation. Consequently, for each fruit growth stage, FD and p_p data, as well as their derivatives (i.e., RGR and RPCR), from East- and West-oriented trees were pooled together for each irrigation treatment. z-scores ranged from negative to positive in the 24-h intervals selected (**Figures 9A,B**). In control trees, FD showed an expected nocturnal increase with a diurnal lag phase during stages I, IIIa, and IIIb. **Figure 9A** shows FD and RGR in a representative day at stage I (51 DAFB). In the warmest hours of the day, p_p increased, being the inverse of p_c, as leaf turgor pressure

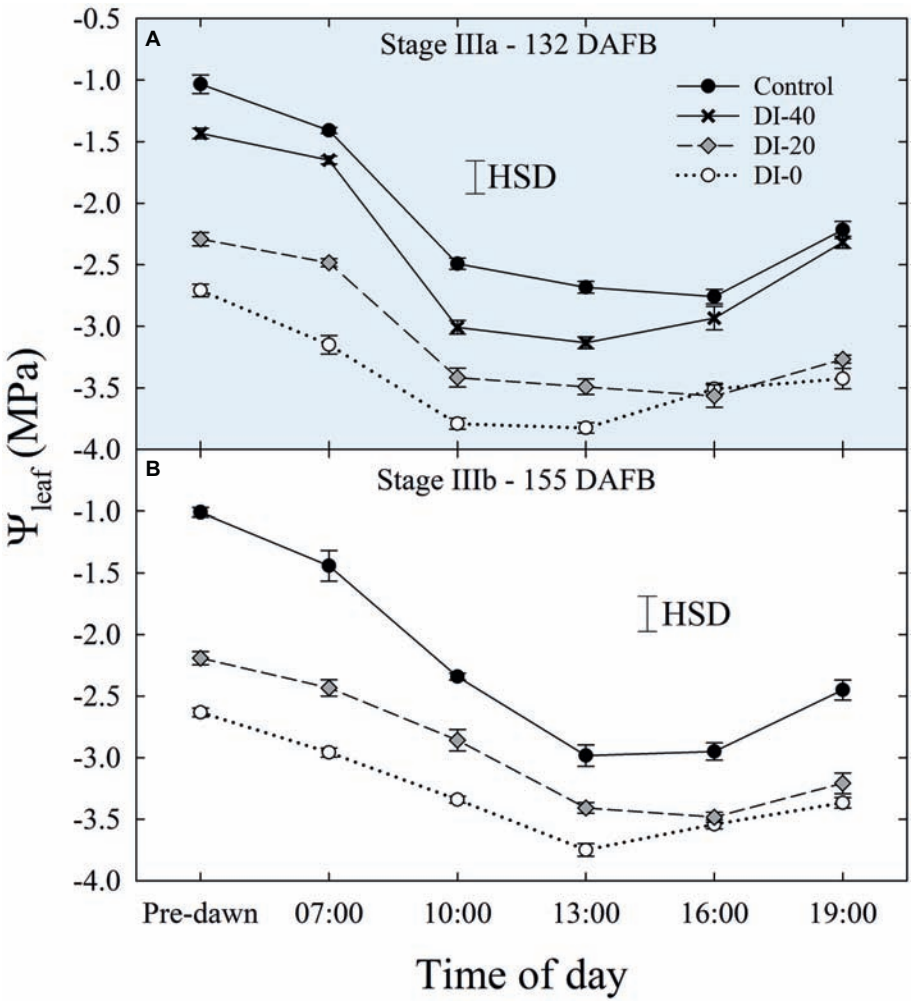

FIGURE 5 | Daily curves of leaf water potential (Ψ_{leaf}) at stages IIIa **(A)** and IIIb **(B)** of 'September Bright' nectarine fruit growth. Trees irrigated to 100% (control), 40% (DI-40), 20% (DI-20), and 0% (DI-0) of crop evapotranspiration. Error bars represent standard errors of means (n = 6). Significant differences determined with analysis of variance and Tukey's honestly significant difference (HSD, $p < 0.05$).

was lost, and a peak of RPCR was observed in the first part of the morning (**Figure 9B**).

Initially, FD and p_p values, corresponding to the time of spot measurements of Ψ_{stem}, Ψ_{leaf}, g_s, and leaf RWC from daily curves, were considered to determine whether any significant linear relationships occurred. Pearson's correlation analyses emphasized in most cases, no significant linear correlation at all between FD and the water status indices, except for the association between FD and Ψ_{leaf} with a low correlation coefficient (**Table 2**). The inverse relationships with the highest correlation coefficients were found between p_p and leaf water status indices. The highest correlation coefficient was found between p_p and Ψ_{leaf}, due to the high influence of leaf turgor pressure on the total Ψ_{leaf}. The use of FD and p_p *per se* to find significant relationships with plant water status indices is likely to hide information as there is an intrinsic delay in the adjustment of water in tissue in response to plant water deficit. Hence, the rates at which FD and p_p change over time are likely to be more strictly related to water potential gradients in particular. Therefore, RGR and RPCR can be used to smooth delay of fruit and leaf responses to water deficit over time. Besides, the use of continuous data from leaves or fruit alone might not provide appropriate information on plant water status. When considered in isolation, data from fruit diameter changes are influenced by fruit development stage and fruit growth, while data of leaf turgor pressure may not be directly related to water balance in the other main organs capable of transpiration. As a consequence, the association of RGR and RPCR dynamics can highlight a ratio of fruit and leaf water exchanges which might reflect more precisely plant water status.

Subsequently, data of diel relationships (i.e., p_p vs. FD and RPCR vs. RGR) at 15-min intervals were plotted for a clear sky day at each stage of fruit development. Scatter plots in **Figure 10** highlight anticlockwise hysteretic relationships between RPCR and RGR. Similar trends were found for p_p vs. FD associations (data not shown). Hysteresis among sensors' outputs and/or water status indicators is common, especially when trunk or leaf indicators are considered (e.g., sap flow density,

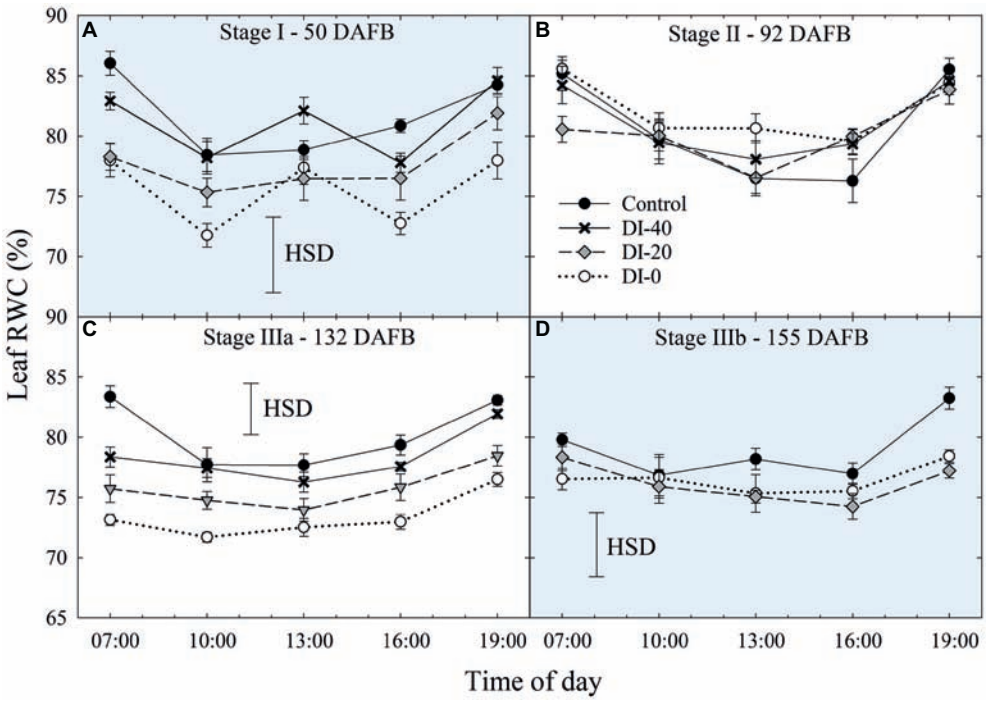

FIGURE 6 | Daily curves of leaf relative water content (RWC) at stages I **(A)**, II **(B)**, IIIa **(C)**, and IIIb **(D)** of 'September Bright' nectarine fruit growth. Trees irrigated to 100% (control), 40% (DI-40), 20% (DI-20), and 0% (DI-0) of crop evapotranspiration. Error bars represent standard errors of means (n = 6). Significant differences determined with analysis of variance and Tukey's honestly significant difference (HSD, $p < 0.05$).

stomatal conductance, diameter variations, Ψ_{leaf}, transpiration), and has been widely documented (Brough et al., 1986; Cruiziat et al., 1989; Granier et al., 1989; Ameglio and Cruiziat, 1992; Tognetti et al., 1996; Fernández, 2017). The hysteretic behavior was observed in all the fruit developmental stages, although it showed different patterns (**Figure 10**). At stage I, there was a gradual increase of the hysteretic loop area as irrigation volume decreased, reaching its maximum size in the DI-0 treatment (**Figure 10A**). Nevertheless, a similar trend in loop area with higher levels of DI was not observed in the other stages (**Figures 10B–D**), suggesting stage-dependent mechanisms of water regulation in fruits and leaves. In addition, the generally low midday Ψ_{stem} at stage IIIa and IIIb (i.e., ≤ −2.00 MPa) may have altered the hysteretic patterns. Hysteresis is likely to be caused by both a lag in tissue water dehydration and rehydration, and nocturnal/diurnal inverted pattern of the RPCR to RGR association. Consequently, diel RGR and RPCR trends were firstly considered alone and then subdivided into diurnal (7:00 to 19:45 h) and nocturnal (20:00 to 6:45 h) data, to investigate associations with midday Ψ_{stem}. The use of RGR and RPCR was favored over FD and p_p, as the former yielded the tightest associations with midday Ψ_{stem}. Diel, diurnal, and nocturnal RGR and RPCR parameters (i.e., RSD, maximum, minimum, sum) from all the irrigation treatments were pooled together and their means were linearly regressed with midday Ψ_{stem}. Among all the significant ($p < 0.05$) regression models obtained using data from all the stages, the highest R^2 were found when nocturnal maximum RGR (MAX_{RGR}) (**Figure 11A**) and minimum diel RPCR (MIN_{RPCR}) (**Figure 11B**) were related to midday Ψ_{stem}. The nonlinear model in **Figure 11A** can be explained with the fact that a limited water deficit is needed for maximum fruit cell expansion due to rehydration (i.e., peak at −1.56 MPa). Oppositely, at Ψ_{stem} near −1.00 MPa, fruit cell turgor is higher and less water is drawn from nearby organs. When Ψ_{stem} reaches particularly low levels (~ −3.50 MPa) maximum RGR tends to zero.

The linear relationship between Ψ_{stem} and diel MIN_{RPCR} showed a loose but direct association (**Figure 11B**), in contrast with findings in olive where Marino et al. (2016), instead, found an inverse linear relationship. In our case, even the linear regression between p_p (the indicator used by Marino et al., 2016), rather than RPCR, and midday Ψ_{stem} resulted in a direct relationship, although with a lower R^2 (0.247) than the former (data not shown). The inverse relationship found by Marino et al. (2016) in olive was expected as p_p is the inverse of turgor pressure, which is instead directly related to Ψ_{stem}. In our case, diel MIN_{RPCR} indicates the maximum rate over 24 h at which partially dehydrated leaves re-establish some turgor pressure by recalling water from nearby organs. Therefore, the direct relationship between diel MIN_{RPCR} and Ψ_{stem} shows that such instantaneous water pulling force increases with water deficit, allowing leaves to maintain minimum hydration and escape desiccation and death. Indeed, a Ψ_{stem} < 3.00 MPa could be fatal for nectarine trees if a drought avoidance mechanism is not activated. On the other

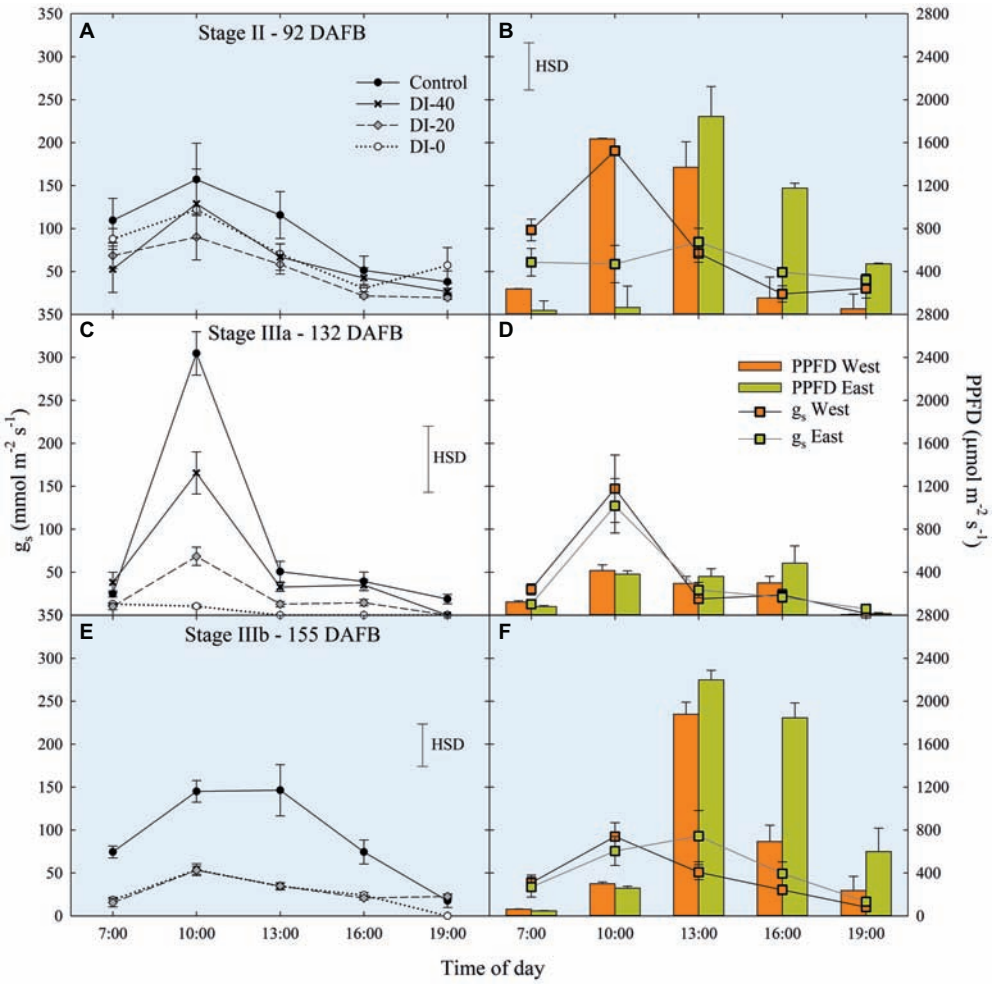

FIGURE 7 | Daily curves of leaf stomatal conductance (g_s) at stages II **(A)**, IIIa **(C)**, and IIIb **(E)** of 'September Bright' nectarine fruit growth, and in West- and East-oriented trees [Stage II **(B)**, IIIa **(D)**, IIIb **(F)**]. Trees irrigated to 100% (control), 40% (DI-40), 20% (DI-20), and 0% (DI-0) of crop evapotranspiration. Bars in panels **(B)**, **(D)**, and **(F)** show means of photosynthetic photon flux density (PPFD) for West- and East-oriented trees. Bars represent standard errors of means (irrigation treatment $n = 6$; canopy orientation $n = 12$). Significant differences determined with analysis of variance and Tukey's honestly significant difference (HSD, $p < 0.05$). The HSD bars in panels **(B,D,F)** represent only differences in g_s, and not in PPFD (only used as a reference).

hand, olive can easily tolerate leaf dehydration at similar levels of Ψ_{stem}.

Insights from **Figures 10, 11** suggested that ratios of RGR to RPCR might be better indicators of midday Ψ_{stem}, by combining fruit and leaf water relations. More specifically, the changes in hysteretic patterns (**Figure 10**) indicated that RGR/RPCR variance may be strictly related to midday Ψ_{stem} variations, as the shape of the loop changed along with increasing water deficit. However, hystereses were also likely to be influenced by intrinsic parameters of diel, diurnal, and nocturnal variations, such as maximum, minimum, and sum. Consequently, linear regression models considered RGR-to-RPCR ratios for all these parameters regressed vs. midday Ψ_{stem}. The only two linear models with $R^2 > 0.3$ were found for nocturnal data using the RSD_{RGR}/RSD_{RPCR} ($R^2 = 0.346$) and MAX_{RGR}/MAX_{RPCR} ($R^2 = 0.318$) ratios. The latter relationship was mostly derived from the significant association found in **Figure 11A**, as the response to midday Ψ_{stem} had a similar peak trend, but with a lower R^2 (0.405). Therefore, the MAX_{RGR}/MAX_{RPCR} ratio was discarded.

Finally, stepping forward to the strongest association with midday Ψ_{stem}, the scatter plot showed an inverse nonlinear association (**Figure 12C**), suggesting that the model might be both composed by a linear phase at higher values of Ψ_{stem} and by an exponential phase at lower Ψ_{stem}. In accordance with our hypothesis, the diurnal regression tended to show an opposite trend, although no significant association was found (**Figure 12B**). The diel regression reflected the unpredictable hysteretic behavior seen in **Figure 10**, resulting in the weakest, nonsignificant association (**Figure 12A**).

The association of nocturnal RSD_{RGR}/RSD_{RPCR} to Ψ_{stem} (**Figure 12C**) shifted from linear to exponential at midday $\Psi_{stem} = -2.3$ MPa, suggesting that this water deficit level might be identified as a threshold under which late-ripening

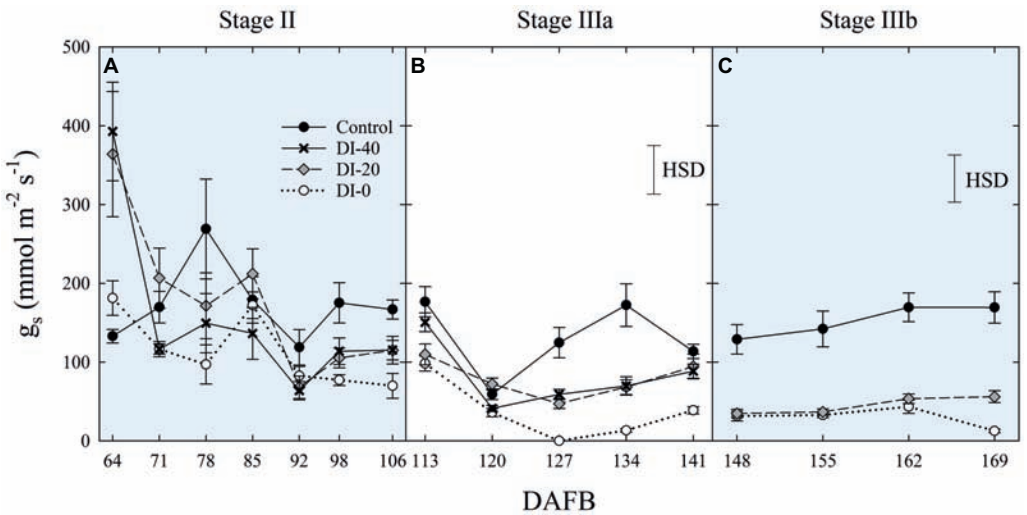

FIGURE 8 | Mid-morning leaf stomatal conductance (g_s) at stages II **(A)**, IIIa **(B)**, and IIIb **(C)** of 'September Bright' nectarine fruit growth. Trees irrigated to 100% (control), 40% (DI-40), 20% (DI-20), and 0% (DI-0) of crop evapotranspiration. Timeline expressed in days after full bloom (DAFB). Error bars represent standard errors of means (n = 6). Significant differences determined with analysis of variance and Tukey's honestly significant difference (HSD, $p < 0.05$).

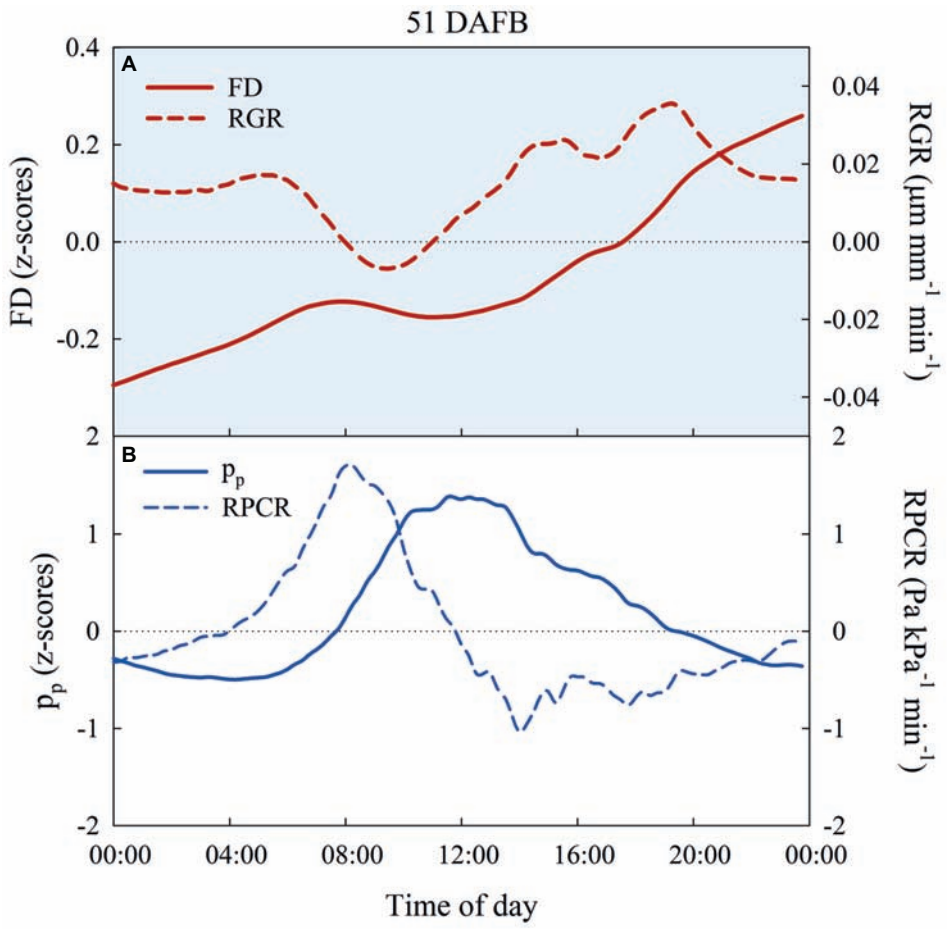

FIGURE 9 | Diel trends of fruit diameter (FD, n = 3) and fruit relative growth rate (RGR, n = 3) **(A)**, attenuated pressure of leaf patches (p_p) and leaf relative pressure change rate (RPCR) **(B)** in control irrigated trees at 51 days after full bloom (DAFB), at stage I of 'September Bright' nectarine fruit growth.

TABLE 2 | Pearson's correlation coefficients for fruit diameter (FD) and attenuated leaf patch clamp pressure (p_p) vs. plant water status (PWS) indicators: stem water potential (Ψ_{stem}), leaf water potential (Ψ_{leaf}), leaf stomatal conductance (g_s), and leaf relative water content (RWC) for all fruit growth stages.

PWS indicator	FD (*z*-scores)	*p*	*n*	p_p (*z*-scores)	*p*	*n*
Ψ_{stem} (MPa)	–0.103	0.184	168	–0.320	<0.001	180
Ψ_{leaf} (MPa)	–0.296	0.009	78	–0.645	<0.001	84
RWC (%)	–0.156	0.066	140	–0.442	<0.001	150
g_s (mmol m^{-2} s^{-1})	0.183	0.090	87	0.186	0.067	97

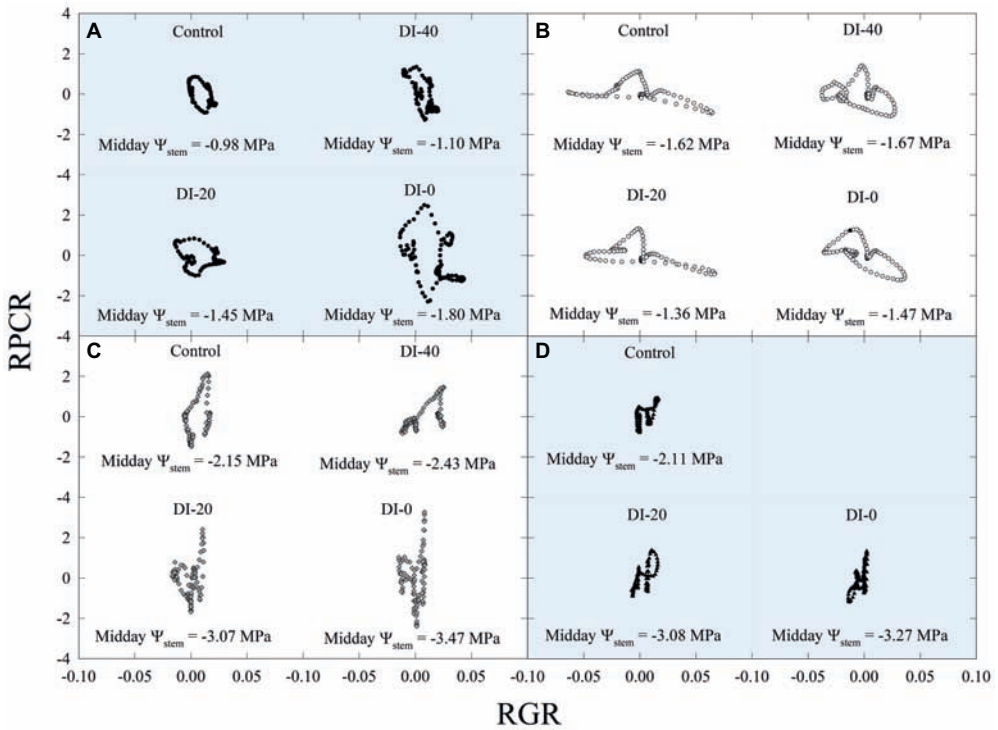

FIGURE 10 | Scatter plots of diel leaf relative pressure change rate (RPCR) and fruit relative growth rate (RGR) at stages I [50 days after full bloom, DAFB **(A)**], II [92 DAFB **(B)**], IIIa [132 DAFB **(C)**], and IIIb [155 DAFB **(D)**] of 'September Bright' nectarine fruit growth. Trees irrigated to 100% (control), 40% (DI-40), 20% (DI-20), and 0% (DI-0) of crop evapotranspiration. Midday Ψ_{stem} for each irrigation treatment and DAFB is reported in its relative panel.

'September Bright' nectarine trees are significantly affected by drought. Below the level of –2.3 MPa, the RSD of nocturnal fruit growth increases with respect to the one of leaf turgor pressure. For instance, the slight decrease in fruit diameter occurring between 154 and 161 DAFB in DI-0 trees (**Figure 2D**) induces an increase in nocturnal RSD_{RGR} while RSD_{RPCR} does not change, generating the observed increase of RSD_{RGR}/RSD_{RPCR}. At stage III, peach and nectarine stomata become dysfunctional (Chalmers et al., 1983) and high transpiration rates can overcome level of phloem and xylem inflows in fruits (Lescourret et al., 2001; Morandi et al., 2007a). This phenomenon generates particularly low fruit water potential and causes an increase in water potential difference between leaves and fruit (McFadyen et al., 1996), as also found in olive by Fernandes et al. (2018). Therefore, the different regulation of water balance in fruit and leaves may provide a very useful parameter for real-time and continuous monitoring of plant water status.

The identified stage-independent threshold of midday Ψ_{stem} (–2.3 MPa) can be used for irrigation management in commercial 'September Bright' nectarine orchards under environmental conditions similar to those in our study. However, during stage I, trees exposed to DI (i.e., mean of DI-0, DI-20 and DI-40) never reached such low levels of Ψ_{stem}, despite yielding fruit with significantly lower final size compared to control irrigated trees (i.e., 53.3 ± 0.44 mm vs. 58.6 ± 0.81 mm for DI and control, respectively). Yet, it is important to acknowledge the limitations of using a significant number of sensors (≥3) on individual fruit and leaves for the appropriate estimation of Ψ_{stem} for each tree, and the damage that they may cause when they are kept on the same organ for prolonged time (e.g., limitation of gas exchange, light interception, and growth). In particular, a regular monitoring (at least at weekly intervals) has to be conducted to clamp sensors on different fruit and leaves and to verify their correct use. Even so, the estimated Ψ_{stem} from a good sample of trees has the potential to be combined

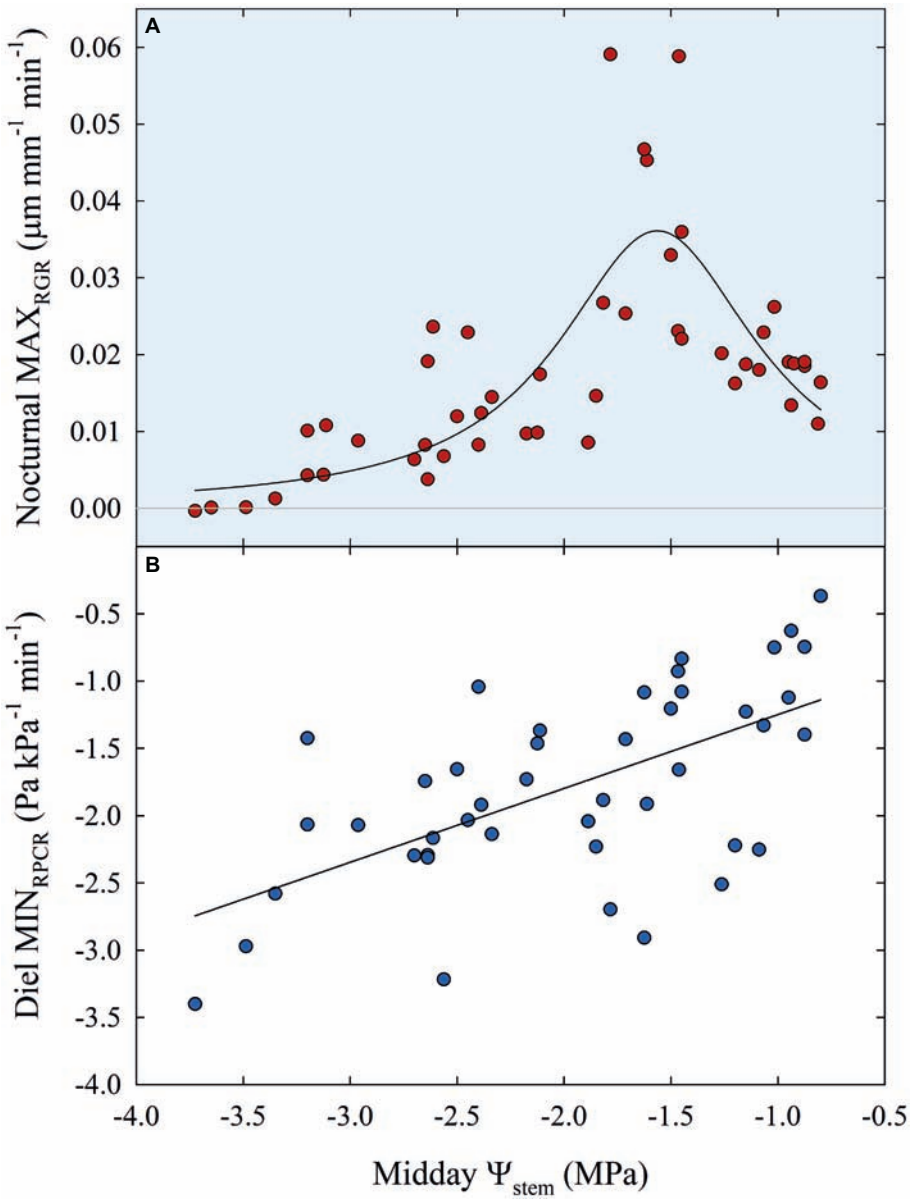

FIGURE 11 | Maximum nocturnal fruit relative growth rate (MAX_{RGR}) vs. midday Ψ_{stem} **(A)** and minimum diel leaf relative pressure change rate (MIN_{RPCR}) vs. midday Ψ_{stem} **(B)** for all fruit growth stages and irrigation treatments. Nonlinear regression in panel **(A)**: $MAX_{RGR} = 0.04/\{1 + [(\Psi_{stem} + 1.56)/0.57]^2\}$, $R^2 = 0.597$, $p < 0.001$. Linear regression in panel **(B)**: $MIN_{RPCR} = -0.70 + 0.55 \times \Psi_{stem}$, $R^2 = 0.369$, $p < 0.001$.

with spatial information (e.g., NDVI and thermal images) for a highly precise irrigation management in modern large orchards.

CONCLUSIONS

Overall, this work highlights a combined fruit and leaf sensing approach for the continuous monitoring of tree water status. On one side, the leaf sensing method guarantees a fast and responsive signal based on leaf turgor pressure that represents a pre-alarm forecast for irrigation management; on the other hand, continuous fruit size sensing provides the precise information on the time-lag and plant dehydration level to which deficit irrigation can be imposed until fruit growth and yield are significantly affected. Both together, leaf and fruit sensing provide a powerful and reliable tool that is not influenced by the fruit development stage and that can be continuously used to detect stem water potential thresholds for irrigation management. In this regard, additional efforts should be made to develop new fruit and leaf sensing technologies that reduce the likelihood to damage organs during the period of data collection. Further investigations need to be carried out to

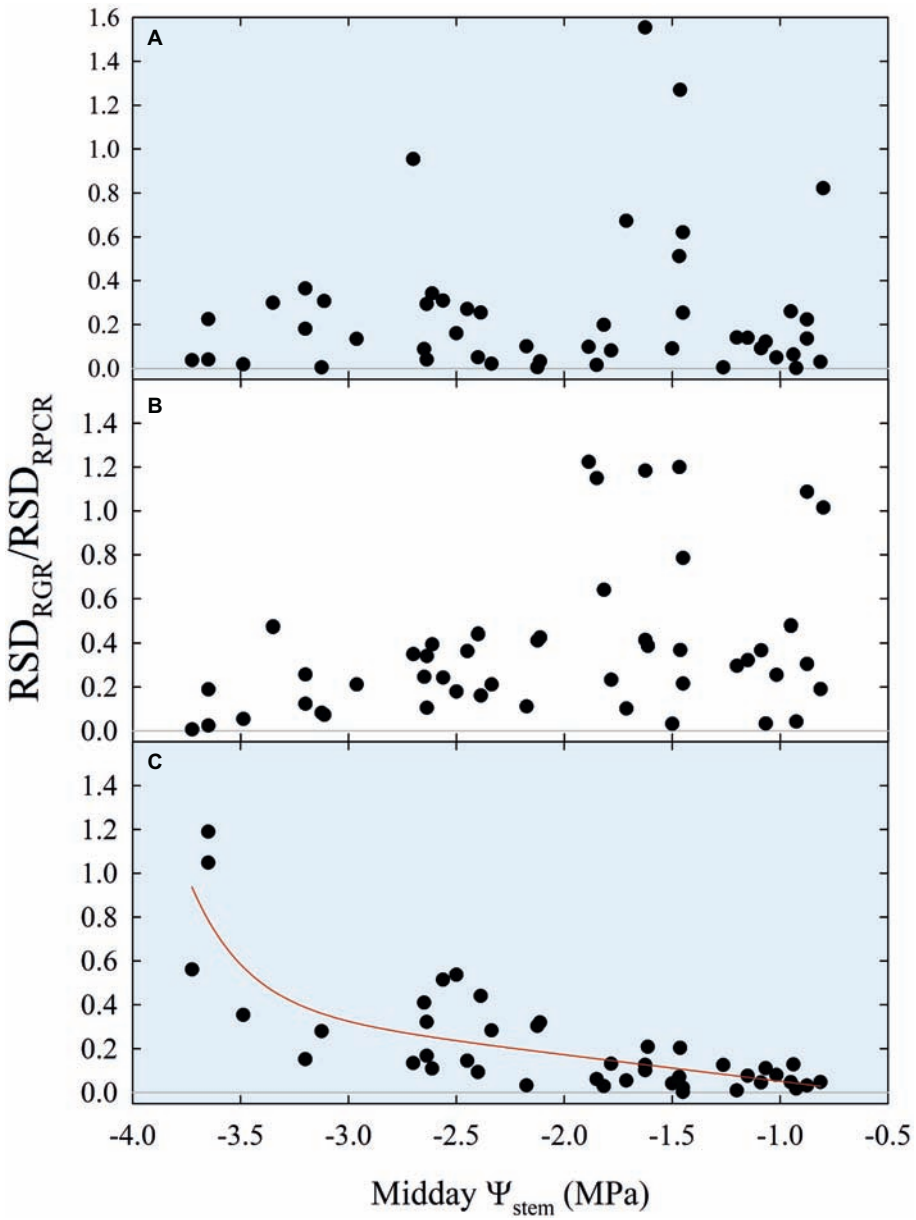

FIGURE 12 | Diel **(A)**, diurnal **(B)**, and nocturnal ratios **(C)** of relative standard deviations of fruit relative growth rate (RSD_{RGR}) and leaf relative pressure change rate (RSD_{RPCR}) vs. midday Ψ_{stem} for all fruit growth stages and irrigation treatments. Expo-linear model in panel **(C)**: $RSD_{RGR}/RSD_{RPCR} = -0.07 + 2.88E\text{-}07 \times \exp.(-3.89 \times \Psi_{stem}) - 0.12 \times \Psi_{stem}$, $R^2 = 0.650$, $p < 0.001$.

promote models that assess the nocturnal to diurnal shift within the diel hysteresis of fruit growth vs. leaf turgor pressure, and the time lag characterizing the hysteretic loop. Nevertheless, our findings represent an innovative and valid plant-based support to rational and sustainable irrigation management.

DATA AVAILABILITY

The datasets for this manuscript are available upon request to Agriculture Victoria. Requests to access the datasets should be directed to Mark Glenn O'Connell, mark.oconnell@ecodev.vic.gov.au.

AUTHOR CONTRIBUTIONS

All authors contributed to conception and design of the study. MOC, DS, and RLB made available the equipment used in the experiment. AS and MOC carried out field measurements. AS and RLB performed the statistical analysis. AS wrote the first draft of the manuscript. All authors

contributed to manuscript revision, read and approved the submitted version.

FUNDING

The experiment was supported by a PhD project funded with a scholarship issued by the Italian Ministry of Education and the University of Palermo, and by the stone fruit experimental orchard project (SF17006 Summerfruit Orchard – Phase II) funded by Hort Innovation using Summerfruit levy and funds from the Australian Government with co-investment from Agriculture Victoria.

ACKNOWLEDGMENTS

The technical support and assistance of Dave Haberfield, Jim Selman, Athulya Jancy Benny, Andrew O'Connell, and Cameron O'Connell and the scientific support provided by Ian Goodwin, Des Whitfield, Subhash Chandra, and Steve Green are gratefully acknowledged.

REFERENCES

Allen, R. G., Pereira, L. S., Raes, D., and Smith, M. (1998). *Crop evapotranspiration – guidelines for computing crop water requirements, FAO irrigation and drainage paper 56*. (Rome: FAO-Food and Agriculture Organisation of the United Nations).

Ameglio, T., and Cruiziat, P. (1992). "Daily variations of stem and branch diameter: short overview from a developed example" in *Mechanics of swelling*. ed. T. K. Karalis (Berlin, Heidelber, Germany: Springer), 193–204.

Ballester, C., Castiella, M., Zimmermann, U., Rüger, S., Martínez Gimeno, M. A., and Intrigliolo, D. S. (2017). Usefulness of the ZIM-probe technology for detecting water stress in clementine and persimmon trees. *Acta Hortic.* 1150, 105–112. doi: 10.17660/ActaHortic.2017.1150.15

Barrs, H. D., and Weatherley, P. E. (1962). A re-examination of the relative turgidity technique for estimating water deficits in leaves. *Aust. J. Biol. Sci.* 15, 413–428. doi: 10.1071/BI9620413

Blanco-Cipollone, F., Lourenço, S., Silvestre, J., Conceição, N., Moñino, M. J., Vivas, A., et al. (2017). Plant water status indicators for irrigation scheduling associated with iso-and anisohydric behavior: vine and plum trees. *Horticulturae* 3, 47–63. doi: 10.3390/horticulturae3030047

Blanke, M. M., and Lenz, F. (1989). Fruit photosynthesis. *Plant Cell Environ.* 12, 31–46. doi: 10.1111/j.1365-3040.1989.tb01914.x

Bonachela, S., Orgaz, F., Villalobos, F. J., and Fereres, E. (2001). Soil evaporation from drip-irrigated olive orchards. *Irrig. Sci.* 20, 65–71. doi: 10.1007/s002710000030

Brough, D. W., Jones, H. G., and Grace, J. (1986). Diurnal changes in water content of the stems of apple trees, as influenced by irrigation. *Plant Cell Environ.* 9, 1–7.

Burquez, A. (1987). Leaf thickness and water deficit in plants: a tool for field studies. *J. Exp. Bot.* 38, 109–114. doi: 10.1093/jxb/38.1.109

Chalmers, D. J., Burge, G., Jerie, P. H., and Mitchell, P. D. (1986). The mechanism of regulation of "Bartlett" pear fruit and vegetative growth by irrigation withholding and regulated deficit irrigation. *J. Amer. Soc. Hort. Sci.* 111, 904–907.

Chalmers, D. J., Mitchell, P. D., and van Heek, L. (1981). Control of peach tree growth and productivity by regulated water supply, tree density, and summer pruning. *J. Amer. Soc. Hort. Sci.* 106, 307–312.

Chalmers, D. J., Olsson, K. A., and Jones, T. R. (1983). "Water relations of peach trees and orchards" in *Additional woody crop plants*. ed. T. T. Kozlowski, Vol. 7 (New York, NY: Academic Press), 197–232.

Chalmers, D. J., and van den Ende, B. (1975). A reappraisal of the growth and development of peach fruit. *Funct. Plant Biol.* 2, 623–634. doi: 10.1071/PP9750623

Chalmers, D. J., and Wilson, I. B. (1978). Productivity of peach trees: tree growth and water stress in relation to fruit growth and assimilate demand. *Ann. Bot.* 42, 285–294.

Conejero, W., Alarcón, J. J., García-Orellana, Y., Nicolás, E., and Torrecillas, A. (2007). Evaluation of sap flow and trunk diameter sensors for irrigation scheduling in early maturing peach trees. *Tree Physiol.* 27, 1753–1759. doi: 10.1093/treephys/27.12.1753

Connors, C. H. (1919). Growth of fruits of peach. *New Jersey Agric. Exp. Stn. Annu. Rep.* 40, 82–88.

Cruiziat, P., Granier, A., Claustres, J. P., and Lachaize, D. (1989). "Diurnal evolution of water flow and potential in an individual spruce: experimental and theoretical study" in *Ann. Sci. Forest*. ed. E. Dreyer, Vol. 46 (France: EDP Sciences), 353–356.

DeJong, T. M., and Goudriaan, J. (1989). Modeling peach fruit growth and carbohydrate requirements: reevaluation of the double-sigmoid growth pattern. *J. Amer. Soc. Hort. Sci.* 114, 800–804.

Ehrenberger, W., Rüger, S., Rodríguez-Domínguez, C. M., Díaz-Espejo, A., Fernández, J. E., Moreno, J., et al. (2012). Leaf patch clamp pressure probe measurements on olive leaves in a nearly turgorless state. *Plant Biol.* 14, 666–674. doi: 10.1111/j.1438-8677.2011.00545.x

Fereres, E., and Soriano, M. A. (2007). Deficit irrigation for reducing agricultural water use. *J. Exp. Bot.* 58, 147–159. doi: 10.1093/jxb/erl165

Fernandes, R. D. M., Cuevas, M. V., Diaz-Espejo, A., and Hernandez-Santana, V. (2018). Effects of water stress on fruit growth and water relations between fruits and leaves in a hedgerow olive orchard. *Agric. Water Manag.* 210, 32–40. doi: 10.1016/j.agwat.2018.07.028

Fernández, J. E. (2017). Plant-based methods for irrigation scheduling of woody crops. *Horticulturae* 3, 35–72. doi: 10.3390/horticulturae3020035

Fernández, J. E., Rodriguez-Dominguez, C. M., Perez-Martin, A., Zimmermann, U., Rüger, S., Martín-Palomo, M. J., et al. (2011). Online-monitoring of tree water stress in a hedgerow olive orchard using the leaf patch clamp pressure probe. *Agric. Water Manag.* 100, 25–35. doi: 10.1016/j.agwat.2011.08.015

Génard, M., and Huguet, J. G. (1996). Modeling the response of peach fruit growth to water stress. *Tree Physiol.* 16, 407–415. doi: 10.1093/treephys/16.4.407

Goldhamer, D. A., Fereres, E., Mata, M., Girona, J., and Cohen, M. (1999). Sensitivity of continuous and discrete plant and soil water status monitoring in peach trees subjected to deficit irrigation. *J. Amer. Soc. Hort. Sci.* 124, 437–444.

Goodwin, I., Whitfield, D. M., and Connor, D. J. (2006). Effects of tree size on water use of peach (*Prunus persica* L. Batsch). *Irrig. Sci.* 24, 59–68. doi: 10.1007/s00271-005-0010-z

Granier, A., Breda, N., Claustres, J. P., and Colin, F. (1989). "Variation of hydraulic conductance of some adult conifers under natural conditions" in *Ann. Sci. Forest*. ed. E. Dreyer, Vol. 46 (France: EDP Sciences), 357–360.

Jones, H. G. (2004). Irrigation scheduling: advantages and pitfalls of plant-based methods. *J. Exp. Bot.* 55, 2427–2436. doi: 10.1093/jxb/erh213

Jones, H. G. (2007). Monitoring plant and soil water status: established and novel methods revisited and their relevance to studies of drought tolerance. *J. Exp. Bot.* 58, 119–130. doi: 10.1093/jxb/erl118

Koide, R. T., Robichaux, R. H., Morse, S. R., and Smith, C. M. (1989). "Plant water status, hydraulic resistance and capacitance" in *Plant physiological ecology*. eds. R. W. Pearcy, J. R. Ehleringer, H. A. Mooney, and P. W. Rundel (Dordrecht, Germany: Springer), 161–183.

Lang, A. (1990). Xylem, phloem and transpiration flows in developing apple fruits. *J. Exp. Bot.* 41, 645–651. doi: 10.1093/jxb/41.6.645

Lescourret, F., Génard, M., Habib, R., and Fishman, S. (2001). Variation in surface conductance to water vapor diffusion in peach fruit and its effects on fruit growth assessed by a simulation model. *Tree Physiol.* 21, 735–741. doi: 10.1093/treephys/21.11.735

Li, S. H., Huguet, J. G., and Bussi, C. (1989b). Irrigation scheduling in a mature peach orchard using tensiometers and dendrometers. *Irrig. Drain.* 3, 1–12.

Li, S. H., Huguet, J. G., Schoch, P. G., and Orlando, P. (1989a). Response of peach tree growth and cropping to soil water deficit at various phenological stages of fruit development. *J. Hortic. Sci.* 64, 541–552.

Lo Bianco, R., and Scalisi, A. (2017). Water relations and carbohydrate partitioning of four greenhouse-grown olive genotypes under long-term drought. *Trees* 31, 717–727. doi: 10.1007/s00468-016-1502-6

Marino, G., Pernice, F., Marra, F. P., and Caruso, T. (2016). Validation of an online system for the continuous monitoring of tree water status for sustainable irrigation managements in olive (*Olea europaea* L.). *Agric. Water Manag.* 177, 298–307. doi: 10.1016/j.agwat.2016.08.010

Marsal, J., and Girona, J. (1997). Relationship between leaf water potential and gas exchange activity at different phenological stages and fruit loads in peach trees. *J. Amer. Soc. Hort. Sci.* 122, 415–421.

Martínez-Gimeno, M. A., Castiella, M., Rüger, S., Intrigliolo, D. S., and Ballester, C. (2017). Evaluating the usefulness of continuous leaf turgor pressure measurements for the assessment of persimmon tree water status. *Irrig. Sci.* 35, 159–167. doi: 10.1007/s00271-016-0527-3

McCutchan, H., and Shackel, K. A. (1992). Stem-water potential as a sensitive indicator of water stress in prune trees (*Prunus domestica* L. cv. French). *J. Amer. Soc. Hort. Sci.* 117, 607–611.

McFadyen, L. M., Hutton, R. J., and Barlow, E. W. R. (1996). Effects of crop load on fruit water relations and fruit growth in peach. *J. Hortic. Sci.* 71, 469–480.

Morandi, B., Losciale, P., Manfrini, L., Zibordi, M., Anconelli, S., Pierpaoli, E., et al. (2014). Leaf gas exchanges and water relations affect the daily patterns of fruit growth and vascular flows in Abbé Fétel pear (*Pyrus communis* L.) trees. *Sci. Hortic.* 178, 106–113. doi: 10.1016/j.scienta.2014.08.009

Morandi, B., Manfrini, L., Losciale, P., Zibordi, M., and Corelli Grappadelli, L. (2010a). The positive effect of skin transpiration in peach fruit growth. *J. Plant Physiol.* 167, 1033–1037. doi: 10.1016/j.jplph.2010.02.015

Morandi, B., Manfrini, L., Losciale, P., Zibordi, M., and Corelli Grappadelli, L. (2010b). Changes in vascular and transpiration flows affect the seasonal and daily growth of kiwifruit (*Actinidia deliciosa*) berry. *Ann. Bot.* 105, 913–923. doi: 10.1093/aob/mcq070

Morandi, B., Manfrini, L., Zibordi, M., Noferini, M., Fiori, G., and Corelli Grappadelli, L. (2007b). A low-cost device for accurate and continuous measurements of fruit diameter. *HortScience* 42, 1380–1382. doi: 10.21273/HORTSCI.42.6.1380

Morandi, B., Rieger, M., and Corelli Grappadelli, L. (2007a). Vascular flows and transpiration affect peach (*Prunus persica* Batsch.) fruit daily growth. *J. Exp. Bot.* 58, 3941–3947. doi: 10.1093/jxb/erm248

Mossad, A., Scalisi, A., and Lo Bianco, R. (2018). Growth and water relations of field-grown 'Valencia' orange trees under long-term partial rootzone drying. *Irrig. Sci.* 36, 9–24. doi: 10.1007/s00271-017-0562-8

Naor, A. (1998). Relations between leaf and stem water potentials and stomatal conductance in three field-grown woody species. *J. Hortic. Sci. Biotechnol.* 73, 431–436. doi: 10.1080/14620316.1998.11510995

Naor, A. (2000). Midday stem water potential as a plant water stress indicator for irrigation scheduling in fruit trees. *Acta Hortic.* 537, 447–454. doi: 10.17660/ActaHortic.2000.537.52

Naor, A. (2006). Irrigation scheduling and evaluation of tree water status in deciduous orchards. *Hortic. Rev.* 32, 111–165. doi: 10.1002/9780470767986.ch3

Naor, A., Hupert, H., Greenblat, Y., Peres, M., Kaufman, A., and Klein, I. (2001). The response of nectarine fruit size and midday stem water potential to irrigation level in stage III and crop load. *J. Amer. Soc. Hort. Sci.* 126, 140–143. doi: 10.21273/jashs.126.1.140

Naor, A., Klein, I., Hupert, H., Grinblat, Y., Peres, M., and Kaufman, A. (1999). Water stress and crop level interactions in relation to nectarine yield, fruit size distribution, and water potentials. *J. Amer. Soc. Hort. Sci.* 124, 189–193. doi: 10.21273/jashs.124.2.189

Paço, T. A., Ferreira, M. I., and Conceição, N. (2006). Peach orchard evapotranspiration in a sandy soil: comparison between eddy covariance measurements and estimates by the FAO 56 approach. *Agric. Water Manag.* 85, 305–313. doi: 10.1016/j.agwat.2006.05.014

Padilla-Díaz, C. M., Rodriguez-Dominguez, C. M., Hernandez-Santana, V., Perez-Martin, A., and Fernández, J. E. (2016). Scheduling regulated deficit irrigation in a hedgerow olive orchard from leaf turgor pressure related measurements. *Agric. Water Manag.* 164, 28–37. doi: 10.1016/j.agwat.2015.08.002

Rodriguez-Dominguez, C. M., Ehrenberger, W., Sann, C., Rüger, S., Sukhorukov, V., Martín-Palomo, M. J., et al. (2012). Concomitant measurements of stem sap flow and leaf turgor pressure in olive trees using the leaf patch clamp pressure probe. *Agric. Water Manag.* 114, 50–58. doi: 10.1016/j.agwat.2012.07.007

Rüger, S., Netzer, Y., Westhoff, M., Zimmermann, D., Reuss, R., Ovadiya, S., et al. (2010). Remote monitoring of leaf turgor pressure of grapevines subjected to different irrigation treatments using the leaf patch clamp pressure probe. *Aust. J. Grape Wine R.* 16, 405–412. doi: 10.1111/j.1755-0238.2010.00101.x

Savitzky, A., and Golay, M. J. (1964). Smoothing and differentiation of data by simplified least squares procedures. *Anal. Chem.* 36, 1627–1639. doi: 10.1021/ac60214a047

Scalisi, A., Bresilla, K., and Simões Grilo, F. (2017). Continuous determination of fruit tree water-status by plant-based sensors. *Italus Hortus.* 24, 39–50. doi: 10.26353/j.itahort/2017.2.3950

Shackel, K. A., Ahmadi, H., Biasi, W., Buchner, R., Goldhamer, D., Gurusinghe, S., et al. (1997). Plant water status as an index of irrigation need in deciduous fruit trees. *HortTechnology* 7, 23–29.

Simonneau, T., Habib, R., Goutouly, J. P., and Huguet, J. G. (1993). Diurnal changes in stem diameter depend upon variations in water content: direct evidence in peach trees. *J. Exp. Bot.* 44, 615–621. doi: 10.1093/jxb/44.3.615

Snyder, R. L. (2017). Climate change impacts on water use in horticulture. *Horticulturae* 3, 27–35. doi: 10.3390/horticulturae3020027

Steppe, K., De Pauw, D. J., and Lemeur, R. (2008). A step towards new irrigation scheduling strategies using plant-based measurements and mathematical modelling. *Irrig. Sci.* 26, 505–517. doi: 10.1007/s00271-008-0111-6

Stöckle, C. O., Marsal, J., and Villar, J. M. (2011). Impact of climate change on irrigated tree fruit production. *Acta Hortic.* 889, 41–52. doi: 10.17660/ActaHortic.2011.889.2

Tognetti, R., Raschi, A., Béres, C., Fenyvesi, A., and Ridder, H. W. (1996). Comparison of sap flow, cavitation and water status of *Quercus petraea* and *Quercus cerris* trees with special reference to computer tomography. *Plant Cell Environ.* 19, 928–938. doi: 10.1111/j.1365-3040.1996.tb00457.x

Tran, N., Bam, P., Black, K., Graham, T., Zhang, P., Dixon, M., et al. (2015). Improving irrigation scheduling protocols for nursery trees by relating cumulative water potential to concurrent vapour pressure deficit©. *Acta Hortic.* 1085, 129–134. doi: 10.17660/ActaHortic.2015.1085.22

Turner, N. C. (1988). Measurement of plant water status by the pressure chamber technique. *Irrig. Sci.* 9, 289–308.

Vera, J., Conejero, W., Conesa, M. R., and Ruiz-Sánchez, M. C. (2019). Irrigation factor approach based on soil water content: a nectarine orchard case study. *Water* 11, 589–603. doi: 10.3390/w11030589

Zimmermann, D., Reuss, R., Westhoff, M., Geßner, P., Bauer, W., Bamberg, E., et al. (2008). A novel, non-invasive, online-monitoring, versatile and easy plant-based probe for measuring leaf water status. *J. Exp. Bot.* 59, 3157–3167. doi: 10.1093/jxb/ern171

Zimmermann, U., Rüger, S., Shapira, O., Westhoff, M., Wegner, L. H., Reuss, R., et al. (2010). Effects of environmental parameters and irrigation on the turgor pressure of banana plants measured using the non-invasive, online monitoring leaf patch clamp pressure probe. *Plant Biol.* 12, 424–436. doi: 10.1111/j.1438-8677.2009.00235.x

Conflict of Interest Statement: The authors declare that the research was conducted in the absence of any commercial or financial relationships that could be construed as a potential conflict of interest.

frontiers in Plant Science

ORIGINAL RESEARCH
published: 23 January 2020
doi: 10.3389/fpls.2019.01695

Transpiration Reduction in Maize (*Zea mays* L) in Response to Soil Drying

Faisal Hayat[1]*, *Mutez Ali Ahmed*[1,2], *Mohsen Zarebanadkouki*[1], *Mathieu Javaux*[3,4], *Gaochao Cai*[1,2] *and Andrea Carminati*[1]

[1] Chair of Soil Physics, University of Bayreuth, Bayreuth, Germany, [2] Division of Soil Hydrology, University of Göttingen, Göttingen, Germany, [3] Earth and Life Institute-Environmental Sciences, Universite Catholique de Louvain, Louvain la Neuve, Belgium, [4] Agrosphere (IBG-3), Forschungszentrum Juelich GmbH, Juelich, Germany

The relationship between leaf water potential, soil water potential, and transpiration depends on soil and plant hydraulics and stomata regulation. Recent concepts of stomatal response to soil drying relate stomatal regulation to plant hydraulics, neglecting the loss of soil hydraulic conductance around the roots. Our objective was to measure the effect of soil drying on the soil-plant hydraulic conductance of maize and to test whether stomatal regulation avoids a loss of soil-plant hydraulic conductance in drying soils. We combined a root pressure chamber, in which the soil-root system is pressurized to maintain the leaf xylem at atmospheric pressure, with sap flow sensors to measure transpiration rate. The method provides accurate and high temporal resolution measurements of the relationship between transpiration rate and xylem leaf water potential. A simple soil-plant hydraulic model describing the flow of water across the soil, root, and xylem was used to simulate the relationship between leaf water potential and transpiration rate. The experiments were carried out with 5-week-old maize grown in cylinders of 9 cm diameter and 30 cm height filled with silty soil. The measurements were performed at four different soil water contents (WC). The results showed that the relationship between transpiration and leaf water potential was linear in wet soils, but as the soil dried, the xylem tension increased, and nonlinearities were observed at high transpiration rates. Nonlinearity in the relationship between transpiration and leaf water potential indicated a decrease in the soil-plant hydraulic conductance, which was explained by the loss of hydraulic conductivity around the roots. The hydraulic model well reproduced the observed leaf water potential. Parallel experiments performed with plants not being pressurized showed that plants closed stomata when the soil-plant hydraulic conductance decreased, maintaining the linearity between leaf water potential and transpiration rate. We conclude that stomata closure during soil drying is caused by the loss of soil hydraulic conductivity in a predictable way.

Keywords: maize (*Zea mays* L), pressure chamber, soil drying, stomatal closure, transpiration rates

OPEN ACCESS

Edited by:
Maren Dubbert, University of Freiburg, Germany

Reviewed by:
Teemu Hölttä, University of Helsinki, Finland
Juliana S. Medeiros, The Holden Arboretum, United Kingdom

***Correspondence:**
Faisal Hayat
Faisal.Hayat@uni-bayreuth.de

Specialty section:
This article was submitted to Technical Advances in Plant Science, a section of the journal Frontiers in Plant Science

Received: *14 May 2019*
Accepted: *02 December 2019*
Published: *23 January 2020*

Citation:
Hayat F, Ahmed MA, Zarebanadkouki M, Javaux M, Cai G and Carminati A (2020) Transpiration Reduction in Maize (Zea mays L) in Response to Soil Drying. Front. Plant Sci. 10:1695. doi: 10.3389/fpls.2019.01695

INTRODUCTION

Drought is a primary constraint to plant growth and crop production worldwide. Mechanisms by which drought impacts plant growth are complex and involve feedbacks between stomata regulation, plant hydraulics and soil drying. A hydraulic framework is helpful to understand the physical constraints to transpiration (Sperry and Love, 2015). The soil-plant atmospheric continuum is described as a network of elements connected in series and in parallel (Cowan, 1965; Sperry et al., 1998; Draye et al., 2010; Mencuccini et al., 2019). Each element is characterized by hydraulic conductances (which can be variable) and capacitances. Water flows from soil to the roots, and then along the xylem till the leaf tissues and stomata, where it evaporates into the atmosphere following the cohesion-tension theory (Pickard, 1981; Sperry et al., 1998). The driving force for transpiration is the water tension generated in the leaves because of the evaporating water. The tension propagates down along the xylem to the roots and to the soil. The hydraulic conductivities of the xylem, of the roots and of the soil are extremely variable. Xylem vessels tend to cavitate at high tension, causing a large drop in the axial conductance of the xylem (Sperry et al., 1998). The radial conductance of the root is also variable and it is affected by anatomical changes as well as by the expression of aquaporin (Ehlert et al., 2009; Redondo et al., 2009; Simonneau et al., 2009; Knipfer et al., 2011; Chaumont and Tyerman, 2014). Finally, the soil hydraulic conductivity determines the ease of water flow through the soil. Its conductivity decreases by several orders of magnitude as the soil dries, and it might become smaller than that of roots (Gardner, 1960; Draye et al., 2010). Eventually, when plants are exposed to severe drying, their roots shrink and lose part of their contact to the soil (Carminati et al., 2013), which further decreases the conductance between rhizosphere and root. On the other hand, plants can close this gap and attenuate the drop in conductivity by secreting mucilage (Carminati et al., 2010) or by growing root hairs (Carminati et al., 2017).

Soil drying triggers a gradual closure of stomata and a reduction in transpiration rate (Carter et al., 1980; Meyer and Green, 1980; Bates et al., 1981; Comstock, 2002; Sinclair et al., 2005). Stomatal closure depends on both hydraulic and hormonal signals, such as abscisic acid (ABA) (Tardieu and Davies, 1993; Brodribb and McAdam, 2017 and Buckley, 2017). Independently from the mechanism by which stomata close, it has been proposed that stomatal regulation avoids excessive drop in leaf water potential by responding to nonlinearities in the relationship between transpiration rate and leaf water potential (Sperry and Love, 2015; Sperry et al., 2016). However, there is limited experimental evidence that stomatal regulation prevents and responds to drop in soil-plant hydraulic conductance. Additionally, most of the studies linking stomatal regulation to plant hydraulics focus on xylem vulnerability as the primary constraint on water flow in soil and plants (Anderegg et al., 2017), neglecting the explicit role of soil hydraulic conductivity.

Our objective was to test whether stomata close when the soil-plant hydraulic conductance drops during soil drying. Here, we use a soil-plant hydraulic model that solves the radial flow of water around a representative single root (Gardner, 1960; Van Lier et al., 2008) and water flow in the plant (Sperry et al., 1998) to test whether the drop in hydraulic conductance can be predicted based on the loss of soil hydraulic conductance.

Experimentally, we applied the pressure chamber method (Passioura, 1980) to maize (*Zea mays* L) growing in silty soil. The root-soil system of intact transpiring plants is pressurized to maintain the leaf xylem at atmospheric pressure. The applied pressure is then equivalent to the tension of water in the leaf xylem (Passioura, 1980). The method allows accurate measurements at high temporal resolution of leaf water potential for varying transpiration rates and soil water potential. Furthermore, we measured transpiration rates for pressurized (in the pressure chamber) and not-pressurized (outside the pressure chamber) plants to test to what extent leaf tension controls stomata closure in drying soils.

MATERIALS AND METHODS

Soil and Plant Preparation

Three replicates of maize (*Zea mays* L.) were grown in PVC pots with 30 cm of height and 9 cm of diameter. The pots were filled with a mixture of silt and quartz sand (1:1 ratio) {{mdash}} which were sieved to a particle diameter < 1 mm. The soil was poured into each pot to achieve a bulk density of 1.4 g cm^{-3}. The soil surface of each pot was covered with fine gravels (2–3.5 mm) to minimize evaporation from the soil surface. Several holes with a diameter of 1.5 mm were drilled at the bottom and sides of the pots to allow, respectively, water drainage and lateral injection of water using a fine needle. Five holes were placed with diameter of 5 mm and with a distance of 5 cm from each other at the sides of the pots to measure soil water content using a TDR (time domain reflectometer, FOM/mts, E-Test (IA PAS), Lublin, Poland). The soil hydraulic properties were estimated using extended evaporation method (Peters and Durner, 2008; Schindler et al., 2010). The implementation of this method using Hyprop (Meters, Munich, Germany) and the parameterization of retention curve and soil hydraulic conductivity has been described in Hayat et al (2018).

Maize seeds were germinated on moist filter paper for 48 h and the seedlings were planted in the containers. The plants were grown for 40 days in a climate room with a photoperiod of 14 h, day/night temperature of 25°C/22°C, relative humidity of 60% and light intensity 200 μmol m^{-2} s^{-1}. During the first three weeks, the plants were irrigated every third day by immersing the pots in a nutrient solution to achieve an average soil water content of 25%. Afterward, the soil water contents were adjusted to the following scenarios: i) water content of 21%–25% (wet soil); ii) water content of 12%–13% (midwet soil); iii) water content of 9%–10% (middry soil); iv) and water content of 6%–6.5% (dry soil). The soil water contents were measured every third day using TDR. The soil moisture content was measured at five different heights (5, 10, 15, 20, 25, and 30 cm).

Transpiration Measurements

Prior to the experiment, we measured soil water contents at five different heights as described above. Afterwards, transpiration rates for each scenario were recorded by Sap Flow Sensors SGA9 (Dynamax Inc, USA). This nonintrusive, energy balance sensor measures the amount of heat carried by the sap and converts into real-time transpiration rate.

Transpiration rates were also measured by weighing the plants before and after the recordings, and the decrease in weight was compared to the cumulative flow measured with the sap flow sensors (**Figure S1A**). A LED lamp (GC 9, photo flux density (15 cm), 2450 μmol m^{-2} s^{-1}, Greenception GmbH, Hamburg) was installed at a distance of 16 cm above the shoots (**Figure S1B**). Transpiration was increased in four steps (from low to high transpiration) by increasing photosynthetic photon intensity. Transpiration was measured for a period of one and a half hour for each step. At the end of transpiration measurements, water was injected in the pot through the holes to bring the soil to the initial soil water content.

Pressure Chamber

Xylem water potential of transpiring plants was measured using the pressure chamber method, based on Passioura (1980). We started the experiment when plants were 40 days old. Briefly, the soil core and the roots were put inside the pressure chamber in such a way that the shoot remained outside and it was carefully sealed to avoid air leakage (**Figure S1B**). One leaf was cut and the pressure in the chamber was increased (using 99.9% vol. N_2) until a water droplet appeared on a cut leaf (**Figure S1C**). The pressure needed to keep a drop of water at the cut end of the leaves is numerically equal to the tension in the xylem (Passioura, 1980). Transpiration was increased stepwise by imposing leaves to four increasing photosynthetic photon intensities. In each step, we let the plant to transpire for 1.5 h. During this time, transpiration was measured using a sap flow sensor that was installed on the stem of the plant. The measurements were performed for four scenarios of moisture levels and four transpiration rates. To reveal the effect of soil and plant pressurizing on the transpiration rate (stomata closure), each measurement was performed with and without pressurizing the soil.

Soil-Plant Hydraulic Model

We used a simple model to estimate the water flow in the soil-plant continuum. The model was represented as a series of hydraulic resistances (and one capacitance in the soil) between the bulk soil and the leaves. The flux of water in the soil q [cm s^{-1}] is calculated using a cylindrical model as a function of radial distance r to the root center:

$$q(r) = -k_{soil}(\psi)\frac{\partial \psi}{\partial r} \tag{1}$$

where k_{soil} is the soil conductivity [cm s^{-1}] (when the matric potential is expressed as hydraulic head, i.e., 1 hPa ≈ 1 cm), which is function of matric potential ψ [hPa], and $\frac{\partial \psi}{\partial r}$ is the gradient in matric potential. As boundary condition at the root-soil interface, we set $q(r_0) = -\frac{T}{2\pi r_0 L}$ where T is the transpiration rate [cm^3 s^{-1}], r_0 is the root radius [cm] and L is the active root length [cm]. We imposed no flow at the outer root radius r_b [cm], i.e., $q(r_b) = 0$, where $r_b = \sqrt{\frac{V}{\pi L}}$ here V is the soil volume [cm^3] and $\psi = \psi_b$.

The soil hydraulic conductivity k_{soil} [cm s^{-1}] is parameterized using Brooks and Corey model (Brooks and Corey, 1964):

$$k_{soil}(\psi) = k_{sat}\left(\frac{\psi}{\psi_o}\right)^{\tau} \tag{2}$$

where k_{sat} is the soil saturated hydraulic conductivity [cm s^{-1}], τ is a fitting parameter [-], ψ_o is the soil air entry value [hPa^{-1}].

Equation (1) is linearized following (van Lier et al., 2006; Schröder et al., 2007), who assumed a steady-rate behavior and used the matric flux potential [cm^2 s^{-1}]:

$$\Phi(\psi) = \int_{-\infty}^{\psi} k(x)dx \tag{3}$$

Following this approach, we obtain:

$$\Phi_{r,s} = -\frac{T}{2\pi r_0 L}\left(\frac{r_0}{2} - r_0 r_b^2 \frac{ln(r_b/r_0)}{r_b^2 - r_0^2}\right) + \Phi_b \tag{4}$$

where Φ_b is obtained from inserting ψ_b in Eq. (2–3). Inverting Eq. 3 and using the parameterization of Eq. 2, from $\Phi_{r,s}$ (Eq. 4) we obtain $\psi_{r,s}$.

Knowing the transpiration rate and the plant hydraulic conductance, K_{plant} [cm^3 hPa^{-1} s^{-1}], the dissipation of water potential within the plant is calculated as:

$$T = K_{plant}\left(\psi_{leaf,x} - \psi_{r,s}\right) \tag{5}$$

where $\psi_{leaf,x}$ is the water potential in the leaf xylem [hPa].

In this model, we assumed that: 1) the total length of the roots taking up water is L; 2) all the roots take up water at similar rate; 3) the soil water potential is at at distance r_b from the root center is equal for all roots; 4) there is no cavitation in the xylem. The last assumption is justified by the fact that during the measurements the plant was maintained pressurized and water in the leaf xylem was at atmospheric pressure. The illustration of these parameters is shown in **Figure S2**.

The model allows to calculate the leaf water potential ψ_{leaf} for varying soil water potential ψ_b and transpiration rates T. The model requires the parameters K_{plant}, L, r_b, r_0 and the function k_{soil} (ψ) (Eq. 2). k_{soil} (ψ) was measured and parameterized independently (**Figure S3**). The root radius r_0 was set to 0.05 cm. r_b is calculated as $r_b = \sqrt{\frac{V}{\pi L}}$. The independent parameters were K_{plant} and L and were adjusted to best reproduce the measured balancing pressure P [hPa] for the different transpiration rates and soil water potentials.

The root pressure chamber is numerically equal to minus of the leaf water potential:

$$P = -\psi_{leaf,x} \tag{6}$$

assuming that gradients in osmotic potential are negligible. Additionally, the root length was independently measured using WinRhizo and then compared to the fitted L.

STATISTICAL ANALYSIS

The effects of soil water content, light intensity, pressurization, and the interactions between them on transpiration were analysed using *N*-way analysis of variance (ANOVA) followed by Tukey-Kramer multiple comparison tests. In all cases, $p < 0.05$ was taken as the lowest level of significance. Matlab (**9.5.0**) and the corresponding statistic packages were used to perform all the statistical analysis.

RESULTS

The soil water retention and unsaturated conductivity curves obtained by fitting the evaporation method are shown in **Figure S3A**. The fitting parameters of the water retention curve were further used to estimate the soil hydraulic conductivity using Brooks and Corey parameterization (Brooks and Corey, 1964) (**Figure S3B**).

The soil water content profiles were measured by the TDR in all replications that are shown in **Figure 1**. The measurements showed that the distribution of water content was relatively homogeneous throughout the soil profile.

We calibrated the sap flow sensors using the gravimetric measurements (**Figure S4**). The transpiration rate measured by sap flow was linearly related to the gravimetric measurements. We repeated the calibration for each measurement (e.g., for each water content and for each sample).

The effect of pressurization and light intensity on averaged transpiration rates (measured with sap flow sensors) with and without pressurization at each water content are shown in **Figure 2**. In general, we observed a slightly higher transpiration rate when the plants were pressurized. This indicates that when plants were pressurized and water in the leaf xylem was at atmospheric pressure, the stomata were more open. However, as long as the soil was wet or the light intensity was low, transpiration rate increased with increasing light intensity under both, pressurized and not pressurized conditions. In contrast, in dry soil (WC = 9.33%) under not pressurized conditions transpiration dropped significantly ($p < 0.05$, Tukey-Kramer test) at high photosynthetic photon intensity (at 2000 μmol m^{-2} s^{-1}) (**Figure 2C**). At the tested soil moistures, pressurization prevented stomatal closure at all soil moistures. **Figure 2E** shows a linear response of transpiration to increasing light intensity and the increase in transpiration was even more marked in dry soil (**Figure 2E**).

We tested the statistical significance of the effect of different factors (i.e., pressurization, soil water content and light intensity) and the interaction on transpiration rate by ANOVA (see **Supplementary Material Table S1**). Transpiration rate was significantly influenced by light intensity and pressurization. The effect of pressurization interacted with that of light intensity on transpiration rate. This implies that for different light intensities the impact of pressurization was different. Soil water content and its interaction with other two factors did not show significant impact, which was possibly because of limited measurements at low soil moistures.

The comprehensive data sets of transpiration rates, measured xylem tension, and the model fitting for different water contents for replication 1 are shown in **Figure 3**. Dots are transpiration rates and leaf water potential measured when plants were pressurized for four imposed photosynthetic photon intensities (550, 1,000, 1,600, and 2,200 μmol m^{-2} s^{-1} marked as 1–4). The solid lines are the fitting of the model. In wet soil (WC = 24.7%),

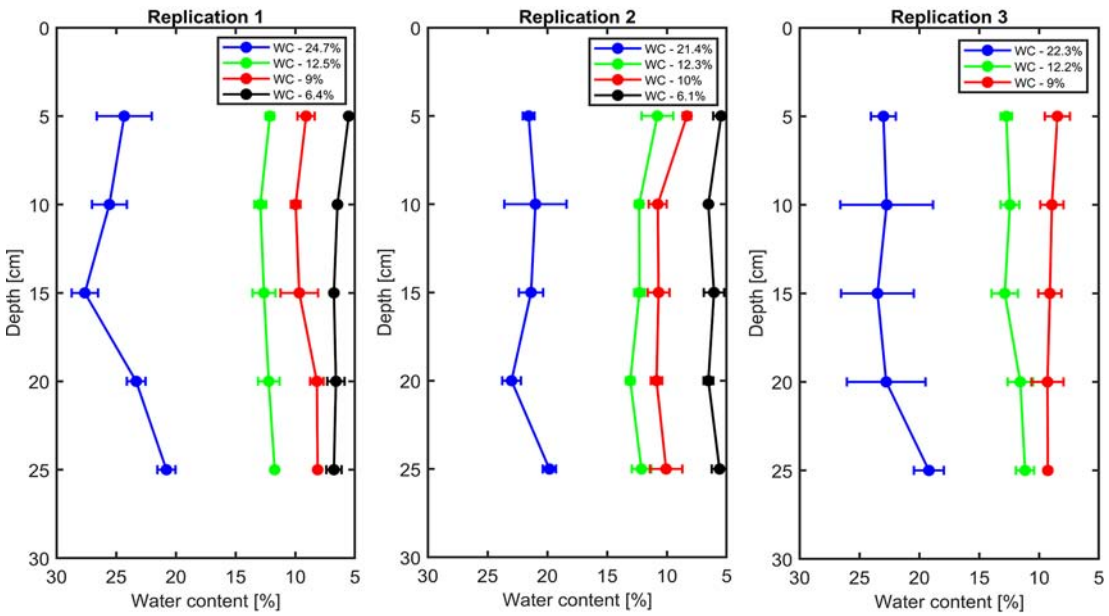

FIGURE 1 | Vertical profiles of volumetric soil water content in each replication.

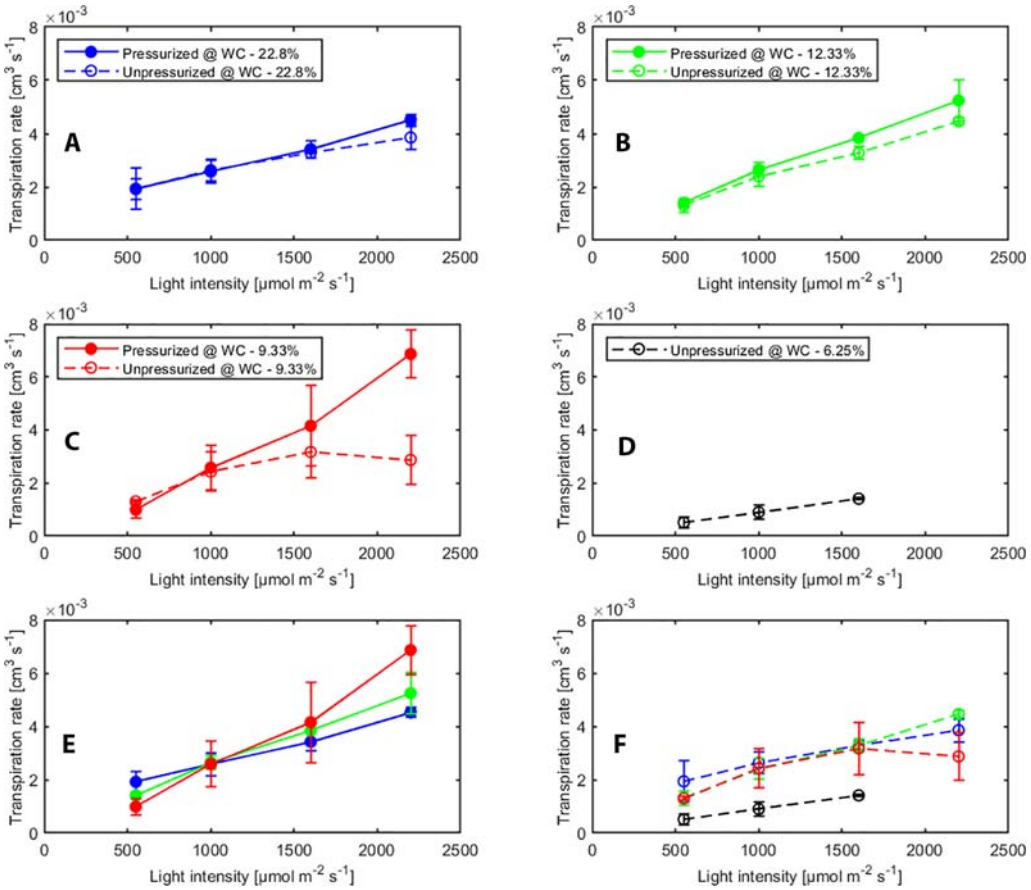

FIGURE 2 | Effect of light intensity and pressurization on transpiration rates for varying soil water contents. **(A–D)** Effect of pressurization on transpiration. **(E)** Effect of light intensity and soil moisture on transpiration in pressurized and **(F)** unpressurized plants.

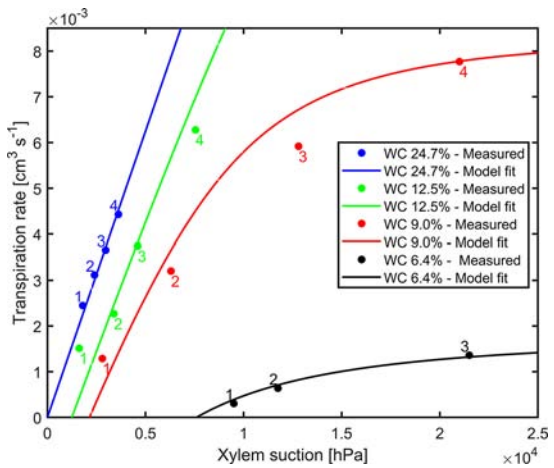

FIGURE 3 | Measured xylem suction and transpiration rate for decreasing water contents (WC) and increasing light intensity (1–4) for replicate 1 (2 and 3 are shown as **Supplementary Material**). The solid lines are the model fits.

the relationship between transpiration rate and xylem tension was linear. As the soil dried (WC = 12.5%, 9% and 6.4%), this relationship became nonlinear at increasing transpiration rates. The slope of linear part of the curve at high water content (at WC = 24.7%) is interpreted as the plant conductance, K_{plant} (i.e., soil resistance is assumed to be negligible). This conductance was used in the simulations. For high water content, the conductance K_{plant} (at WC = 24.7%) was 1.25×10^{-6} [cm^3 hPa^{-1} s^{-1}]. The total soil-plant conductance reduced dramatically in dry soils at high transpiration rates due to the drop of soil hydraulic conductivity around the roots, which is well reproduced by the soil hydraulic model. The relation between transpiration rates, measured xylem tension, and the model fitting for different water contents for replication 2 & 3 are shown in **Supplementary Material** (**Figure S5**). Conductance of the root system, active root length used in the model, and coefficient of correlation for each replication are shown in **Table 1**.

The effect of light intensity and water content on normalized soil-plant conductance k^* is shown in **Figure 4**. The k^* value is the ratio of soil-plant conductance to the maximum conductance measured in wet soil and low light intensity. In general, soil water

TABLE 1 | The conductance of soil-root system, active root length optimized for the model and R^2 in each replication.

Replication	K_{plant}	L	R^2
	[cm^3 hPa^{-1} s^{-1}]	[cm]	
1	1.25×10^{-6}	700	0.9808
2	1.05×10^{-6}	200	0.3518
3	5.63×10^{-5}	350	0.8991

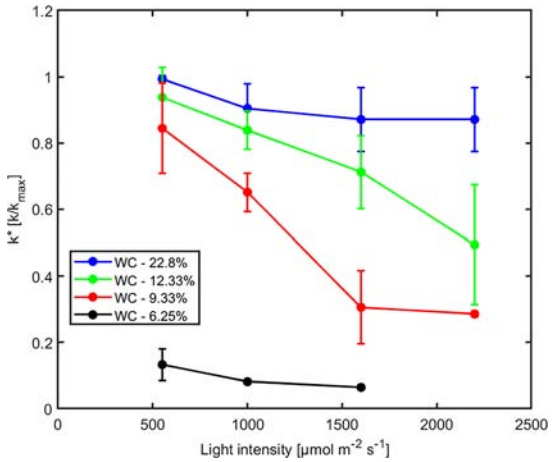

FIGURE 4 | Effect of light intensity on normalized soil-plant conductance $k^* = k/k_{max}$ (where k_{max} is the soil-plant conductance in the wettest soil and lowest light intensity) at varying soil water contents (WC). Relative soil-plant conductance k* decreased with increasing light intensity due to higher transpiration rates and with decreasing soil water contents due to the decreasing soil hydraulic conductivity.

content and light intensity and their interaction affected k^* extremely significantly ($p < 0.01$, **Table S2**). k^* is approximately constant in wet soil at each imposed light intensity. In drier soil (WC = 12.33% and 9.33%), k^* reduced with increasing light intensity. The reduction was extremely significant ($p < 0.01$, Tukey-Kramer test) at WC = 9.33% where it occurred at light intensity of ca. 1,500–2,000 µmol m^{-2} s^{-1}. At WC = 12.33% the drop was only significant ($p < 0.05$, Tukey-Kramer test) at light intensity above 2,000 µmol m^{-2} s^{-1}. Note that these were the conditions when transpiration was reduced in the unpressurized plants (**Figures 2B, C**). The relationship between P_0 [hPa] (intercept of xylem pressure and transpiration rate) and minus the soil matric potential [hPa] is plotted in **Figure 5**. In principle, these values should fit unless there was a large osmotic gradient between the xylem and the soil. In dry soil, the values fitted rather well (consider that the estimation of the soil matric potential based on water retention curve are prone to errors in the dry range). In wet soil, (i.e., WC between 21.4% and 24.7%), the soil matric potential was slightly more negative than the fitted P_0, which indicates a more positive pressure in the xylem than in the soil, possibly caused by a more negative osmotic potential in the xylem than in the soil. The difference of ca. 50 –100 hPa is not detectable at more negative soil water potential (as explained in the note above).

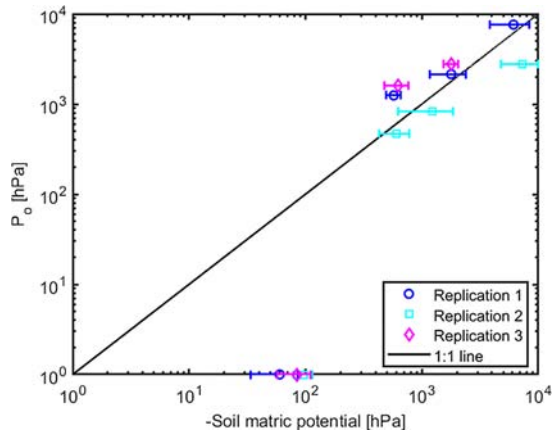

FIGURE 5 | The relation between intercept (Po) and the soil matric potential. The points below (above) the 1:1 line indicate a more negative (positive) osmotic potential in the leaf xylem than in the soil.

DISCUSSION AND CONCLUSIONS

We measured the relationship between leaf water potential and transpiration rates in maize at various soil water contents and light intensity. From this relationship, we estimated the soil-plant hydraulic conductance and its decrease with increasing transpiration rates and decreasing soil moistures. In parallel, we have measured the transpiration rates (for unpressurized plants). We have found that reductions in transpiration occurred in correspondence to reductions in soil-plant hydraulic conductance, which were caused by the loss of soil hydraulic conductivity around roots.

Pressurization increased the transpiration rates almost at all soil water contents and each imposed light intensity (see **Figure 2**). However, this effect was particularly visible only in dry soil conditions and high light intensity. At WC = 9.33% and high light intensity (2,200 µmol m^{-2} s^{-1}) pressurization increased transpiration by a factor of 3 (**Figure 2C**) compared to unpressurized plants. At this condition, the leaf potential would have been around −2.1 MPa if the plant had not been pressurized (**Figure 3**) and the relationship between leaf water potential and transpiration rate would have been extremely nonlinear (**Figure 3**, red line, point 4). At low soil water content and high light intensity the soil-plant hydraulic conductance was significantly reduced. Interestingly, the soil-plant hydraulic conductance was already reduced in wetter soil (WC = 12.33%) and at lower light intensity (WC = 9.33%, LI ≈ 1600 µmol m^{-2} s^{-1}). This suggests that the drop in hydraulic conductance anticipated (and possibly triggered) the reduction in transpiration. It also shows that stomatal regulation (prevented in the pressurized plants) occurred when the soil-plant hydraulic conductance decreased.

The relationship between leaf xylem tension and transpiration rate (under pressure) was linear in wet soils and became nonlinear at drier soil conditions and increasing transpiration rates (**Figure 3**). The nonlinearity in this

relationship corresponds to a decrease in soil-plant conductance shown in **Figure 4**. This finding is consistent with previous measurements with barley (*Hordeum vulgare*) (Carminati et al., 2017) and wheat (*Triticum*) (Passioura, 1980), and fits well with early model of root water uptake (Gardner and Ehlig, 1963).

The soil-root hydraulics model was capable to reproduce the measured relationship between xylem tension and transpiration rate. The only unknown parameters of the model were: 1) the plant conductance K_{plant}, equal to the inverse of the slope of the xylem suction versus transpiration rate at high WC; and 2) the active root length L, which is the effective length of the roots actually taking up water, and which determines the onset of nonlinearity in the curves. The best fits were obtained with L = 200, 350, and 700 cm. Note that the measured total root length was much higher in the order of ca. 30,000 cm. The active root length thus only represented 0.7%–2.5% of the total root length. In reality, all roots might take up water, but at variable rates. For instance, Ahmed et al. (2018) showed that in mature maize most of the water uptake are taken up by crown roots were seminal roots and their lateral had a minor contribution to root water uptake. In addition, L might compensate experimental errors in measuring the soil conductivity or in assuming that soil and rhizosphere hydraulic properties are similar. Therefore, these values are fitting parameters and they should be cautiously interpreted.

Note also that active root length and root conductance are physically linked to each other, i.e., the longer the root, the larger its interface to soil and the bigger its conductance. These two variables were treated as independent in this study but this could be further investigated using allometric relations (Meunier et al., 2017; Meunier et al., 2018).

The relation of estimated plant hydraulic conductivity and imposed matric potential for each replication showed that the soil-plant hydraulic conductance was constant in the wet soil and that the drop in soil-plant hydraulic conductance observed at increasing transpiration rate and decreasing soil water content were well explained by the loss of soil hydraulic conductivity around the roots taking up water. Due to pressurization, xylem cavitation was likely to be prevented during the measurements and thus the decrease in conductivity was caused by soil drying.

In conclusion, we have shown that stomatal regulation reduces transpiration when soil-plant hydraulic conductance drops, preventing marked nonlinearities in the relationship between leaf water potential and transpiration rate, as hypothesized in Sperry and Love (2015). Soil-plant hydraulic conductance decreased at high transpiration rates and low soil water contents, as predicted by hydraulic models (Sperry et al., 1998). This result provides novel experimental evidence supporting the use of soil-plant hydraulic models to predict stomatal response to soil drying. Compared to studies focusing on xylem vulnerability (e.g., Anderegg et al., 2017), here we focused on soil drying as the cause of hydraulic limitation. Contrary to Anderegg et al. (2017), who found that stomata close much before the xylem cavitates, we found that stomata close when the soil hydraulic conductivity dropped. It means that for the tested maize in the silt-sand mixture, loss of soil hydraulic conductivity is the primary constraint to transpiration.

DATA AVAILABILITY STATEMENT

All datasets generated for this study are included in the article/ **Supplementary Material**.

AUTHOR CONTRIBUTIONS

FH carried out the experiments and drafted the manuscript. MAA and AC participated in the design of the experimental setup and results evaluation. MZ and MJ helped in simulation of data. GC contributed in revision and performing statistical analysis. MZ and MJ helped in simulation of data.

FUNDING

FH was funded by the Ministry of Higher Education Commission, Pakistan under contract No. 50015636. GC was funded by BMBF, project 02WIL1489 (Deutsche Israelische Wassertechnologie Kooperation). The authors acknowledge the Deutsche Forschungsgemeinschaft (DFG, German Research Foundation) for funding of the priority program 2089, project numbers 403670197 "Emerging effects of root hairs and mucilage on plant scale soil water relations" to MAA, MJ and AC.

ACKNOWLEDGMENT

We thank Andreas Kolb (University of Bayreuth) for his precious technical support.

SUPPLEMENTARY MATERIAL

The Supplementary Material for this article can be found online at: https://www.frontiersin.org/articles/10.3389/fpls.2019.01695/full#supplementary-material

FIGURE S1 | **(A)** Transpiration measurements using the sap flow sensor and balance; **(B)** plant in the pressure chamber with sap flow sensor connected; **(C)** water bleeding from the cut leaf.

FIGURE S2 | Schematic of the model used for simulation of leaf water potential. Here, ψ_b, $\psi_{r,s}$ and $\psi_{leaf,x}$ are the matric flux potential in the bulk soil, soil-root interface and in leaf xylem, respectively.

FIGURE S3 | Brooks and Corey parameterization of hydraulic properties of soil: **(A)** fitted soil water retention curve, **(B)** fitted hydraulic conductivity curve. The dots show water the potential and the hydraulic conductivity of soil at different measured water contents for each replication.

FIGURE S4 | Calibration of transpiration rates measured by sap flow with gravimetric measurements.

FIGURE S5 | Measured xylem suction and transpiration rate for replication 2 & 3.

TABLE S1 | The analysis of variance (N-way ANOVA) for the influence of different factors on transpiration rate ($P < 0.001$***, $P < 0.01$**, $P < 0.05$*).

TABLE S2 | The analysis of variance (N-way ANOVA) for the influence of different factors on k* ($P < 0.001$***, $P < 0.01$**, $P < 0.05$*).

REFERENCES

Ahmed, M.A., Zarebanadkouki, M., Meunier, F., Javaux, M., Kaestner, A., and Carminati, A. (2018). Root type matters: measurement of water uptake by seminal, crown, and lateral roots in maize. *J. Exp. Bot.* 69, 1199–1206. doi: 10.1093/jxb/erx439

Anderegg, W. R. L., Wolf, A., Arango-Velez, A., Choat, B., Chmura, D. J., Jansen, S., et al. (2017). Plant water potential improves prediction of empirical stomatal models. *PloS One* 12, 1–17. doi: 10.1371/journal.pone.0185481

Bates, L. M., Hall, A. E., and Sciences, P. (1981). Stomatal closure with soil water depletion not associated with changes in bulk leaf water status. *Oecologia* 50, 62–65. doi: 10.1007/BF00378794

Brodribb, T. J., and McAdam, S. A. M. (2017). Evolution of the stomatal regulation of plant water content. *Plant Physiol.* 174, 639–649. doi: 10.1104/pp.17.00078

Brooks, R. H., and Corey, A. T. (1964). *Hydraulic properties of porous media* (USA: Color. State Univ. Hydrol. Pap. Collins). https://doi.org/citeulike-article-id:711012

Buckley, T. N. (2017). Modeling stomatal conductance. *Plant Physiol.* 174, 572–582. doi: 10.1104/pp.16.01772

Carminati, A., Moradi, A. B., Vetterlein, D., Vontobel, P., Lehmann, E., Weller, U., et al. (2010). Dynamics of soil water content in the rhizosphere. *Plant Soil* 332, 163–176. doi: 10.1007/s11104-010-0283-8

Carminati, A., Vetterlein, D., Koebernick, N., Blaser, S., Weller, U., and Vogel, H. J. (2013). Do roots mind the gap? *Plant Soil* 367, 651–661. doi: 10.1007/s11104-012-1496-9

Carminati, A., Passioura, J. B., Zarebanadkouki, M., Ahmed, M. A., Ryan, P. R., Watt, M., et al. (2017). Root hairs enable high transpiration rates in drying soils. *New Phytol.* 216, 771–781. doi: 10.1111/nph.14715

Carter, J. N., Jensen, M. E., and Traveller, D. J. (1980). Effect of mid- and late-season water stress on sugarbeet growth and yield. *Agron. J.* 72, 806–815. doi: 10.2134/agronj1980.00021962007200050028x

Chaumont, F., and Tyerman, S. D. (2014). Aquaporins: highly regulated channels controlling plant water relations. *Plant Physiol.* 164, 1600–1618. doi: 10.1104/pp.113.233791

Comstock, J. P. (2002). Hydraulic and chemical signalling in the control of stomatal conductance and transpiration. *J. Exp. Bot.* 53, 195–200. doi: 10.1093/jexbot/53.367.195

Cowan, I. R. (1965). Transport of water in the soil-plant-atmosphere system. *J. Appl. Ecol.* 2, 221–239. doi: 10.2307/2401706

Draye, X., Kim, Y., Lobet, G., and Javaux, M. (2010). Model-assisted integration of physiological and environmental constraints affecting the dynamic and spatial patterns of root water uptake from soils. *J. Exp. Bot.* 61, 2145–2155. doi: 10.1093/jxb/erq077

Ehlert, C., Maurel, C., Tardieu, F., and Simonneau, T. (2009). Aquaporin-mediated reduction in maize root hydraulic conductivity impacts cell turgor and leaf elongation even without changing transpiration. *Plant Physiol.* 150, 1093–1104. doi: 10.1104/pp.108.131458

Gardner, W. R., and Ehlig, C. F. (1963). The influence of soil water on transpiration by plants. *J. Geophys. Res.* 68, 5719–5724. doi: 10.1029/JZ068i020p05719

Gardner, W. R. (1960). Dynamic aspects of water availability to plants. *Soil Sci.* 89 (2) 63–73 doi: 10.1097/00010694-196002000-00001

Hayat, F., Ahmed, M. A., Zarebanadkouki, M., Cai, G., and Carminati, A. (2018). Measurements and simulation of leaf xylem water potential and root water uptake in heterogeneous soil water contents. *Adv. Water Resour.* 124, 96–105. doi: 10.1016/J.ADVWATRES.2018.12.009

Knipfer, T., Besse, M., Verdeil, J. L., and Fricke, W. (2011). Aquaporin-facilitated water uptake in barley (Hordeum vulgare L.) roots. *J. Exp. Bot.* 62, 4115–4126. doi: 10.1093/jxb/err075

Mencuccini, M., Manzoni, S., and Christoffersen, B. (2019). Modelling water fluxes in plants: from tissues to biosphere. *New Phytol.* 222, 1207–1222. doi: 10.1111/nph.15681

Meunier, F., Couvreur, V., Draye, X., Vanderborght, J., and Javaux, M. (2017). Towards quantitative root hydraulic phenotyping : novel mathematical functions to calculate plant-scale hydraulic parameters from root system functional and structural traits. *J. Math. Biol.* 75, 1133–1170. doi: 10.1007/s00285-017-1111-z

Meunier, F., Zarebanadkouki, M., Ahmed, M. A., Carminati, A., Couvreur, V., and Javaux, M. (2018). Hydraulic conductivity of soil-grown lupine and maize unbranched roots and maize root-shoot junctions. *J. Plant Physiol.* 227, 31–44. doi: 10.1016/j.jplph.2017.12.019

Meyer, W. S., and Green, G. C. (1980). Water use by wheat and plant indicators of available soil water1. *Agron. J.* 72, 253–257. doi: 10.2134/agronj1980.00021962007200020002x

Passioura, J. B. (1980). The transport of water from soil to shoot in wheat seedlings. *J. Exp. Bot.* 31, 333–345. doi: 10.1093/jxb/31.1.333

Peters, A., and Durner, W. (2008). Simplified evaporation method for determining soil hydraulic properties. *J. Hydrol.* 356, 147–162. doi: 10.1016/j.jhydrol.2008.04.016

Pickard, W. F. (1981). The ascent of sap in plants. *Prog. Biophys. Mol. Biol.* 37, 181–229. doi: 10.1016/0079-6107(82)90023-2

Redondo, E., Hachez, C., Parent, B., Tardieu, F., Chaumont, F., and Simonneau, T. (2009). Drought and abscisic acid effects on aquaporin content translate into changes in hydraulic conductivity and leaf growth rate: a trans-scale approach. *Plant Physiol.* 149, 2000–2012. doi: 10.1104/pp.108.130682

Schindler, U., Durner, W., Unold, G. V., Mueller, L., and Wieland, R. (2010). The evaporation method : extending the measurement range of soil hydraulic properties using the air-entry pressure of the ceramic cup. *J. Plant Nutr. Soil Sci.* 173, 563–572. doi: 10.1002/jpln.200900201

Schröder, T., Javaux, M., Vanderborght, J., and Vereecken, H. (2007). Comment on "Root water extraction and limiting soil hydraulic conditions estimated by numerical simulation". *Vadose Zone J.* 6, 524–526. doi: 10.2136/vzj2007.0042l

Simonneau, T., Ehlert, C., Maurel, C., and Tardieu, F. (2009). Integrated control of leaf growth by cell turgor in response to combinations of evaporative demands and aquaporin-mediated reductions in root hydraulic conductivity. *Comp. Biochem. Physiol. Part A Mol. Integr. Physiol.* 153A, S228. doi: 10.1016/j.cbpa.2009.04.572

Sinclair, T. R., Holbrook, N. M., and Zwieniecki, M. A. (2005). Daily transpiration rates of woody species on drying soil. *Tree Physiol.* 25, 1469–1472. doi: 10.1093/treephys/25.111469

Sperry, J. S., and Love, D. M. (2015). What plant hydraulics can tell us about responses to climate-change droughts. *New Phytol.* 207, 14–27. doi: 10.1111/j.1469-8137.2010.03195.x

Sperry, J. S., Adler, F. R., Campbell, G. S., and Comstock, J. P. (1998). Limitation of plant water use by rhizosphere and xylem conductance: results from a model. *Plant Cell Environ.* 21, 347–359. doi: 10.1046/j.1365-3040.1998.00287.x

Sperry, J. S., Wang, Y., Wolfe, B. T., Mackay, D. S., Anderegg, W. R. L., Mcdowell, N. G., et al. (2016). Pragmatic hydraulic theory predicts stomatal responses to climatic water deficits. *New Phytol.* 212, 577–589. doi: 10.1111/nph.14059

Tardieu, F., and Davies, W. J. (1993). Integration of hydraulic and chemical signalling in the control of stomatal conductance and water status of droughted plants. *Plant Cell Environ.* 16, 341–349. doi: 10.1111/j.1365-3040.1993.tb00880.x

van Lier, Q., de, J., Metselaar, K., and van Dam, J. C. (2006). Root water extraction and limiting soil hydraulic conditions estimated by numerical simulation. *Vadose Zone J.* 5, 1264–1277. doi: 10.2136/vzj20060056

Van Lier, Q. D. J., Van Dam, J. C., Metselaar, K., De Jong, R., and Duijnisveld, W. H. M. (2008). Macroscopic root water uptake distribution using a matric flux potential approach. *Vadose Zone J.* 7, 1065–1078. doi: 10.2136/vzj20070083

Conflict of Interest: The authors declare that the research was conducted in the absence of any commercial or financial relationships that could be construed as a potential conflict of interest.

frontiers in Plant Science

OPINION
published: 03 February 2020
doi: 10.3389/fpls.2019.01742

Blind Spots in Water Management, and How Natural Sciences Could Be Much More Relevant

Ignacio Cazcarro[1,2]* *and Jorge Bielsa*[2]

[1] Fundacion Agencia Aragonesa para la Investigacion y el Desarrollo (ARAID), Zaragoza, Spain, [2] Department of Economic Analysis, Faculty of Economics and Business Studies, Agrifood Institute of Aragon (IA2), Zaragoza, Spain

Keywords: plant water use and dynamics, water cycle and balance, water footprint, socioeconomic analysis, economic and political ecology

OPEN ACCESS

Edited by:
Maren Dubbert,
University of Freiburg, Germany

Reviewed by:
Maite M. Aldaya,
Observatorio del Agua, Fundación Botín, Spain

***Correspondence:**
Ignacio Cazcarro
icazcarr@unizar.es

Specialty section:
This article was submitted to Technical Advances in Plant Science, a section of the journal Frontiers in Plant Science

Received: *31 October 2019*
Accepted: *11 December 2019*
Published: *03 February 2020*

Citation:
Cazcarro I and Bielsa J (2020) Blind Spots in Water Management, and How Natural Sciences Could Be Much More Relevant. Front. Plant Sci. 10:1742. doi: 10.3389/fpls.2019.01742

INTRODUCTION

Estimates of crop evapotranspiration (ET) to measure the freshwater use indicator water footprint (WF) have undoubtedly been popular and implemented (Chapagain and Hoekstra, 2004), as well as the more recent extension to subnational regions and watersheds (Mekonnen and Hoekstra, 2010a; Hoekstra and Mekonnen, 2012; Mekonnen and Hoekstra, 2012). As reviewed by (Chenoweth et al., 2014; Lovarelli et al., 2016), these studies have gone from estimating products' water trade on a global scale, to rigorous quantification for specific crops and geographical areas. Many studies have extended the coverage and precision of estimates. However, when it comes to the implementation of these improvements in local and river-basin water management, we find management problems that are ultimately unaddressed. It is here that, in our opinion, the Plant Water Sciences (PWS) have to shed light on these "blind spots." We also illustrate these general ideas with two examples.

Blind Spots in Recent Literature on Water Footprint: Fields for Future Research, Especially for Plant Water Sciences

Firstly, defining boundaries on what to account for human appropriation is a multidisciplinary and, to this point, open debate regarding WF calculations. Launiainen et al. (2014) questioned WF's appropriateness for evaluating the water use in forestry and forest-based production. They pleaded for the exclusion of rain-fed forestry and forest-based production in WF, arguing that managed forest ET is indistinguishable from those of unmanaged forests. At a global level, there were case studies on some forest products such as paper WF (van Oel and Hoekstra, 2012), but these were not as systematic as those for crops and livestock WF. Nevertheless, we do need a clear split between both human and natural water usage in order to manage existing water resources.

Secondly, to further improve estimates, we find areas where WF can benefit from more precise studies of plant water ET and dynamics. Recent studies (Schyns et al., 2017; Schyns and Vanham, 2019) have estimated the WF (of production) of wood for lumber, pulp, paper, fuel, and firewood, but more can be done to calculate the WF on the consumer side, computing the responsibility of the demand (typically households/individuals) in the WF. Regarding livestock WF, the challenges involve discerning dry matter composition (concentrates/roughages). Furthermore, WF would probably benefit from updated estimates on roughages ET/WF, especially pasture/grass (estimated and briefly explained in Mekonnen and Hoekstra, 2010a). The relation and distinction of

evaporation (E) to transpiration (T), absent in many studies until very recently, is very important from an economic perspective since T is *productive* and E is not (E can occur from soil but also from intercepted water on leaves). Recently, Nouri et al. (2019) found that mulching reduced irrigation needs by 3.6%, and when combined with drip irrigation, by 4.7%. There is thus an important need for studies on "partitioning" of ET and T (see review in Kool et al., 2014).

Thirdly, while there have been great advances in developing spatial and temporally explicit information, there is a divergence between the geographic and temporal units used by natural scientists and those used by social scientists for resource management (typically, river basins and long periods of time). If plant sciences do not provide information for the geographic areas in which decisions are taken, their work will be overlooked by social scientists. Regarding the temporal dimension, there are a lack of studies looking beyond a point in time (even when the evaluations of evapotranspiration are averaged over periods of time), and looking at the effects derived from land use and cover changes. In other words, studies looking at the dynamics of the resource rather than a static picture are needed. In summary, very detailed and methodical studies from the natural sciences coexist with rough approximations and simulations of data, such as those used by hydro-economic models (see for example Harou et al., 2009; Kahil et al., 2018 for a review of this form of work).

Fourthly, there are also blind spots regarding the estimation of historical WF time series. Historic economic analyses on water consumption usually rely on multiple sources of information: censuses, statistics on climate, precipitation, irrigation systems, agricultural production, yield, inputs used, water uses, etc. Information on crop water consumption (in m^3 per unit of production) was also used in the past, relating it to scarcity and sustainability. How do we estimate the evolution of these coefficients over time? The answer likely lies in developing a methodology that allows us to obtain them from data on changes in irrigation systems, yields, harvest indexes, soils, etc. Dalin et al. (2012) and Duarte et al. (2014) initiated attempts to generalize coefficient changes over time based on yield changes. There is room for improvement in these estimates, e.g., incorporating not only the effect of changes in yield (as crop output per unit area), but also the changes in the harvest index (the ratio of grain yield to biomass when the crop matures), notably being increased (greater part of the biomass allocated to the grain) in many countries with the Green Revolution.

Some Ideas on How to Improve Relevance in Practical Water Management

As happened previously with the concept of Integrated Water Resources Management (IWRM), a vast literature and discussion of a topic does not directly entail practical utility. One step further is needed. We cannot expect one indicator to be able to resolve everything, but we can provide additional data to complement it (e.g., Vanham et al., 2016, investigated whether the WF indicator addresses the food–energy–water ecosystem nexus, finding potential components to be included). Lund (2015) correctly highlighted that water management has always required not only physical sciences, but also social ones. Indeed, natural sciences have often not counted so much as it should on water management practices.

The present and future of the world's food requirements and water needs have already been at the forefront since studies like those of Rockström et al. (1999). Greater water needs could lead to decisions that affect nature in the future. Derived from this, some researchers have tried to combine policy recommendations that take into account the management of local and global, acknowledging interrelations, especially between use and scarcity through trade (see Vörösmarty et al., 2015). However, the apparent remoteness of some phenomena (indirect chains of impacts) and the absence of monetary valuations beyond their relationship with agricultural production, have impeded their prominence in practice.

For the most part, economists' contributions to the virtual water (VW) and WF literature have not been as comprehensive as it should either. These contributions have focused on: a) computing VW and WF through economic tools such as multi-regional input-output tables and models (Duarte and Yang, 2011; Tian et al., 2018); b) criticize or highlight limitations on the concept of VW based on the theory of comparative advantage (Wichelns, 2011; Gawel, 2014; Mateo-Sagasta et al., 2015; Wichelns, 2015); c) defend it or further explain factors completing the picture (Gawel, 2014; Afkhami et al., 2018; Zhao et al., 2019); and d) relate WF with scarcity and profitability, to obtain a visible 'water productivity' (Garrido et al., 2010; Cazcarro et al., 2019).

However, although most of these latest studies are focused on trying to reflect the shortage and opportunity costs, the recommendations of Lowe et al. (2018) for incorporating environmental valuation are necessary because it has not really been done. Along these lines, we extend this argument by stating that, in general, both economic valuations have not dealt with WF and economic analysis has not served to make WF socially relevant, which is a very desirable goal.

Therefore, we propose to go beyond the recommendations of Lowe et al. (2018), arguing that the economic valuation of water should also be based on measurements of WF, their scarcity, and the equivalence of their opportunity costs when regarding alternative uses or environmental costs generated.

There are other ways of making economic valuations of water, such as the literature of environmental valuation and that of ecosystem services (Martin-Ortega et al., 2015; Liu et al., 2016). The literature of hydro-economic models (HE) also pursues that goal (e.g., Escriva-Bou et al., 2018; Kahil et al., 2018).

We also emphasize the importance of working together with HE (more biophysical) models, and of incorporating broader perspectives and tools (political, economic, and social ecology). For example, Hellegers and van Halsema (2019) argue that valuation is very useful for decision-making and that it must go beyond economics. We also have examples of more social assessments (Rodríguez-Labajos and Martínez-Alier, 2015; Wright-Contreras, 2018) and more in the realm of ecological economics (Kallis et al., 2013; Gómez-Baggethun and Martín-López, 2015). All this literature

TABLE 1 | Selected review of literature on water footprint (WF) notably related to plant water sciences (PWS) and dynamics, and key gaps for water management (WM).

Study/ies (physical)	Class and methods	Advances	Gaps or aspects not covered	Relevance for PWS and dynamics
(Mekonnen and Hoekstra, 2010a; Mekonnen and Hoekstra, 2010b; Hoekstra and Mekonnen, 2012; Mekonnen and Hoekstra, 2012)	ET, VW, and WF computation	WF of crop and livestock products.	Temporal dimension other than averages of a period (TDOTAOAP). Rough results on grasslands WFs.	Need of PWS to compute other temporal dimensions and grasslands WFs
(Liu et al., 2016) (Mekonnen & Hoekstra, 2010b)	VW and WF computation, notably of gray WF.	Gray WF computation making 1st assumptions on leaching and run-off of nitrogen fertilizers.	TDOTAOAP. Lack of other pollutant than N. Lack of sensitivity analyses on key assumptions	Need of PWS to test sensitivity to some fixed assumptions on leaching and run-off.
(Schyns et al., 2015)	Review and classification of indicators of green water availability and scarcity.	Advances on defining and measuring green water scarcity.	Choosing and making operational the green water scarcity indicators discussed.	Need of PWS to determine which part of the green water flow is productive.
(Schyns et al., 2017; Schyns & Vanham, 2019)	ET, VW, and WF computation, notably of forestry products WF.	WF of forest products.	TDOTAOAP. Full accounting by more detailed tree types and locations.	Need of PWS to obtain results more detailed tree types and locations.
(Shtull-Trauring et al., 2016)	Combination of high resolution WFs with GIS to analyze impacts of different factors.	Finds insufficient classic WF yield parameter (m^3/ton) alone to compare different crops; and strong impact in gray WF of the water quality standards used.	TDOTAOAP. Lack of wider picture of the full social benefit and costs.	An example to follow. Great attempt of linking and making useful PWS for WM at relevant scales.
(Nouri et al., 2019)	E and T distinction	E and T distinction, introducing the effect of mulching on WF.	Lack of study of the feasibility and practicality of the strategies proposed.	Shows the relevance of this distinction for WF studies (e.g., water-saving effect of mulching and drip irrigation).
Study/ies (economics)	**Class and methods**	**Advances**	**Gaps or aspects not covered**	**Relevance for PWS and dynamics**
(Wichelns, 2011; Mateo-Sagasta et al., 2015; Wichelns, 2015)	Critiques to WF related to comparative advantage	Some fair critiques to WF related to comparative advantage.	Full understanding of the searched goals with VW and WF, and the implications of comparative advantage	Show a wider picture of how PWS results feed and are fundamental for WF and derived global and comprehensive studies: water content of consumption, effects and scenarios from different diets, population projections, etc.
(Daniels et al., 2011; Duarte and Yang, 2011; Tian et al., 2018)	Multi-region models, input-output	Highlight the role of the full global chains for water (not just agri-food, energy, paper).	Typically, less precision in the agri-food WFs, and short temporal spans.	
(Garrido et al., 2010; Cazcarro et al., 2019)	WF, scarcity, and water apparent productivity	Highlight the role of dryland/ irrigated land, and the relation of WF to scarcity and water apparent productivities.	Lack of other economic valuation of water and WF than that of the market (prices, monetary values, etc.).	Shows very different economic relevance of rainfed/irrigated/grass/land for WFs and the need of PWS to properly account them.
Dalin et al. (2012); Duarte et al. (2014), Konar et al. (2013)	Historical WFs computations	Attempts to get and use historical WFs to obtain relations of water pressures and socioeconomic variables	Simplistic methods of computing historical WFs based on yields	Researchers in PWS are better suited to obtain estimates of historical WFs.
(Lund, 2015; Lowe et al., 2018)	Review of integrating social with physical sciences for WM accomplishments. Comment on the need of linking WF and economic valuation. Literature review.	Highlight of the needs of linking natural and social sciences for water management, and of the use of economic valuation.	Focus only on a sub-discipline of environmental economics without citing ecological and political ecology options.	Shows the importance of problem-solving focus. Provides perspective on the valuation of ecosystem services, etc.
This Opinion article	Opinion on the cited WF blind spots and proposals to make more relevant PWS and economics in WM.	Identification of WF literature gaps especially related to PWS and proposals to make them more relevant in WM.	Lacks empirical application other than brief examples. Does not explain in full detail some of the arguments presented.	Finds blind spots in which PWS could shed light on WF calculation. Extends perspectives on how to make PWS research more useful and consistent with socioeconomic analysis for practical WM.

has one element in common: it is about following, as Lund (2015) points out, a problem-based approach rather than a discipline-based approach.

If the above seems too "ethereal," we propose a couple of concrete examples below.

Two Examples for Practical Relevance

First example: the management of forests and other types of vegetation. This entails biodiversity, erosion, emissions, lack of management, which affects the risk of fires, but also its effect on water availability (in Blanco (2017), existing paradigms on the relation between forests and water are even challenged). Indeed, existing blue-green water relations and substitutability are often ignored by analyzing them as if they were two distinct areas. As reviewed in D'Odorico et al. (2018), decades of research on deforestation have highlighted the profound hydroclimatic impacts of land use and land cover change (Perugini et al., 2017). Although it is very difficult to generalize conclusions for different kinds of forests, climates, soils, etc. (for which more studies on grassland *vs*. agroforestry are needed), Kay et al. (2018) show consistently for six case studies in Europe how groundwater recharge rate tends to be higher in agricultural landscapes without agroforestry systems. On rain-fed farmland *vs*. forestry, the former is found to sustain lower evapotranspiration rates because of the smaller leaf area index, surface roughness, root depth, and greater albedo (Bonan, 2008; Perugini et al., 2017; D'Odorico et al., 2018). On closed *vs*. open forest, the first reduces more infiltration (Gracia et al., 2011; Di Prima et al., 2017). All in all, both ET and runoff go against infiltration. The reason is that, although truly runoff does not increase on site storing, water remains within the basin, while with ET water escapes from it. For example, in the Ebro basin, Bielsa et al. (2011) and López-Moreno et al. (2008; 2014) found surprisingly small water volumes in downstream gauges which lead them to identify increasing natural revegetation as a potential explanatory factor. We believe plant sciences have a great deal to contribute to river basin water management since land-use changes, particularly forest extent and coverage, can modify forest water demand and hence blue water availability. Some policy makers only take action when they grasp, if roughly, the economic implications of these water losses or water pollution.

Consider a second example. As highlighted by Shtull-Trauring et al. (2016), high-resolution studies can provide data to inform policy makers and farmers about the appropriate crops and cultivation practices that lower the WF by increasing water use efficiency and reducing the negative impact on the environment. On that basis, we would also add that policy makers will only take appropriate decisions knowing the whole picture of the benefits and costs for society. We know that the market economic valuation instruments are not usually appropriate for this cost-benefit calculations (see e.g., Van der Zaag and Savenije, 2006). Therefore, a key aspect is the consideration of many water services as public goods. This implies requiring some type of agency that considers social costs and benefits [be they public administrators/non-governmental organizations (NGOs), etc.] to manage it. Only if the water cycle (and thus the green side of it) is fully known, can informed and sound decisions be made. Clearly, plant water dynamics have much to contribute in this area. **Table 1** summarizes advances, gaps and relevance for PWS of a selection of the cited literature.

CONCLUDING REMARKS

As we have argued based on the critical analysis of recent literature on water management and on WF, new advances in the study of plant water dynamics have great potential to improve the understanding and management of the water cycle. These have to do with the data from the ET measurements and their dynamics. This need is important for pastures, forests, and vegetation and, in particular, for economically and politically relevant areas and periods of time. The ultimate goal is to develop work based on problems and not on disciplines. However well-known that principle is, it is still not applied in many scientific areas.

AUTHOR CONTRIBUTIONS

IC and JB contributed equally to the analysis and writing of the article.

FUNDING

IC acknowledges the financial support from the Ramón Areces Foundation, grant CISP15A3198.

REFERENCES

Afkhami, M., Bassetti, T., Ghoddusi, H., and Pavesi, F. (2018). Virtual water trade: the implications of capital scarcity. *SSRN Electron. J.* 1–38. doi: 10.2139/ssrn.3166874

Bielsa, J., Cazcarro, I., and Sancho, Y. (2011). Integration of hydrological and economic approaches to water and land management in Mediterranean climates: an initial case study in agriculture. *Spanish J. Agric. Res.* 9, 1076–1088. doi: 10.5424/sjar/20110904-500-10

Blanco, J. A. (2017). Bosques, suelo y agua: explorando sus interacciones. *Ecosistemas* 26, 1–9. doi: 10.7818/ECOS.2017.26-2.01

Bonan, G. B. (2008). *Ecological climatology* (New York, NY, USA: Cambridge University Press).

Cazcarro, I., Martín-Retortillo, M., and Serrano, A. (2019). Reallocating regional water apparent productivity in the long term: methodological contributions and application for Spain. *Reg. Environ. Change* 19, 1455–1468. doi: 10.1007/s10113-019-01485-9

Chapagain, A. K., and Hoekstra, A. Y. (2004). Water Footprints of Nations. *Value Water Res. Rep. Ser.* 16.

Chenoweth, J., Hadjikakou, M., and Zoumides, C. (2014). Quantifying the human impact on water resources: a critical review of the water footprint concept. *Hydrol. Earth Syst. Sci.* 18, 2325–2342. doi: 10.5194/hess-18-2325-2014

D'Odorico, P., Davis, K. F., Rosa, L., Carr, J. A., Chiarelli, D., Dell'Angelo, J., et al. (2018). The global food-energy-water nexus. *Rev. Geophys.* 56, 456–531. doi: 10.1029/2017RG000591

Dalin, C., Konar, M., Hanasaki, N., Rinaldo, A., and Rodriguez-Iturbe, I. (2012). Evolution of the global virtual water trade network. *Proc. Natl. Acad. Sci.* 109, 5989–5994. doi: 10.1073/pnas.1203176109

Daniels, P. L., Lenzen, M., and Kenway, S. J. (2011). The ins and outs of water use – a review of multi-region input–output analysis and water footprints for regional sustainability analysis and policy. *Econ. Syst. Res.* 23, 353–370. doi: 10.1080/09535314.2011.633500

Di Prima, S., Bagarello, V., Angulo-Jaramillo, R., Bautista, I., Cerdà, A., Del Campo, A., et al. (2017). Impacts of thinning of a Mediterranean oak forest on soil properties influencing water infiltration. *J. Hydrol. Hydromechanics* 65, 276–286. doi: 10.1515/johh-2017-0016

Duarte, R., and Yang, H. (2011). Input–output and water: introduction to the special issue. *Econ. Syst. Res.* 23, 341–351. doi: 10.1080/09535314.2011.638277

Duarte, R., Pinilla, V., and Serrano, A. (2014). The effect of globalisation on water consumption: a case study of the Spanish virtual water trade, 1849–1935. *Ecol. Econ.* 100, 96–105. doi: 10.1016/j.ecolecon.2014.01.020

Escriva-Bou, A., Lund, J. R., Pulido-Velazquez, M., Hui, R., and Medellín-Azuara, J. (2018). Developing a water-energy-GHG emissions modeling framework: insights from an application to California's water system. *Environ. Model. Software* 109, 54–65. doi: 10.1016/j.envsoft.2018.07.011

Garrido, A., Llamas, M. R., C., V.-O., Novo, P., Rodríguez-Casado, R., and Aldaya, M. M. (2010). *Water footprint and virtual water trade in Spain: policy implications* (New York: Springer- Fundación Marcelino Botín).

Gawel, E. (2014). "Virtual water and trade: a critical economic review," in *The Global Water System in the Anthropocene: Challenges for Science and Governance*. Eds. A. Bhaduri, J. Bogardi, J. Leentvaar and S. Marx (Cham: Springer International Publishing), 27–43.

Gómez-Baggethun, E., and Martín-López, B. (2015). "Ecological economics perspectives on ecosystem services valuation," in *Handbook of Ecological Economics*. Eds. J. Martínez-Alier and R. Muradian, 260–282. doi: 10.4337/9781783471416.00015

Gracia, C., Vanclay, J., Daly, H., Sabate, S., and Gyenge, J. (2011). "Securing water for trees and people: possible avenues: a challenging balance," in Water for Forests and People in the Mediterranean Region,. Eds. Y. Birot, C. Gracia, and M. Palahi. (Finland: European Forest Institute) 83–91.

Harou, J. J., Pulido-Velazquez, M., Rosenberg, D. E., Medellín-Azuara, J., Lund, J. R., and Howitt, R. E. (2009). Hydro-economic models: concepts, design, applications, and future prospects. *J. Hydrol.* 375, 627–643. doi: 10.1016/j.jhydrol.2009.06.037

Hellegers, P., and van Halsema, G. (2019). Weighing economic values against societal needs: questioning the roles of valuing water in practice. *Water Policy* 21, 514–525. doi: 10.2166/wp.2019.048

Hoekstra, A. Y., and Mekonnen, M. M. (2012). The water footprint of humanity. *Proc. Natl. Acad. Sci.* 109, 3232–3237. doi: 10.1073/pnas.1109936109

Kahil, T., Parkinson, S., Satoh, Y., Greve, P., Burek, P., Veldkamp, T. I. E., et al. (2018). A continental-scale hydroeconomic model for integrating water-energy-land Nexus solutions. *Water Resour. Res.* 54, 7511–7533. doi: 10.1029/2017WR022478

Kallis, G., Gómez-Baggethun, E., and Zografos, C. (2013). To value or not to value? *That is not question. Ecol. Econ.* 94, 97–105. doi: 10.1016/j.ecolecon.2013.07.002

Kay, S., Crous-Duran, J., Ferreiro-Domínguez, N., García de Jalón, S., Graves, A., Moreno, G., et al. (2018). Spatial similarities between European agroforestry systems and ecosystem services at the landscape scale. *Agrofor. Syst.* 92, 1075–1089. doi: 10.1007/s10457-017-0132-3

Konar, M., Hussein, Z., Hanasaki, N., Mauzerall, D. L., and Rodriguez-Iturbe, I. (2013). Virtual water trade flows and savings under climate change. *Hydrol. Earth Syst. Sci.* 17, 3219–3234. doi: 10.5194/hess-17-3219-2013

Kool, D., Agam, N., Lazarovitch, N., Heitman, J. L., Sauer, T. J., and Ben-Gal, A. (2014). A review of approaches for evapotranspiration partitioning. *Agric. For. Meteorol.* 184, 56–70. doi: 10.1016/j.agrformet.2013.09.003

Launiainen, S., Futter, M. N., Ellison, D., Clarke, N., Finér, L., Högbom, L., et al. (2014). Is the water footprint an appropriate tool for forestry and forest products: the Fennoscandian case. *Ambio* 43, 244–256. doi: 10.1007/s13280-013-0380-z

Liu, Z., Davis, S. J., Feng, K., Hubacek, K., Liang, S., Anadon, L. D., et al. (2016). Targeted opportunities to address the climate-trade dilemma in China. *Nat. Clim. Change* 6, 201–206. doi: 10.1038/nclimate2800

López-Moreno, J. I., Beniston, M., and García-Ruiz, J. M. (2008). Environmental change and water management in the Pyrenees: facts and future perspectives for Mediterranean mountains. *Glob. Planet. Change* 61, 300–312. doi: 10.1016/j.gloplacha.2007.10.004

López-Moreno, J. I., Zabalza, J., Vicente-Serrano, S. M., Revuelto, J., Gilaberte, M., Azorin-Molina, C., et al. (2014). Impact of climate and land use change on water availability and reservoir management: scenarios in the upper aragón River, Spanish Pyrenees. *Sci. Total Environ.* 493, 1222–1231. doi: 10.1016/j.scitotenv.2013.09.031

Lovarelli, D., Bacenetti, J., and Fiala, M. (2016). Water footprint of crop productions: a review. *Sci. Total Environ.* 548–549, 236–251. doi: 10.1016/j.scitotenv.2016.01.022

Lowe, H. B., Oglethorpe, R. D., and Choudhary, S. (2018). Marrying Unmarried literatures: the water footprint and environmental (Economic) valuation. *Water* 10, 1815. doi: 10.3390/w10121815

Lund, J. R. (2015). Integrating social and physical sciences in water management. *Water Resour. Res.* 51, 5905–5918. doi: 10.1002/2015WR017125

Martin-Ortega, J., Ferrier, R. C., Gordon, I. J., and Khan, S. (2015). *Water ecosystem services: a global perspective*. (Cambridge University Press).

Mateo-Sagasta, J., Raschid-Sally, L., and Thebo, A. (2015). "Global Wastewater and Sludge Production, Treatment and Use," in *Wastewater: Economic Asset in an Urbanizing World*. Eds. P. Drechsel, M. Qadir and D. Wichelns (Dordrecht: Springer Netherlands), 15–38.

Mekonnen, M. M., and Hoekstra, A. Y. (2010a). A global and high-resolution assessment of the green, blue and grey water footprint of wheat. *Hydrol. Earth Syst. Sci.* 14, 1259–1276. doi: 10.5194/hess-14-1259-2010

Mekonnen, M. M., and Hoekstra, A. Y. (2010b). The green, blue and grey water footprint of farm animals and animal products, 1. doi: 10.5194/hess-15-1577-2011

Mekonnen, M. M., and Hoekstra, A. Y. (2012). A global assessment of the water footprint of farm animal products. *Ecosystems* 15, 401–415. doi: 10.1007/s10021-011-9517-8

Nouri, H., Stokvis, B., Galindo, A., Blatchford, M., and Hoekstra, A. Y. (2019). Water scarcity alleviation through water footprint reduction in agriculture: the effect of soil mulching and drip irrigation. *Sci. Total Environ.* 653, 241–252. doi: 10.1016/j.scitotenv.2018.10.311

Perugini, L., Caporaso, L., Marconi, S., Cescatti, A., Quesada, B., de Noblet-Ducoudré, N., et al. (2017). Biophysical effects on temperature and precipitation due to land cover change. *Environ. Res. Lett.* 12, 53002. doi: 10.1088/1748-9326/aa6b3f

Rockström, J., Gordon, L., Folke, C., Falkenmark, M., and Engwall, M. (1999). Linkages among water vapor flows, food production, and terrestrial ecosystem services. *Ecol. Soc.* 3. doi: 10.5751/ES-00142-030205

Rodríguez-Labajos, B., and Martínez-Alier, J. (2015). Political ecology of water conflicts. *Wiley Interdiscip. Rev. Water* 2, 537–558. doi: 10.1002/wat2.1092

Schyns, J. F., and Vanham, D. (2019). The water footprint of wood for energy consumed in the European Union. *Water (Switzerland)* 11, 1–11. doi: 10.3390/w11020206

Schyns, J. F., Booij, M. J., and Hoekstra, A. Y. (2017). The water footprint of wood for lumber, pulp, paper, fuel and firewood. *Adv. Water Resour.* 107, 490–501. doi: 10.1016/j.advwatres.2017.05.013

Schyns, J. F., Hoekstra, A. Y., and Booij, M. J. (2015). Review and classification of indicators of green water availability and scarcity. *Hydrol. Earth Syst. Sci. Discuss.* 12, 5519–5564. doi: 10.5194/hessd-12-5519-2015

Shtull-Trauring, E., Aviani, I., Avisar, D., and Bernstein, N. (2016). Integrating high resolution water footprint and GIS for promoting water efficiency in the agricultural sector: a case study of plantation crops in the Jordan Valley. *Front. Plant Sci.* 7, 1877. doi: 10.3389/fpls.2016.01877

Tian, X., Sarkis, J., Geng, Y., Qian, Y., Gao, C., Bleischwitz, R., et al. (2018). Evolution of China's water footprint and virtual water trade: a global trade assessment. *Environ. Int.* 121, 178–188. doi: 10.1016/j.envint.2018.09.011

Vörösmarty, C. J., Hoekstra, A. Y., Bunn, S. E., Conway, D., and Gupta, J. (2015). Fresh water goes global. *Science (80-.)*, 349,478–479. doi: 10.1126/science.aac6009

Van der Zaag, P., and Savenije, H. H. (2006). Water as an economic good: the value of pricing and the failure of markets. *Value Water Res. Rep. Ser.* 19, 1–32.

van Oel, P. R., and Hoekstra, A. Y. (2012). Towards quantification of the water footprint of paper: a first estimate of its consumptive component. *Water Resour. Manage.* 26, 733–749. doi: 10.1007/s11269-011-9942-7

Vanham, D., del Pozo, S., Pekcan, A. G., Keinan-Boker, L., Trichopoulou, A., and Gawlik, B. M. (2016). Water consumption related to different diets in Mediterranean cities. *Sci. Total Environ.* 573, 96–105. doi: 10.1016/j.scitotenv.2016.08.111

Wichelns, D. (2011). Do the virtual water and water footprint perspectives enhance policy discussions? *Int. J. Water Resour. Dev.* 27, 633–645. doi: 10.1080/07900627.2011.619894

Wichelns, D. (2015). Virtual water and water footprints: overreaching into the discourse on sustainability, efficiency, and equity. *Water Altern.* 8, 396–414.

Wright-Contreras, L. (2018). A transnational urban political ecology of water infrastructures: global water policies and water management in Hanoi. *Public Work. Manage. Policy* 24, 195–212. doi: 10.1177/1087724X18780045

Zhao, D., Hubacek, K., Feng, K., Sun, L., and Liu, J. (2019). Explaining virtual water trade: a spatial-temporal analysis of the comparative advantage of land, labor and water in China. *Water Res.* 153, 304–314. doi: 10.1016/j.watres.2019.01.025

Conflict of Interest: The authors declare that the research was conducted in the absence of any commercial or financial relationships that could be construed as a potential conflict of interest.

frontiers in Plant Science

PERSPECTIVE
published: 19 March 2020
doi: 10.3389/fpls.2020.00302

Fungal Aquaporins in Ectomycorrhizal Root Water Transport

Hao Xu[1]* *and Janusz J. Zwiazek*[2]

[1] Summerland Research and Development Centre, Agriculture and Agri-Food Canada, Summerland, BC, Canada,
[2] Department of Renewable Resources, University of Alberta, Edmonton, AB, Canada

Ectomycorrhizal fungi influence root water transport of host plants. To delineate the exact mechanisms of how fungal partner alters root water relations, it is important to understand the functions of fungal transmembrane water channels, i.e., aquaporins, the key component in the symplastic pathways. In this paper, we discussed what roles the fungal aquaporins may play in root water transport. We also highlighted the opportunities of using integrated approaches to address rising questions in future hotspots of aquaporin and root water relations research.

Keywords: hypha, major intrinsic protein, plant–fungal interaction, symplastic pathway, transport capacity

OPEN ACCESS

Edited by:
Juan Pedro Ferrio, Fundación Agencia Aragonesa para la Investigación y el Desarrollo, Spain

Reviewed by:
Sabine Dagmar Zimmermann, Délégation Languedoc Roussillon (CNRS), France
Jose Eduardo Marqués-Gálvez, University of Murcia, Spain

***Correspondence:**
Hao Xu
hao.xu@canada.ca

Specialty section:
This article was submitted to Technical Advances in Plant Science, a section of the journal Frontiers in Plant Science

Received: *19 December 2019*
Accepted: *02 March 2020*
Published: *19 March 2020*

Citation:
Xu H and Zwiazek JJ (2020) Fungal Aquaporins in Ectomycorrhizal Root Water Transport. Front. Plant Sci. 11:302. doi: 10.3389/fpls.2020.00302

IMPACTS OF ECTOMYCORRHIZA ON ROOT WATER RELATIONS

Ectomycorrhizal (EcM) fungi develop mutualistic associations with roots of Pinaceae and many hardwood species. Through their highly specialized structures, EcM fungi supply mineral nutrients and water to the roots of host plants in exchange for photosynthates.

EcM fungi colonize the lateral roots extracellularly at the water permeable root tips, typically forming three compartments that alter water transport in the rhizosphere distinctly. They are the extraradical network of free-living mycelia, mantle sheath and Hartig net. The free-living fungal mycelia extend by cell elongation and infinite cell division, into an extensive extraradical network in the soil (Smith and Read, 2008). The hyphae at the growing mycelial front are actively involved in water and nutrient acquisition. Some hyphae go through different degrees of morphological differentiation and form specialized rope-like strands called rhizomorphs for medium-distance and long-distance soil exploration (Agerer, 2001). Vessel hyphae in rhizomorphs are enlarged with highly modified or absent septa that facilitate efficient water movement. Some peripheral hyphae in rhizomorphs display thickened and pigmented cell walls that may help to reduce water loss (Agerer, 2001; Peterson et al., 2004). Nutrients and water are transported along rhizomorphs to two structures at hyphae-root interface – the hyphal mantle sheath that envelops the root tip and forms an outwardly sealed compartment mainly for storage, and the intercellular Hartig net of hyphae surrounding the plant epidermal and outer cortical cells for substrate exchange (**Figure 1A**; Smith and Read, 2008).

While water travels along the water potential gradient in roots by apoplastic and symplastic pathways (Steudle and Peterson, 1998), the presence of EcM fungi can drastically change the dynamics of plant water relations and root hydraulic properties, by altering both pathways, particularly around the root epidermal and cortical cells (**Figure 1A**; Marjanović et al., 2008; Smith and Read, 2008; Lehto and Zwiazek, 2011). Firstly, the presence of EcM fungi can substantially alter root anatomy and the hydrophilic properties of root apoplastic pathway (Nylund, 1987; Muhsin and Zwiazek, 2002). Secondly, the extensive hyphal network of mycorrhizas can significantly increase water supply toward the roots (Lehto and Zwiazek, 2011). Water availability in root cortex is subsequently altered. Root aquaporins – the water transporting Major intrinsic proteins (MIPs) located on cellular membranes – respond to the change in water availability, and rule the water permeability of symplastic pathway in root cortex and in endodermis where the apoplastic pathway is thought to be hindered by Casparian band (**Figure 1A**).

ROLES OF FUNGAL AQUAPORINS IN ECTOMYCORRHIZAL ROOT WATER TRANSPORT

To understand root hydraulic properties of EcM plants, water transfer between both partners should be elucidated as a plant–fungi continuity. Theoretically, water can move in the extracellular space and in the cell walls of hydrophilic hyphae in a manner equivalent to the apoplastic pathway in plant roots. While in the hyphal protoplasts, water travels efficiently cross septa between adjacent cells with minimal barrier (Agerer, 2001; Peterson et al., 2004).

When water travels cross the cellular membrane of hyphal cells from apoplastic into symplastic space, or vice versa, its movement is regulated by an array of fungal MIPs with water permeability (Pettersson et al., 2005; Maurel and Plassard, 2011). These water channel proteins belong to the clusters of orthodox aquaporins or facultative aquaporins (Xu et al., 2013; **Figure 2A**), and are commonly referred as fungal aquaporins for their roles in determining water permeability of cellular membranes and water transport efficiency of symplastic pathway. They have 250–330 amino acids, forming six transmembrane domains, with three loops in the extracellular space, and two loops and two termini in the cytoplasm (**Figure 2B**). They also possess signature motifs for water selectivity and key residues for gating. Their subcellular localization on plasma membrane, secretory pathway or mitochondrial membrane can be predicted based on the motifs in the N-terminus (**Figure 2C**). The transport capacity can be predicted by how their sequences cluster into the phylogenetic relations, and be confirmed by functional assays of protein expression. A dozen of aquaporins have been functionally characterized in EcM fungus *Laccaria bicolor* and ectendomycorrhizal fungus *Terfezia claveryi*. The studies demonstrate their strong to moderate capacity of transporting water, urea, glycerol, ammonia, and CO_2. Their expression can be altered by mycorrhization or abiotic cues such as drought, salt, low temperature, or pH (Dietz et al., 2011; Navarro-Ródenas et al., 2012, 2013; Xu et al., 2015), suggesting their multiple roles in plant–fungal interactions, and their involvement in water transport and nutrient transfer of the mycorrhizal partners. Differential expressions of fungal aquaporins were also observed in a cell-specific pattern, in EcM root tips, free-living mycelium, fungal mantle, Hartig net, and fruiting body. The accumulation of transcripts of *Tuber melanosporum* aquaporins in the mantle of mycorrhizal tips (Hacquard et al., 2013), the upregulation of several aquaporins in the formation of the fruiting body of *L. bicolor* (Xu et al., 2016), and the striking upregulation of two aquaporin genes of EcM *Cenococcum geophilum* induced by the symbiosis interaction with *Pinus silvestris* (Peter et al., 2016), are some examples of the physiological significance of fungal aquaporins in hyphal cells and at hypha-root interface.

Fungal aquaporins regulate the acquisition and release of water by the hyphae, and therefore play essential physiological roles in hyphal cell expansion, division, and hyphal fusion. Because of their significance in the processes of water entry and exit of the symplastic pathway, understanding their roles is key to elucidate the precise pathways for water transport from the fungal partner to the host roots in mycorrhizal associations. Firstly, fungal aquaporins regulate the amount of water acquired by the hyphae at mycelial front and subsequently transported into rhizomorphs. Secondly, the abundance and activity of fungal aquaporins could impact water availability in root extracellular space in Hartig net (**Figures 1A,B**). Ultimately, by changing the hydration in the apoplastic space, it can influence root aquaporin regulation and the overall root water uptake (Javot and Maurel, 2002; Marjanović et al., 2005; Lee et al., 2010; Dietz et al., 2011; Navarro-Ródenas et al., 2013; Xu et al., 2015; Calvo-Polanco et al., 2019).

The involvement of fungal aquaporins in root water transport was proven by the enhancement of root hydraulic conductance in *Picea glauca* roots mycorrhizal with the *L. bicolor* strains that overexpressed the fungal water-transporting aquaporins (Xu et al., 2015). As the conceptual model based on this study shows (**Figure 1A**), the contribution of *L. bicolor* hyphae to root water transport in *P. glauca* could involve increased apoplastic water transport in the root intercellular spaces, which may be attributed to water released from the hyphae and may lead to increased hydration at the fungal-root interface, and consequently impact aquaporin expression in mycorrhizal roots (**Figure 1B2**). Moderate increase in fungal aquaporin expression may lead to a further increase in hydration in the root intercellular space; therefore, apoplastic water transport in roots may be further enhanced (**Figure 1B3**). Under adverse conditions such as low temperatures, upregulation of fungal aquaporins to a furthest extent may lead to the increase in water influx into hyphal cells and the decrease in hydration in the root intercellular space, which consequently affects root aquaporin regulation and reduces root hydraulic conductance in the host plant. This suggests that the role of fungal aquaporins in EcM root water

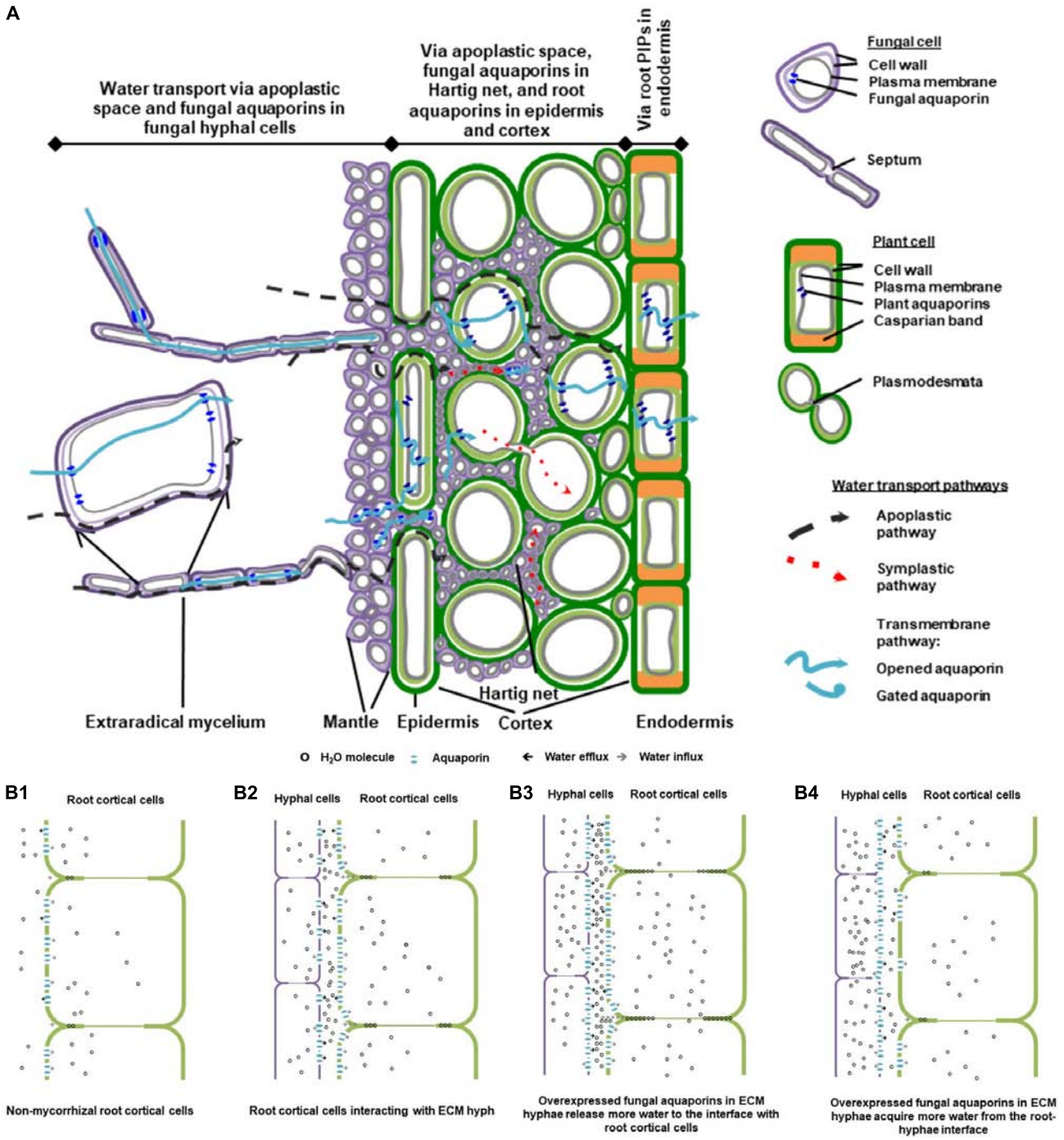

FIGURE 1 | A schematic diagram of water transport pathways and aquaporin involvement in ectomycorrhizal (EcM) association. **(A)** A conceptual model of water pathways through EcM hypha-root continuity. The diagram was drawn based on the composite model of root water transport (Steudle and Peterson, 1998), with reference to that of the EcM root water transport suggested by Lehto and Zwiazek (2011). **(B)** Involvement of fungal and plant aquaporins in water transport at the hypha-root interface in EcM. The simplified model is postulated according to a study on the roles of fungal aquaporin *Laccaria bicolor* JQ585595 in EcM interaction and root hydraulic dynamics of the host plant *Picea glauca* (Xu et al., 2015). **(B1)** Water is transported in apoplastic space and cell-to-cell pathways in cortical cells in non-mycorrhizal root tips; **(B2)** In mycorrhizal root tips, root water transport in apoplastic, and cell-to-cell pathways is altered by the presence of mycorrhizal hyphae, as water released from mycorrhizal hyphae increases the hydration in the intercellular space of cortical cells, and the root aquaporins are engaged for transmembrane water transport; **(B3)** When transcript abundance of the fungal aquaporins is up-regulated, a moderate increase in fungal aquaporins contributes to the increase in water efflux from hyphal cells and in hydration of root intercellular space, which leads to further enhancement of apoplastic water availability to root; **(B4)** Conditionally, increased abundance of fungal aquaporins may cause more water influx into hyphal cells and less water in intercellular space available for root transport. The diagrams were modified from Xu (2015) with the author's permission.

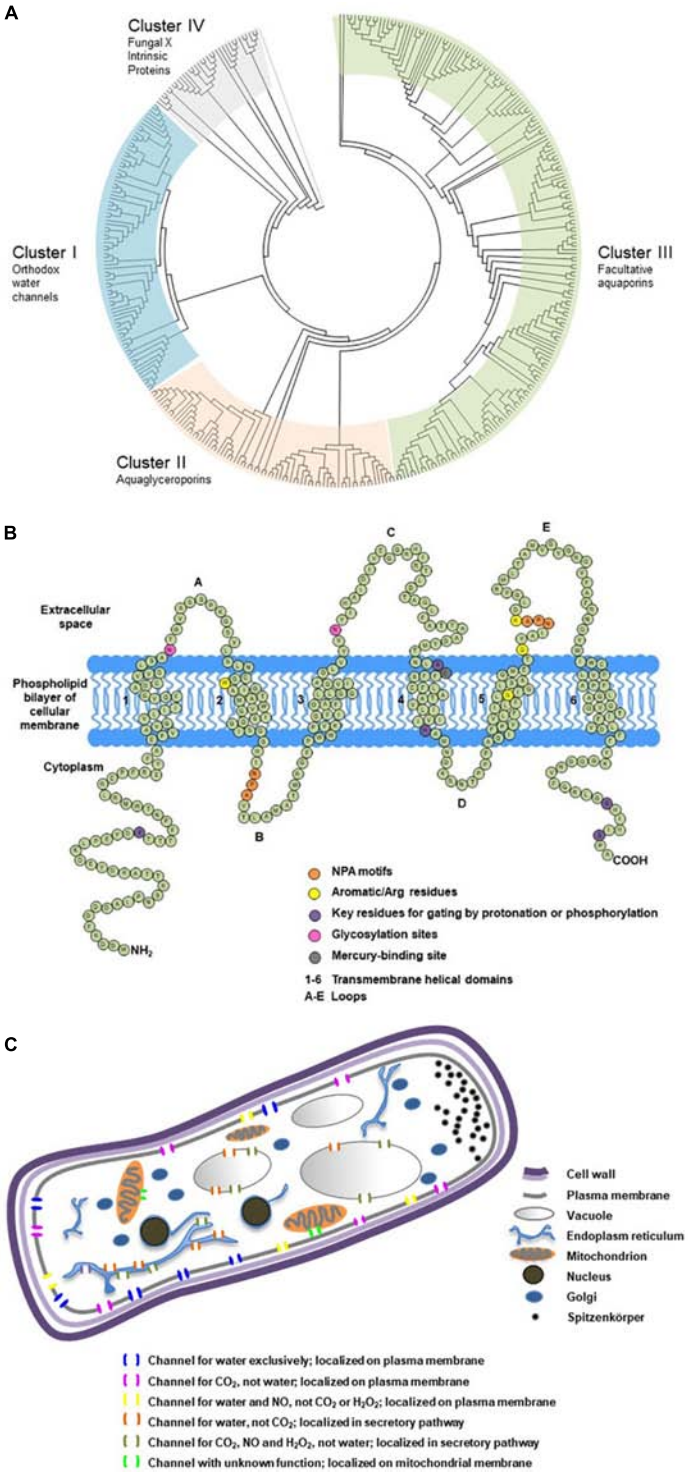

FIGURE 2 | Phylogenetic classification, secondary structure and cellular localization of ectomycorrhizal fungal aquaporins. **(A)** Phylogenetic analysis of 376 fungal major intrinsic proteins (MIPs), including 152 sequences from 32 EcM fungi categorized into four clusters. The sequences were retrieved from public databases in JGI and NCBI. The classification referred to Xu et al. (2013). Divergence times for all branching points in the topology were calculated using the Maximum Likelihood method based on the JTT matrix-based model (Jones et al., 1992; Tamura et al., 2012) in MEGA 7 (Kumar et al., 2016). The tree was outgrouped to the aquaporin sequences of AqpZ from *Escherichia coli* and AQP1 from *Mus musculus*. **(B)** Transmembrane domains and signature motifs of fungal aquaporins. Protein secondary structure was predicted using SOSUI (Hirokawa et al., 1998). The diagram was reproduced from Xu (2015) with the author's permission. **(C)** Possible subcellular localizations and transport functions of fungal aquaporins. Subcellular localization was predicted using TargetP (Emanuelsson et al., 2007). The diagram was modified from Xu (2015) with the author's permission.

transport is highly dynamic and reversible. Further studies on the synchronization of fungal and plant aquaporins need to be conducted in the context of abiotic stresses, as well as under stimulation of stress-related and mycorrhiza-related phytohormones (Zargar et al., 2017; Lanfranco et al., 2018; Calvo-Polanco et al., 2019).

INTEGRATED TOOLKITS AND FUTURE PERSPECTIVES FOR FUNGAL AQUAPORIN RESEARCH

In the last two decades, aquaporin research has been accelerated substantially by the integrated approaches of bioinformatics, functional assays in singular cell expression systems, and molecular tools for abundance analysis and *in situ* visualization of aquaporin RNAs and proteins.

Phylogenetic reconstruction and peptide secondary structure prediction (Hirokawa et al., 1998; Emanuelsson et al., 2007) are usually the first steps and relatively rapid tools to screen putative fungal aquaporins that are retrieved from the expanding resource of sequenced fungal genomes. To date, Mycorrhizal Genomics Initiative (Martin et al., 2011, 2016; Nordberg et al., 2014; van der Heijden et al., 2015) has released the annotated genomes of more than 90 EcM fungal species (**Figure 2A**), which provides an unprecedented platform for *in silico* analysis of fungal MIPs and for selection of promising aquaporins of functional and physiological importance.

Functional assay can be considered as phenotyping of transmembrane porters. Using the singular cell expression systems of *Xenopus* oocytes and yeasts, researchers have unveiled diverse transport capacities of fungal aquaporins and postulated their versatile physiological functions (**Figure 2C**). One aquaporin may possess multiple transport functions, whereas different aquaporins may be permeable to similar substrates. Transport capacities of water and other small neutral molecules by fungal aquaporins, and their interaction with other transmembrane porters of amino acids, sugars and ions, are important areas to explore. Studies showed that a variety of fungal transmembrane porters were simultaneously upregulated by EcM interaction, which indicated the increased substrate exchange between the symbionts (Martin et al., 2010; Peter et al., 2016). In addition, the orchestrated gating and trafficking of aquaporins and other transmembrane porters may play important roles in cellular signaling; however, this area remains largely unexplored. The findings will contribute to the understanding of their multiple crucial roles in fungal growth and interaction with mycorrhizal plants (Nehls and Dietz, 2014; Verma et al., 2014).

Physiological roles of aquaporins with known transport capacities can be inferred by the alteration and synchronization of their expressions in response to abiotic stresses and stress-related phytohormones such as abscisic acid, cytokinins, salicylic acid, and strigolactones (Zargar et al., 2017; Lanfranco et al., 2018; Calvo-Polanco et al., 2019). The functional importance of aquaporins is also implied by the differential expressions of fungal aquaporins in extraradical mycelium, mantle and Hartig net, and of plant aquaporins in epidermis, cortex and endodermis (**Figure 1A**). In addition to RNA-seq differential expression analysis for the identification of significantly upregulated aquaporins (Martin et al., 2010; Peter et al., 2016), techniques such as qRT-PCR in combination with laser capture microdissection RNA extraction and mRNA *in situ* hybridization, allow researchers to examine the transcript abundance of plant aquaporins in different cell types along root water transport pathways (Almeida-Rodriguez and Hacke, 2012; Gambetta et al., 2013), and of fungal aquaporins in different hyphal compartments in mycorrhizal roots (Hacquard et al., 2013). In addition, transgenic fungal constructs that overexpress or silence water-transporting aquaporins, are powerful tools to confirm the physiological contributions of fungal aquaporins in mycorrhizal roots (Xu et al., 2015).

On a finer scale, advances in antibody and immunofluorescence techniques will facilitate the research on aquaporin subcellular localization and post-translational modifications such as phosphorylation, protonation and heteromerization. This will help to elucidate how the gating and trafficking mechanisms of fungal and plant aquaporins are linked to the changes in root hydraulic conductivity, as responses to mycorrhizal symbiosis, and abiotic cues.

DATA AVAILABILITY STATEMENT

The datasets generated for this study can be found in the JGI, https://mycocosm.jgi.doe.gov/Mycorrhizal_fungi/Mycorrhizal_fungi.info.html, by inquiring EcM fungal genomes with the keyword "aquaporin".

AUTHOR CONTRIBUTIONS

HX and JZ conceptualized and wrote the manuscript.

FUNDING

The research was supported by two research grants provided by the Agriculture and Agri-Food Canada (Project IDs J-002199 and J-002265).

ACKNOWLEDGMENTS

We thank the cited researchers for their work on delineating the processes of ectomycorrhizal root water transport and Mycorrhizal Genomics Initiative for sharing bioinformatics resources.

REFERENCES

Agerer, R. (2001). Exploration types of ectomycorrhizae—a proposal to classify ectomycorrhizal mycelial systems according to their patterns of differentiation and putative ecological importance. *Mycorrhiza* 11, 107–114. doi: 10.1007/s005720100108

Almeida-Rodriguez, A. M., and Hacke, U. G. (2012). Cellular localization of aquaporin mRNA in hybrid poplar stems. *Am. J. Bot.* 99, 1249–1254. doi: 10.3732/ajb.1200088

Calvo-Polanco, M., Armada, E., Zamarreño, A. M., García-Mina, J. M., and Aroca, R. (2019). Local root ABA/cytokinin status and aquaporins regulate poplar responses to mild drought stress independently of the ectomycorrhizal fungus *Laccaria bicolor*. *J. Exp. Bot.* 70, 6437–6446. doi: 10.1093/jxb/erz389

Dietz, S., von Bülow, J., Beitz, E., and Nehls, U. (2011). The aquaporin gene family of the ectomycorrhizal fungus *Laccaria bicolor*: lessons for symbiotic functions. *New Phytol.* 190, 927–940. doi: 10.1111/j.1469-8137.2011.03651.x

Emanuelsson, O., Brunak, S., Heijne, G., and Nielsen, H. (2007). Locating proteins in the cell using TargetP, SignalP, and related tools. *Nat. Protoc.* 2, 953–971. doi: 10.1038/nprot.2007.131

Gambetta, G. A., Fei, J., Rost, T. L., Knipfer, T., Matthews, M. A., Shackel, K. A., et al. (2013). Water uptake along the length of grapevine fine roots: developmental anatomy, tissue-specific aquaporin expression, and pathways of water transport. *Plant Physiol.* 163, 1254–1265. doi: 10.1104/pp.113.221283

Hacquard, S., Tisserant, E., Brun, A., Legué, V., Martin, F., and Kohler, A. (2013). Laser microdissection and microarray analysis of *Tuber melanosporum* ectomycorrhizas reveal functional heterogeneity between mantle and Hartig net compartments. *Environ. Microbiol.* 15, 1853–1869. doi: 10.1111/1462-2920.12080

Hirokawa, T., Boon-Chieng, S., and Mitaku, S. (1998). SOSUI: classification and secondary structure prediction system for membrane proteins. *Bioinformatics* 14, 378–379. doi: 10.1093/bioinformatics/14.4.378

Javot, H., and Maurel, C. (2002). The role of aquaporins in root water uptake. *Ann. Bot.* 90, 301–313. doi: 10.1093/aob/mcf199

Jones, D. T., Taylor, W. R., and Thornton, J. M. (1992). The rapid generation of mutation data matrices from protein sequences. *Comput. Appl. Biosci.* 8, 275–282. doi: 10.1093/bioinformatics/8.3.275

Kumar, S., Stecher, G., and Tamura, K. (2016). MEGA7: molecular evolutionary genetics analysis version 7.0 for bigger datasets. *Mol. Biol. Evol.* 33, 1870–1874. doi: 10.1093/molbev/msw054

Lanfranco, L., Fiorilli, V., Venice, F., and Bonfante, P. (2018). Strigolactones cross the kingdoms: plants, fungi, and bacteria in the arbuscular mycorrhizal symbiosis. *J. Exp. Bot.* 69, 2175–2188. doi: 10.1093/jxb/erx432

Lee, S. H., Calvo-Polanco, M., Chung, G. C., and Zwiazek, J. J. (2010). Role of aquaporins in root water transport of ectomycorrhizal jack pine (*Pinus banksiana*) seedlings exposed to NaCl and fluoride. *Plant Cell Environ.* 33, 769–780. doi: 10.1111/j.1365-3040.2009.02103.x

Lehto, T., and Zwiazek, J. J. (2011). Ectomycorrhizas and water relations of trees: a review. *Mycorrhiza* 21, 71–90. doi: 10.1007/s00572-010-0348-9

Marjanović, Ž, Nehls, U., and Varma, A. (eds) (2008). "Ectomycorrhiza and water transport," in *Mycorrhiza*, (Berlin: Springer), 149–159. doi: 10.1007/978-3-540-78826-3_8

Marjanović, Ž, Uehlein, N., Kaldenhoff, R., Zwiazek, J. J., Weiss, M., Hampp, R., et al. (2005). Aquaporins in poplar: what a difference a symbiont makes. *Planta* 222, 258–268.

Martin, F., Cullen, D., Hibbett, D., Pisabarro, A., Spatafora, J. W., Baker, S. E., et al. (2011). Sequencing the fungal tree of life. *New Phytol.* 190, 818–821.

Martin, F., Kohler, A., Murat, C., Balestrini, R., Coutinho, P. M., Jaillon, O., et al. (2010). Périgord black truffle genome uncovers evolutionary origins and mechanisms of symbiosis. *Nature* 464, 1033–1038.

Martin, F., Kohler, A., Murat, C., Veneault-Fourrey, C., and Hibbett, D. S. (2016). Unearthing the roots of ectomycorrhizal symbioses. *Nat. Rev. Microbiol.* 14, 760–773. doi: 10.1038/nrmicro.2016.149

Maurel, C., and Plassard, C. (2011). Aquaporins: for more than water at the plant–fungus interface? *New Phytol.* 190, 815–817.

Muhsin, T. M., and Zwiazek, J. J. (2002). Ectomycorrhizas increase apoplastic water transport and root hydraulic conductivity in *Ulmus americana* seedlings. *New Phytol.* 153, 153–158.

Navarro-Ródenas, A., Bárzana, G., Nicolás, E., Carra, A., Schubert, A., and Morte, A. (2013). Expression analysis of aquaporins from desert truffle mycorrhizal symbiosis reveals a fine-tuned regulation under drought. *Mol. Plant Microbe Int.* 26, 1068–1078. doi: 10.1094/MPMI-07-12-0178-R

Navarro-Ródenas, A., Ruíz-Lozano, J. M., Kaldenhoff, R., and Morte, A. (2012). The aquaporin TcAQP1 of the desert truffle *Terfezia claveryi* is a membrane pore for water and CO2 transport. *Mol. Plant Microbe Int.* 25, 259–266.

Nehls, U., and Dietz, S. (2014). Fungal aquaporins: cellular functions and ecophysiological perspectives. *Appl. Microbiol. Biotechnol.* 98, 8835–8851. doi: 10.1007/s00253-014-6049-0

Nordberg, H., Cantor, M., Dusheyko, S., Hua, S., Poliakov, A., Shabalov, I., et al. (2014). The genome portal of the department of energy joint genome institute: 2014 updates. *Nucleic Acids Res.* 42, D26–D31. doi: 10.1093/nar/gkt1069

Nylund, J. E. (1987). The ectomycorrhizal infection zone and its relation to acid polysaccharides of cortical cell walls. *New Phytol.* 106, 505–516.

Peter, M., Kohler, A., Ohm, R. A., Kuo, A., Krützmann, J., Morin, E., et al. (2016). Ectomycorrhizal ecology is imprinted in the genome of the dominant symbiotic fungus *Cenococcum geophilum*. *Nat. Commun.* 7, 1–15. doi: 10.1038/ncomms12662

Peterson, R. L., Massicotte, H. B., and Melville, L. H. (2004). *Mycorrhizas: Anatomy and Cell Biology*. Ottawa: NRC Research Press.

Pettersson, N., Filipsson, C., Becit, E., Brive, L., and Hohmann, S. (2005). Aquaporins in yeasts and filamentous fungi. *Biol. Cell* 97, 487–500.

Smith, S. E., and Read, D. J. (2008). *Mycorrhizal Symbiosis*, 3rd Edn, Cambridge: Academic Press.

Steudle, E., and Peterson, C. A. (1998). How does water get through roots? *J. Exp. Bot.* 49, 775–788.

Tamura, K., Battistuzzi, F. U., Billing-Ross, P., Murillo, O., Filipski, A., and Kumar, S. (2012). Estimating divergence times in large molecular phylogenies. *Proc. Natl. Acad. Sci. U.S.A.* 109, 19333–19338. doi: 10.1073/pnas.1213199109

van der Heijden, M. G. A., Martin, F. M., Selosse, M. A., and Sanders, I. R. (2015). Mycorrhizal ecology and evolution: the past, the present, and the future. *New Phytol.* 205, 1406–1423. doi: 10.1111/nph.13288

Verma, R. K., Prabh, N. D., and Sankararamakrishnan, R. (2014). New subfamilies of major intrinsic proteins in fungi suggest novel transport properties in fungal channels: implications for the host-fungal interactions. *BMC Evol. Biol.* 14:173. doi: 10.1186/s12862-014-0173-4

Xu, H. (2015). *Major INTRINSIC PRoteins of Laccaria Bicolor: Characterization, Transcript Profiling and Functions in Ectomycorrhizal Associations with Picea glauca*. Ph.D. thesis, University of Alberta, Edmonton.

Xu, H., Cooke, J. E., and Zwiazek, J. J. (2013). Phylogenetic analysis of fungal aquaporins provides insight into their possible role in water transport of mycorrhizal associations. *Botany* 91, 495–504.

Xu, H., Kemppainen, M., El Kayal, W., Lee, S. H., Pardo, A. G., Cooke, J. E., et al. (2015). Overexpression of *Laccaria bicolor* aquaporin JQ585595 alters root water transport properties in ectomycorrhizal white spruce (*Picea glauca*) seedlings. *New Phytol.* 205, 757–770. doi: 10.1111/nph.13098

Xu, H., Navarro-Ródenas, A., Cooke, J. E., and Zwiazek, J. J. (2016). Transcript profiling of aquaporins during basidiocarp development in *Laccaria bicolor* ectomycorrhizal with *Picea glauca*. *Mycorrhiza* 26, 19–31. doi: 10.1007/s00572-015-0643-6

Zargar, S. M., Nagar, P., Deshmukh, R., Nazir, M., Wani, A. A., Masoodi, K. Z., et al. (2017). Aquaporins as potential drought tolerance inducing proteins: towards instigating stress tolerance. *J. Proteom.* 169, 233–238. doi: 10.1016/j.jprot.2017.04.010

Conflict of Interest: The authors declare that the research was conducted in the absence of any commercial or financial relationships that could be construed as a potential conflict of interest.

frontiers in Plant Science

ORIGINAL RESEARCH
published: 24 March 2020
doi: 10.3389/fpls.2020.00340

A Cultivar-Sensitive Approach for the Continuous Monitoring of Olive (*Olea europaea* L.) Tree Water Status by Fruit and Leaf Sensing

Alessio Scalisi[1,2], Giulia Marino[1,3], Francesco Paolo Marra[1], Tiziano Caruso[1] and Riccardo Lo Bianco[1]*

[1] Department of Agricultural, Food and Forest Sciences (SAAF), University of Palermo, Palermo, Italy, [2] Agriculture Victoria, Department of Jobs, Precincts and Regions, Tatura, VIC, Australia, [3] Department of Plant Sciences, University of California, Davis, Davis, CA, United States

Sustainable irrigation is crucial to reduce water use and management costs in modern orchard systems. Continuous plant-based sensing is an innovative approach for the continuous monitoring of plant water status. Olive (*Olea europaea* L.) genotypes can respond to drought using different leaf and fruit physiological and morphological mechanisms. This study aimed to identify whether fruit and leaf water dynamics of two different olive cultivars were differently affected by water deficit and their response to changes of midday stem water potential (Ψ_{stem}), the most common indicator of plant water status. Plant water status indicators such as leaf stomatal conductance (g_s) and Ψ_{stem} were measured in the Sicilian olive cultivars Nocellara del Belice (NB) and Olivo di Mandanici (MN), in stage II and III of fruit development. Fruit gauges and leaf patch clamp pressure probes were mounted on trees and their raw data were converted in relative rates of fruit diameter change (RR_{fruit}) and leaf pressure change (RR_{leaf}), sensitive indicators of tissue water exchanges. The analysis of diel, diurnal and nocturnal fluctuations of RR_{fruit} and RR_{leaf} highlighted differences, often opposite, between the two cultivars under water deficit. A combination of statistical parameters extrapolated from RR_{fruit} and RR_{leaf} diurnal and nocturnal curves were successfully used to obtain significant multiple linear models for the estimation of midday Ψ_{stem}. Fruit and leaf water exchanges suggest that olive cultivar can either privilege fruit or leaf water status, with MN likely preserving leaf water status and NB increasing fruit tissue elasticity under severe water deficit. The results highlight the advantages of the integration of fruit and leaf water dynamics to estimate plant water status and the need for genotype-specific models in olive.

Keywords: drought, fruit diameter, sustainable irrigation, turgor pressure, water deficit, water potential

OPEN ACCESS

Edited by:
Juan Pedro Ferrio, Fundacion Agencia Aragonesa para la Investigacion y el Desarrollo, Spain

Reviewed by:
Antonio Diaz Espejo, Institute of Natural Resources and Agrobiology of Seville (CSIC), Spain
Salvatore Camposeo, University of Bari Aldo Moro, Italy

****Correspondence:***
Alessio Scalisi
alessio.scalisi@agriculture.vic.gov.au;
alessio.scalisi@unipa.it

Specialty section:
This article was submitted to Technical Advances in Plant Science, a section of the journal Frontiers in Plant Science

Received: *06 December 2019*
Accepted: *06 March 2020*
Published: *24 March 2020*

Citation:
Scalisi A, Marino G, Marra FP, Caruso T and Lo Bianco R (2020) A Cultivar-Sensitive Approach for the Continuous Monitoring of Olive (Olea europaea L.) Tree Water Status by Fruit and Leaf Sensing. Front. Plant Sci. 11:340. doi: 10.3389/fpls.2020.00340

INTRODUCTION

In recent years, sustainable irrigation has become a crucial aspect of orchard management to reduce inputs in agricultural systems. In the current global warming and desertification scenario, both environmentally and economically oriented reasons provide the basis for a water saving approach, which has become paramount in irrigated orchards. Automated irrigation management is even

more important in high-density systems in which growers tend to increase orchard productivity and reduce management costs by mechanizing operations. In the past, irrigation management was commonly based on soil water status or environmental indices. However, tree water status provides the most precise drought stress indices, in spite of soil and environmental conditions. Indeed, plants represent the intermediate component of the soil-plant-atmosphere continuum, and their physiological responses are the result of an integration of both soil and environment. This implies an advantage of plant-based over soil-based methods for an accurate irrigation scheduling (Fernández, 2017).

Plant water requirements differ among species and even cultivars, making irrigation scheduling and management a complex task for growers. The physiological responses of plants to decreasing water availability are various and depend on evolutionary adaptation and acclimation to new climatic conditions. The olive species (*Olea europaea* L.) has a very wide genetic pool, and includes genotypes that can respond to drought using different mechanisms of leaf dehydration tolerance and leaf morphological and structural adaptations (Bacelar et al., 2004, 2006; Ennajeh et al., 2010; Lo Bianco and Scalisi, 2017; Scalisi et al., 2019a). Gucci et al. (2000) and Lo Bianco and Scalisi (2017) found different leaf stomatal regulation among olive cultivars. Connor (2005) suggested that olive genotypes use avoidance (i.e., low leaf conductance, low leaf area, low xylem hydraulic conductivity and large roots) and tolerance mechanisms (i.e., high turgor through cell osmotic adjustments, small cell size, and changes in cell-wall elasticity) under drought. Midday stem water potential (Ψ_{stem}) is considered a very sensitive parameter of plant water status for irrigation management (Moriana and Fereres, 2002; Fernández et al., 2006; Moriana et al., 2012, Marino et al., 2018). However, Ψ_{stem} is mostly measured by the Scholander pressure chamber, which does not allow for continuous monitoring and automated irrigation.

Recently, plant-based sensing technologies are taking hold for the continuous plant water status monitoring in fruit trees. In most of cases, sensors are mounted on aboveground organs such as stem, fruit and leaves (Fernández, 2014, 2017; Scalisi et al., 2017). In olive, trunk dendrometers have been associated with tree water stress thresholds and proposed for irrigation management due to their relatively easy installation and stability across the season (Moreno et al., 2006; Cuevas et al., 2010; Fernández et al., 2011b).

In the last few years, emphasis has been given to the use of leaf patch clamp pressure (LPCP) probes for the continuous assessment of olive leaf water status (Fernández et al., 2011a; Ehrenberger et al., 2012; Rodriguez-Dominguez et al., 2012, 2019; Marino et al., 2016; Padilla-Díaz et al., 2016; Fernándes et al., 2017). The output of LPCP probes is expressed as attenuated pressure of leaf patches (p_p), which is inversely related to cell turgor pressure (p_c) (Zimmermann et al., 2008). Therefore, the highest values of p_p occur around solar noon, as that is the moment in which leaf cell turgor is the lowest. Ben-Gal et al. (2010) found an inversion of the p_p curve in severely drought-stressed olive trees. Thereafter, Fernández et al. (2011a) classified water deficit states based on the degree of inversion of the curve. State I represented no drought stress and leaves with a non-inverted curve, state II grouped leaves experiencing partial inversion of the curve and mild water deficit, and state III enclosed all leaves experiencing severe water deficit and full inversion of the curve.

Fruit-based probes based on linear variable displacement transducers (LVDTs) can provide good information on fruit growth, which on a diel scale is mostly dominated by water in- and out-flows, rather than carbon gain; thus, fruit diameter (FD) variations respond to water deficit (Scalisi et al., 2017). Fernandes et al. (2018) studied olive FD dynamics in response to water deficit, suggesting the appropriateness of fruit gauges for continuous plant water status monitoring. Although FD and p_p are strictly related to soil water availability and plant water status, they are also influenced by environmental variables, crop load, genetic factors and phenology. The derived values of FD and p_p (namely relative rate of fruit diameter change, RR_{fruit} and relative rate of leaf pressure change, RR_{leaf}) represent good indicators of the rate at which water enters and exits leaf or fruit, respectively. The reasoning behind this assumption resides in the fact that they both represents rates of changes – pressure and diameter, respectively – from an initial state, which, in the short term ($\leq$15-minute intervals) are mainly driven by tissue water exchanges. The combined use of RR_{fruit} and RR_{leaf} was recently introduced to estimate water deficit in nectarine (Scalisi et al., 2019b,c). Plants modulate water movements to and from the two main transpiring organs (i.e., leaf and fruit) using several strategies such as osmotic adjustments, stomatal closure or cell-wall elasticity regulation. As a result, we hypothesized that either leaf or fruit water status might be privileged under increasing water deficit in olive genotypes with different drought tolerance/avoidance mechanisms.

This work aimed to study olive fruit and leaf water dynamics in relation to tree water status. Our hypothesis was that, similarly to what found in nectarine (Scalisi et al., 2019c), the combination of RR_{fruit} and RR_{leaf} might provide an even more accurate identification of plant water status, rather than monitoring each parameter independently. In addition, this study aimed to identify cultivar-specific RR_{fruit}/RR_{leaf} relationships to determine whether the genotypes under study preserve leaf or fruit water exchanges under increasing water deficit, as sink power for water might differ among genotypes.

MATERIALS AND METHODS

Experimental Design

The experiment was carried out in summer 2016 in a high-density (6 × 3 spacing, ∼ 555 trees/ha) olive orchard located near Sciacca, in South-western Sicily (37°29′56.8″ N and 13°12′13.4″ E, 138 m a.s.l.). Three-year-old self-rooted trees were trained to "free palmette" along a hedgerow in North-to-South rows. The experimental orchard is part of a large survey on the Sicilian autochthonous germplasm (Marino et al., 2019). Olive alternates high and low cropping seasons and this experiment considered only trees in an ON-year (heavy crop load). In this trial, the two Sicilian cultivars Nocellara del Belice (NB) and Olivo di Mandanici (MN) were selected for their different vigor and fruit

characteristics (Marino et al., 2016, 2017). Trees belonging to NB have low vigor, spreading canopy habit and yield large fruit, mainly processed as table olives, whereas MN trees show high vigor, upright canopy habit and yield smaller fruit, exclusively utilized for olive oil extraction. NB trees are particularly sensitive to leaf dehydration (Lo Bianco and Scalisi, 2017) and to water deficit overall (Scalisi et al., 2019a). The soil was a sandy clay loam (60% sand, 18% silt, and 22% clay) with pH of 7.7 and <5% of active carbonates. Trees were regularly fertilized and pruned according to conventional practices.

Meteorological data were retrieved from the meteorological station of Sciacca (Servizio Informativo Agrometeorologico Siciliano). Reference evapotranspiration (ET_0) and vapor pressure deficit (VPD) were calculated using the methods described by Allen et al. (1998). Crop evapotranspiration (ET_c) was estimated by weighing ET_0 with an average K_c of 0.50 ± 0.05 (Allen et al., 1998).

Trees were irrigated at weekly intervals using self-compensating in-line drippers delivering 16 L/h. Four irrigation levels were imposed to generate a large variability in tree water status: full irrigation (FI) supplied with a volume of water equal to 100% of ET_c, and three sustained deficit irrigation levels at 66% (DI-66), 33% (DI-33), and 0% (DI-0) of FI. Six, four, two and no drippers per plant were used for FI, DI-66, DI-33, and DI-0, respectively. Trees were arranged according to a completely randomized experimental design, with twelve tree-replicate per cultivar, and three trees for each irrigation level. Measurements were carried out at stages II (pit-hardening) and III (cell enlargement) of fruit development, as during the stage I (mid-May/beginning July) spring rainfall saturated the soil and canceled any possible effect of deficit irrigation. Data are reported in local time.

Plant Water Status

Leaf stomatal conductance (g_s) was measured using a Delta-T AP4 dynamic porometer (Delta-T Devices LTD, Cambridge, United Kingdom) on three sun-exposed leaves in three trees per irrigation level. Daily measurements of g_s were taken at 2-hour intervals, from 0800 to 2000 h in a day at stage II (day of the year, DOY = 209) and from 0800 to 1800 h in a day at stage III (DOY = 287).

A pressure chamber (PMS Instrument Co., Corvallis, OR, United States) was used for the determination of Ψ_{stem}, on twigs covered by plastic and aluminum foil 1 h before measurement, as described by Turner (1988). Daily measurements of Ψ_{stem} were carried out on three twigs per tree, on the same trees and DOY of g_s measurements, at 2-hour intervals and from pre-dawn (0430 h) to 2000 h at DOY 209, and to 1800 h at DOY 287. Midday Ψ_{stem} was measured at around 1400 h, once a week from 196 to 287 DOY, and using three twigs per tree.

Fruit- and Leaf-Based Sensing

The fruit gauges based on LVDT sensors described by Morandi et al. (2007) were installed on olive drupes for continuous FD measurements. Gauges were wired to four CR-1000 data loggers (Campbell scientific, Inc., Logan, UT, United States) and data were downloaded manually. A total of 16 gauges (eight on each cultivar, two trees per irrigation level) were mounted on sun exposed fruit at medium canopy height (1.5 m above ground). In addition, early in the morning, LPCP probes (Yara International, Oslo, NO, United States) were clamped on sun exposed, mature leaves for continuous measurement of p_p. LPCP clamping was done a day after irrigation to ensure optimal leaf turgor, carefully avoiding central leaf nerves and placing the piezoresistive sensor on the abaxial side of leaves. The initial LPCP clamping pressure ranged from 15 to 25 kPa. Data of p_p were recorded continuously and sent to an online server through a system equipped with radio transmitters and a main GPRS/radio controller. LPCP probes were mounted on leaves nearby the fruit monitored with fruit gauges, using the same number of sensors (i.e., 16). Both fruit gauges and LPCP probes were mounted on the same trees used for g_s and Ψ_{stem} measurements.

Fruit gauges and LPCP probes were set to record FD and p_p at 15-minute intervals for 8 days at fruit growth stages II and III. A buffer period corresponding to the first 3 days after sensor mounting was discarded to allow adjustments and/or re-clamping in fruit and leaves. Raw FD and p_p data were processed using a 15-point convoluted spline function (Savitzky and Golay, 1964) to smooth the sensor signal and erase noise. Following data filtering, FD and p_p values were standardized by using z-scores [i.e., $z = (x-\text{mean})/\text{standard deviation}$) to allow comparison among fruits with different initial diameter or leaf with different initial turgor pressure when sensors were mounted. After standardization, FD and p_p obtained from different sensors on the same tree were averaged. Second derivatives of FD and p_p were calculated to determine RR_{fruit} and RR_{leaf} as shown in Eqs. 1, 2, respectively. A standardization of RR_{fruit} and RR_{leaf} was not carried out as they are based on standardized FD and p_p, allowing possible comparisons among outputs from different sensors.

$$RR_{fruit} = (\ln FD_2 - \ln FD_1)/(t_2 - t_1) \quad (1)$$

$$RR_{leaf} = (\ln p_{p2} - \ln p_{p1})/(t_2 - t_1) \quad (2)$$

where, FD_2 and FD_1 are FD at time 2 (t_2) and 1 (t_1), and p_{p2} and p_{p1} are p_p at t_2 and t_1, respectively.

Diel data were subdivided in diurnal (0600 to 2000 h) and nocturnal (2015 to 0545 h) intervals. Subsequently, diel, diurnal and nocturnal statistical parameters were extrapolated from data series for RR_{fruit} and RR_{leaf} in order to find the best predictor of midday Ψ_{stem}. The parameters considered for each time interval (i.e., 24 h, night or day) were: (a) the minimum value (MIN), (b) the maximum value (MAX), (c) the summation of values at 15-minute intervals (SUM), and (d) the difference between MAX and MIN (RANGE). The relative standard deviation (standard deviation divided by the mean, RSD) was calculated as an additional parameter to allow comparison among variances expressed in different units. A graphical representation of all RR_{fruit} statistical parameters calculated on diel basis is shown in **Figure 1**. Similarly, all parameters were calculated for diurnal and nocturnal intervals. Raw data obtained from sensors that either caused damage to the organs or that were displaced by strong wind were discarded.

For each cultivar, the statistical parameters from nocturnal and diurnal timeframes were fitted into multiple regression models to

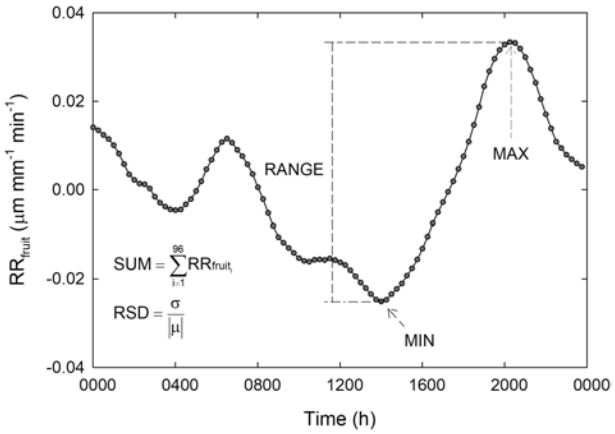

FIGURE 1 | Schematization of statistical parameters calculated on a relative rate of fruit diameter change (RR_{fruit}) diel curve. MIN = minimum value of RR_{fruit}, MAX = maximum value of RR_{fruit}, RANGE = MAX-MIN, SUM = summation of RR_{fruit} values taken at 15-minute intervals from 1 (0000 h) to 96 (2345 h), RSD = relative standard deviation, where σ is the standard deviation and |μ| is the absolute value of the mean.

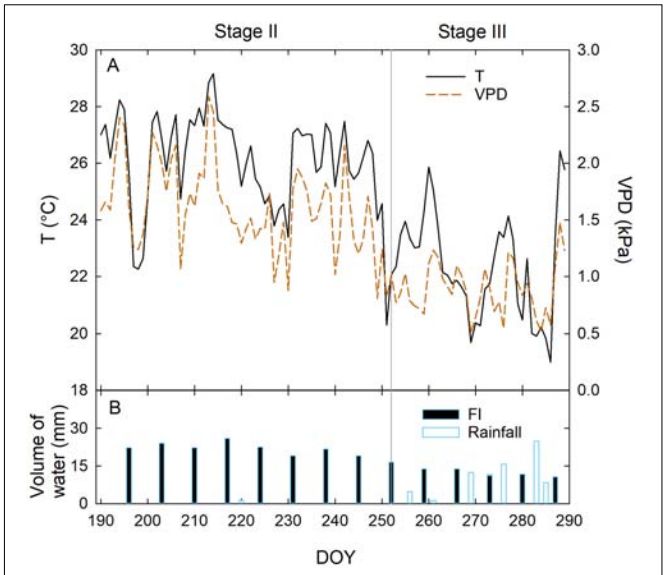

FIGURE 2 | Daily mean temperature (T) and vapor pressure deficit (VPD) **(A)**, daily volumes of water supplied with full irrigation (FI) and rainfall **(B)** at fruit growth stages II and III, from 190 to 290 days of the year (DOY).

predict midday Ψ_{stem}. A backward stepwise procedure was used to discard the parameters that did not significantly contribute to Ψ_{stem} estimation.

RESULTS AND DISCUSSION

Weather Conditions and Irrigation

As expected, temperature (T) and vapor pressure deficit (VPD) were the highest in the measured fraction of stage II, as it occurred in full summer (Jul 8 to Sep 8) (**Figure 2A**). Relatively low T and VPD were recorded in stage III from 280 to 290 DOY (**Figure 2A**), due to frequent precipitations. In stage II, only sporadic rainfall occurred, and irrigation was approximately constant, ranging from 19 to 26 mm per week in FI trees. Lower weekly volumes of water were supplied in stage III due to the precipitations occurred from 252 to 289 DOY (**Figure 2B**). However, at this stage, precipitation led to an average higher weekly crop water supply (CWS, i.e., irrigation + rainfall) compared to stage II (**Figure 2B**). Specifically, in stage II the total CWS was mainly made up of irrigation water (**Table 1**), whereas precipitations at stage III contributed to the 63, 72, 83, and 100% of CWS in FI, DI-66, DI-33, and DI-0 trees, respectively.

TABLE 1 | Crop water supply (CWS) in FI (full irrigated, 100% of crop evapotranspiration), DI-66 (66% of FI), DI-33 (33% of FI) and DI-0 (rainfed) olive trees at fruit growth stages II and III.

Fruit growth stage	CWS	Volume of water (mm)			
		FI	DI-66	DI-33	DI-0
II	Irrigation	197	130	64	0
	Rainfall	1	1	1	1
	Sub-total	198	131	65	1
III	Irrigation	112	74	38	0
	Rainfall	188	188	188	188
	Sub-total	300	262	226	188
Total		438	393	291	189

Data represent averages of 'Nocellara del Belice' and 'Olivo di Mandanici.'

Fruit Characteristics

The two cultivars showed different fruit shape (i.e., NB fruit were almost spherical whereas MN fruit were oblong in shape) from the beginning of fruit diameter measurements at stage II until harvest. Fruit size was also consistently greater in NB than in MN (**Figure 3**), with nearly no fruit growth during stage II in either cultivars, as expected in the pit hardening stage (Scalisi et al., 2019c). Stage III was characterized by a faster fruit diameter increment in MN compared to NB. The latter is related to the first part of stage III (i.e., the part shown in **Figure 3**), as in the remaining part of stage III until harvest, MN fruit reached an average final diameter of ∼16 mm. On the other hand, NB fruit reached an average final diameter of ∼23 mm at harvest, suggesting that they had a steeper growth after the end of the period considered in this study (i.e., after 290 DOY).

Linear regression analyses between fruit diameter and weight highlighted a different relationship of these two fruit parameters in both stages II (**Figure 4A**) and III (**Figure 4B**), as the slopes were significantly higher in NB than in MN ($P < 0.001$ from t-test) due to different pulp-stone ratios. These findings confirm once again the different fruit morphological characteristics of the two cultivars under study.

Plant Water Status

Results from daily g_s measurements carried out at 209 and 287 DOY did not show significantly different patterns between the 2 days of measurements and among irrigation levels. **Figure 5**

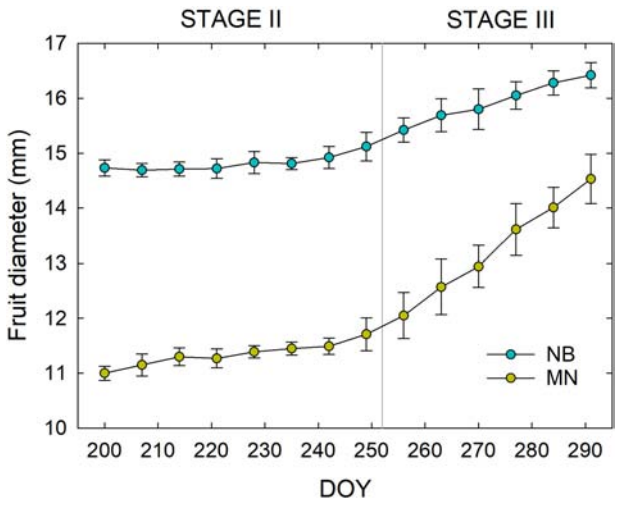

FIGURE 3 | Weekly fruit diameter variations in 'Nocellara del Belice' (NB) and 'Olivo di Mandanici' (MN) olive cultivars at fruit growth stages II and III from 200 to 291 days of the year (DOY). Error bars represent standard deviations of means (n = 60).

shows g_s trends in NB and MN at stage II (A) and III (B). In MN, an overall peak of g_s occurred at mid-morning (1000 h) with a subsequent sudden decrease at 1200 h in response to increasing noon T and VPD. On the other hand, NB leaves did not show a clear peak of g_s in the morning and kept stomatal aperture stable from 0800 h to 1800 h (**Figures 5A,B**), with a significant drop at 2000 h (**Figure 5A**). MN leaves showed significantly higher g_s than NB at 1000 h, implying a likely higher tree water consumption in the morning. This hypothesis is supported by dynamics of sap flux density measured with thermal dissipation probes in the previous year (Marino et al., unpublished), where MN trees showed higher daily water consumption, especially because of greater flows in the first part of the morning. In the afternoon, NB leaves showed higher g_s than MN, with significant differences occurring at 1800 h (**Figures 5A,B**), suggesting a tendency to maintain higher photosynthetic activity late in the day, when T and VPD are lower.

Daily curves of Ψ_{stem} at stages II (209 DOY) and III (287 DOY) showed the typical overall decreasing potential at solar noon in both cultivars, with a subsequent increase late in the afternoon (**Figure 6**). When tested with ANOVA, only Ψ_{stem} in stage III showed significant differences among irrigation levels and a significant interaction with time (i.e., **Figures 6B,D**), with the lowest daily values always occurring between 1400 and 1600 h and in DI-0 trees (**Figures 6B,D**). During the pit hardening phase (i.e., stage II), it is well established that deficit irrigation has little effect on Ψ_{stem} (Dell'Amico et al., 2012). The minimum Ψ_{stem} was significantly lower in NB (−2.53 MPa ± 0.03) than in MN (−2.33 MPa ± 0.03, $P < 0.001$). Pre-dawn observations at stage III suggest a different behavior in the two cultivars, with only MN trees fully recovering to FI levels during the night in DI-0 and DI-33 levels (**Figures 6B,D**). A rise of Ψ_{stem} was observed in NB and MN trees at 1800 h, with DI-0 MN trees recovering completely to FI levels (**Figure 6D**).

Weekly measurements of midday Ψ_{stem} from 196 to 287 DOY generally reflected the irrigation levels (**Figure 7**). Indeed, DI-0 trees experienced the lowest midday Ψ_{stem} both in stages II and III. As expected, midday Ψ_{stem} was higher at stage II than at stage III, although T and VPD were generally higher in the former (**Figure 2**). In this phenological phase, water deficit

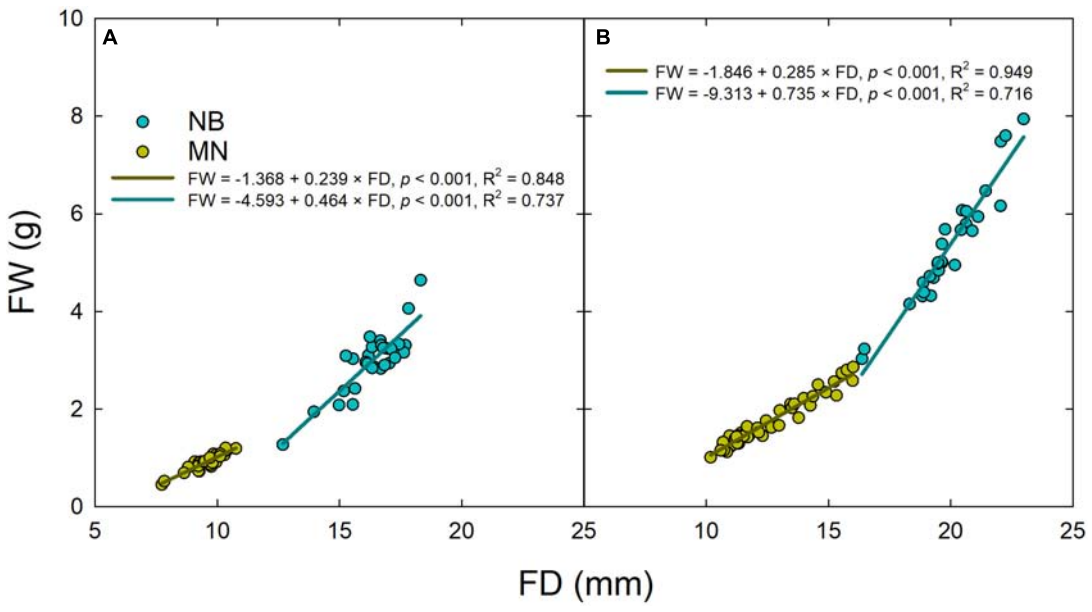

FIGURE 4 | Linear regressions of fruit weight (FW) vs. fruit diameter (FD) in 'Nocellara del Belice' (NB) and 'Olivo di Mandanici' (MN) olive sampled at stage II **(A)** and stage III **(B)** of fruit development.

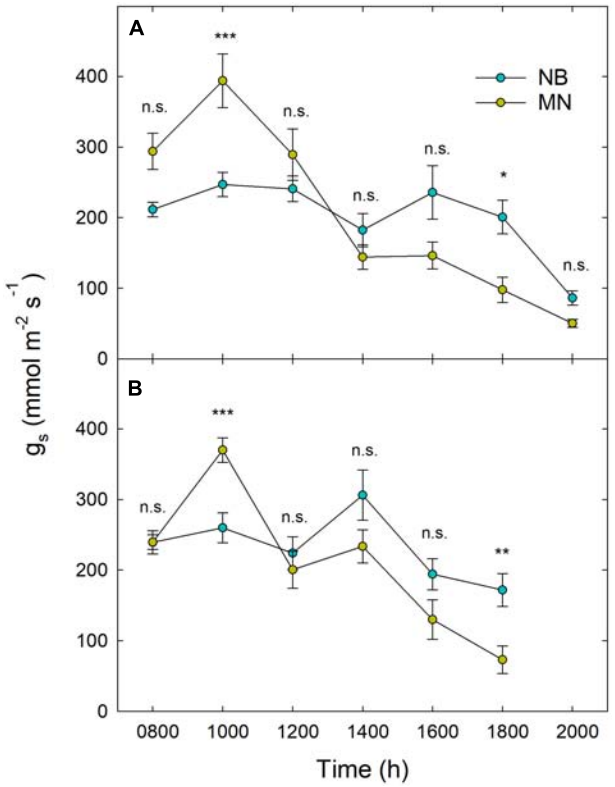

FIGURE 5 | Daily curves of stomatal conductance (g_s) in 'Nocellara del Belice' (NB) and 'Olivo di Mandanici' (MN) olive leaves at fruit growth stages II **(A)** and III **(B)**. Data averaged across different irrigation levels at 209 **(A)** and 287 **(B)** days of the year. Error bars indicate standard deviations of means. N.s., non-significant; *, significantly different for $P < 0.05$; **, significantly different for $P < 0.01$; ***, significantly different for $P < 0.001$ by Tukey's test.

slows down the overall plant activity, inducing a reduction of vegetative growth and photosynthesis, which in turn might limit transpiration (Parent et al., 2009). Indeed, even g_s was similar in stages II and III (**Figure 5**), despite differences in T and VPD (**Figure 2**). Consequently, as water loss by transpiration is likely to be reduced, plants under deficit irrigation at stage II do not reach as low Ψ_{stem} as when the same irrigation is applied in stages I and III. The only exception occurred at 244 DOY, where DI-0 trees experienced a very low Ψ_{stem} in both cultivars, due to both particularly high T and VPD (**Figure 2A**) and to the transition toward the beginning of stage III which was completed the following week. In stage III, the sudden steep increases of Ψ_{stem} at 287 DOY was determined by high precipitations (**Figure 2**). Overall, the cultivars showed a significantly different drop of midday Ψ_{stem} in response to DI-0 (*t*-test $P < 0.05$). Indeed, across the monitoring period, rainfed NB trees showed a lower average midday Ψ_{stem} (-2.75 ± 0.07 MPa) than MN trees (-2.54 ± 0.08 MPa). Combining observations on g_s and Ψ_{stem}, it can be said that MN avoids excessive Ψ_{stem} lowering, not by reduced stomatal aperture, as g_s is significantly higher in MN than in NB in the morning (**Figure 5**), but by other mechanisms. Despite deficit irrigation, NB trees kept their stomata open in the afternoon (**Figure 5**), when ET_0 is highest, and might have not been able to limit water loss from transpiration, inducing low Ψ_{stem}. Marino et al. (2016) suggested that osmotic adjustments might be responsible of the relatively higher Ψ_{stem} in a clone of MN. Furthermore, changes in the leaf cell elastic modulus occur in other olive genotypes under drought (Karamanos, 1984; Dichio et al., 2003; Bacelar et al., 2006). Both osmotic adjustments and reduced cell wall elasticity contribute to turgor preservation (Patakas and Noitsakis, 1997) and might have led to the high Ψ_{stem} found in MN.

Fruit and Leaf-Based Sensing

After removing the three-day buffer period from FD, pp, RR_{fruit}, and RR_{leaf} data, a 5-day interval in stage II was obtained (**Figure 8**). Trends of FD (**Figures 8A,E**) did not highlight different fruit growth dynamics among irrigation levels in stage II, for both NB and MN. FI induced sharper fruit shrinkage than deficit irrigation at 222 and 223 DOY, as fruit with an optimal water status are likely to exchange more water in the warmest hours of the day.

Dynamics of p_p highlighted the typical inversion phenomenon of the diel curve in olive leaves from trees under deficit irrigation (Fernández et al., 2011a). In NB, DI-66 and DI-33 leaves exhibited the half-inverted state (state II), whereas DI-0 leaves showed a total inversion of the curve (state III) (**Figure 8B**). In MN trees, a clear shift from state I to II was not observed, despite the slight tendency to enter state II at 219 and 221 DOY, with no apparent differences among irrigation levels (**Figure 8F**). This suggests that MN leaves can maintain high cell turgor, probably by reduced cell wall elasticity or osmotic adjustments, as found in other olive genotypes (Bacelar et al., 2009; Dichio et al., 2009; Lo Bianco and Scalisi, 2017).

The highest RR_{fruit} always occurred early in the night as fruit quickly rehydrated their tissues (**Figures 8C,G**). As expected, the most negative RR_{fruit} rate (i.e., the highest fruit shrinkage rate) always occurred in the warmest hours of the day. RR_{fruit} dynamics were also affected by deficit irrigation in NB, as the diel RANGE was greater in DI-0 and DI-33 than in DI-66 and FI fruit (**Figure 8C**). A completely different behavior was observed in MN fruit, which instead had the widest diel RANGE in FI trees (**Figure 8G**). In addition, the overall diel RANGE of RR_{fruit} in MN was almost double than in NB, implying larger water in- and out-flows per unit of fruit volume in the former, determined by high fruit sink power for water.

A general positive peak of RR_{leaf} was exhibited early in the morning (**Figures 8D,F**), representing a quick leaf turgor loss (i.e., RR_{leaf} is equivalent to the inverse of the relative change in p_c) after pre-dawn highest turgor in the 24-hour timeframe. Even in this case, the two cultivars responded differently to water deficit, with NB DI-0 trees exhibiting minimal diel fluctuations (i.e., RANGE) while MN DI-0 trees showing the largest RANGE. This suggested that the oscillations of RR_{leaf} might be linked to those of RR_{fruit}.

Another 5-day interval was considered at stage III of fruit development (**Figure 9**). Differently from stage II, FD responses were characterized by an evident diameter increase across the 5 days and within the 24-hour period in both cultivars

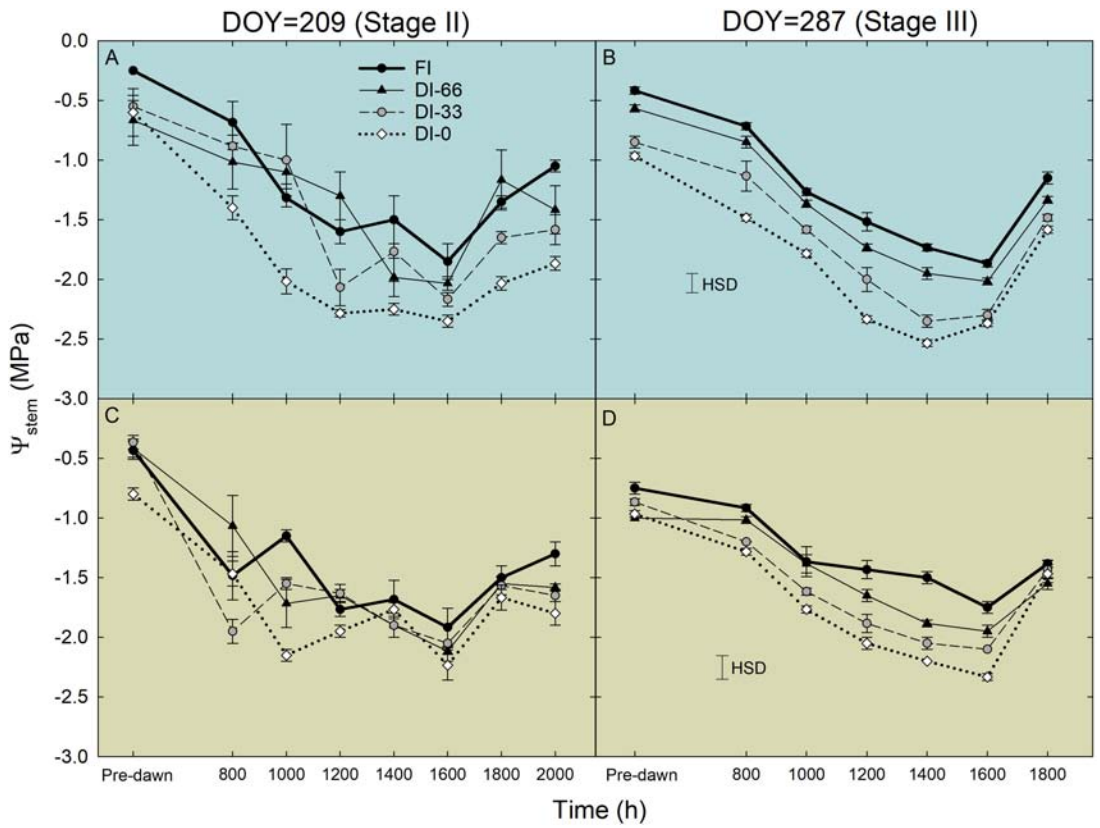

FIGURE 6 | Daily curves of stem water potential (Ψ_{stem}) in 'Nocellara del Belice' (NB) **(A,B)** and 'Olivo di Mandanici' (MN) **(C,D)** olive trees under full irrigation (FI), 66% of FI (DI-66), 33% of FI (DI-33) and no irrigation (DI-0) at 209 (stage II) and 287 (stage III) days of the year (DOY). Error bars represent standard deviations of means (n = 3). Significant differences determined by Tukey's Honestly Significant Difference (HSD, $P < 0.05$).

(**Figures 9A,E**), as in stage III fruit are in full cell enlargement phase (**Figures 9A,E**). Daily curves of p_p (**Figures 9B,F**) did not show pronounced inversion phenomena, as this week was characterized by high rainfall (**Figure 2B**) and general higher midday Ψ_{stem} (**Figure 7**). Only NB DI-0 trees showed a partially inverted p_p curve. Diel RANGE of RR_{fruit} was found to be greatly reduced at stage III (**Figures 9C,G**) compared to stage II (**Figures 8C,G**). In the former, low VPD (**Figure 2A**) and good soil water availability determined by abundant precipitations (**Figure 2B**) led to an increase of water content in fruit and lower fruit water exchanges. For similar reasons, the diel RANGE of RR_{leaf} was reduced in stage III (**Figures 9D,H**), although NB and MN maintained the same differences in response to deficit irrigation levels observed at stage II (**Figures 8D,H**).

Considering the interesting findings from RR_{fruit} and RR_{leaf} dynamics, these two indices were further related to each other regressing their diel data at 15-minute intervals in a day at stage II (DOY = 223) and stage III (DOY = 287). Scatter plots in **Figure 10** show anti-clockwise hysteretic relationships between RR_{fruit} and RR_{leaf}, both for NB (**Figures 10A,B**) and MN (**Figures 10C,D**). Hysteresis are common when relating outputs from different sensors of plant water status mounted on different organs (Tognetti et al., 1996; Fernández, 2017), as there is generally a lag in tissue water de- and re-hydration, and in our case, also a likely different pattern of the RR_{leaf} to RR_{fruit} relationship between day and night. An overall decrease of the hysteretic loop area occurred from stage II (DOY 223) to stage III (DOY 287) in both cultivars (i.e., for NB **Figures 10A,B**, and for MN **Figures 10C,D**). This is probably driven by the different fruit growth pattern at stages II and III which induced a reduction of the RR_{fruit} diel range (**Figures 9C,G**). In both DOY 223 and 287, the hysteretic loops in NB progressively flattened along the RR_{fruit} axis with increasing water deficit (**Figures 10A,B**) due to the change in the ratio between RR_{fruit} and RR_{leaf}. In other words, on one hand, at increasing water deficit and in a diel interval, it seems that NB leaves significantly reduce water exchanges, as the values of RR_{leaf} stay around 0 Pa kPa^{-1} min^{-1}. On the other hand, increasing water deficit caused MN loops to flatten along the RR_{leaf} axis (**Figures 10C,D**), with MN leaves keeping high water exchanges at low Ψ_{stem}, while fruit water exchanges were significantly reduced, as RR_{fruit} did not change much from 0 μm mm^{-1} min^{-1}.This opposite trend suggests a completely different mechanism of leaf and fruit water exchanges in response to increasing water deficit in the two cultivars, which might be driven by different osmotic adjustments, cell-wall elasticity and tissue water content.

The statistical diel, nocturnal and diurnal parameters of RR_{fruit} (i.e., MIN, MAX, SUM, RANGE, and RSD) were associated

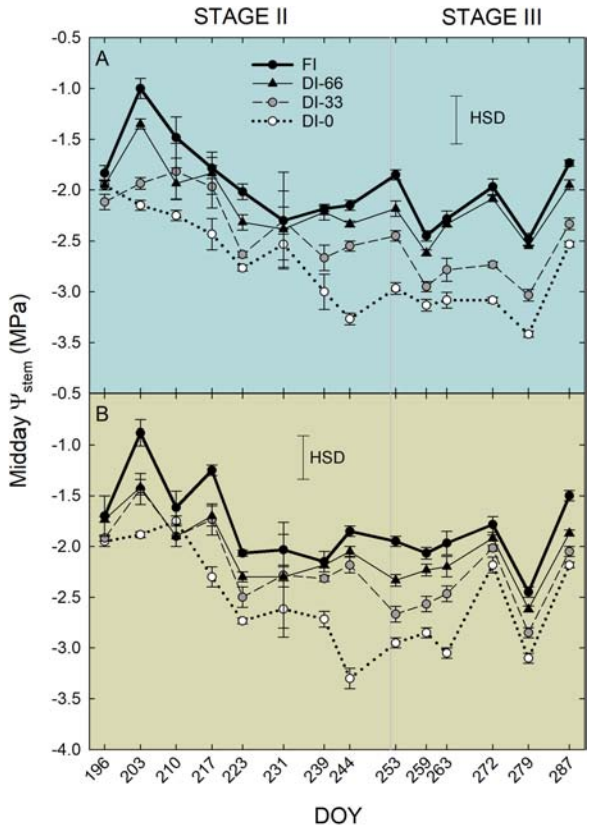

FIGURE 7 | Midday stem water potential (Ψ_{stem}) in 'Nocellara del Belice' (NB) **(A)** and 'Olivo di Mandanici' (MN) olive trees **(B)** under full irrigation (FI), 66% of FI (DI-66), 33% of FI (DI-33) and no irrigation (DI-0) during stage II (from 196 to 252 DOY) and stage III (from 253 to 287 DOY) of fruit growth. Error bars represent standard deviations of means ($n = 3$). Significant differences determined by Tukey's Honestly Significant Difference (HSD, $P < 0.05$).

to the corresponding RR_{leaf} parameters to assess fruit and leaf responses to water deficit. Subsequently, data were analyzed by MANOVA to determine whether the combined response of parameters was affected by cultivars, irrigation levels, and cultivar × irrigation interaction. The cultivar did not influence significantly diel, diurnal and nocturnal RR_{fruit}/RR_{leaf} when statistical parameters were considered together (**Table 2**). Diel and diurnal RR_{fruit}/RR_{leaf} parameters changed significantly in response to irrigation levels, but the cultivar × irrigation interaction had the strongest effect (**Table 2**), indicating that RR_{fruit}/RR_{leaf} responses to deficit irrigation differ between the two genotypes under study. Specifically, the highest F was found in the MANOVA that tested diurnal RR_{fruit}/RR_{leaf} responses to cultivar × irrigation. These results suggest that, under increasing water deficit, the differences in genotype-specific fruit and leaf sink power to water are predominant in day hours.

Ratios between RR_{fruit} and RR_{leaf} diel, diurnal and nocturnal parameters were often linearly related to midday Ψ_{stem} (**Figure 11**). Interestingly, linear regression models highlighted opposite trends in the two cultivars for many of the several associations tested. In NB, $RANGE_{diel}$ [diel RANGE(RR_{fruit})/diel RANGE(RR_{leaf})] was higher at lower midday Ψ_{stem}, suggesting more marked water exchanges (e.g., in and out) in fruit rather than leaves at pronounced water deficit (**Figure 11A**). An opposite trend was observed in MN, in which decreasing midday Ψ_{stem} lead to higher leaf water exchanges (**Figure 11B**). This inverted trend agrees with RR_{fruit} and RR_{leaf} fluctuations shown in **Figures 8C,D,G,H**. In NB, during the day MIN_{diur} [diurnal MIN(RR_{fruit})/diurnal MIN(RR_{leaf})] increased along increasing water deficit (**Figure 11C**). This indicates that as water deficit increases, the highest diurnal speed of fruit water loss becomes higher compared to the highest speed of leaf turgor gain. Even in this case, an opposite trend is found in MN, with the diurnal rate of fruit water loss being higher than leaf rehydration rate at low midday Ψ_{stem} (**Figure 11D**). In NB, SUM_{noct} [nocturnal SUM(RR_{fruit})/nocturnal SUM(RR_{leaf})] decreased with increasing water deficit, with leaf rehydration being favored over fruit water gain (**Figure 11E**). Oppositely, in MN the SUM_{noct} ratio was inversely related to midday Ψ_{stem} (**Figure 11F**), suggesting a stronger nocturnal sink power for water of fruit compared to leaves under more severe water deficit.

All the insights obtained so far suggest that fruit to leaf relationships in terms of RR_{fruit} and RR_{leaf} dynamics at different times of the day can be strictly related to midday Ψ_{stem}, thus, to plant water status.

The backward stepwise multiple regression analysis for NB indicated that most of the statistical parameters significantly contributed to the model in Eq. 3 ($P < 0.05$), and only MIN_{diur}, RSD_{diur} [diurnal RSD(RR_{fruit})/diurnal RSD(RR_{leaf})] and MIN_{noct} [nocturnal MIN(RR_{fruit})/nocturnal MIN(RR_{leaf})] were discarded. RSD_{noct} [nocturnal RSD(RR_{fruit})/nocturnal RSD(RR_{leaf})] provided the greatest contribution to the model ($P < 0.001$, $F = 29.400$). In the multiple regression model obtained for MN (Eq. 4), only four parameters were significant ($P < 0.05$): $RANGE_{diur}$ [diurnal RANGE(RR_{fruit})/diurnal RANGE(RR_{leaf})], RSD_{diur}, MIN_{diur} and RSD_{noct}. Also in this case, RSD_{noct} represented the parameter exhibiting the most relevant effect to the prediction of midday Ψ_{stem} ($P < 0.001$, $F = 24.569$).

$$NB\ \Psi_{stem} = -1.96 + (65.54 \times MAX_{diur}{}^{r}) - (106.84 \times RANGE_{diur}{}^{s}) - (21.27 \times SUM_{diur}{}^{t}) - (3.20 \times MAX_{noct}{}^{u}) + (89.56 \times RANGE_{noct}{}^{v}) + (25.96 \times SUM_{noct}{}^{w}) - (0.365 \times RSD_{noct}{}^{x}) \quad (P < 0.001,\ R^2 = 0.924,\ S.E. = 0.14) \qquad (3)$$

$$MN\ \Psi_{stem} = -1.35 - (40.01 \times RANGE_{diur}) - (0.11 \times RSD_{diur}{}^{y}) - (21.649 \times MIN_{diur}{}^{z}) - (0.280 \times RSD_{noct})\ (P < 0.001,\ R^2 = 0.879,\ S.E. = 0.17) \qquad (4)$$

where, ^{r} = diurnal [MAX (RR_{fruit})/MAX (RR_{leaf})]; ^{s} = diurnal [RANGE (RR_{fruit})/RANGE (RR_{leaf})]; ^{t} = diurnal [SUM

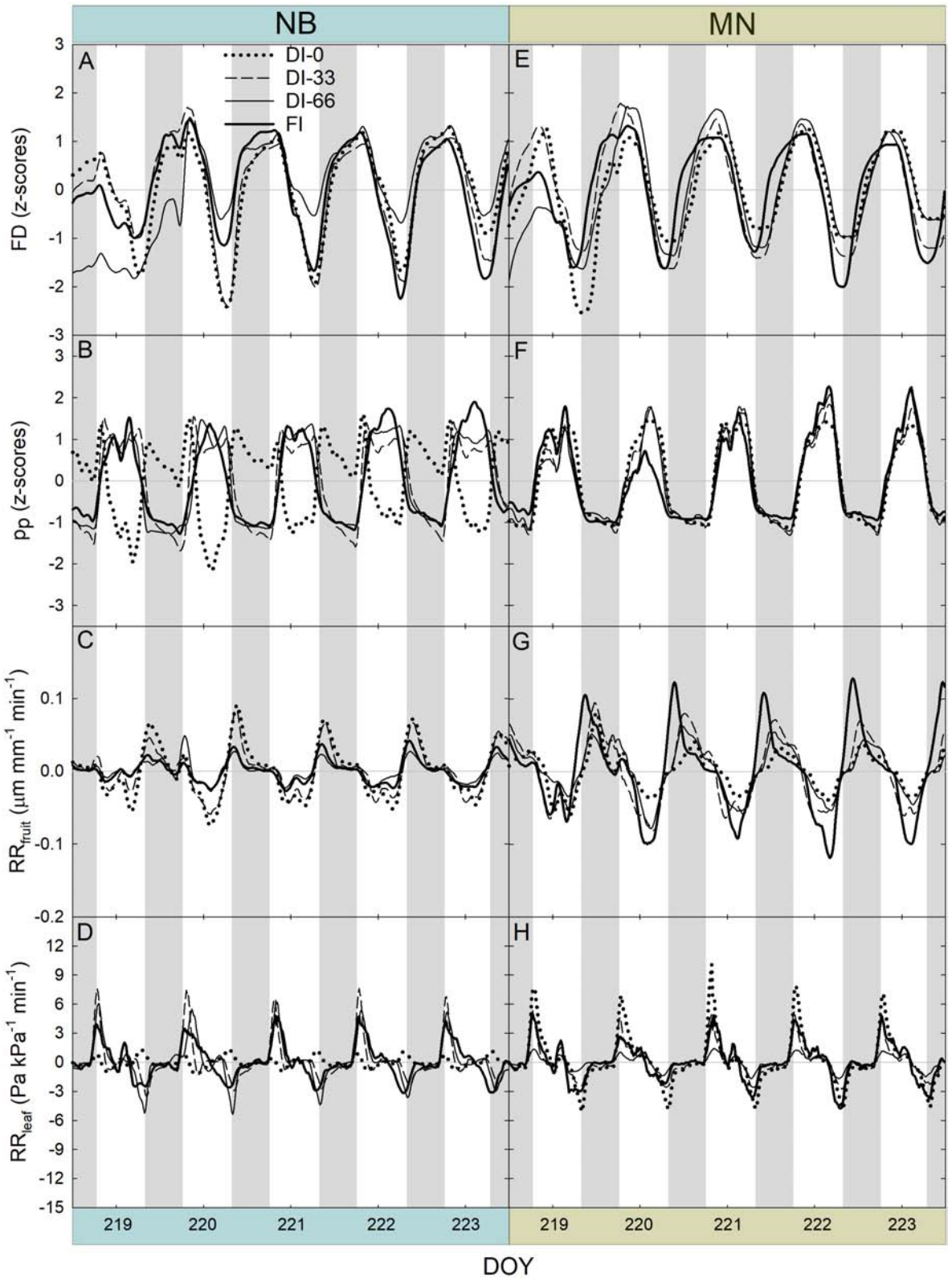

FIGURE 8 | Fruit diameter (FD), leaf patch clamp pressure (p_p), relative rate of fruit diameter change (RR_{fruit}) and relative rate of leaf pressure change (RR_{leaf}) recorded at 15-minute intervals for 5 days during stage II of fruit growth in 'Nocellara del Belice' (NB) **(A–D)** and 'Olivo di Mandanici' (MN) olive trees **(E–H)** under full irrigation (FI), 66% of FI (DI-66), 33% of FI (DI-33) and no irrigation (DI-0). Gray and white areas show nocturnal and diurnal hours, respectively.

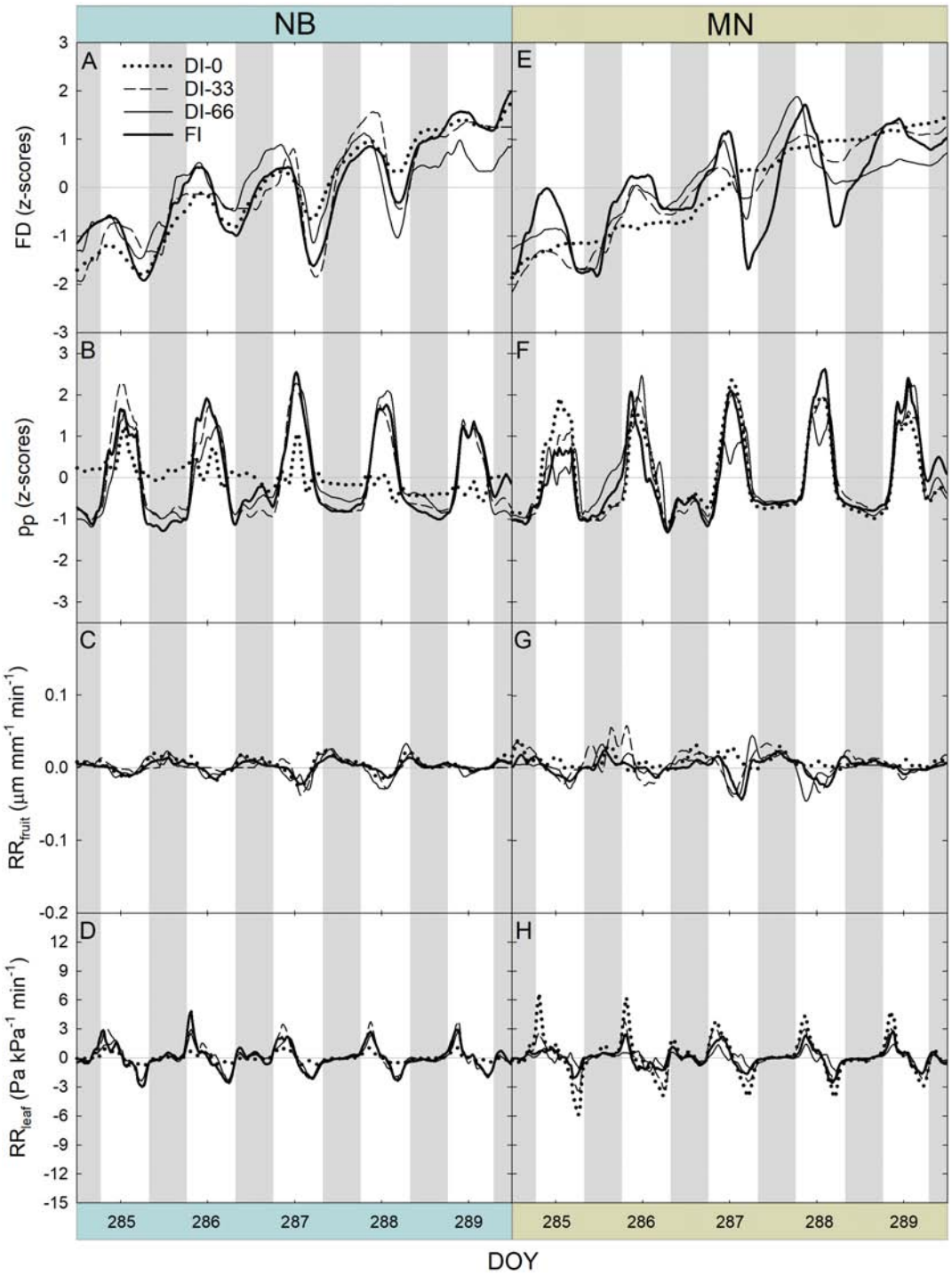

FIGURE 9 | Fruit diameter (FD), leaf patch clamp pressure (p_p), relative rate of fruit diameter change (RR_{fruit}) and relative rate of leaf pressure change (RR_{leaf}) recorded at 15-minute intervals for 5 days during stage III of fruit growth in 'Nocellara del Belice' (NB) **(A–D)** and 'Olivo di Mandanici' (MN) olive trees **(E–H)** under full irrigation (FI), 66% of FI (DI-66), 33% of FI (DI-33) and no irrigation (DI-0). Gray and white areas show nocturnal and diurnal hours, respectively.

(RR_{fruit})/SUM (RR_{leaf})]; ^{u} = nocturnal [MAX(RR_{fruit})/MAX (RR_{leaf})]; ^{v} = nocturnal [RANGE (RR_{fruit})/RANGE (RR_{leaf})]; ^{w} = nocturnal [SUM (RR_{fruit})/SUM (RR_{leaf})]; ^{x} = nocturnal [RSD (RR_{fruit})/RSD (RR_{leaf})]; ^{y} = diurnal [RSD (RR_{fruit})/RSD (RR_{leaf})]; ^{z} = diurnal [MIN (RR_{fruit})/MIN (RR_{leaf})].

A similar highly significant relationship of RSD_{noct} and midday Ψ_{stem} was also observed in nectarine

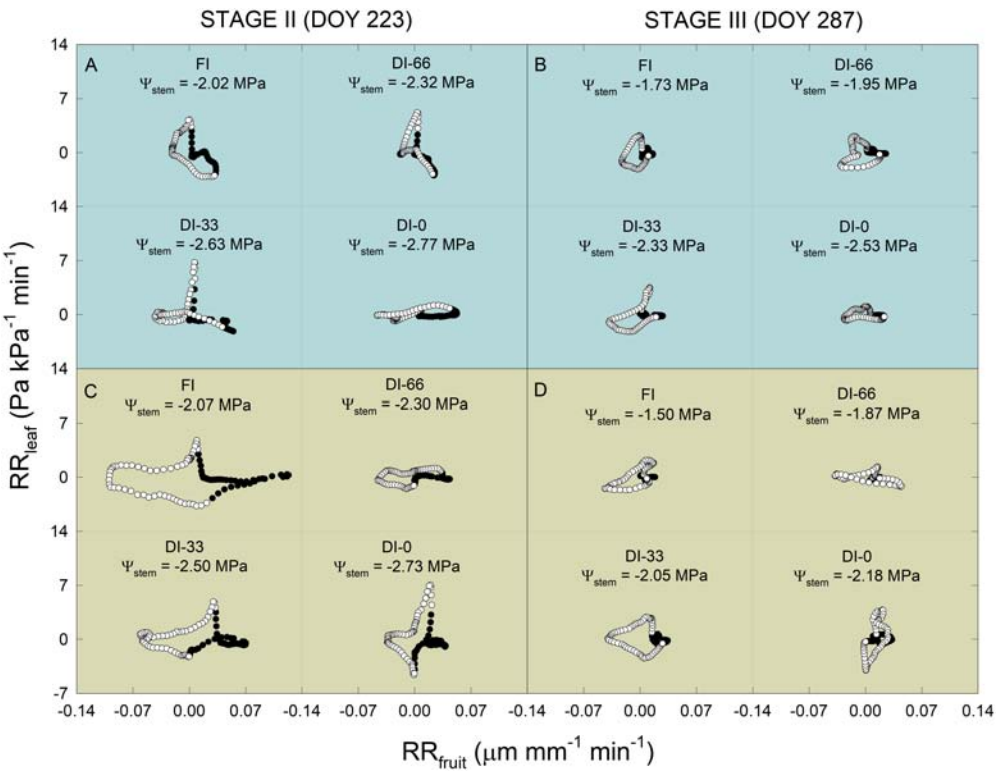

FIGURE 10 | Scatter plots of relative rate of leaf pressure change (RR_{leaf}) vs. relative rate of fruit diameter change (RR_{fruit}) in 'Nocellara del Belice' **(A,B)** and 'Olivo di Mandanici' olive trees **(C,D)** under full irrigation (FI), 66% of FI (DI-66), 33% of FI (DI-33) and no irrigation (DI-0), at 223 (stage II) and 287 (stage III) days of the year (DOY). Midday stem water potential (Ψ_{stem}) reported for each cultivar × DOY × irrigation level combination. White and black circles represent diurnal and nocturnal data in a diel interval, respectively.

(Scalisi et al., 2019c), and in both cases (i.e., olive and nectarine), the relationship of RSD_{noct} to Ψ_{stem} was negative (RSD_{noct} linear components in Eqs. 3, 4), suggesting that the variability of RR_{fruit} at lower Ψ_{stem} is higher than the one of RR_{leaf}. In other words, being the night the fraction of the 24 h at which both fruit and leaf tissues import water, when trees are severely stressed, fruit water import are relatively higher than leaf's when compared to the same relationship in no water-deficit conditions. However, the two olive cultivars under study show different patterns of fruit and leaf water-exchange regulation at other times of the day under increasing water deficit gradients. NB seems to favor fruit water exchanges over leaf's when water deficit increases (**Figure 11A**), as indicated by the wide fluctuations of fruit water in- and out-flows in trees under DI-0 conditions (**Figure 8C**). At the same time, DI-0 leaves reduce their transpiration and water in-flow leading to minimum turgor gain (**Figure 8D**). On the contrary, MN leaf water exchanges become predominant compared to fruit under water deficit conditions, whereas fluctuations of fruit water in- and out-flows are wider than leaf's in FI trees (**Figures 8G,H**, **11B**). This differentiation in the response to drought is likely to be due to both fruit and leaf characteristics. Indeed, the water potential in NB leaves is likely to go negative, as suggested by daily g_s (**Figure 5**) and Ψ_{stem} (**Figures 6A,B**) trends. This leads to a higher loss of leaf cell turgor in NB, despite similar midday Ψ_{stem} to MN (**Figure 7**), as confirmed by the inversion of the p_p curve at 223 DOY (**Figures 8C,D**). In turn, the low turgor leads to a decrease of RR_{leaf} diel fluctuations. The most pronounced loss of turgor in

TABLE 2 | Multivariate analyses of variance (MANOVAs) testing the effects of cultivar, irrigation and the cultivar × irrigation interaction on the ratios of statistical parameters extrapolated from the relative rate of fruit diameter change (RR_{fruit}) and the relative rate of leaf pressure change (RR_{leaf}) at diel, diurnal and nocturnal intervals.

Factor	Time frame	Significance level for Wilk's Lambda test	F
Cultivar	Diel	0.495	0.894
	Diurnal	0.260	1.365
	Nocturnal	0.104	1.991
Irrigation	Diel	0.025	1.965
	Diurnal	0.001	2.783
	Nocturnal	0.238	1.266
Cultivar × Irrigation	Diel	<0.001	5.195
	Diurnal	<0.001	6.515
	Nocturnal	0.031	1.907

Each line represents a single MANOVA based on the following ratios of statistical parameters: MIN = MIN(RR_{fruit})/MIN(RR_{leaf}); MAX = MAX(RR_{fruit})/MAX(RR_{leaf}); SUM = SUM(RR_{fruit})/SUM(RR_{leaf}); RANGE = [(MAX(R_{fruit}) − MIN (RR_{fruit})]/[(MAX(RR_{leaf}) − MIN(RR_{leaf})]; and RSD = RSD(RR_{fruit})/RSD(RR_{leaf}). Significance levels and F shown for each MANOVA.

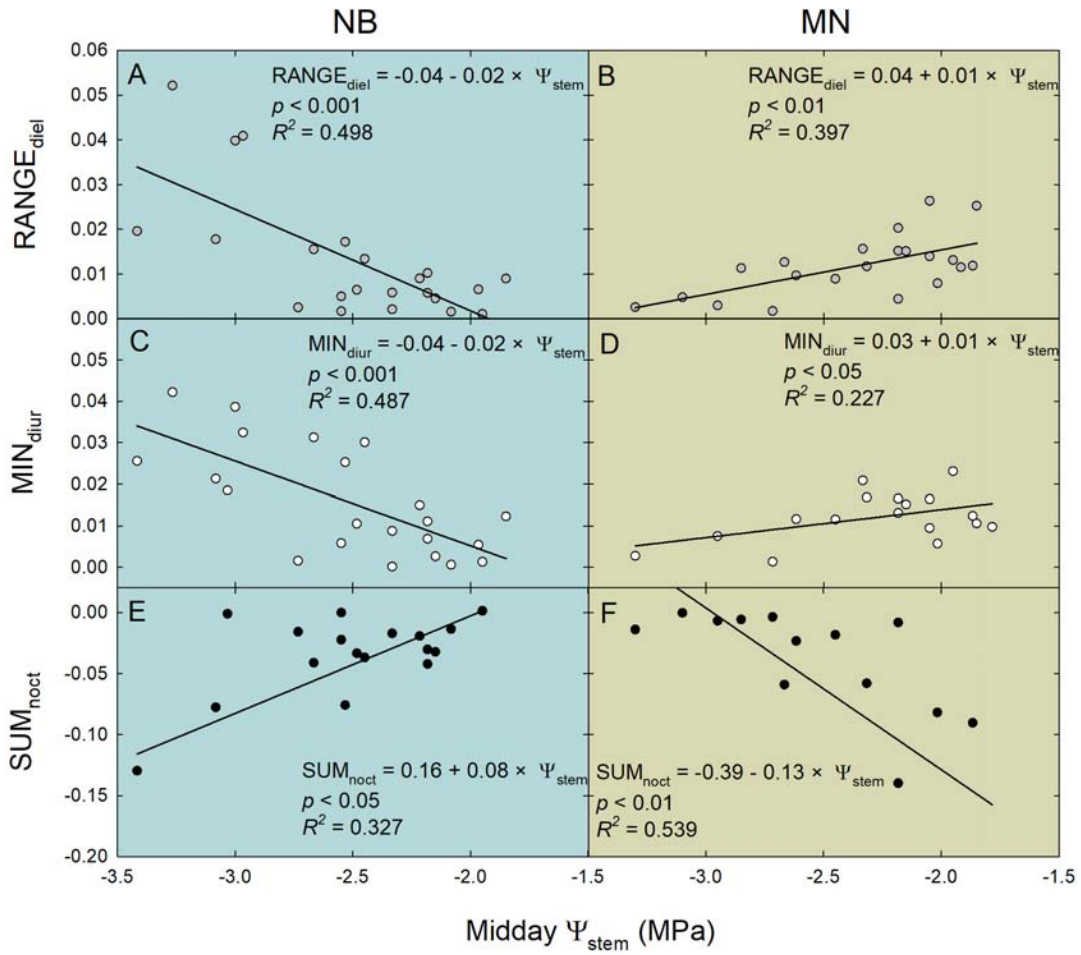

FIGURE 11 | Linear relationships of ratios between the statistical parameters of the relative rate of fruit diameter change (RR_{fruit}) and the relative rate of leaf pressure change (RR_{leaf}) vs. midday stem water potential (Ψ_{stem}). $RANGE_{diel}$ = diel [$RANGE(RR_{fruit})/RANGE(RR_{leaf})$] **(A,B)**; MIN_{diur} = diurnal [$MIN(RR_{fruit})/MIN(RR_{leaf})$] **(C,D)**; SUM_{noct} = nocturnal [$SUM(RR_{fruit})/SUM(RR_{leaf})$] **(E,F)**. Gray, white and black circles represent diel, diurnal and nocturnal data, respectively, for "Nocellara del Belice" (NB) and "Olivo di Mandanici" (MN) olive trees.

NB leaves might also be driven by a lower leaf cell-wall elasticity in this cultivar than in MN, a trait that Bacelar et al. (2009) associated to less drought-tolerant genotypes. Concomitantly, NB fruit increase their RR_{fruit} fluctuations in DI-0 conditions, perhaps driven by high cell-wall elasticity, acting as the main pump of water, fruit-to-leaf vascular flows. The generally significantly higher midday Ψ_{stem} exhibited by MN can also be associated to a relatively higher water potential in the leaves compared to NB, as also in this case stomatal regulation did not differ among irrigation levels. The hypothesized higher leaf osmotic adjustments and cell-wall elasticity in MN under drought may also be confirmed by the low tendency to an inversion of the p_p curve (**Figure 8F**). In addition, the positive relationship between $RANGE_{diel}$ and midday Ψ_{stem} in MN (**Figure 8B**) is determined by the lower fruit water exchanges at DI-0 levels (**Figure 8G**), which may be driven by lower fruit cell-wall elasticity in MN compared to NB.

The different mechanisms in the two cultivars were observed in an -ON year, and it would be interesting to further study tree responses in -OFF years, as Dell'Amico et al. (2012) and Girón et al. (2015) observed that in "Manzanillo" trees crop load influenced the ability of fruit and leaves to act as sinks for water. Changes in osmotic adjustments (Dichio et al., 1997, 2009; Lo Bianco and Scalisi, 2017) and cell-wall elasticity (Xiloyannis et al., 1993; Bacelar et al., 2009) along water deficit gradients have been reported for leaves. However, to the best of our knowledge, no consideration has been previously given to concomitant changes of similar drought tolerance mechanisms in fruit. Divergent physiological responses of fruit and leaf to drought might also be affected by different productive performance, fruit number and tree vigor. At harvest, MN showed significantly higher yield (Y = 7.30 ± 0.60 kg/tree), trunk cross-sectional area (TCSA = 51.3 ± 1.97 cm^2), yield efficiency (YE = 0.14 ± 0.01 kg cm^{-2}) and crop load (CL = 4562 ± 615 n. of fruit) compared to NB (Y = 3.78 ± 0.66 kg/tree, TCSA = 41.37 ± 1.49 cm^2, YE = 0.09 ± 0.01 kg cm^{-2} and CL = 510 ± 100 n. of fruit). The greatly higher number of fruits in MN may represent a

conspicuous water reservoir for the tree and be involved in a buffer effect on plant response to drought. NB compensates its low fruit number with an average fruit water content six-fold higher than MN (data not shown), for a total tree water storage in fruit tissues almost equivalent to MN trees. A divergent evolution of the two genotypes may have favored the development of diversified protective mechanisms that control fruit and leaf water exchanges under drought.

CONCLUSION

The results of this work suggest that overall a lower amount of water can be used for irrigation in MN, as this cultivar tends to lose leaf cell turgor at lower Ψ_{stem} than NB and therefore can be considered a drought-tolerant genotype. The behavior of NB is instead more compatible with drought-avoidance, as leaf stomatal conductance was moderate compared to MN, and in accordance with Scalisi et al. (2019a) who reported an increased root/leaf biomass ratio in NB under drought. Our findings reveal different strategies of fruit and leaf water exchanges in droughted trees, suggesting that olive genotypes can favor the water status of one organ over the other in conditions of water scarcity. The use of genotype-dependent models is therefore essential to determine how leaf and fruit water exchanges can be related to plant water status. These models can provide the basis for an automated modulation of irrigation in response to pre-defined thresholds of water deficit. The two models described in Eqs. 3, 4 can be used for a precise day-by-day assessment of midday Ψ_{stem} in the two cultivars under study, and in -ON years. Future studies should integrate responses from stage I in the multiple regression models.

Overall, this work confirms the advantages of combining fruit and leaf water dynamics for the prediction of plant water status in olive, whose suitability was just confirmed in a nectarine study (Scalisi et al., 2019c). Nevertheless, technologies that sense fruit and leaves water dynamics are still independent and need to be fit in a unique system for real-time monitoring. The use of this combined approach in other fruit species of horticultural interest is highly recommended, despite the complexity of a correct management of a large network of sensors.

DATA AVAILABILITY STATEMENT

The raw data supporting the conclusions of this article will be made available by the authors, without undue reservation, to any qualified researcher.

AUTHOR CONTRIBUTIONS

All authors contributed to conception and design of the study. FM, TC, and RL made available the equipment used in the experiment. AS carried out the field measurements and wrote the first draft of the manuscript. AS and RL performed the statistical analysis. GM, FM, TC, and RL contributed to the data interpretation. All authors contributed to manuscript revision, read and approved the submitted version.

FUNDING

The experiment was supported by a Ph.D. project funded with a scholarship issued by the Italian Ministry of Education and the University of Palermo.

ACKNOWLEDGMENTS

We gratefully acknowledge the technical support and field assistance provided by Federico Costa, Silvia Fretto, Laura Macaluso, Filipa Simões Grilo, Placido Volo, and the scientific support of Luca Corelli Grappadelli and Bartolomeo Dichio. This research was partly supported by a Ph.D. project funded with a scholarship issued by the Italian Ministry of Education and the University of Palermo.

REFERENCES

Allen, R. G., Pereira, L. S., Raes, D., and Smith, M. (1998). *Crop Evapotranspiration-Guidelines for Computing Crop Water Requirements-FAO Irrigation and Drainage Paper 56*. Rome: FAO.

Bacelar, E. A., Correia, C. M., Moutinho-Pereira, J. M., Gonçalves, B. C., Lopes, J. I., and Torres-Pereira, J. M. (2004). Sclerophylly and leaf anatomical traits of five field-grown olive cultivars growing under drought conditions. *Tree physiol.* 24, 233–239. doi: 10.1093/treephys/24.2.233

Bacelar, E. A., Moutinho-Pereira, J. M., Gonçalves, B. C., Lopes, J. I., and Correia, C. M. (2009). Physiological responses of different olive genotypes to drought conditions. *Acta Physiol. Plant* 31, 611–621. doi: 10.1007/s11738-009-0272-9

Bacelar, E. A., Santos, D. L., Moutinho-Pereira, J. M., Gonçalves, B. C., Ferreira, H. F., and Correia, C. M. (2006). Immediate responses and adaptative strategies of three olive cultivars under contrasting water availability regimes: changes on structure and chemical composition of foliage and oxidative damage. *Plant Sci.* 170, 596–605. doi: 10.1016/j.plantsci.2005.10.014

Ben-Gal, A., Kool, D., Agam, N., van Halsema, G. E., Yermiyahu, U., Yafe, A., et al. (2010). Whole-tree water balance and indicators for short-term drought stress in non-bearing 'Barnea' olives. *Agric. Water Manag.* 98, 124–133. doi: 10.1016/j.agwat.2010.08.008

Connor, D. J. (2005). Adaptation of olive (*Olea europaea* L.) to water-limited environments. *Aust. J. Agric. Res.* 56, 1181–1189. doi: 10.1071/AR05169

Cuevas, M. V., Torres-Ruiz, J. M., Álvarez, R., Jiménez, M. D., Cuerva, J., and Fernández, J. E. (2010). Assessment of trunk diameter variation derived indices as water stress indicators in mature olive trees. *Agric. Water Manag.* 97, 1293–1302. doi: 10.1016/j.agwat.2010.03.011

Dell'Amico, J., Moriana, A., Corell, M., Girón, I. F., Morales, D., Torrecillas, A., et al. (2012). Low water stress conditions in table olive trees (*Olea europaea* L.) during pit hardening produced a different response of fruit and leaf water relations. *Agric. Water Manag.* 114, 11–17. doi: 10.1016/j.agwat.2012.06.004

Dichio, B., Margiotta, G., Xiloyannis, C., Bufo, S. A., Sofo, A., and Cataldi, T. R. (2009). Changes in water status and osmolyte contents in leaves and roots of olive plants (*Olea europaea* L.) subjected to water deficit. *Trees* 23, 247–256. doi: 10.1007/s00468-008-0272-1

Dichio, B., Nuzzo, V., Xiloyannis, C., Celano, G., and Angelopoulos, K. (1997). Drought stress-induced variation of pressure-volume relationships in *Olea europaea* L. Cv. "Coratina". *Acta Hortic.* 449, 401–410. doi: 10.17660/ActaHortic.1997.449.56

Dichio, B., Xiloyannis, C., Angelopoulos, K., Nuzzo, V., Bufo, S. A., and Celano, G. (2003). Drought-induced variations of water relations parameters in *Olea europaea*. *Plant Soil* 257, 381–389. doi: 10.1023/a:1027392831483

Ehrenberger, W., Rüger, S., Rodríguez−Domínguez, C. M., Díaz−Espejo, A., Fernández, J. E., Moreno, J., et al. (2012). Leaf patch clamp pressure probe measurements on olive leaves in a nearly turgorless state. *Plant Biol.* 14, 666–674. doi: 10.1111/j.1438-8677.2011.00545.x

Ennajeh, M., Vadel, A. M., Cochard, H., and Khemira, H. (2010). Comparative impacts of water stress on the leaf anatomy of a drought-resistant and a drought-sensitive olive cultivar. *J. Hortic. Sci. Biotechnol.* 85, 289–294. doi: 10.1080/14620316.2010.11512670

Fernandes, R. D. M., Cuevas, M. V., Diaz-Espejo, A., and Hernandez-Santana, V. (2018). Effects of water stress on fruit growth and water relations between fruits and leaves in a hedgerow olive orchard. *Agric. Water Manag.* 210, 32–40. doi: 10.1016/j.agwat.2018.07.028

Fernández, R. D. M., Cuevas, M. V., Hernandez-Santana, V., Rodriguez-Dominguez, C. M., Padilla-Díaz, C. M., and Fernández, J. E. (2017). Classification models for automatic identification of daily states from leaf turgor related measurements in olive. *Comput. Electron. Agric.* 142, 181–189. doi: 10.1016/j.compag.2017.09.005

Fernández, J. E. (2014). Plant-based sensing to monitor water stress: Applicability to commercial orchards. *Agric. Water Manag.* 142, 99–109. doi: 10.1016/j.agwat.2014.04.017

Fernández, J. E. (2017). Plant-based methods for irrigation scheduling of woody crops. *Horticulturae* 3:35. doi: 10.3390/horticulturae3020035

Fernández, J. E., Díaz-Espejo, A., Infante, J. M., Durán, P., Palomo, M. J., Chamorro, V., et al. (2006). Water relations and gas exchange in olive trees under regulated deficit irrigation and partial rootzone drying. *Plant Soil* 284, 273–291. doi: 10.1007/s11104-006-0045-9

Fernández, J. E., Rodriguez-Dominguez, C. M., Perez-Martin, A., Zimmermann, U., Rüger, S., Martín-Palomo, M. J., et al. (2011a). Online-monitoring of tree water stress in a hedgerow olive orchard using the leaf patch clamp pressure probe. *Agric. Water Manag.* 100, 25–35. doi: 10.1016/j.agwat.2011.08.015

Fernández, J. E., Torres-Ruiz, J. M., Díaz-Espejo, A., Montero, A., Álvarez, R., Jiménez, M. D., et al. (2011b). Use of maximum trunk diameter measurements to detect water stress in mature 'Arbequina' olive trees under deficit irrigation. *Agric. Water Manag.* 98, 1813–1821. doi: 10.1016/j.agwat.2011.06.011

Girón, I. F., Corell, M., Galindo, A., Torrecillas, E., Morales, D., Dell'Amico, J., et al. (2015). Changes in the physiological response between leaves and fruits during a moderate water stress in table olive trees. *Agric. Water Manag.* 148, 280–286. doi: 10.1016/j.agwat.2014.10.024

Gucci, R., Grimelli, A., Costagli, G., Tognetti, R., Minnocci, A., and Vitagliano, C. (2000). Stomatal characteristics of two olive cultivars "Frantoio" and "Leccino". *Acta Hortic.* 586, 541–544. doi: 10.17660/ActaHortic.2002.586.113

Karamanos, A. J. (1984). "Ways of detecting adaptive responses of cultivated plants to drought. An agronomic approach," in *Being Alive On Land. Tasks For Vegetation Science*, Vol. 13, eds N. S. Margaris, M. Arianoustou-Faraggitaki, and W. C. Oechel, (Dordrecht: Springer), 91–101. doi: 10.1007/978-94-009-6578-2_12

Lo Bianco, R., and Scalisi, A. (2017). Water relations and carbohydrate partitioning of four greenhouse-grown olive genotypes under long-term drought. *Trees* 31, 717–727. doi: 10.1007/s00468-016-1502-6

Marino, G., Caruso, T., Ferguson, L., and Marra, F. P. (2018). Gas exchanges and stem water potential define stress thresholds for efficient irrigation management in olive (*Olea europea* L.). *Water* 10, 342. doi: 10.3390/w10030342

Marino, G., Macaluso, L., Grilo, F., Marra, F. P., and Caruso, T. (2019). Toward the valorization of olive (*Olea europaea* var. *europaea* L.) biodiversity: horticultural performance of seven Sicilian cultivars in a hedgerow planting system. *Sci. Hortic.* 256:108583. doi: 10.1016/j.scienta.2019.108583

Marino, G., Macaluso, L., Marra, F. P., Ferguson, L., Marchese, A., Campisi, G., et al. (2017). Horticultural performance of 23 Sicilian olive genotypes in hedgerow systems: vegetative growth, productive potential and oil quality. *Sci. Hortic.* 217, 217–225. doi: 10.1016/j.scienta.2017.01.046

Marino, G., Pernice, F., Marra, F. P., and Caruso, T. (2016). Validation of an online system for the continuous monitoring of tree water status for sustainable irrigation managements in olive (*Olea europaea* L.). *Agric. Water Manag.* 177, 298–307. doi: 10.1016/j.agwat.2016.08.010

Morandi, B., Manfrini, L., Zibordi, M., Noferini, M., Fiori, G., and Corelli Grappadelli, L. (2007). A low-cost device for accurate and continuous measurements of fruit diameter. *HortScience* 42, 1380–1382. doi: 10.21273/hortsci.42.6.1380

Moreno, F., Conejero, W., Martín-Palomo, M. J., Girón, I. F., and Torrecillas, A. (2006). Maximum daily trunk shrinkage reference values for irrigation scheduling in olive trees. *Agric. Water Manag.* 84, 290–294. doi: 10.1016/j.agwat.2006.03.005

Moriana, A., and Fereres, E. (2002). Plant indicators for scheduling irrigation of young olive trees. *Irrig. Sci.* 21, 83–90. doi: 10.1007/s00271-001-0053-8

Moriana, A., Pérez-López, D., Prieto, M. H., Ramírez-Santa-Pau, M., and Pérez-Rodriguez, J. M. (2012). Midday stem water potential as a useful tool for estimating irrigation requirements in olive trees. *Agric. Water Manag.* 112, 43–54. doi: 10.1016/j.agwat.2012.06.003

Padilla-Díaz, C. M., Rodriguez-Dominguez, C. M., Hernandez-Santana, V., Perez-Martin, A., and Fernández, J. E. (2016). Scheduling regulated deficit irrigation in a hedgerow olive orchard from leaf turgor pressure related measurements. *Agric. Water Manag.* 164, 28–37. doi: 10.1016/j.agwat.2015.08.002

Parent, B., Hachez, C., Redondo, E., Simonneau, T., Chaumont, F., and Tardieu, F. (2009). Drought and abscisic acid effects on aquaporin content translate into changes in hydraulic conductivity and leaf growth rate: a trans-scale approach. *Plant Physiol.* 149, 2000–2012. doi: 10.1104/pp.108.130682

Patakas, A., and Noitsakis, B. (1997). Cell wall elasticity as a mechanism to maintain favorable water relations during leaf ontogeny in grapevines. *Am. J. Enol. Viticult.* 48, 352–356.

Rodriguez-Dominguez, C. M., Ehrenberger, W., Sann, C., Rüger, S., Sukhorukov, V., Martín-Palomo, M. J., et al. (2012). Concomitant measurements of stem sap flow and leaf turgor pressure in olive trees using the leaf patch clamp pressure probe. *Agric. Water Manag.* 114, 50–58. doi: 10.1016/j.agwat.2012.07.007

Rodriguez-Dominguez, C. M., Hernandez-Santana, V., Buckley, T. N., Fernández, J. E., and Diaz-Espejo, A. (2019). Sensitivity of olive leaf turgor to air vapour pressure deficit correlates with diurnal maximum stomatal conductance. *Agric. Forest Meteorol.* 272, 156–165. doi: 10.1016/j.agrformet.2019.04.006

Savitzky, A., and Golay, M. J. (1964). Smoothing and differentiation of data by simplified least squares procedures. *Anal. Chem.* 36, 1627–1639. doi: 10.1021/ac60214a047

Scalisi, A., Bresilla, K., and Simões Grilo, F. (2017). Continuous determination of fruit tree water-status by plant-based sensors. *Italus Hortus* 24, 39–50. doi: 10.26353/j.itahort/2017.2.3950

Scalisi, A., Marra, F. P., Caruso, T., Illuminati, C., Costa, F., and Lo Bianco, R. (2019a). Transpiration rates and hydraulic conductance of two olive genotypes with different sensitivity to drought. *Acta Hortic.* 1253, 421–428. doi: 10.17660/ActaHortic.2019.1253.55

Scalisi, A., O'Connell, M. G., Lo Bianco, R., and Stefanelli, D. (2019b). Continuous detection of new plant water status indicators in stage I of nectarine fruit growth. *Acta Hortic.* 1253, 9–16. doi: 10.17660/ActaHortic.2019.1253.2

Scalisi, A., O'Connell, M. G., Stefanelli, D., and Lo Bianco, R. (2019c). Fruit and leaf sensing for continuous detection of nectarine water status. *Front. Plant Sci.* 10:805. doi: 10.3389/fpls.2019.00805

Tognetti, R., Raschi, A., Béres, C., Fenyvesi, A., and Ridder, H. W. (1996). Comparison of sap flow, cavitation and water status of *Quercus petraea* and *Quercus cerris* trees with special reference to computer tomography. *Plant Cell Environ.* 19, 928–938. doi: 10.1111/j.1365-3040.1996.tb00457.x

Turner, N. C. (1988). Measurement of plant water status by the pressure chamber technique. *Irrig. Sci.* 9, 289–308. doi: 10.1007/bf00296704

Xiloyannis, C., Dichio, B., and Nuzzo, V. (1993). "Meccanismi di risposta dell'olivo alla carenza idrica," *Atti del convegno Tecniche, Norme e Qualitá in Olivicoltura*. Potenza, Italy: 123–136.

Zimmermann, D., Reuss, R., Westhoff, M., Geßner, P., Bauer, W., Bamberg, E., et al. (2008). A novel, non-invasive, online-monitoring, versatile and easy plant-based probe for measuring leaf water status. *J. Exp. Bot.* 59, 3157–3167. doi: 10.1093/jxb/ern171

Conflict of Interest: The authors declare that the research was conducted in the absence of any commercial or financial relationships that could be construed as a potential conflict of interest.

frontiers in Plant Science

ORIGINAL RESEARCH
published: 14 April 2020
doi: 10.3389/fpls.2020.00387

Water Stable Isotopes in Ecohydrological Field Research: Comparison Between *In Situ* and Destructive Monitoring Methods to Determine Soil Water Isotopic Signatures

Angelika Kübert[1]†, Sinikka Paulus[1,2†], Adrian Dahlmann[1], Christiane Werner[1], Youri Rothfuss[3], Natalie Orlowski[4‡] and Maren Dubbert[1‡]*

[1] Ecosystem Physiology, University of Freiburg, Freiburg, Germany, [2] Department of Biogeochemical Integration, Max Planck Institute for Biogeochemistry, Jena, Germany, [3] Institute of Bio- and Geosciences, Agrosphere Institute (IBG-3), Jülich, Germany, [4] Chair of Hydrology, University of Freiburg, Freiburg, Germany

OPEN ACCESS

Edited by:
Pietro Franceschi, Fondazione Edmund Mach, Italy

Reviewed by:
Xiaoying Gong, Fujian Normal University, China
Xuefa Wen, Chinese Academy of Sciences (CAS), China

***Correspondence:**
Angelika Kübert
angelika.kuebert@cep.uni-freiburg.de

†These authors have contributed equally to this work

‡These authors share senior authorship

Specialty section:
This article was submitted to Technical Advances in Plant Science, a section of the journal Frontiers in Plant Science

Received: *10 September 2019*
Accepted: *18 March 2020*
Published: *14 April 2020*

Citation:
Kübert A, Paulus S, Dahlmann A, Werner C, Rothfuss Y, Orlowski N and Dubbert M (2020) Water Stable Isotopes in Ecohydrological Field Research: Comparison Between In Situ and Destructive Monitoring Methods to Determine Soil Water Isotopic Signatures. Front. Plant Sci. 11:387. doi: 10.3389/fpls.2020.00387

Ecohydrological isotope based field research is often constrained by a lack of temporally explicit soil water data, usually related to the choice of destructive sampling in the field and subsequent analysis in the laboratory. New techniques based on gas permeable membranes allow to sample soil water vapor *in situ* and infer soil liquid water isotopic signatures. Here, a membrane-based *in situ* soil water vapor sampling method was tested at a grassland site in Freiburg, Germany. It was further compared with two commonly used destructive sampling approaches for determination of soil liquid water isotopic signatures: cryogenic vacuum extraction and centrifugation. All methods were tested under semi-controlled field conditions, conducting an experiment with dry-wet cycling and two isotopically different labeling irrigation waters. We found mean absolute differences between cryogenic vacuum extraction and *in situ* vapor measurements of 0.3–14.2‰ ($\delta^{18}O$) and 0.4–152.2‰ ($\delta^{2}H$) for soil liquid water. The smallest differences were found under natural abundance conditions of ^{2}H and ^{18}O, the strongest differences were observed after irrigation with labeled waters. Labeling strongly increased the isotopic variation in soil water: Mean soil water isotopic signatures derived by cryogenic vacuum extraction were -11.6 ± 10.9‰ ($\delta^{18}O$) and +61.9 ± 266.3‰ ($\delta^{2}H$). The *in situ* soil water vapor method showed isotopic signatures of -12.5 ± 9.4‰ ($\delta^{18}O$) and +169.3 ± 261.5‰ ($\delta^{2}H$). Centrifugation was unsuccessful for soil samples due to low water recovery rates. It is therefore not recommended. Our study highlights that the *in situ* soil water vapor method captures the temporal dynamics in the isotopic signature of soil water well while the destructive approach also includes the natural lateral isotopic heterogeneity. The different advantages and limitations of the three methods regarding

setup, handling and costs are discussed. The choice of method should not only consider prevailing environmental conditions but the experimental design and goal. We see a very promising tool in the *in situ* soil water vapor method, capturing both temporal developments and spatial variability of soil water processes.

Keywords: *in situ* soil water vapor sampling technique, cryogenic vacuum extraction, centrifugation, water stable isotopes, soil water, ecohydrology

INTRODUCTION

Water stable isotopes (^{2}H and ^{18}O) are considered as ideal tracers to study water fluxes within the soil-plant-atmosphere continuum (Rothfuss and Javaux, 2017; Dubbert and Werner, 2019). In order to retrieve the water isotopic signature of soil water, soil material is predominantly sampled destructively and containing water extracted in the laboratory (Orlowski et al., 2016b). The most commonly used methods are cryogenic vacuum extraction, centrifugation or high pressure mechanical squeezing, but also new methods such as microwave extraction and direct vapor equilibration have been developed and compared (Orlowski et al., 2016b). These destructive methods, however, are very limited in terms of data point sampling and therewith restrict the study of ecohydrological processes. Berry et al. (2018) addressed the methodological state of the art in stable isotope ecohydrology as "shotgun" or "snapshot methods", referring to the lack of continuous measurements. Laboratory based water extraction methods are currently highly debated due to their inaccuracy and non-comparability of the obtained isotope results (Orlowski et al., 2019). Issues observed with laboratory based methods are mainly due to interferences with soil texture, water contents, interactions with cations, and the different pore spaces that may or may not be extracted via the different approaches (Meißner et al., 2014; Oerter et al., 2014; Orlowski et al., 2016b, 2018).

Several authors have addressed the lack of methodological consistency in water stable isotope research and called for an improvement of spatial and temporal resolution of soil pore water, vapor fluxes and plant transpiration measurements (Vereecken et al., 2015; Volkmann et al., 2016b; Berry et al., 2018; Dubbert and Werner, 2019). Techniques based on laser spectroscopy allow to measure online and *in situ* water vapor isotopic signature at high precision and frequency (Helliker and Noone, 2010; Werner et al., 2012). Combining laser spectroscopy with other techniques also allows for measuring different water compartments and fluxes at high temporal resolution, such as soil pore water (e.g., Rothfuss et al., 2013; Volkmann and Weiler, 2014; Gaj et al., 2016), xylem water (Volkmann et al., 2016a) or transpiration (Wang et al., 2012; Simonin et al., 2013; Dubbert et al., 2017). Microporous polypropylene membranes, for instance, enabled the sampling of soil water vapor isotope compositions *in situ* and non-destructively once installed (Rothfuss et al., 2013; Volkmann and Weiler, 2014; Gaj et al., 2016).

So far, this *in situ* soil water vapor technique has been mainly applied for continuous measurements under controlled laboratory conditions (Rothfuss et al., 2015; Quade et al., 2018), or on short timescales in the field (maximum 11 consecutive days) (Gaj et al., 2016; Volkmann et al., 2016b) and only few times during long-term experiments under field conditions (Oerter et al., 2017; Quade et al., 2019). Despite few applications, the potential of *in situ* long-term monitoring experiments has been addressed by numerous studies and reviews within the field of ecohydrology (Sprenger et al., 2015, 2019; Berry et al., 2018; Penna et al., 2018; Stumpp et al., 2018). With continuous *in situ* isotope measurements of soil and xylem water vapor, Volkmann et al. (2016a), for instance, were able to show how different tree species under drought varied in their reaction toward an artificial precipitation pulse. Their results showed that the response was visible within one to four hours after the irrigation event and that the travel times were species specific. More experiments of this type are needed in order to evaluate the relevance of the observed patterns for different soil and vegetation types and over longer time scales. In particular, high uncertainties exist concerning the reaction of ecosystems in dry conditions with low soil water availability when plants need to optimize cost and benefit between transpiration and biomass production (Schymanski et al., 2008). An enhanced understanding of these processes would open the path to improve physically based modeling approaches of actual and future water fluxes of different ecohydrological compartments (Rothfuss and Javaux, 2017). Furthermore, it could help to develop management and conservation strategies to sustain water resources as well as augment eco- and agricultural system resilience (Mahindawansha et al., 2018; Penna et al., 2018). In particular, the management and conservation of grasslands are of economic and ecological interest. They provide important ecosystem services such as biodiversity conservation and carbon storage (White et al., 2000; Millennium Ecosystem Assessment, 2005; Stoate et al., 2009; Schnyder et al., 2010; Maestre et al., 2012). Global change induced threats such, as extreme drought or heavy rainfall can, however, substantially threat their stable functioning and hence the provided ecosystem services (Habel et al., 2013; IPBES, 2018).

The central objective of our study was the comparison between *in situ* and destructive estimates of soil water isotopic signatures observed in a semi-controlled field experiment at a grassland site (Freiburg, Germany). The applied *in situ* method was a membrane based monitoring method developed by Rothfuss et al. (2013) for soil water vapor. We compared the *in situ* water vapor method for soil water with the two commonly used destructive soil water sampling approaches – cryogenic vacuum extraction and centrifugation. We characterized the temporal dynamics of the isotopic signature of soil water in different soil depths.

We tested the three approaches under (semi-controlled) field conditions by conducting an experiment with dry-wet cycling and isotopically labeled water in order to test their application (i) under varying micrometeorological conditions, (ii) for different soil water contents, and (iii) for different ranges of isotopic signature (natural and labeled abundance). For this purpose, we artificially created water limited conditions (14 days) under isotopic natural abundance conditions, and subsequently applied two severe rain pulses (20 mm per 70 min and 35 mm per 90 min), each followed by a period of drought (12 and 18 days). The two pulses differed in their isotopic signatures, one pulse being strongly depleted in both isotopologues (^{18}O and ^{2}H) and one pulse being heavily deuterated relative to natural abundance.

The different advantages and limitations of the three methods are discussed in detail (including not only their accuracy but also related expenses of time and costs for setup and use) in order to enhance future consideration about methodological approaches to address ecohydrological and soil water processes related questions.

MATERIALS AND METHODS

The measured or inferred values of water hydrogen and oxygen stable isotopic ratios are reported relative to the values of the Vienna Standard Mean Ocean Water and expressed as isotopic signatures (respectively, δ^2H and $\delta^{18}O$) in per mill (‰) (Gonfiantini, 1978). All isotopic analysis was performed with a cavity ring-down laser spectroscope (L2130-i; Picarro, Santa Clara, United States).

Study Site

The study was performed at the experimental research site Freiburg Flugplatz in South West Germany at 238 m a.s.l. (48°1′22″N; 7°49′57″O). The site represents a temperate, perennial grassland with ruderal vegetation. Mean annual temperature is 11.4°C and mean annual rainfall is 662.1 mm (reference period 1988–2017, Deutscher Wetterdienst [DWD], 2018). The soil is classified as a skeleton-rich Anthrosol on former fluvial deposition and displays pronounced differences between soil horizons. Top layer is brown earth (0–10 cm), followed by a sandy, medium grain gravel layer (10–35 cm) with consolidated clay beneath 40 cm depth. Between 0 and 40 cm depth, soil texture consisted of 37.8% sand, 48.6% silt, and 13.7% clay. Porosities in the soil ranged between 57% in the topsoil and 36% in the gravel layer (K. Kühnhammer, personal communication). Dominant species during the time of our experiment were *Agrostis tenuis* L., *Carex hirta* L. and *C. jacea.*

Generating Varying Soil Water Contents and Isotopic Signatures

Different water contents and isotopic signature values were imposed in the soil profile by excluding natural precipitation and simulating irrigation events. For this, we installed a plot of 4 m × 3 m inner size which could be covered up by a transparent rainout shelter in 145 to 210 cm height above the canopy. These shelters included a buffering zone of approximately 100 cm at each side to prevent subsurface lateral flow from adjacent soil. First measurements started on June 15, 2018. Natural precipitation was excluded from the plot after June 7, 2018. Shelters were set up exclusively before forecasted rain events.

Irrigation events took place on June 20 and July 2 in the late evening (22:00–23:10; 22:00–23.30 CET, respectively). The water of the first irrigation event (referred to as "label 1") was labeled with $\delta^{18}O = -56.9 \pm 0.8‰$ and $\delta^{2}H = -181.7 \pm 5.2‰$ and simulated a rain event of 20 mm per 70 min. The water of the second irrigation event (referred to as "label 2", deuterated) was labeled with $\delta^{18}O = -10.3 \pm 0.2‰$ and $\delta^{2}H = +396.0 \pm 16.4‰$ and simulated a rain event of 35 mm per 90 min. The chosen irrigation amounts correspond to rain events classified as "severe precipitation events" and "storm warning", respectively, according to the classification of the German Meteorological Service DWD. Irrigation was performed at night to minimize evaporative losses during tracer application. Irrigation was applied by moving, 1 m above the plot in regular intervals, a 3 m long tubing, perforated each centimeter with a 1/16″ diameter tube.

In the following, the three experimental phases will be distinguished according to the irrigation events, i.e., between natural abundance, label 1 and label 2. The time is expressed in Day after Labeling (after label 1, DaL), i.e., natural abundance (before labeling, DaL = 0), label 1 (DaL 1–12) and label 2 (DaL 12–30). During all phases, natural precipitation was excluded by setting up a shelter before forecasted events.

Micrometeorological Data

Environmental data were collected throughout the whole experiment. Photosynthetic photon flux density (S-LIA-M003, Onset, Bourne, MA, United States), air temperature and relative humidity (S-THB-M008, Onset, Bourne, MA, United States) were measured in a distance of 10 m from the experimental site in 1 m height above ground and logged as five-minute averages (HOBOH21-002 U30, Onset, Bourne, MA, United States). Natural bulk precipitation was sampled by a self-built precipitation collector. The collector consisted of glass funnel (diameter 80 cm^2, at 1 m height above ground level) which was connected by an insulated PTFE (Polytetrafluoroethylene) tube to a glass bottle, buried in the ground. In the funnel, a coarse filter mesh was used to prevent contamination as much as possible. Bulk water samples were collected after each rain event, filtered to remove organic compounds (glass fiber, retention capacity 1–2 μm, KC98.1, Roth, Karlsruhe, Germany) and their isotopic signatures determined.

Soil Water Content and Soil Temperature Measurements

Volumetric soil water contents (10 HS Decagon Devices, WA, United States) and soil temperatures (T108, Campbell Scientific, Logan, UT, United States) were monitored in −2, −5, −20 and −40 cm depth (n = 3). Sensors were set up on March 26–12 weeks before measurement start (June 15) – in order to minimize the impact on the vegetation cover. A 60 cm × 50 cm hole was excavated, and sensors were installed in the wall

of the undisturbed soil. Soil excavation material was carefully emplaced trying to imitate original stratifications and eliminate the formation of preferential flow pathways. Sensor data was stored as five-minute averages with a data logger (CR1000, Campbell Scientific, Logan, UT, United States). The soil water content sensors' readings were calibrated against values obtained gravimetrically from destructive sampling. Soil gravimetric water content was converted to volumetric water content by taking the soil dry bulk density (1.4 ± 0.2 g/cm^3) into account.

In Situ Isotopic Measurements of Soil Pore Water

Setup and Data Collection

The isotopic signature (δ_{S_v}, i.e., δ^2H and δ^{18}O in ‰) and mixing ratio of soil water vapor (MR, i.e., the ratio of the mass of soil water vapor to the mass of dry air in a given volume in ppm) were measured non-destructively on a daily basis between 8:30 AM and 19:00 CET in −2, −5, −20 and −40 cm depth (n = 3), at the same depth as soil water content and temperature sensors were installed (**Figure 1**). It was done by following the method of Rothfuss et al. (2013), i.e., by sampling the water vapor intruding a piece of gas permeable (GP) microporous polypropylene tubes (Accurel GP V8/2HF, 3M, Germany; 0.155 cm wall thickness, 0.55 cm i.d., 0.86 cm o.d.) inserted in the soil. The water vapor contained in the tube eventually reaches isotopic thermodynamic equilibrium, i.e., has an isotopic signature function of that of liquid water and soil temperature (Majoube, 1971; Horita and Wesolowski, 1994). The soil water vapor is then flushed at a flow with dry synthetic air and directed toward the laser spectroscope for online determination of its isotopic signature.

GP tubes were installed on March 26 at the three sides of the excavated hole. During installation of the setup, two belowground connections of GP tubes were damaged (replicate 3, depths −2 and −40 cm) and, therefore, excluded from the experiment. The final setup comprised a total of 10 observation depths for δ_{S_v}. The GP tubes were of 20 cm length (54.0 cm^2 outer, 34.6 cm^2 inner surface area, 4.8 cm^3 inner volume) and extended at both ends with insulated PFA (Perfluoroalkoxy alkanes) and PTFE (Polytetrafluoroethylene) tubing systems (1/4″ and 1/8″). Dry synthetic air (Messer, Bad Soden, Germany) flow introduced to the tubes' inlet could be distributed via electric valve manifolds (Oxygen Clean Manifold, Clippard Instruments, OH, United States) to a desired tube section from which the respective water vapor sample was directed to the laser spectroscope. Air flow was controlled by a Mass Flow Controller (MFC; model FC-260, Tylan, Torrance, CA, United States with a read-out box RO-7010).

δ_{S_v} of each GP tube was determined on a daily basis between 8:30 AM and 19:00 CET by directing synthetic dry air into the GP tubes at an average flow rate of 110 ml min^{-1}. Before measurements, valve boxes and gas lines (excluding the GP soil gas sampling tubes) were flushed with synthetic dry air via bypass lines at a flow rate of 300 to 700 ml min^{-1} to evacuate water vapor or condensed droplets of previous measurements in the sampling system. In wet measurement periods (relative humidity

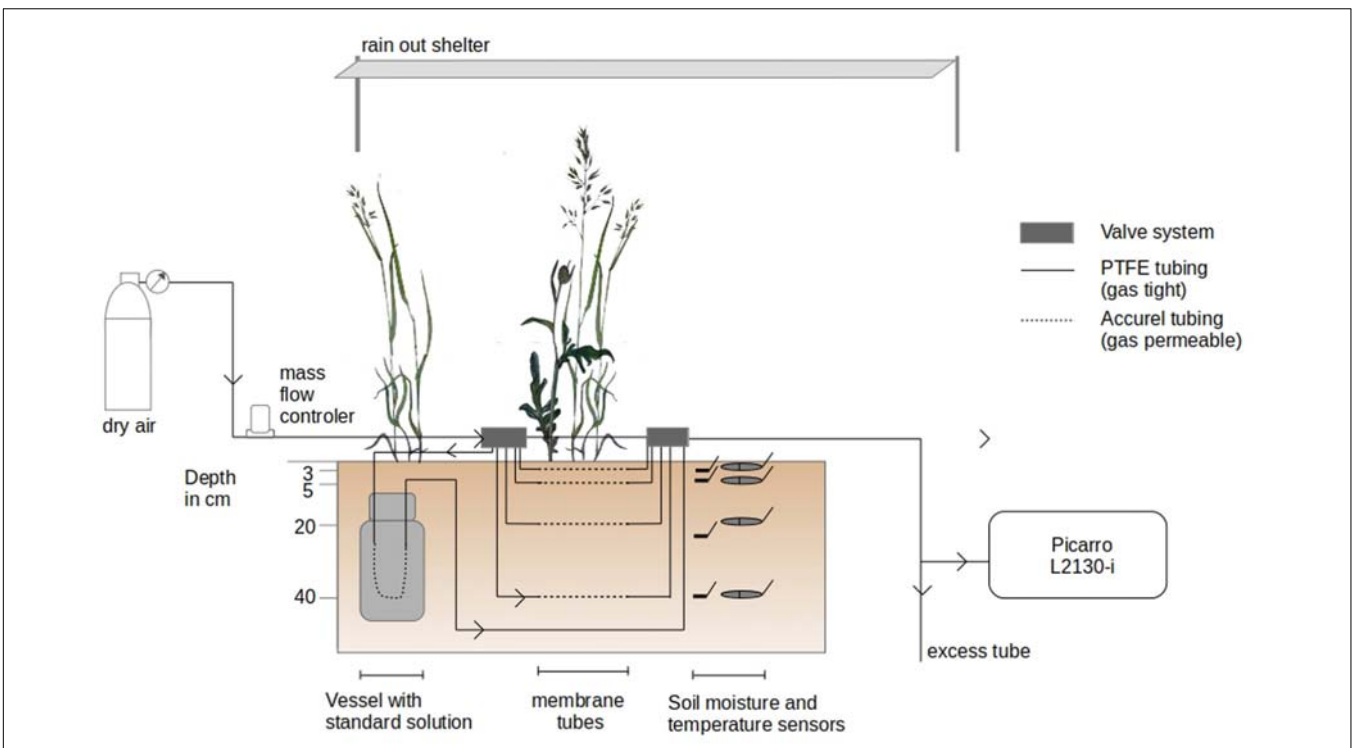

FIGURE 1 | Experimental setup of the *in situ* soil water vapor measurements. Soil water vapor was sampled across the soil profile from the vicinity of a series of gas permeable polypropylene tubing. The *in situ* soil water vapor sampling method was coupled to a laser spectroscope (Picarro L2130-i) for isotope measurements.

>80% and/or soil volumetric water content in 3 cm > 15%), each GP tube was flushed for five minutes at a flow rate of 300 ml min^{-1}. During drier time periods, no flushing of the GP tubes was necessary. Additionally, before/after each GP tube measurement, the tube system was flushed for five minutes via bypass lines. Steady values in MR and δ_{S_v} were, generally, reached after 10–20 min of sampling. Soil water vapor was sequentially sampled from the GP tubes in the following order for each profile: −20, −2, −40, and −5 cm depth. In total, δ_{S_v} was measured for each GP tube once a day during the experiment except on weekends.

For calibration of the raw δ_{S_v} values, water vapor was sampled sequentially from three custom-built soil standards (one isotopically 'light' standard STD_L, one 'medium' standard STD_M, and one heavy standard STD_H) once a day following the above described method. For this, three laboratory containers equipped with gas permeable GP tubes were filled with quartz sand (0.3–0.8 mm) and saturated (i.e., approx. 35 % vol. SWC) with water of known isotopic signature (STD_L: $\delta^{18}O = -78.8 \pm 0.04‰$; $\delta^{2}H = -263.3 \pm 0.71‰$; STD_M: $\delta^{18}O = -9.3 \pm 0.07‰$; $\delta^{2}H = -65.3 \pm 0.32‰$; STD_H: $\delta^{18}O = -9.3 \pm 0.2‰$; $\delta^{2}H = +865.0 \pm 0.21‰$). The STD_L and STD_H were measured last in order to prevent carry-over (memory) effects in the laser spectroscope. All standards were buried, together with a temperature sensor (T108, Campbell Scientific, Logan, UT, United States), in −60 cm depth in the soil at a distance of approximately 4 m from the center of the experimental plot. Insulating material was placed between standard vessel lids and topsoil material to keep changes of temperature of standards as small as possible.

Data Processing

Assuming thermodynamic equilibrium, collected data on δ_{S_v} were converted to liquid soil isotopic signatures δ_{S_l} after Majoube (1971) (Eq. 1 and 2) using the soil temperature of the respective soil depth. For the soil water vapor standards, the temperature of the adjacent buried sensor was used.

$$\delta_{S\_l} = (\delta_{S\_v} + 1) \times \alpha^{+} - 1 \quad (1)$$

$$\ln \alpha^{+} = a\frac{10^6}{T^2} + b\frac{10^3}{T} + c \quad (2)$$

With α^{+} being the equilibrium fractionation factor, T the reaction temperature in Kelvin. α^{+} was calculated based on the coefficients a, b, c from the experimental results of Majoube (1971) (i.e., for δ_{s_l} of ^{2}H: a = 24.844, b = −76.248 and c = 52.612; for δ_{s_l} of ^{18}O: a = 1.137, b = −0.4156, c = −2.0667).

To check for dependencies between MR and δs_l, the linear relationship between MR and the deviation of the measured δs_l value from the true δs_l value was determined based on the measurements of the soil standard vessels (Schmidt et al., 2010). No significant relationships were found and, therefore, no corrections applied ($\delta^{2}H$: $p = 0.15$, $R^2 = 0.11$; $\delta^{18}O$: $p = 0.8$, $R^2 = -0.04$, **Supplementary Figure S1**).

Subsequently, plateaus of steady values in MR, $\delta^{2}H$, and $\delta^{18}O$ (liquid) were determined by moving averages of the coefficients of variation (cv, 3 min period). Intervals of steady values were identified by finding the time period (x) when the sum of the cvs (MR, $\delta^{2}H$, and $\delta^{18}O$) was the smallest. Finally, isotopic signatures of selected intervals were averaged and calibrated against the ones of STD_M by drift correction. STD_L and STD_H were not used for calibration due to continuous problems with carry over effects.

Soil Destructive Sampling for Isotope Analysis

For comparison with the *in situ* method, soil samples were destructively taken every three days (13 days in total). All samples were taken within distances of maximum 1.80 m from the corners of the *in situ* measurement setup (**Figure 1**). Soil cores were collected with a soil auger (core diameter 20 mm, Pürckhauer, ecoTech Umwelt-Meßsysteme GmbH, Bonn, Germany) and stratified into portions of 0–3 cm, 3–8 cm, 18–23 cm, and 38–43 cm depth to correspond to the positioning of the *in situ* GP tubes (−2, −5, −20, and −40 cm depth). For each soil depth, three replicates were sampled per day ($n = 3$), except for centrifugation of soil ($n = 2$). Moreover, sampling for centrifugation was stopped 11 days before the other methods since the water recovery rates of soil samples were low (see section 3.3). Soil samples were always taken between 14:30 and 15:00 CET. Immediately after sampling, samples were split into two subsamples: 1) gas-tight 10-ml septum-capped glass vials for cryogenic extraction and 2) gas-tight centrifuge tubes (20 ml Pall Macrosep Advance) and sealed with Parafilm (Bemis, Oshkosh, WI, United States). All samples were kept in a cool box during transportation and stored at −20°C until further analysis.

Cryogenic Vacuum Extraction and Centrifugation

Soil destructive samples were extracted via: (1) cryogenic vacuum extraction, and (2) centrifugation. For cryogenic vacuum extraction, samples were heated up to approximately 95°C for 90 min under a vacuum of 0.1 mbar (XDS10 vacuum pump, Edwards, Burgess Hill, United Kingdom) and water vapor was trapped in liquid N_2 traps (custom-built vacuum line, similar to Ehleringer and Dawson (1992); design of R. Siegwolf). For centrifugation, samples were defrosted in the gas-tight centrifuge tubes, sealed with Parafilm. After defrosting, they were spun for 1 h at 5000 rpm at a temperature of 40°C on a Rotina centrifuge [Rotina 48 R, Hettich, Tuttlingen, Germany, similar to Millar et al. (2018)]. After water extraction, liquid water samples were stored in thread glass vials (ND9, LLG, Meckenheim, DE) with closed lids at 4°C until isotope analysis. Isotope analysis was conducted with a V1102-i vaporization module coupled to a A0325 robotic autosampler (both accessories of the L2130-i laser spectroscope, Picarro Inc., Santa Clara, CA, United States) and then measured with the same laser spectroscope which was used in the field. Extracted water samples were calibrated against three laboratory standards (Newman et al., 2009). All laboratory standards and soil standards were calibrated against international standards: V-SMOW, SLAP, and GISP (IAEA, Vienna). Water vapor mixing ratios did not strongly vary (16,143 ± 1,402 ppmv), and, therefore, no correction was applied to the isotope measurement results (see section 2.5). In addition, isotope

results of extracted water samples were post-processed with ChemCorrect^{TM} (Picarro Inc., Santa Clara, CA, United States) to detect organic contamination.

In order to quantify the effect of soil properties on cryogenic vacuum extraction, we fully dried soil samples from the field site (105°C for >48 h) and added water of known isotopic signature (spike test, Thielemann et al., 2019). Since water contents have shown to affect the soil water isotopic signature, this spike test was run for two different volumetric water contents (15% and 30%, n = 10, respectively). Soil samples were kept frozen and subsequently extracted cryogenically.

For both extraction methods, water recovery rates [%] were calculated on basis of the weight loss (mC-1 Laboratory LC 620, Sartorius AG, Göttingen, Germany) after oven drying (at 100°C for 48 h) of the extracted samples.

Statistical Analysis and Evaluation

Statistical analysis was conducted in R [R Core Team (2017), version 3.6.0]. Results were presented as mean values ± 1 standard deviation (SD) if not stated differently.

Dual-isotope graphical representation was used to compare between *in situ* and destructive laboratory-based isotope measurements. Locally estimated scatterplot smoothing (loess) was applied to find significant differences between extraction methods (only for experimental phases label 1 and label 2). Only data of at least two replicates per date and depth were included in the analysis. Centrifugation soil data was excluded due to the small sample size. Methods were considered significantly different if the confidence intervals (95%) of their respective loess functions did not overlap [software package ggplot2 by Wickham (2016)]. This approach was chosen because of the small and unequal sample size of the different methods and the repetitive measurement character of the *in situ* soil water vapor method.

Based on the same data, boxplots were created (showing also the sample size of each method per experimental phase) and the mean and SD across experimental phases calculated (per date as well as over the whole phase; per depth and across all depths) including error propagation. Moreover, the difference between soil water isotopic signature mean values (over the experimental phase) before and after the labelling pulses was calculated to determine the effect of labelling pulses 1 and 2.

Linear regression analysis was employed to evaluate the relationship between water vapor mixing ratios and isotopic signatures obtained by the *in situ* soil water vapor sampling method and further to determine the local meteorological water line (LMWL, based on year 2017) of the field site. Before analysis, residual versus fitted plots and quantile-quantile plots based on the model were plotted to validate the assumptions of homogenous variance and normal distribution of residuals of linear regression analysis.

RESULTS

Micrometeorological Conditions

Air temperature showed a strong amplitude during the experiment and ranged from 0.9 up to 43.3°C (**Figure 2**). The prevailing development of the mean air temperature during the day was characterized by a strong increase from 11.1°C at 5:00 CET, reaching a stable maximum at noon of around 31.2°C, before declining slowly toward the evening again. Topsoil temperatures (−2 cm depth) followed the same pattern, although the amplitude was less pronounced and approximately 2 h delayed from the air temperature, reaching its mean temperature maximum of 22.0°C around 18:00 CET. Daily temperature amplitudes were strongest in the topsoil and decreased with decreasing depth (data not shown). The photosynthetic photon flux density was highest at 13:00 CET reaching mean intensities of 1422.4 μmol m^{-2} s^{-1}. Air relative humidity was inversely related to air temperature, reaching its mean daily minimum of 35.5% around 4 pm whereas maximum values of 94.7% could be observed around 5:00 CET in the morning.

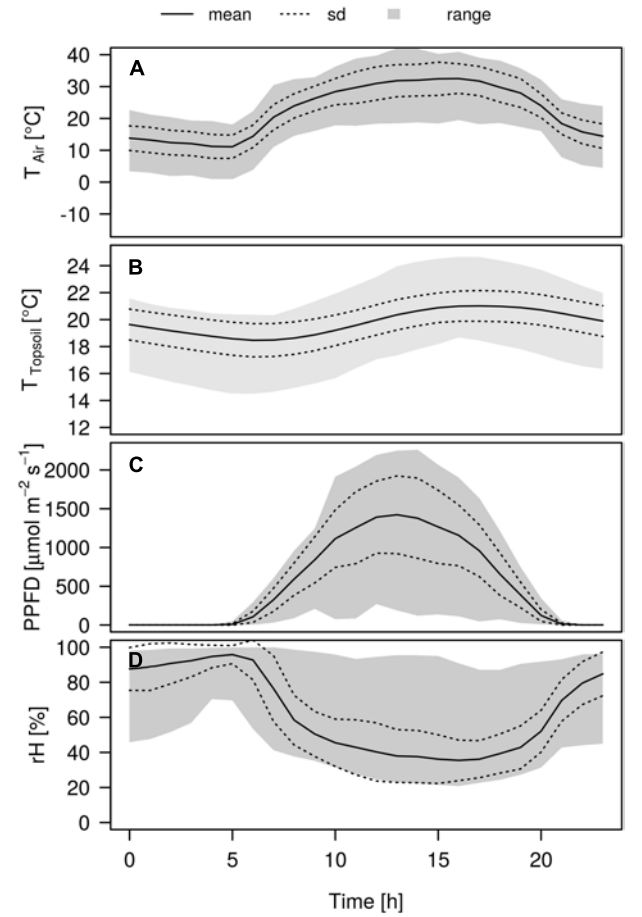

FIGURE 2 | Variation in micrometeorological conditions during the day over the course of the experiment. **A** Air temperature T_{Air} [°C], **(B)** topsoil temperature T_{Soil} [°C], **(C)** photosynthetic photon flux density PPFD [μmol m^{-2} s^{-1}], and **(D)** Relative humidity rH [%]. Mean (solid lines) ± 1 SD (dashed lines) and range (gray shaded).

Soil Water Contents

During the whole experiment, only few precipitation events occurred, with the strongest one on July 5, amounting to 9 mm

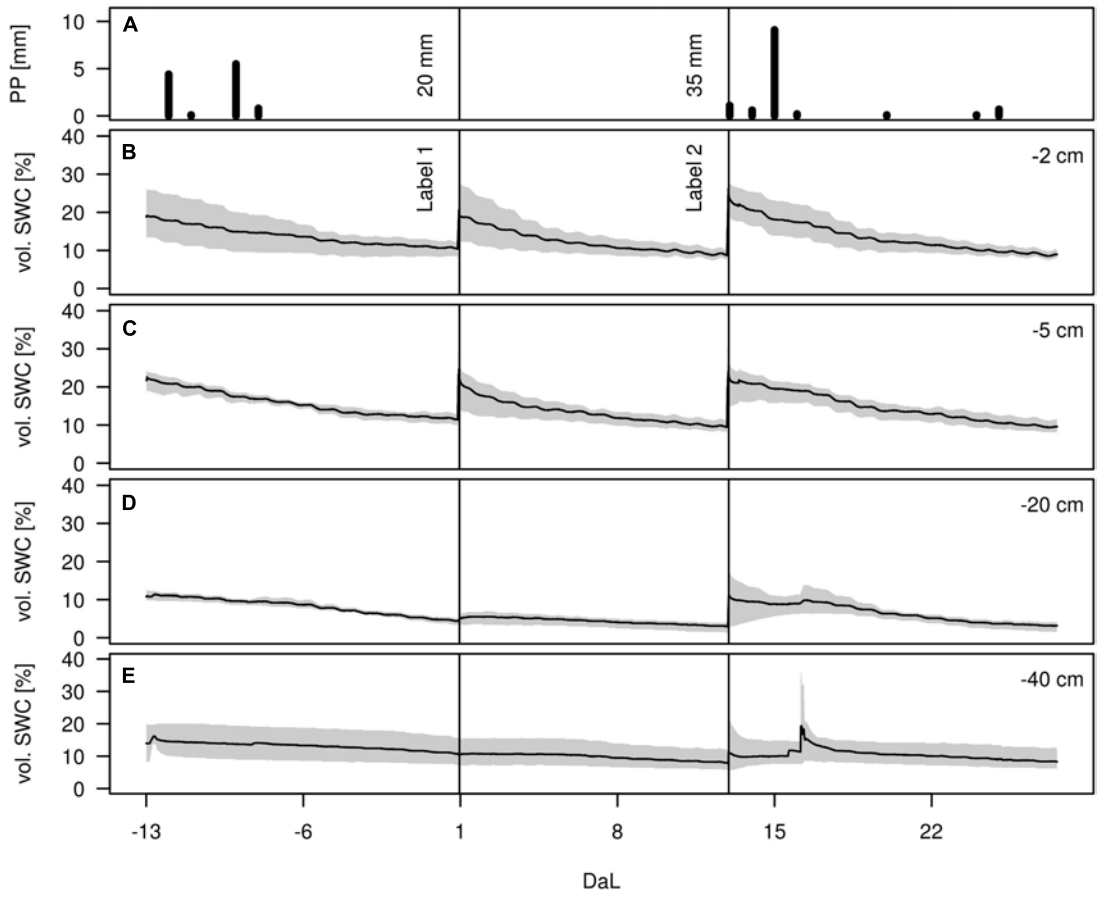

FIGURE 3 | (A) Precipitation height [mm], **(B–E)** Volumetric soil water content (vol. SWC, in %) in −2, −5, −20, and −40 cm during the experiment (Day after Labelling DaL). Black lines indicate irrigation events: label 1 and label 2. Mean (solid range) and range (gray shaded), $n = 3$.

(**Figure 3**). The effects of the rain-out shelter and simulated rain events were clearly visible from the temporal dynamics of the volumetric soil water content (vol. SWC) in all depths, which spanned from 3 to 36%. Infiltration of irrigation water was most visible in the upper soil depths (−2 and −5 cm) whereas the lower depths (−20 and −40 cm) were less affected and showed overall more stable vol. SWC values. Variation among replicates showed to be highest in −2 cm and in −40 cm depth, as well as after each applied irrigation event. After the above-mentioned rainfall event on July 5, a short peak was observable in the two deeper soil horizons, most likely due to preferential flow along soil cracks. Except for this peak value in −40 cm, highest differences of vol. SWC during the measurement period were observed at −2 cm, with values ranging from 7 to 36%.

Extraction Efficiency of Cryogenic Vacuum Extraction and Centrifugation

Generally, the water recovery rate of cryogenic vacuum extraction was higher compared to that of the centrifugation. In our study, the centrifugation of soils was strongly limited by sampled material and soil water content. Out of 64 samples for centrifugation, only 22 delivered enough liquid water for isotope analysis, i.e., more than 65% samples could not be measured. The limit for centrifugation was a vol. SWC of 7% in the lower soil depths (−20 and −40 cm). In the upper soil depths (−2 and −5 cm) with higher organic content the limit for centrifugation was 13%. However, we often could not obtain enough water for higher vol. SWC values in all depths, either. Generally, more soil material (here >15 ml/35 g) would have been needed to successfully determine the isotopic signature of soil water with centrifugation.

None of the soil samples were found to be organically contaminated (Chem Correct results).

Isotopic signatures could be measured from 92% of the soil water samples cryogenically extracted. Loss of samples was mainly related to difficulties in sample collection in the lower soil horizons (extraction efficiency of 75% in soil depths −20 and −40 cm).

Performance of *In Situ* and Destructive Isotope Measurements

The mean measurement precision of GP tubes in the medium soil standard (STD_M: $\delta^{18}O = -9.3 \pm 0.07‰$; $\delta^{2}H = -65.3 \pm 0.32‰$) deviated by 0.3‰ and 0.5‰ from the target value for $\delta^{18}O$ and

δ^2H, respectively. This expresses the average correction applied to values from *in situ* derived soil water measurements to account for drift correction of the laser spectroscope due to fluctuating background conditions. No apparent drift in standard isotope ratios was observed.

The measurement precision of the laser spectroscope in the laboratory, i.e., the precision for the destructive approach, was 0.3 ± 0.4‰ for δ^{18}O and 1.2 ± 6.2‰ for δ^2H, and again no drift was observed.

The accuracy of the cryogenic extraction, tested on spiked replicates from Freiburg field site, showed that mean deviations from the target value were 0.6 ± 0.2‰ for δ^{18}O and 3.0 ± 1.2‰ for δ^2H, respectively. This was less precise than results of our repeated *in situ* soil standard measurements in sand, and laboratory results with GP tubing (data not shown) in the same soil as used in the spike tests.

Method Comparison

Derived Isotopic Signature Values

During the natural abundance measurement phase, mean isotopic signatures of all extraction methods (method centrifugation excluded) for soil water were similar to mean precipitation values (−7.3 ± 4‰ in δ^{18}O and −48.3 ± 28‰ in δ^2H): Mean *in situ* measured values (across soil depths) were −7.1 ± 1‰ for δ^{18}O and −48.6 ± 8‰ for δ^2H. Cryogenic vacuum extraction obtained higher values for δ^{18}O with −5.5 ± 2‰, but lower for δ^2H with −50.1 ± 11‰ (**Supplementary Table S1**). After irrigation with labelled waters, isotopic signatures of both soil water extraction methods clearly showed that antecedent and newly incoming water mixed (**Figure 4**). Soil waters, observed after the two labelling pulses, strongly differed in dual isotope space (δ^{18}O, δ^2H). The *in situ* soil water vapor method, generally, showed the strongest deviation of isotopic signatures from preconditions (**Figure 5**). This effect was most visible in −2 and −5 cm depth and diminished with depths. While the isotopic response was more pronounced for δ^{18}O following labelling pulse 1 (label strongly depleted in ^{18}O relative to natural abundance), δ^2H was more affected after labelling pulse 2 (strongly enriched in ^{2}H). After labelling pulse 1, the isotopic signature inferred from cryogenic vacuum extraction was higher, with an average difference of 3.4‰ for δ^{18}O and 5.0‰ for δ^2H over all depths (**Supplementary Table S2**). Significant differences were found for δ^{18}O in −2 and −20 cm depth (no overlap of confidence intervals, **Figure 5**). After labelling pulse 2, mean differences in δ^{18}O were minor between methods (0.9‰), but high in δ^2H with 107.5‰ (with high standard deviations for both methods >260‰). Differences in isotopic signatures were significant for the observations in depths −2 and −5 cm (no overlap, **Figure 5**). Soil isotopic signature at −40 cm depth was visibly affected by the second labelled irrigation only when it diverged from natural abundance. This could be observed by both methods but was more pronounced for the *in situ* soil water vapor method.

Temporal Evolution and Variation of δ^{18}O and δ^2H in Soil Profiles

Depth profiles of soil water isotopic signatures obtained from the *in situ* and cryogenic vacuum extraction methods are presented in **Figure 6**. At initial conditions (DaL = 0), soil water isotope profiles showed a typical exponential shape, with the strongest enrichment of both isotopologues in −2 cm depth. The first labelling pulse substantially decreased mean signatures of δ^{18}O and δ^2H in the topsoil (from DaL 0 to DaL 5). For the *in situ*

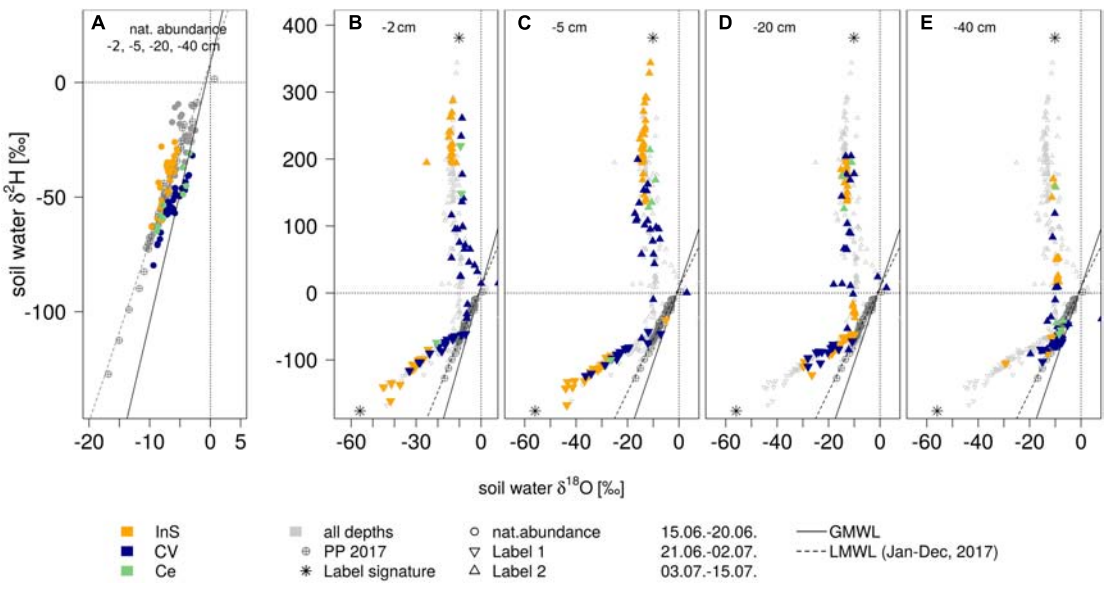

FIGURE 4 | Dual isotopes plots of soil water (δ^{18}O vs. δ^2H): **(A)** before (all soil depths) and **(B–E)** after the irrigation events (per depth) resulting from different extraction methods (*in situ* gas permeable tubing InS, cryogenic vacuum extraction CV and centrifugation Ce, in: yellow, blue, green resp.). Global meteoric water line GMWL and local meteoric water line (LMWL, based on 2017 data). *indicate isotopic signatures of irrigation events.

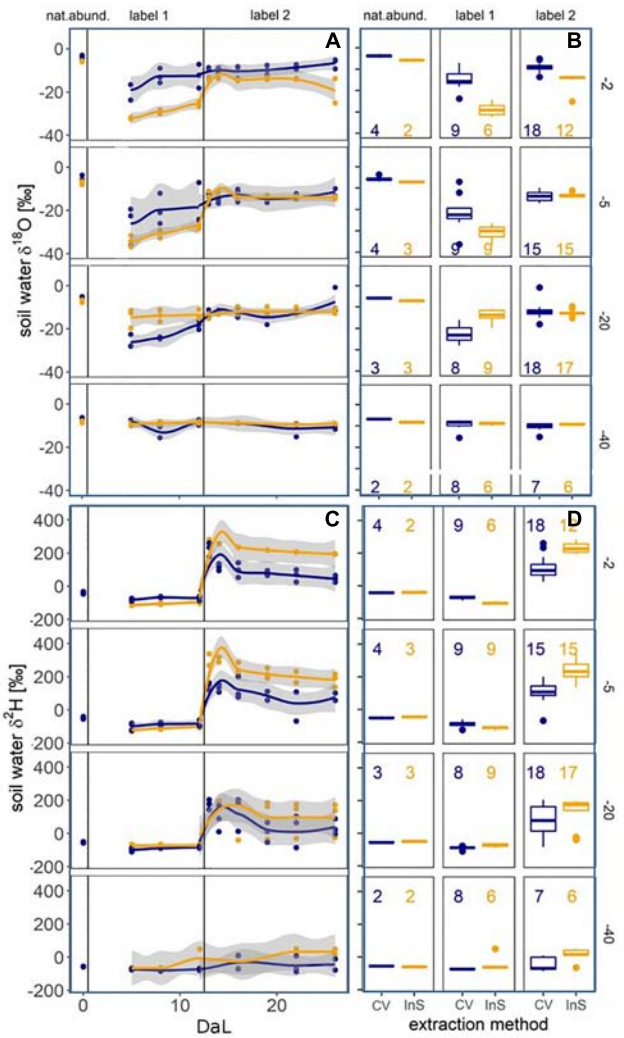

FIGURE 5 | Soil water $\delta^{18}O$ **(A,B)** and $\delta^{2}H$ **(C,D)** values measured at −2, −5, −20, and −40 cm depth by cryogenic vacuum extraction (CV, blue) and *in situ* gas permeable tubing (InS, yellow). Left panels **(A,C)**: Evolution over time (Day after labelling, DaL). Right panels **(B,D)**: Boxplots per experimental phase with sample size (at least $n = 2$ per time, depth and method). Methods were considered significantly different if confidence intervals of loess regressions did not overlap.

method in −2 cm depth, we observed a decrease from −5.7 to −32.0‰ ($\delta^{18}O$) and from −40.1 to −113.2‰ ($\delta^{2}H$). For the cryogenic vacuum extraction, we saw a decrease from −3.8 to −33.1‰ ($\delta^{18}O$) and −40.4 to −116.3‰ ($\delta^{2}H$). The second labelling pulse increased $\delta^{18}O$ values of cryogenically extracted soil water from −12.8 to −8.9‰ and increased $\delta^{2}H$ values from −70.8 to +224.1‰ in −2 cm depth. For the *in situ* method, we found an increase from −25.5 to −13.7‰ for $\delta^{18}O$; from −97.0 to +271.5‰ for $\delta^{2}H$.

Under natural abundance conditions, average SD in soil water $\delta^{18}O$ and $\delta^{2}H$ measured across depths was, generally, in a similar range, with 1.2‰ and 3.5‰, respectively, for the *in situ* soil water vapor method and 1.9‰, and 9.9‰ for cryogenic vacuum extraction (**Supplementary Table S1**). Irrigation events increased the range of soil water isotopic signatures considerably for both methods and therewith the isotopic differences between these methods.

TABLE 1 | Overview over costs [€] and time [h] needed in this experiment for extraction of water, per 100 samples.

	Destructive		*In situ*
	Cryo. vacuum extraction	**Centrifuge**	**Polyprop.**
Equipment	8,000	5,000	1,775
Tubing			14.2[2]
Labor intensity	Intense	Low	Low
Time [h][1]	60[3]	58.3[3]	25
Running costs[1]	120	610	–
Know-how for setup and handling	Medium	Easy	Medium-difficult

Not included are the time required for calibration of isotopic signatures, as well as costs for power and gas supply. [1]per 100 sample, [2]per soil depth, and [3]including laser measurement with 6 injections per sample.

While the *in situ* soil water vapor method clearly showed the temporal development of the soil water vapor isotopic signature (**Supplementary Figure S2**) of the same undisturbed soil volume, it has to be taken into account that the cryogenic vacuum extraction method based on destructive sampling at different location captured both the temporal variability and lateral heterogeneity of the soil profile. For the *in situ* method, isotopic differences across soil depths were better distinguishable, especially after the labelling pulses. Rothfuss et al., 2013, observed a memory effect associated with *in situ* GP tubes under saturated conditions (pure water). This was not the case in our experiment, since the soil was never fully saturated, even not directly after irrigation events.

Time and Cost Expenses

In terms of effort and costs, each extraction method had its advantages and disadvantages (**Table 1**). The time required for *in situ* soil sampling in our experiment was approximately 25 h per 100 samples, i.e., on average 15 min per sample, not including calibration and flushing of the system with dry air. Additionally, two entire days were needed for installation of the experimental setup. The equipment needed for the *in situ* soil method is cheaper than for the destructive methods and no material, despite of gas and electricity, is consumed. For the setup and handling of the *in situ* system an experienced person is needed, and further tests are necessary before the system is ready for operational use.

In total, it took 36 min per sample (without calibration) from soil sampling over cryogenic vacuum extraction to isotope analysis in the lab via laser spectroscope.

DISCUSSION

Methodological Differences

All extraction methods but centrifugation were able to generate isotopic signatures for soil water. However, some samples

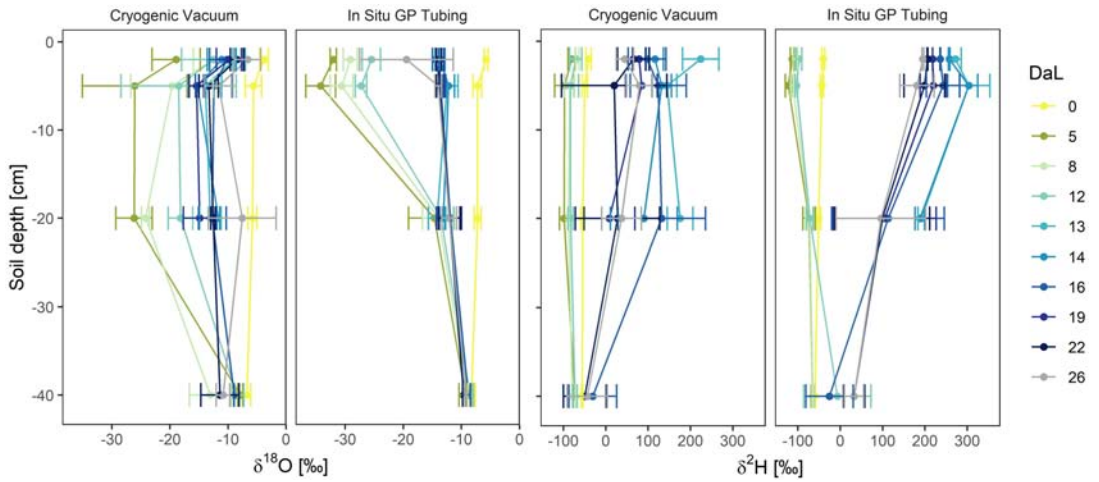

FIGURE 6 | Temporal dynamics of soil water $\delta^{18}O$ and $\delta^{2}H$ profiles (Day of Labelling, DaL) obtained by cryogenic vacuum extraction and *in situ* gas permeable (GP) tubing (n = 2–3). Mean values ± 1 SD. Labelling pulse 1 was applied in the night after DaL 0, label 2 in the night after DaL 12.

from deeper soil depths did not contain enough water for cryogenic vacuum extraction and subsequent liquid isotope analysis (i.e., 25% samples from −20 cm and −40 cm depth). The *in situ* monitoring method worked well for lower soil water contents and under stable environmental conditions (no rain and low rH), which both lowered the risk of condensation in the GP tubing.

We found the strongest impact of labelled water on the soil water in the uppermost soil layer, decreasing isotopic variation (i.e., smaller SDs) with depth, and relatively constant isotopic values in −40 cm depth for both methods throughout the whole experiment (**Figures 5**, **6**). Several studies reported a damping of incoming precipitation signals in the soil profile and a decreasing variability of soil water isotopes with depth, independently from sampling strategies (Orlowski et al., 2016a; Sprenger et al., 2016). They concluded that this observed damping was related to soil water mixing and capillary rise of groundwater. This dampening effect was observed for all extraction methods in all depths and therefore mixing seems to always occur to some degree.

We observed substantial differences between cryogenically extracted and *in situ* soil water vapor measurements, particularly after label 2 which was strongly enriched in ^{2}H (**Figures 5**, **6**). A generally lower effect of the labelled water to the on the cryogenically extracted soil water was found.

The fraction of soil water sampled by different extraction methods is currently one of the main questions faced by the ecohydrological research community (Berry et al., 2018; Penna et al., 2018; Sprenger et al., 2018; Orlowski et al., 2019). In comparison to the direct water vapor equilibration method, cryogenic vacuum extraction can likely also access hygroscopic and biologically bound water (Koeniger et al., 2011; Sprenger et al., 2015; Orlowski et al., 2016b). When testing different soil types with varying soil water contents, generally higher $\delta^{18}O$ and $\delta^{2}H$ values have been reported for the direct water vapor equilibration method in comparison to cryogenic vacuum extraction (Orlowski et al., 2016b). However, we did not find higher $\delta^{18}O$ and $\delta^{2}H$ values for the *in situ* soil water vapor method here.

Some authors (Oerter and Bowen, 2017) could observe systematically higher values (5.7‰ for $\delta^{2}H$ and 1.1‰ for $\delta^{18}O$) between *in situ* GP and cryogenically derived isotopic signatures under natural conditions while others did not observe systematic offsets (Volkmann and Weiler, 2014 and Gaj et al., 2016). Oerter and Bowen (2017) concluded that a physical separation of soil water, related to the characteristics of the soil material (like particle size) occurring in their studied system, was the reason for that difference. The initial water content and the size of particles were found to influence how antecedent water was replaced by subsequent water infiltration events (Gouet-Kaplan et al., 2012). This means that the *in situ* GP method, which always monitored the identical area, could not capture the spatial isotopic heterogeneity of the soil system. The destructive sampling for the cryogenic vacuum extraction, however, included the soil system's spatial isotopic variation. By adding labeled water with an isotopic signature which strongly differed from natural abundance, we highly increased the isotopic gradients in the soil. In addition, even though the amount of added water was high for a rainfall event, it did not completely saturate the soil. This further increased the spatial heterogeneity of water isotopic signatures in the soil. Hence, we could observe a high isotopic variation in our soil which likely caused the offset of 107.5‰ in $\delta^{2}H$ between cryogenic vacuum extraction and *in situ* derived $\delta^{2}H$, linked to the (spatially different) sampling of the methods. The *in situ* soil water vapor method always sampled the identical soil area while the soil samples for the cryogenic vacuum extraction were taken from different areas and thus covered a wider lateral range.

Strength and Limitations of Soil Water Vapor *In Situ* Method

A main constrain for the *in situ* soil water vapor method is the access to power and gas supply in the field, as well

as the possibility to set up the equipment in an, ideally air conditioned, shelter. One further crucial point of the *in situ* soil water vapor method is the installation of the sampling tubes in the field. It can substantially alter the soil's natural structure and therewith impact water flow pathways, especially in highly heterogeneous soils, as the one of our field site, with distinct horizons from fluvial depositions. Therefore, this destructive impact should be kept minimal during installation. Installations are recommended ahead of time (>60 days) to allow soil to settle and vegetation to fully regrow before starting *in situ* measurements. A potential source of error can arise from condensations effect. We impeded condensation effects by establishment of a flushing routine which was checked regularly and if necessary adapted based on the actual requirements. A dilution routine right after the sampling point (Quade et al., 2019) or a temperature control system [i.e., a heating system, Oerter and Bowen (2017)] would be an ideal countermeasure against condensation if the experimental setup allows it, in particular for measurements under wet and cool ambient conditions. It should be further monitored how soil conditions, sampling procedure and timeframe affect the measurement results. Rothfuss et al. (2015) reported no impact on the isotopic signature of water vapor after sampling over long periods and high flow rates under laboratory conditions (soil type: FH31 sand). Similarly, we could not observe an impact of sampling, i.e., an isotopic enrichment of our standard vessels, either. Moreover, sampling was not limited by low soil water contents and could repeatedly take place at the identical soil location. Strengths and limitations of the *in situ* soil water vapor method are discussed in more detail in Quade et al. (2018, 2019).

How to Choose Which Method to Use?

In terms of effort and costs, each extraction method had its advantages and disadvantages (**Table 1**). While the centrifugation is less labor-intensive than the other two extraction methods, it is relatively expensive and limited in its application for soil samples, regarding the soil water content and soil type (Orlowski et al., 2016b).

The *in situ* method was, generally, the fastest method (i.e., 25 h for 100 samples) to derive isotopic signature of soil water and the cheapest regarding the initial equipment. It was also relatively cheap during operation since it only consumed power and gas (i.e., laser spectroscope related consumables which are needed for all extraction methods). The initial investments of time and expertise for the *in situ* method are compensated by shorter sampling times and lower operating costs, in particular if the system is automated.

The *in situ* soil water vapor method had a high measurement precision of 0.3‰ for $\delta^{18}O$ and 0.2‰ for $\delta^{2}H$. With a deviation of -0.6 ± 0.2‰ for $\delta^{18}O$ and $+3.0 \pm 1.2$‰ for $\delta^{2}H$ from the target value (spike test), our system for cryogenic vacuum extraction did not meet the criteria of an acceptable performance ($\pm$0.2‰ for $\delta^{18}O$ and $\pm$ 2‰ for $\delta^{2}H$, Wassenaar et al., 2012; Orlowski et al., 2016b). The application of cryogenic vacuum extraction is currently strongly discussed in ecohydrological research and associated with strong varying results dependent on soil texture, soil water contents and laboratory procedure (Orlowski et al., 2013, 2016b, 2018). In the worldwide comparison of cryogenic vacuum extraction systems, our system delivered a relatively high precision (Orlowski et al., 2018). The measurement with the laser spectroscope further decreased the measurement precision (laser spectroscope: 0.3 ± 0.4‰ for $\delta^{18}O$ and 1.2 ± 6.2‰ for $\delta^{2}H$). The heterogeneity and higher variation of cryogenic vacuum extraction (**Figure 6**), associated with the destructive sampling bias and the extraction procedure, led to a wide range of observed isotopic signatures. This high variation can impede the use of isotopic signatures to distinguish between different soil depths and, hence, to trace water flow pathways. By sampling the identical soil area, the *in situ* soil water vapor method can exclude the bias of destructive sampling and decrease sampling related heterogeneity. This is of significant advantage when applying isotopically labelled waters in heterogeneous soil systems. Labeling approaches have been widely applied in ecohydrological studies [e.g. Volkmann et al. (2016a), Quade et al. (2018)] and are a powerful tool to trace water fluxes. They allow a statistically robust distinction between different water sources (Seeger and Weiler, 2016), which is important for statistical mixing source water models [e.g., *SIAR* by Parnell et al. (2010)]. By sampling the identical soil area and avoiding sampling related heterogeneity, the *in situ* soil water vapor method will further increase the accuracy of these models. To capture the vertical as well as the natural lateral isotopic heterogeneity of a system and their temporal dynamics, several soil profiles with *in situ* GP tubes could be laterally distributed to obtain 3D high temporal resolution soil isotopic profiles.

The choice of method should not only consider the prevailing soil conditions (Orlowski et al., 2016b) but also the experimental design and goal, i.e., which spatial and/or temporal resolution of processes should be captured (Dubbert and Werner, 2019). The two different approaches (destructive vs. *in situ*) aim at different spatial and temporal scales and resolutions. In this study, the isotopic signatures obtained by cryogenic vacuum extraction only represented 10 cm^3 of the soil volume. Our *in situ* soil water vapor method could sample 42 cm^3 under near-saturated, and even up to 526 cm^3 under dry conditions (Quade et al., 2019). The destructive approach only delivers data for one specific point in time, the time of destructive sampling. The *in situ* method, however, can resolve processes occurring at very small time scales. It is only temporally limited in the availability of the laser spectroscope for measurements.

So far, the *in situ* method has been applied mainly at smaller spatial scales, and more research is needed to also implement this technique at wider spatial scales. Longer tubing could be applied (Gangi et al., 2015) to sample larger soil volumes and increase the spatial extent. But longer tubing increases the risk of dry air leaving the gas permeable tubing, in particular under dry conditions (Quade et al., 2019). To assess soil water processes and soil-plant interactions adequately and identify underlying mechanisms, high temporal resolution observations for both soil and plant related processes are pivotal. More research is

needed to also implement the *in situ* soil water vapor method on larger spatial scales. We see a very promising tool in the *in situ* soil water vapor method to capture temporal developments and spatial variability of soil water and ecohydrological processes, in particular in combination with *in situ* xylem or transpiration monitoring techniques.

DATA AVAILABILITY STATEMENT

The datasets generated for this study are available on request to the corresponding author.

AUTHOR CONTRIBUTIONS

AK wrote the manuscript. SP helped writing the manuscript. AK, MD, YR, and NO conceived the study design. AK and MD planned the experiment. SP, AK, and AD set up the experiment and collected the data. SP and AK analyzed the data. All authors reviewed the manuscript.

FUNDING

Funding was provided by the DFG (DU1688/1-1), the "Innovationsfond Forschung" and "Landesgraduiertenförderung" of the federal state of Baden-Württemberg. The article processing charge was funded by the German Research Foundation (DFG) and the University of Freiburg in the funding program Open Access Publishing.

ACKNOWLEDGMENTS

We thank the Chair of Geobotany for being able to use the field site Flugplatz in Freiburg. We thank Isabel Kunz for her help during the field work and Stefan Seeger for advice.

SUPPLEMENTARY MATERIAL

The Supplementary Material for this article can be found online at: https://www.frontiersin.org/articles/10.3389/fpls.2020.00387/full#supplementary-material

REFERENCES

Berry, Z. C., Evaristo, J., Moore, G., Poca, M., Steppe, K., Verrot, L., et al. (2018). The two water worlds hypothesis: addressing multiple working hypotheses and proposing a way forward. *Ecohydrology* 11:e1843. doi: 10.1002/eco.1843

Dubbert, M., Kübert, A., and Werner, C. (2017). Impact of leaf traits on temporal dynamics of transpired oxygen isotope signatures and its impact on atmospheric vapor. *Front. Plant Sci.* 8:5. doi: 10.3389/fpls.2017.00005

Dubbert, M., and Werner, C. (2019). Water fluxes mediated by vegetation: emerging isotopic insights at the soil and atmosphere interfaces. *New Phytol.* 221, 1754–1763. doi: 10.1111/nph.15547

Deutscher Wetterdienst [DWD] (2018). *Historische tägliche Stationsbeobachtungen (Temperatur, Druck, Niederschlag, Sonnenscheindauer, etc.) für Deutschland.* Offenbach: Deutscher Wetterdienst.

Ehleringer, J. R., and Dawson, T. E. (1992). Water uptake by plants: perspectives from stable isotope composition. *Plant Cell Environ.* 15, 1073–1082. doi: 10.1111/j.1365-3040.1992.tb01657.x

Gaj, M., Beyer, M., Koeniger, P., Wanke, H., Hamutoko, J., and Himmelsbach, T. (2016). In situ unsaturated zone water stable isotope (^{2}H and ^{18}O) measurements in semi-arid environments: a soil water balance. *Hydrol. Earth Syst. Sci.* 20, 715–731. doi: 10.5194/hess-20-715-2016

Gangi, L., Tappe, W., Vereecken, H., and Brüggemann, N. (2015). Effect of short-term variations of environmental conditions on atmospheric CO 18 O isoforcing of different plant species. *Agricult. Forest Meteorol.* 201, 128–140. doi: 10.1016/j.agrformet.2014.10.015

Gonfiantini, R. (1978). Standards for stable isotope measurements in natural compounds. *Nature* 271:534.

Gouet-Kaplan, M., Arye, G., and Berkowitz, B. (2012). Interplay between resident and infiltrating water: Estimates from transient water flow and solute transport. *J. Hydrol.* 458–459, 40–50. doi: 10.1016/j.jhydrol.2012.06.026

Habel, J. C., Dengler, J., Janišová, M., Török, P., Wellstein, C., and Wiezik, M. (2013). European grassland ecosystems: threatened hotspots of biodiversity. *Biodivers. Conserv.* 22, 2131–2138. doi: 10.1007/s10531-013-0537-x

Helliker, B. R., and Noone, D. (2010). "Novel approaches for monitoring of water vapor isotope ratios: plants, lasers and satellites," in *Isoscapes: Understanding Movement, Pattern, and Process on Earth Through Isotope Mapping*, eds J. B. West, G. J. Bowen, T. E. Dawson, and K. P. Tu (Dordrecht: Springer), 71–88. doi: 10.1007/978-90-481-3354-3_4

Horita, J., and Wesolowski, D. J. (1994). Liquid-vapor fractionation of oxygen and hydrogen isotopes of water from the freezing to the critical temperature. *Geochim. Cosmochim. Acta* 58, 3425–3437. doi: 10.1016/0016-7037(94)90096-5

IPBES (2018). in *Summary for Policymakers of the Regional Assessment Report on Biodiversity and Ecosystem Services for Europe and Central Asia of the Intergovernmental Science-Policy Platform on Biodiversity and Ecosystem Services*, eds M. Fischer, M. Rounsevell, A. Torre-Marin Rando, A. Mader, A. Church, and M. Elbakidze (Bonn: IPBES Secretariat), 48.

Koeniger, P., Marshall, J. D., Link, T., and Mulch, A. (2011). An inexpensive, fast, and reliable method for vacuum extraction of soil and plant water for stable isotope analyses by mass spectrometry. *Rapid Commun. Mass Spectrom.* 25, 3041–3048. doi: 10.1002/rcm.5198

Maestre, F. T., Quero, J. L., Gotelli, N. J., Escudero, A., Ochoa, V., Delgado-Baquerizo, M., et al. (2012). Plant species richness and ecosystem multifunctionality in global drylands. *Science* 335, 214–218. doi: 10.1126/science.1215442

Mahindawansha, A., Orlowski, N., Kraft, P., Rothfuss, Y., Racela, H., and Breuer, L. (2018). Quantification of plant water uptake by water stable isotopes in rice paddy systems. *Plant Soil* 429, 281–302. doi: 10.1007/s11104-018-3693-7

Majoube, M. (1971). Oxygen-18 and deuterium fractionation between water and steam (in French). *J. Chim. Phys. Phys. Chim. Biol.* 68, 1423–1436.

Meißner, M., Köhler, M., Schwendenmann, L., Hölscher, D., and Dyckmans, J. (2014). Soil water uptake by trees using water stable isotopes (δ2H and δ18O)-a method test regarding soil moisture, texture and carbonate. *Plant Soil* 376, 327–335. doi: 10.1007/s11104-013-1970-z

Millar, C., Pratt, D., Schneider, D. J., and McDonnell, J. J. (2018). A comparison of extraction systems for plant water stable isotope analysis. *Rapid Commun. Mass Spectrom.* 32, 1031–1044. doi: 10.1002/rcm.8136

Millennium Ecosystem Assessment (2005). *Ecosystems and Human Well-Being: Synthesis*. Washington, DC: Island Press.

Newman, B., Tanweer, A., and Kurttas, T. (2009). *IAEA Standard Operating Procedure for the Liquid-Water Stable Isotope Analyser*. Vienna: International Atomic Energy Agency, 27.

Oerter, E., Finstad, K., Schaefer, J., Goldsmith, G. R., Dawson, T., and Amundson, R. (2014). Oxygen isotope fractionation effects in soil water via interaction with cations (Mg, Ca, K, Na) adsorbed to phyllosilicate clay minerals. *J. Hydrol.* 515, 1–9. doi: 10.1016/j.jhydrol.2014.04.029

Oerter, E. J., and Bowen, G. (2017). In situ monitoring of H and O stable isotopes in soil water reveals ecohydrologic dynamics in managed soil systems. *Ecohydrology* 10:e1841. doi: 10.1002/eco.1841

Oerter, E. J., Perelet, A., Pardyjak, E., and Bowen, G. (2017). Membrane inlet laser spectroscopy to measure H and O stable isotope compositions of soil and sediment pore water with high sample throughput. *Rapid Commun. Mass Spectrom.* 31, 75–84. doi: 10.1002/rcm.7768

Orlowski, N., Breuer, L., Angeli, N., Boeckx, P., Brumbt, C., Cook, C. S., et al. (2018). Inter-laboratory comparison of cryogenic water extraction systems for stable isotope analysis of soil water. *Hydrol. Earth Syst. Sci.* 22, 3619–3637. doi: 10.5194/hess-22-3619-2018

Orlowski, N., Frede, H.-G., Brüggemann, N., and Breuer, L. (2013). Validation and application of a cryogenic vacuum extraction system for soil and plant water extraction for isotope analysis. *J. Sens. Sens. Syst.* 2, 179–193. doi: 10.5194/jsss-2-179-2013

Orlowski, N., Kraft, P., Pferdmenges, J., and Breuer, L. (2016a). Exploring water cycle dynamics by sampling multiple stable water isotope pools in a developed landscape in Germany. *Hydrol. Earth Syst. Sci.* 20, 3873–3894. doi: 10.5194/hess-20-3873-2016

Orlowski, N., Pratt, D. L., and McDonnell, J. J. (2016b). Intercomparison of soil pore water extraction methods for stable isotope analysis: intercomparison of soil pore water extraction methods. *Hydrol. Process.* 30, 3434–3449. doi: 10.1002/hyp.10870

Orlowski, N., Pratt, D. L., and McDonnell, J. J. (2019). Intercomparison of soil pore water extraction methods for stable isotope analysis and interpretation of hillslope runoff sources. *Hydrol. Process.* 33, 2939–2954. doi: 10.1002/hyp.13539

Parnell, A. C., Inger, R., Bearhop, S., and Jackson, A. L. (2010). Source partitioning using stable isotopes: coping with too much variation. *PLoS One* 5:e9672. doi: 10.1371/journal.pone.0009672

Penna, D., Hopp, L., Scandellari, F., Allen, S. T., Benettin, P., Beyer, M., et al. (2018). Ideas and perspectives: tracing terrestrial ecosystem water fluxes using hydrogen and oxygen stable isotopes – challenges and opportunities from an interdisciplinary perspective. *Biogeosciences* 15, 6399–6415. doi: 10.5194/bg-15-6399-2018

Quade, M., Brüggemann, N., Graf, A., Vanderborght, J., Vereecken, H., and Rothfuss, Y. (2018). Investigation of kinetic isotopic fractionation of water during bare soil evaporation. *Water Resour. Res.* 54, 6909–6928. doi: 10.1029/2018wr023159

Quade, M., Klosterhalfen, A., Graf, A., Brüggemann, N., Hermes, N., Vereecken, H., et al. (2019). In-situ monitoring of soil water isotopic composition for partitioning of evapotranspiration during one growing season of sugar beet (*Beta vulgaris*). *Agricult. Forest Meteorol.* 266–267, 53–64. doi: 10.1016/j.agrformet.2018.12.002

R Core Team (2017). *R: A Language and Environment for Statistical Computing*. Vienna: R Foundation for Statistical Computing.

Rothfuss, Y., and Javaux, M. (2017). Reviews and syntheses: isotopic approaches to quantify root water uptake: a review and comparison of methods. *Biogeosciences* 14, 2199–2224. doi: 10.5194/bg-14-2199-2017

Rothfuss, Y., Merz, S., Vanderborght, J., Hermes, N., Weuthen, A., Pohlmeier, A., et al. (2015). Long-term and high-frequency non-destructive monitoring of water stable isotope profiles in an evaporating soil column. *Hydrol. Earth Syst. Sci.* 19, 4067–4080. doi: 10.5194/hess-19-4067-2015

Rothfuss, Y., Vereecken, H., and Brüggemann, N. (2013). Monitoring water stable isotopic composition in soils using gas-permeable tubing and infrared laser absorption spectroscopy: monitoring water stable isotopic composition in soils. *Water Resour. Res.* 49, 3747–3755. doi: 10.1002/wrcr.20311

Schmidt, M., Maseyk, K., Lett, C., Biron, P., Richard, P., Bariac, T., et al. (2010). Concentration effects on laser-based δ^{18}O and δ^{2}H measurements and implications for the calibration of vapour measurements with liquid standards: concentration effects on CRDS. *Rapid Commun. Mass Spectrom.* 24, 3553–3561. doi: 10.1002/rcm.4813

Schnyder, H., Isselstein, J., Taube, F., Auerswald, K., Schellberg, J., Wachendorf, M., et al. (eds). (2010). *Grassland in a Changing World*. Duderstadt: Mecke Druck und Verlag.

Schymanski, S. J., Sivapalan, M., Roderick, M. L., Beringer, J., and Hutley, L. B. (2008). An optimality-based model of the coupled soil moisture and root dynamics. *Hydrol. Earth Syst. Sci.* 12, 913–932. doi: 10.5194/hess-12-913-2008

Seeger, S., and Weiler, M. (2016). *Optimizing Plant Water Uptake Source Depths Estimation by Stable Water Isotope Labeling*. Vienna: EGU General Assembly, doi: 10.13140/RG.2.2.24558.10560

Simonin, K. A., Roddy, A. B., Link, P., Apodaca, R., Tu, K. P., Hu, J., et al. (2013). Isotopic composition of transpiration and rates of change in leaf water isotopologue storage in response to environmental variables: Isotopic non-steady-state transpiration. *Plant Cell Environ.* 36, 2190–2206. doi: 10.1111/pce.12129

Sprenger, M., Herbstritt, B., and Weiler, M. (2015). Established methods and new opportunities for pore water stable isotope analysis. *Hydrol. Process.* 29, 5174–5192. doi: 10.1002/hyp.10643

Sprenger, M., Leistert, H., Gimbel, K., and Weiler, M. (2016). Illuminating hydrological processes at the soil-vegetation-atmosphere interface with water stable isotopes: review of water stable isotopes. *Rev. Geophys.* 54, 674–704. doi: 10.1002/2015RG000515

Sprenger, M., Stumpp, C., Weiler, M., Aeschbach, W., Allen, S. T., Benettin, P., et al. (2019). The demographics of water: a review of water ages in the critical zone. *Rev. Geophys.* 57, 800–834. doi: 10.1029/2018RG000633

Sprenger, M., Tetzlaff, D., Buttle, J., Laudon, H., Leistert, H., Mitchell, C. P. J., et al. (2018). Measuring and modeling stable isotopes of mobile and bulk soil water. *Vadose Zone J.* 17:170149. doi: 10.2136/vzj2017.08.0149

Stoate, C., Báldi, A., Beja, P., Boatman, N. D., Herzon, I., van Doorn, A., et al. (2009). Ecological impacts of early 21st century agricultural change in Europe – a review. *J. Environ. Manage.* 91, 22–46. doi: 10.1016/j.jenvman.2009.07.005

Stumpp, C., Brüggemann, N., and Wingate, L. (2018). Stable isotope approaches in vadose zone research. *Vadose Zone J.* 17:180096. doi: 10.2136/vzj2018.05.0096

Thielemann, L., Gerjets, R., and Dyckmans, J. (2019). Effects of soil-bound water exchange on the recovery of spike water by cryogenic water extraction. *Rapid Commun. Mass Spectrom.* 33, 405–410. doi: 10.1002/rcm.8348

Vereecken, H., Huisman, J. A., Franssen, H. J. H., Brüggemann, N., Bogena, H. R., Kollet, S., et al. (2015). Soil hydrology: recent methodological advances, challenges, and perspectives. *Water Resour. Res.* 51, 2616–2633. doi: 10.1002/2014WR016852

Volkmann, T. H. M., Haberer, K., Gessler, A., and Weiler, M. (2016a). High-resolution isotope measurements resolve rapid ecohydrological dynamics at the soil-plant interface. *New Phytol.* 210, 839–849. doi: 10.1111/nph.13868

Volkmann, T. H. M., Kühnhammer, K., Herbstritt, B., Gessler, A., and Weiler, M. (2016b). A method for *in situ* monitoring of the isotope composition of tree xylem water using laser spectroscopy: *In situ* monitoring of xylem water isotopes. *Plant Cell Environ.* 39, 2055–2063. doi: 10.1111/pce.12725

Volkmann, T. H. M., and Weiler, M. (2014). Continual in situ monitoring of pore water stable isotopes in the subsurface. *Hydrol. Earth Syst. Sci.* 18, 1819–1833. doi: 10.5194/hess-18-1819-2014

Wang, L., Good, S. P., Caylor, K. K., and Cernusak, L. A. (2012). Direct quantification of leaf transpiration isotopic composition. *Agricult. Forest Meteorol.* 154–155, 127–135. doi: 10.1016/j.agrformet.2011.10.018

Wassenaar, L. I., Ahmad, M., Aggarwal, P., van Duren, M., Pöltenstein, L., Araguas, L., et al. (2012). Worldwide proficiency test for routine analysis of δ2H and δ18O in water by isotope-ratio mass spectrometry and laser absorption spectroscopy. *Rapid Commun. Mass Spectrom.* 26, 1641–1648. doi: 10.1002/rcm.6270

Werner, C., Schnyder, H., Cuntz, M., Keitel, C., Zeeman, M. J., Dawson, T. E., et al. (2012). Progress and challenges in using stable isotopes to trace plant carbon and water relations across scales. *Biogeosciences* 9, 3083–3111. doi: 10.5194/bg-9-3083-2012

White, R. P., Murray, S., Rohweder, M., Prince, S. D., and Thompson, K. M. (2000). *Grassland Ecosystems*. Washington, DC: World Resources Institute.

Wickham, H. (2016). *ggplot2: Elegant Graphics for Data Analysis*. New York, NY: Springer-Verlag.

Conflict of Interest: The authors declare that the research was conducted in the absence of any commercial or financial relationships that could be construed as a potential conflict of interest.

frontiers in Plant Science

ORIGINAL RESEARCH
published: 15 April 2020
doi: 10.3389/fpls.2020.00358

Borehole Equilibration: Testing a New Method to Monitor the Isotopic Composition of Tree Xylem Water *in situ*

John D. Marshall[1*†], *Matthias Cuntz*[2†], *Matthias Beyer*[3,4†], *Maren Dubbert*[5,6†] *and Kathrin Kuehnhammer*[3,5†]

[1] Department of Forest Ecology and Management, Swedish University of Agricultural Sciences, Umeå, Sweden, [2] Université de Lorraine, AgroParisTech, INRAE, UMR Silva, Nancy, France, [3] IGOE, Umweltgeochemie, Technische Universität Braunschweig, Braunschweig, Germany, [4] Department B2.3: Groundwater Resources and Dynamics, German Federal Institute for Geosciences and Natural Resources (BGR), Hanover, Germany, [5] Ecosystem Physiology, University Freiburg, Freiburg, Germany, [6] IGB Berlin, Landscape Ecohydrology, Berlin, Germany

Forest water use has been difficult to quantify. One promising approach is to measure the isotopic composition of plant water, e.g., the transpired water vapor or xylem water. Because different water sources, e.g., groundwater versus shallow soil water, often show different isotopic signatures, isotopes can be used to investigate the depths from which plants take up their water and how this changes over time. Traditionally such measurements have relied on the extraction of wood samples, which provide limited time resolution at great expense, and risk possible artifacts. Utilizing a borehole drilled through a tree's stem, we propose a new method based on the notion that water vapor in a slow-moving airstream approaches isotopic equilibration with the much greater mass of liquid water in the xylem. We present two empirical data sets showing that the method can work in practice. We then present a theoretical model estimating equilibration times and exploring the limits at which the approach will fail. The method provides a simple, cheap, and accurate means of continuously estimating the isotopic composition of the source water for transpiration.

Keywords: transpiration, continuous sampling, root water uptake, Craig-Gordon model, $\delta^{18}O$, $\delta^{2}H$, isotopic labeling, xylem water

OPEN ACCESS

Edited by:
Lars Hendrik Wegner, Foshan University, China

Reviewed by:
Vadim Volkov, London Metropolitan University, United Kingdom
Ping Ren, Chinese Academy of Sciences (CAS), China

***Correspondence:**
John D. Marshall
john.marshall@slu.se

†ORCID:
John D. Marshall
orcid.org/0000-0002-3841-8942
Matthias Cuntz
orcid.org/0000-0002-5966-1829
Matthias Beyer
orcid.org/0000-0002-1618-6036
Maren Dubbert
orcid.org/0000-0002-2352-8516
Kathrin Kuehnhammer
orcid.org/0000-0001-5266-2207

Specialty section:
This article was submitted to Technical Advances in Plant Science, a section of the journal Frontiers in Plant Science

Received: *30 October 2019*
Accepted: *11 March 2020*
Published: *15 April 2020*

Citation:
Marshall JD, Cuntz M, Beyer M, Dubbert M and Kuehnhammer K (2020) Borehole Equilibration: Testing a New Method to Monitor the Isotopic Composition of Tree Xylem Water in situ. Front. Plant Sci. 11:358. doi: 10.3389/fpls.2020.00358

INTRODUCTION

A large proportion of the precipitation falling into a forest ecosystem is returned to the atmosphere via evapotranspiration of trees and soils. The remainder eventually flows into streams and recharges groundwater. The returns can be divided into transpiration and evaporation, where transpiration refers to the uptake and loss of water from the interiors of plants and evaporation refers to all the rest, including evaporation from soils and plant surfaces (Jarvis and McNaughton, 1986). Finally, the responses to environmental conditions differ qualitatively and quantitatively between transpiration and evaporation; a satisfactory mechanistic description would therefore include separate controls over each component. Although hydrologists have traditionally lumped transpiration with evaporation, they show increasing interest in measuring and modeling the isolated fluxes (Jasechko et al., 2013; Evaristo et al., 2015; Dubbert and Werner, 2019). In contrast,

ecophysiologists have long been interested in describing transpiration, in part because it links the carbon and water budgets of plants (Granier, 1987; Barr et al., 2007; Dubbert et al., 2013; Poyatos et al., 2016).

The transpiration flux can be distinguished from other evaporative fluxes by its unique stable-isotopic signature (e.g., Yakir and da Sternberg, 2000). In general, evaporating water undergoes two fractionations (Dongmann et al., 1974). The first, termed the equilibrium fractionation, is associated with the phase change, where the lighter isotope moves into the vapor phase somewhat more rapidly than the heavier one. The second fractionation occurs as the water vapor diffuses away from the evaporating surface. Termed the kinetic fractionation, it likewise favors the lighter isotope. Integrated over longer time intervals (>days), the isotopic signature of transpired water vapor occurs at steady-state, which means that the isotopic signature is equal to its water source and also equal to the signature of water transported in the xylem. This makes it easily distinguishable from strongly depleted soil evaporation (e.g., Dubbert et al., 2013). However, environmental conditions change so quickly that transpiration at isotopic steady-state is disrupted frequently over the diurnal course and environmentally stable periods are too short for leaves to return to isotopic steady-state (e.g., Simonin et al., 2013; Dubbert et al., 2014). Consequently, the isotopic signature of transpired water vapor follows a distinct diurnal pattern, being most depleted compared to source water during the morning hours, approaching isotopic steady-state throughout the day and being strongly enriched compared to its water source during night (e.g., Dubbert et al., 2014).

The source for transpired water is the water taken up by the roots and transported through the tree xylem. In contrast to the strong fractionation that occurs during transpiration, xylem water is generally taken up and transported without fractionation (Wershaw et al., 1966), though a growing number of exceptions are reported (Lin and Sternberg, 1993; Ellsworth and Williams, 2007; Vargas et al., 2017; Barbeta et al., 2019; Poca et al., 2019). One might expect that the xylem water would be identical to precipitation, but precipitation varies over the year, creating depth profiles in the soil. Moreover, many trees have access to groundwater, which may originate elsewhere (Busch et al., 1992; Beyer et al., 2018). Hence, xylem water isotopic composition is of particular interest for root water uptake studies (Schulze et al., 1996; Moreira et al., 2000; Kulmatiski et al., 2010; Rothfuss and Javaux, 2016) and when investigating hydraulic redistribution (Priyadarshini et al., 2016; Rothfuss and Javaux, 2016; Sprenger et al., 2016). Partitioning of evapotranspiration into its evaporation and transpiration components requires knowledge of the isotopic composition of the two components. Transpiration has been measured by collecting water that evaporates directly from the leaves, both as condensate in bags (Beyer et al., 2016) and as water vapor in chamber outflows (Haverd et al., 2011). In addition, one can also derive the isotopic signature of transpired vapor, either by assuming isotopic steady state (xylem water = transpired water vapor isotopic signature) or modeling transpired water vapor isotopic signature allowing for isotopic non-steady state (e.g., Dongmann et al., 1974; Cuntz et al., 2007; Farquhar et al., 2007).

There is a long tradition of describing the isotopic composition of xylem water via cryogenic distillation of the water held in plant xylem (White et al., 1985; Flanagan et al., 1992). The prerequisite for this method is the completeness of the extraction, which minimizes opportunities for isotopic fractionation between the original sample water and the resulting collected water. However, the approach has several weaknesses. First, it simultaneously distills other volatile organic compounds, especially from leaves (Martín-Gómez et al., 2015). These organic compounds are of little concern if the samples are analyzed by IRMS, but they are problematic in analyses using laser-based absorption techniques (West et al., 2010, 2011). The isotopolog-specific water peaks may be interfered with, especially by alcohol peaks. A second problem is that cryogenic extraction may extract water that is not moving in the xylem, for example water held in cell walls (Barbeta et al., 2018) and heartwood (White et al., 1985; Busch et al., 1992). In these cases, it would not represent the correct uptake source. At best, cryogenic extraction is laborious, slow, and can only represent a point in time (Koeniger et al., 2011). Other methods have been used for extracting soil water (Sprenger et al., 2016), but many of these are ineffective at the low water potentials typical of plant xylem.

When laser-based systems appeared on the market, it became possible to monitor the isotopic composition of water vapor continuously. It was soon recognized that this not only allowed for direct measurements of the isotopic signal of ambient, transpired and evaporated water vapor but also the continuous measurement of liquid water in soils and stems. This can be done by calculating the liquid isotopic composition from vapor phase values assuming equilibrium fractionation (Majoube, 1971) and requires recording temperature and a means of preventing condensation between the equilibration site and the instrument. This led first to several devices for *in situ* studies of soil water isotopes (Herbstritt et al., 2012; Soderberg et al., 2012; Rothfuss et al., 2013; Volkmann and Weiler, 2014), and then to a modification for tree xylem (Volkmann et al., 2016). The xylem system was able to detect unequivocally the arrival of a tracer pulse in the xylem water. However, it had difficulty matching the predicted isotopic composition of $\delta^{18}O$ at natural abundance. It was inspiring as proof-of-concept, but it was worrisome for its complexity and the unexplained offset in the $\delta^{18}O$ data.

We supposed that the problem might be simplified if only the liquid water in the xylem would continue to evaporate into a flowing airstream that passed through the stem of the tree. The isotopic effects might be particularly simple if we could ensure that the airstream reached isotopic equilibrium with the xylem water as it passed through the stem (**Figure 1**). To test this idea, we conducted two experiments and developed a model describing the isotopic equilibration of borehole vapor with liquid xylem water. The experiments tested whether the method was capable of returning the expected values. The model tested different assumptions about the physical processes behind the method and was used to explore its practical limits.

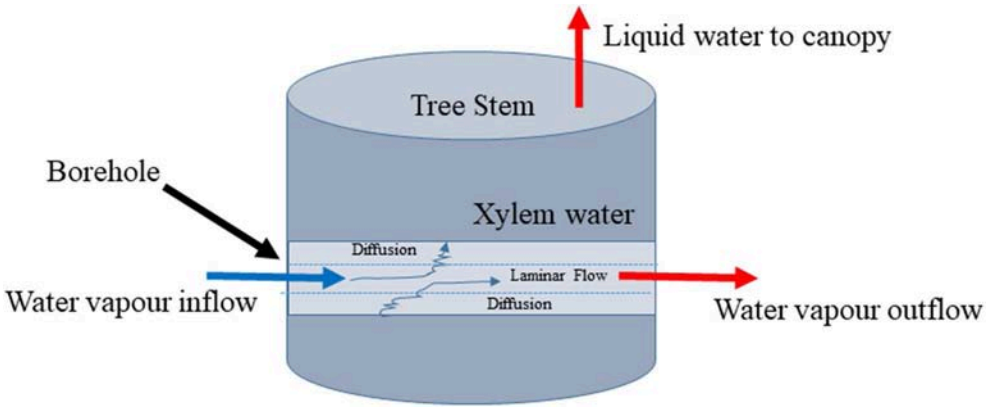

FIGURE 1 | Conceptual diagram of stem borehole technique for measuring xylem water stable isotopic composition by equilibration.

METHODS AND MATERIALS

Cut-Stem Greenhouse Experiment

A preliminary test of the technique was conducted in a greenhouse at the Swedish University of Agricultural Sciences (SLU) in Umeå, Sweden in March, 2014. This experiment was artificial in the sense that a cut stem is unnatural, however, the power of an experiment is always that it controls some sources of variation. In this case, it allowed us to provide a known water source directly into the xylem at a precisely known point in time and at a precisely known distance from the borehole. A field-grown Scots pine (*Pinus sylvestris* L.) tree was cut near Vindeln, in northern Sweden. In the glasshouse it was recut underwater (to avoid cavitation) and, with the crown intact, the cut end was placed several centimeters below the water surface in a bucket containing liquid water of known isotopic composition. The water sources were exchanged for the next several days while the stems transpired and sucked the water up into the xylem. A borehole 6 mm in diameter was drilled through the stem ∼30 cm vertically from the cut end, where the tree diameter was 12 cm. The borehole was rinsed with acetone to reduce pitch production from the resin canals inside. Because the acetone is both volatile and soluble in water, it was rapidly removed from the system. Apart from removing and blocking pitch production, it had no other obvious effects on the tree. The borehole was then plumbed into a Picarro L2130-i cavity ring-down absorption spectrometer (CRDAS) by screwing the pipe threads of a Swagelok connector into the borehole and attaching FEP Teflon tubing of 6 mm outside diameter (Swagelok, Solon, OH, USA) to the other side. The CRDAS analyzed the concentration and isotopic composition of water vapor in the air that had passed through the borehole. It was calibrated against known liquid water standards injected to the evaporator system at the beginning and end of the experiment. A copper-constantan thermocouple was inserted through the tubing and the fitting and placed in contact with the xylem inside the borehole, monitoring xylem temperature continuously throughout the experiment, recorded by a datalogger (CR10X, Campbell Scientific, Logan, USA).

As noted above, the water in the bucket was replaced approximately daily with water of a different isotopic composition to create cycles in the isotopic composition of the xylem water. The deionized Umeå tap water source had $\delta^2H = -177$ to -181 ‰ and $\delta^{18}O$ of -22.1 to -22.9 ‰. This can be considered the control. The enriched source had δ^2H -93.5 ‰ and $\delta^{18}O$ $+8.1$ ‰; it was produced by evaporating deionized Umeå tap water to approximately 3% of its original volume. The bucket water was analyzed on an IRMS (Thermo-Finnigan details, SLU stable isotope lab, Umeå, Sweden) to check its composition at the end of each cycle. Sample lines were removed from the tree whenever condensation was visible, which occurred only in the morning when greenhouse temperatures were coolest. In this case, the lines were dried with air drawn through a tube filled with drying agent until the CRDAS water-vapor concentration and isotopic composition indicated that condensed water had completely evaporated.

The mean arrival time of the label was estimated from the midpoint of the breakthrough curves. The midpoint was calculated as the mean of the steady-state values at the beginning and end of the cycle. This analysis was done on the first cycle because it was the only one that occurred entirely in daylight, meaning that transpiration continuously moved the water up the stem during the breakthrough period. The other cycles included periods of twilight or darkness and so presumably delayed the arrival of the label. The arrival time was compared to estimates of sap flow velocity for Scots pine trees in the field and from the same area. It is unfortunate that we neglected to measure the water uptake rates directly from the buckets; this limitation partially motivated the second experiment.

Intact-Root Greenhouse Experiment

The second greenhouse experiment was conducted in the Institute for Ecosystem Physiology, Freiburg, Germany in November and December 2018. One pine tree (*Pinus pinea* L.)

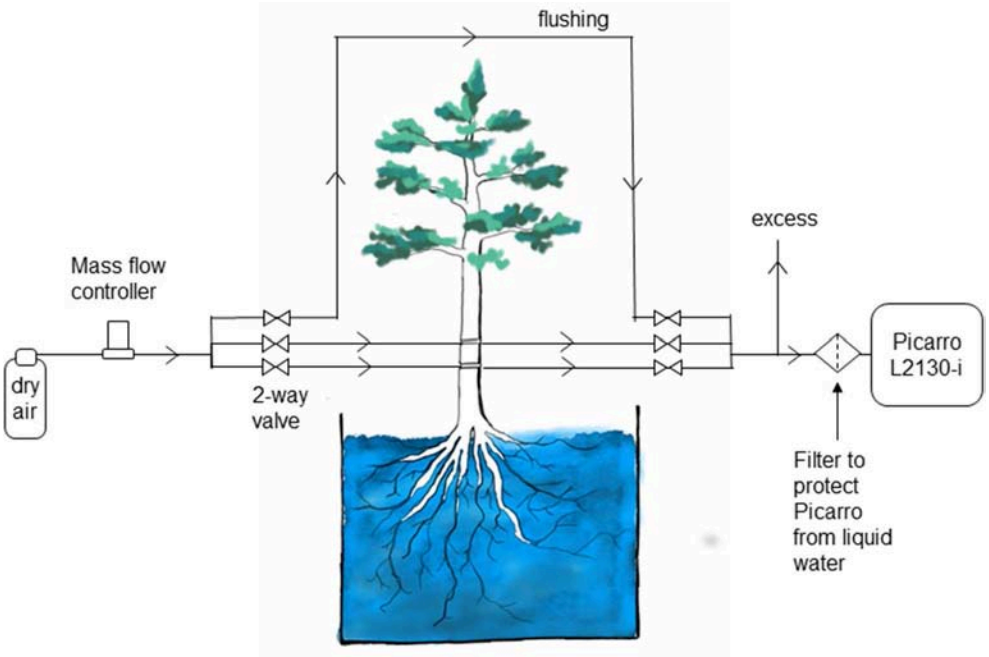

FIGURE 2 | Schematic of the setup for measuring water stable isotopes in tree xylem *in situ* in the Freiburg experiment.

was placed in a large pot under artificial light (12 h light, 12 h dark, switching on automatically at 07:00 o'clock). Two stem boreholes, positioned in parallel, were drilled through the trunk at 15 and 65 cm stem height, respectively. The boreholes were 10 mm in diameter and passed through the entire stem. Trunk diameter was 9.9 cm at the lower borehole and 8 cm at the upper one. Boreholes were flushed, as in the first experiment, with Acetone (Rotipuran, $\geq$ 99.8%, Carl Roth, Germany). Commercially available Swagelok connectors were then inserted at both sides of each borehole and PTFE tubing was attached.

Measurements in different boreholes as well as a control water vapor standard and a flushing line were combined in one automatic system. Automatic switching between individual measurements was realized with solenoid magnetic valves (2-Way Elec. Valve, EC-2-12, Clippard Minimatic, USA). For each measurement, a pair of valves (one at the inflow, one at the outflow) was opened and 80 mL min^{-1} of dry air, regulated via a mass flow controller (FC 260, Tylan General TCA GmbH, Germany), was pushed through the selected borehole or flow path. Water vapor was exchanged at areas with contact to liquid water and sampled gas was directed into a cavity ring-down spectroscopy analyzer (L2130-I, Picarro Inc., USA) to determine its water vapor isotopic composition. **Figure 2** shows a schematic drawing of the experimental setup.

In this experiment, we submerged intact tree roots in water of known isotopic composition ($\delta^{18}O = -8.43 \pm 0.05$ ‰, $\delta^{2}H = -59.28 \pm 0.24$ ‰). We included the roots in this second experiment out of concern for the impact of soil evaporation and potential isotopic fractionation due to the soil matrix (Orlowski et al., 2013, 2016; Gaj et al., 2017), which might therefore cause isotopic heterogeneity across the root system. This also had the advantage of enabling regular, uncomplicated sampling of the tree's source water. To avoid anoxic conditions, the water was well aerated using mini-pumps. On 21 November we changed the tree's source water to $^{2}H_2O$ labeled water ($\delta^{18}O = -9.22 \pm 0.19$ ‰, $\delta^{2}H = +297.57 \pm 3.08$ ‰) and monitored the subsequent change of the isotopic composition in the tree xylem at high time resolution. Weekly refilling to replace transpired water impacted source water isotopic composition. Samples were collected before and after each refilling. The isotopic composition of source water samples was measured with the same laser used for *in situ* measurements but using a vaporizer and switching the measurement mode to liquid injections.

Temperature and relative humidity (RH) of ambient air were recorded every 30 min (OM-EL-USB-2-PLUS, Omega Engineering Inc., United States, accuracy: RH: 2%, T: 0.3°C). Sap flow velocity was estimated with a sap flow sensor (heat pulse velocity sensor, Edaphic Scientific, Australia), installed 20 cm above and perpendicular to the upper borehole. After installation the sensor was thermally insulated. A baseline value for a sap flow velocity of 0 was determined after the experiment by inserting the sensor into a tree without leaves. For calculating sap flow velocities the method described in Hogg et al. (1997) was used.

Data Processing

Individual measurements lasted for 15 min and were preceded by a 5 min period of flushing the valve system with dry air. This on the one hand removed water vapor of the previous measurement from the tubing, while on the other hand allowed for detection and (to some extent) removal of condensed water. Mean values

for each measurement were calculated over the last 3 min of each cycle, when values of measured water vapor and isotopic composition were stable. Data points with a standard deviation greater than 0.5 ‰ and 1.5 ‰ for $\delta^{18}O$ and $\delta^{2}H$ raw values, respectively, were excluded from the data set. This was true for 2.4% of all measurements. On average boreholes were sampled every 3 h.

Temperature (T, °C) was recorded every minute with Type-T thermocouples (copper-constantan) in the bottom borehole and used to calculate equilibrium fractionation (Majoube (1971), as well as saturation vapor pressure inside the borehole (Murray, 1966). The water vapor concentration measured by the cavity-ringdown spectrometer was then compared to the saturated specific humidity at stem temperature T to obtain an estimate of relative humidity in the borehole. The relative humidity was used to assess whether full saturation with water vapor was achieved inside the borehole, indicating whether the assumption of equilibrium conditions inside the borehole was valid. It also revealed potential condensation under the given environmental conditions. Ideally, relative humidity h should approach 1.0. We arbitrarily chose an h of 0.8 as an indication that the dry air pushed into the borehole did not approach saturation. Data points with relative humidity below 0.8 were therefore excluded from the final, processed data set. Thus, excluded were 0.7 and 2.4% of the measurements from the bottom and top borehole, respectively.

Standardization of isotope measurements was done by manually sampling the headspace in four water vapor standards, once per day in the morning. The standards were held in airtight coffee bags (WEBAbag CB400-420BRZ, Weber Packaging GmbH, Germany) each filled with 50 ml of isotopically distinct water with −14.9, −9.4, 3.4 and −9.2 ‰ $\delta^{18}O$ and −110.8, −66.3, 3.8 and 367.7 ‰ $\delta^{2}H$, for light, medium, heavy, and label standard, respectively, and inflated with dry air. After each sampling, bags were refilled with dry air and kept in an insulated box, in which temperature was recorded throughout the day. Analogously to borehole measurements, liquid isotopic compositions were calculated from measured vapor values and T, assuming thermodynamic equilibrium. For quality control, a water vapor standard in an airtight glass container (Duran 1,000 ml, Schott AG, Germany) was integrated into the system and its headspace was automatically sampled (every 2–3 h). After processing collected data in the same way as the other measurements, derived isotopic compositions were 0.61 and 1.12 ‰ lighter compared to reference values of liquid water inside the bottle for $\delta^{18}O$ and $\delta^{2}H$, respectively.

Model Description

The model describes the isotopic composition of water vapor in air as it leaves the borehole and flows toward the isotope analyzer. It describes air flowing through a borehole of radius r in a tree stem of diameter l. The air inside the borehole of Volume $V = \pi r^2 l$ is turned over once after the time $t_u = V/u_o$. If the flow rate u_o is given in mol/s, then V has to be divided by the molar volume $V_{1mol} = 22.414/1000 \cdot T/T_0 \cdot p_0/p$ to give $\tilde{V} = V/V_{1mol}$, with standard temperature $T_0 = 273.15$ K and standard pressure $p_0 = 101\,325$ Pa.

We want to estimate whether this turnover time t_u is sufficient to allow full equilibration of incoming air with the water around the borehole walls. If the airflow is laminar, air is transported by molecular diffusion from the airstream to and from the borehole walls. The maximum diffusion time t_d is hence:

$$t_d = \frac{r^2}{4D} \tag{1}$$

with the diffusivity of vapor in air $D = D_0 \cdot p_0/p \cdot (T/T_0)^{1.88}$ and $D_0 = 2.12 \cdot 10^{-5}$ m^2/s. The velocity profile within the borehole is then parabolic with maximum velocity in the center of the air stream being twice the mean velocity, which is the measured velocity u_{obs}. We take hence $u_o = 2u_{obs}$ during the rest of the manuscript. The turnover time of the borehole volume by the air stream is then:

$$t_u = \frac{\tilde{V}}{2u_{obs}} \tag{2}$$

By comparing t_u and t_d, we can get an indication of whether the passage of air through the borehole is sufficiently slow to allow diffusion, which requires time t_d, to occur into the central air stream before the air stream leaves the borehole, which requires time t_u. Ideally, t_u would be much greater than t_d.

Total Water Vapor in the Borehole

We next sought to determine whether the borehole water vapor concentration would reach saturation before leaving the borehole. We note that air enters the borehole with flowrate u_i and mole fraction w_i and leaves the borehole with flowrate u_o and mole fraction w_o. If u_o is measured on moist air, then the flow rate is the same as the incoming flow rate u_i. If u_o is measured on dry air, then the incoming air flow must be corrected by the different vapor mole fractions of incoming and outgoing air: $u_i = u_o(1-w_o)/(1-w_i)$ (von Caemmerer and Farquhar, 1981). The change of the mole fraction within the borehole is hence the difference between incoming and outgoing moist air flow plus any evaporation E from the borehole surface A:

$$\tilde{V}\frac{dw_o}{dt} = u_i w_i - u_o w_o + \tilde{A}E \tag{3}$$

with $\tilde{A} = A/V_{1mol}$. If we assume that the surface of the borehole is not drying out, meaning that water is continuously supplied to the surface, then E is the exchange flux between the water vapor partial pressure above the borehole surface at stem temperature T_s and the air stream. The exchange flux happens by molecular diffusion $E = D \cdot dw/dr$, which gives:

$$\tilde{V}\frac{dw_o}{dt} = u_i w_i - u_o w_o + \frac{\tilde{A}D}{r}(w_{sat} - w_o) \tag{4}$$

with $w_{sat} = e_{sat}(T_s)/p$ and the saturation partial pressure over liquid water e_{sat}. Note that $A/r = 2\pi l.$, i.e. independent of the radius of the borehole r.

If $u_i = u_o$, this gives the non-steady-state development of the water vapor mole fraction within the borehole as:

$$w_o(t+dt) = w_o^{ss} + \left(w_o(t) - w_o^{ss}\right) e^{-\frac{dt}{t_w}} \tag{5}$$

with the steady-state mole fraction:

$$w_o^{ss} = \frac{u_o w_i + \frac{\tilde{A}D}{r} w_{sat}}{u_o + \frac{\tilde{A}D}{r}} \quad (6)$$

and the time constant:

$$t_w = \frac{\tilde{V}}{u_o + \frac{\tilde{A}D}{r}} \quad (7)$$

The steady-state mole fraction in the borehole is hence a weighted mean of the incoming mole fraction and the vapor coming from the borehole surface. Both airflow and diffusion help to reach steady state (Equation 6).

Isotopic Composition of Total Water Vapor in the Borehole

All mole fractions in Equation (7) carry an isotopic signature. There is a kinetic fractionation α_k (>1) during diffusion, but laminar airflow does not fractionate. This leads to the corresponding differential equation for the development of the isotopic composition in the borehole:

$$\tilde{V}\frac{dw_o R_o}{dt} = u_i w_i R_i - u_o w_o R_o + \frac{\tilde{A}}{r}\frac{D}{\alpha_k}(w_{sat} R_s - w_o R_o) \quad (8)$$

If the isotopic composition of the vapor partial pressure above the borehole surface R_s is in isotopic equilibrium with xylem water $R_s = R_x/\alpha^+$, and $u_i = u_o$, then the non-steady state development of the isotopic composition of water vapor in the borehole writes equivalent to Equations (5–7):

$$R_o(t+dt) = R_o^{ss} + \left(R_o(t) - R_o^{ss}\right) e^{-\frac{dt}{t_x}} \quad (9)$$

with the steady-state mole fraction:

$$R_o^{ss,x} = \frac{u_o w_i R_i + \frac{\tilde{A}D}{r} w_{sat}\frac{R_x}{\alpha_k \alpha^+}}{u_o w_i + \frac{\tilde{A}D}{r}\left[w_{sat} - \left(1 - \frac{1}{\alpha_k}\right) w_o\right]} \quad (10)$$

and the time constant:

$$t_{x,x} = \frac{\tilde{V} w_o}{u_o w_i + \frac{\tilde{A}D}{r}\left[w_{sat} - \left(1 - \frac{1}{\alpha_k}\right) w_o\right]} \quad (11)$$

where the index x indicates the assumption $R_s = R_x/\alpha^+$. It can be shown that $t_{x,x} \geq t_w$ and $t_{x,x} = t_w$ if $\alpha_k = 1$. Note that only $\alpha_k = 1$ gives a steady-state isotopic composition, which is a simple weighted mean of the isotopic compositions of incoming air and xylem water.

$R_s = R_x/\alpha^+$ assumes that water at the borehole surface is not changing but staying constant at the isotopic composition of xylem water R_x, even when exchanging isotopically with vapor in the borehole. If the borehole is not drying out, there must be a supply of water to the borehole surface. The water at the borehole surface might hence tend to a steady-state isotopic composition, where the evaporated water has the isotopic composition of the supply water, similar to leaf water enrichment (Craig and Gordon, 1965). Assuming that supply water has the xylem isotopic composition R_x, this means that the last term of Equation (11) is replaced by $\tilde{A}ER_x$ and the steady state composition is:

$$R_o^{ss,C} = \frac{u_o w_i R_i + \tilde{A}E R_x}{u_o w_i + \tilde{A}E} \quad (12)$$

and the time constant:

$$t_{x,C} = \frac{\tilde{V} w_o}{u_o w_i + \tilde{A}E} \quad (13)$$

with E given in Equations (6) and (7), and the index C indicating the Craig and Gordon steady-state assumption.

Water Vapor and Its Isotopic Composition Along the Borehole

The above derivations assume well-mixed borehole air, which is opposite to the idea of laminar flow. There will rather be a progressive development of water vapor saturation and then isotopic equilibrium from the inflow of the borehole to the outflow of the borehole. Each borehole segment passes on water vapor to the next after interacting with the water on the borehole walls. This would lead to a 2D advection-diffusion equation similar to Equation (20) of Ogée et al. (2007). We do not attempt to solve such a partial differential equation here. We rather discretize the borehole in N segments along the air flow path, where the outflow of one segment is the inflow of the next segment, i.e. that w_o and R_o of segment $i-1$ is w_i and R_i of segment i. Such a procedure approaches the exact solution when using small segments, i.e., large N.

We calculate in the following only solutions to the steady-state equations, assuming rather steady conditions of incoming air, i.e., w_i and R_i. We note that atmospheric concentrations near a forest floor can change rapidly due to emanation from or exchange with the ground. Such rapid fluctuations can be alleviated using a buffer volume. We hence present the following calculations assuming steady state conditions in vapor isotopic composition in all N segments.

We further differentiate three cases:

(3.1) constant isotopic composition of borehole surface water, $R_s = R_x/\alpha^+$,

(3.2) Craig-Gordon steady state for the water at the borehole surface, $R_s = R_C/\alpha^+$, where the borehole surface is in steady state with the vapor isotopic composition of the current segment, and

(3.3) a mixture of both, assuming mixing of unenriched xylem water with the evaporating water at the borehole surface, $R_s = f R_x/\alpha^+ + (1-f) R_C/\alpha^+$.

The model cases are used to assess the isotopic composition across a range of conditions. These include variations in flow rate, tree diameter, incoming water vapor concentrations, and fractional mixing of xylem water with water in isotopic equilibrium with borehole vapor.

RESULTS

Cut-Stem Greenhouse Experiment

When the label was taken up by a cut stem, the asymptotic values at the end of each labeling cycle confirmed that the measured isotopic composition matched the expected values well (**Figures 3A,B**). It took several hours after a change in water source before this agreement was reached because it took several hours for the label to reach the borehole. The yellow bars in **Figure 3** show the time elapsed between the change in source water and the time when the change in label intensity reached its midpoint. We use that time as an estimate of the average arrival time for the label. Only the first cycle was used because it was entirely during the light period, meaning that transpiration continued throughout this period. We estimate that the decline required 4:55 h for $\delta^{18}O$ and 5:21 for $\delta^{2}H$ to reach this inflection point.

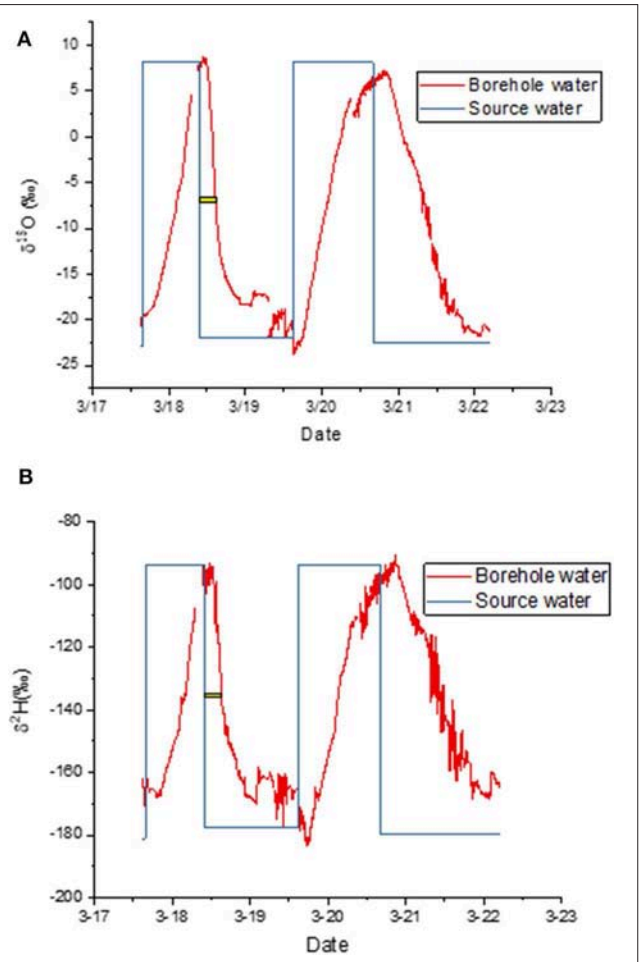

FIGURE 3 | (A,B) Measured isotopic composition of water vapor exiting the borehole (red) and water vapor composition predicted from source water, i.e., source water isotopic composition plus equilibrium fractionation (blue). The yellow bar shows the lag between the change in source water and the mean arrival time in the borehole. Panels show time courses for **(A)** $\delta^{18}O$ and **(B)** $\delta^{2}H$.

There was evidence of condensation in the early morning during this first experiment (**Figure 3**). We therefore disconnected the lines each morning and attached a Drierite column to the borehole inlet. We then pumped dehumidified air through the tubing until the water vapor concentration fell to nearly zero. This dry-down was accompanied by a typical Rayleigh distillation curve as the residual water evaporated (not shown).

Whole-Root Greenhouse Experiment

Our second experiment tested the method using trees with intact root systems. During this experiment, ambient air T and RH averaged 17.3 ± 1.7°C and 46 ± 6% and featured a pronounced diurnal course corresponding to the prevalent light cycle (**Figure 4A**). The variation was large because these diurnal curves represent diurnal patterns over 6 weeks in an indoor hangar not designed to maintain constant conditions. T measured inside the borehole was on average 16.8 ± 1.3°C and therefore 0.5°C lower than the ambient air. Sap flow had a mean velocity of 0.97 ± 0.39 cm h^{-1} and it showed a distinct daytime increase. Mean values with standard deviations over the diurnal course are displayed in **Figure 4B**.

We used the model to estimate time constants for the borehole geometries, which are presented in **Table 1**. The much higher values of t_u compared to those of t_d or t_s again suggest that the air was inside the borehole long enough for the diffusion and evaporation to cause the water vapor in the borehole to approach equilibrium.

For this second experiment, we again compared measured isotopic composition to predictions based on source water values. We present the time courses of liquid xylem water isotopic composition in relation to the trees' source water in **Figure 5**. From these data, we calculated mean deviations of the *in situ* liquid xylem water measured from that of source water during periods that showed stable isotope values for $\delta^{2}H$. The measurements before 22 November represent natural abundance, those after 3 December 2018 show the effect of the label. A negative deviation signifies that *in situ* isotopic composition was more negative compared to source water. For the bottom borehole, the deviations were nearly zero. This means that the derived xylem water isotopic composition agreed with the source water values according to the model assumption 3.1 for both natural abundance ($\delta^{18}O = -0.1 \pm 0.6$ (SD) ‰, $\delta^{2}H = 1.8 \pm$

TABLE 1 | Tree and borehole characteristics, as well as time constants for air flow and diffusion.

Borehole	Height	Tree diameter	t_d	t_u	t_w
Top	65 cm	8 cm	0.24 s	1.77 s	0.46 s
Bottom	15 cm	9.9 cm	0.24 s	2.33 s	0.47 s

t_d is the time constant for diffusion across the unstirred layer at the edge of the borehole, t_u is the time constant for passage through the stem, and t_w is the time constant to reach water vapor saturation. These values suggest that the air passing through the borehole had adequate time to approach isotopic equilibrium.

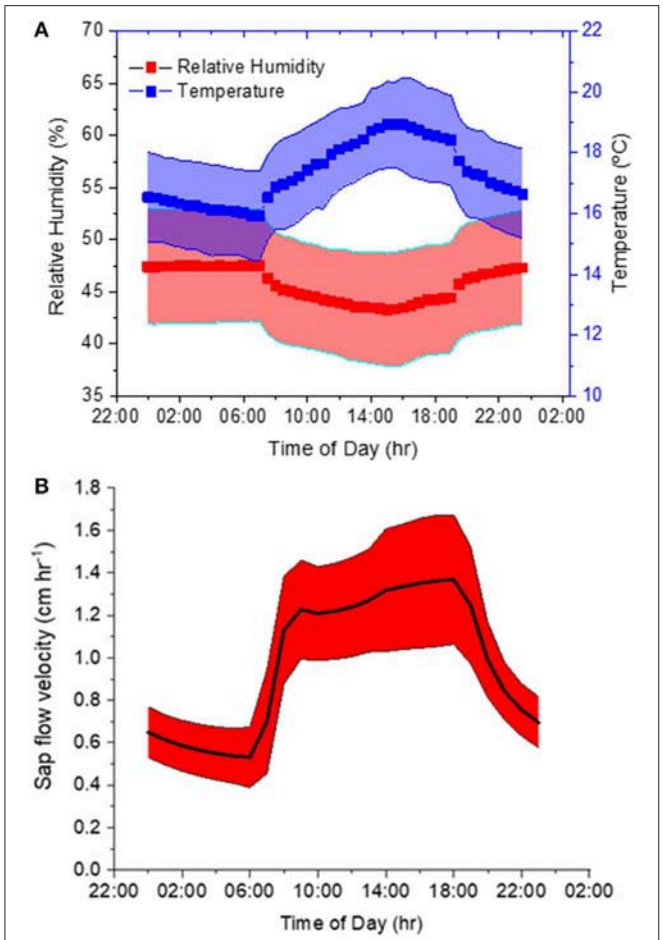

FIGURE 4 | (A,B) Diurnal variations of **(A)** ambient temperature (T) and relative humidity (RH), as well as **(B)** sap flow velocity averaged over the six-week course of the experiment.

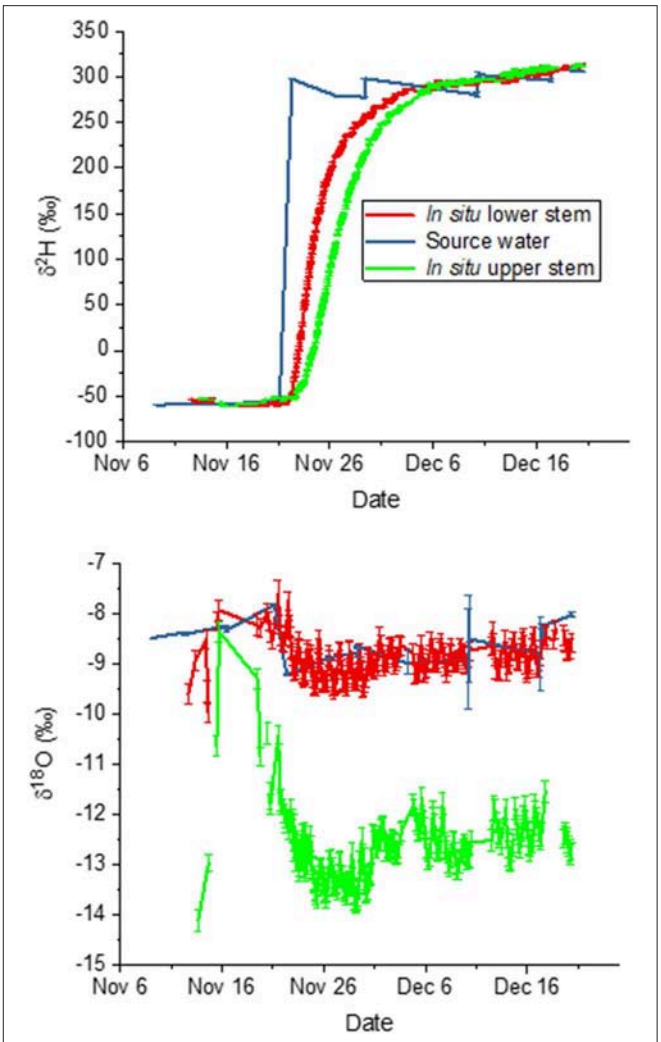

FIGURE 5 | Time course of liquid xylem water isotopic compositions derived *in situ* from measured vapor phase values for the top and bottom borehole in relation to the tree's source water.

2.3 ‰) and the label phase ($\delta^{18}O = -0.25 \pm 0.22$ ‰, $\delta^{2}H = 0.09 \pm 7.8$ ‰). In contrast, the top borehole showed systematic deviations from source water values for both $\delta^{18}O$ and $\delta^{2}H$. $\delta^{18}O$ xylem values were depleted in ^{18}O in relation to source water by -2.8 ± 1.5 ‰ and -3.9 ± 0.3 ‰ for the natural abundance and label phase, respectively. The $\delta^{2}H$ xylem values were more similar in ^{2}H to source water, differing by only 5.3 ± 3.0 and 1.9 ± 8.5 ‰.

In both boreholes $\delta^{2}H$ increased in a similar pattern from initial source water values (natural abundance) to the labeled water value after the change in source water on 21 November. However, in the top borehole the increase was delayed and less steep. We compared the lags in arrival of the label to measured sap flow velocities. The velocity estimated by the sap flow probes was 0.97 ± 0.4 cm hr^{-1}. If we estimate time to the midpoint in the $\delta^{2}H$ increase over time, which provides an estimate of the average uptake velocity, we find it after 70 h at the lower borehole and 124 h at the upper one. The lag time between the two was thus 54 h, yielding 1.08 cm hr^{-1} on average. When compared to the mean sap flow velocity, the agreement is very good.

Although the model predicted that the borehole water vapor should be at saturation, we wished to confirm that the borehole air had reached water vapor saturation by the time it left the borehole. This was important because it might influence whether the water vapor had approached isotopic equilibrium. We therefore calculated relative humidity corrected to borehole temperature for every measurement (see Material and Methods section). On average relative humidity was 98 ± 2% for the bottom borehole and 88 ± 3% for the top borehole.

Modeling

We used the model to test the feasibility and limits of the borehole method. We first estimated the time constants for diffusion of water vapor to and from the borehole wall, and for the flowing airstream in the center of the borehole. If the diffusion were much faster than the passage through the borehole, it would be reasonable to assume that the isotopic composition of the water vapor in the borehole reflects that of the xylem water on the walls. We began by assuming the size of the borehole (10 mm), the flow rate (40 mL min^{-1}, the flow rate induced by the vacuum pump)

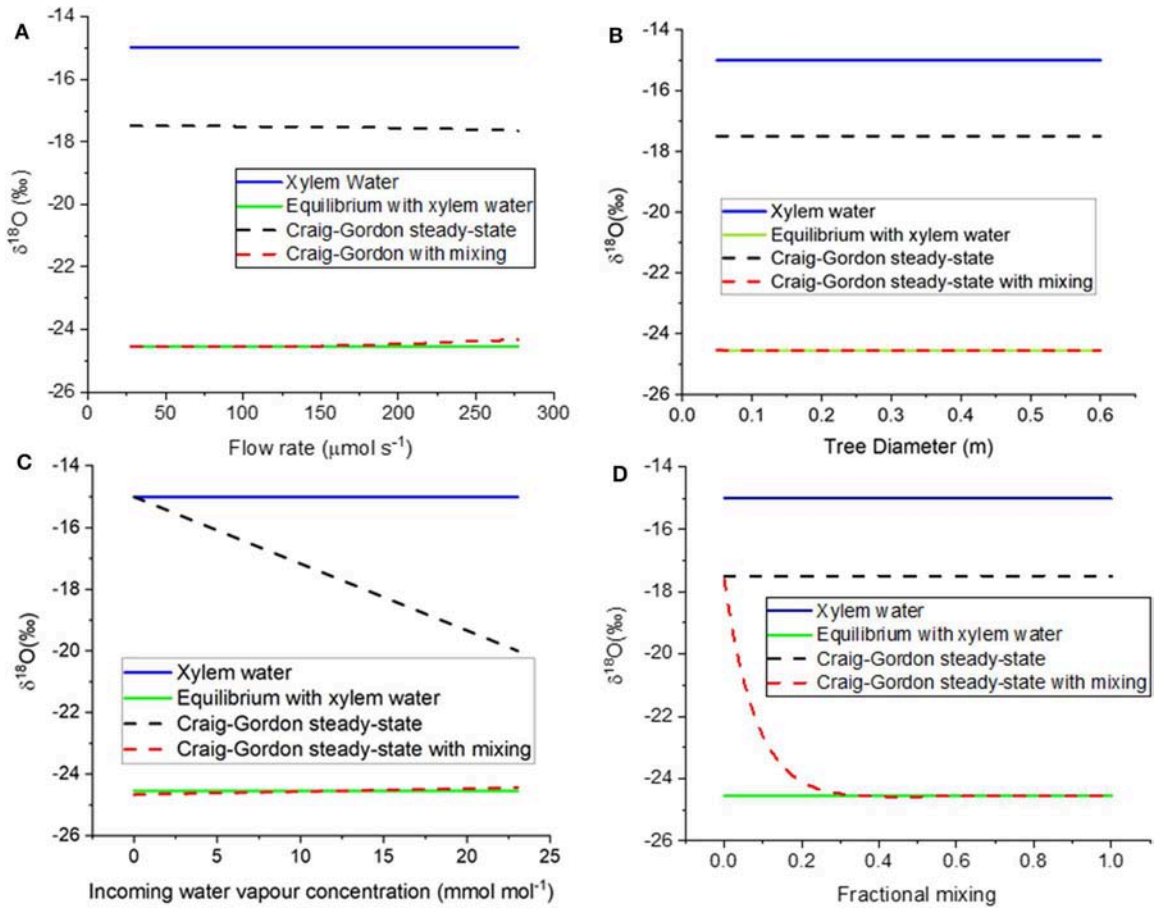

FIGURE 6 | (A–D) Modeled $\delta^{18}O$ of borehole xylem water. The figures show responses to variation in **(A)** flow rate through the stem, **(B)** stem diameter, and therefore wetted length of the borehole, **(C)** incoming water vapor concentration, and **(D)** fractional mixing of unenriched xylem water with borehole surface water in Craig-Gordon steady state. The four curves in each panel show the liquid stem water (blue solid line), water vapor in equilibrium with stem water (green solid line, model assumption 3.1), borehole surface water in Craig-Gordon steady-state (black dashed line, model assumption 3.2), and constant renewal of 35% of enriched borehole surface water with unenriched xylem water (red dashed line, model assumption 3.3).

and temperature (10°C), we found that the throughflow time (t_u) was 5.9 s. The time for diffusion (t_d) was 0.28 s, more than 20 times faster. This result supported the notion that the borehole water vapor could come almost to equilibrium with the xylem water during its passage through the stem.

The model describes the relative humidity in the borehole both at steady-state and non-steady state conditions (Equations 6–10). Using the parameter values above, and adding an inflow relative humidity of 50%, we estimated that relative humidity would reach 99% after thrice the time constant ($t_w = 0.24$ s) inside the borehole. Not surprisingly, t_w is almost the same as the t_d estimate above.

The model solves for the isotopic composition of water vapor in the airstream leaving the borehole when the water vapor was passed from one segment in the stem to the next. We assumed the xylem water had an isotopic composition of −15 ‰ and that the incoming water vapor was −20 ‰. The rapid increase in humidity described above is accompanied by diffusion to and from the walls of any water vapor in the laminar airstream. These vapor fluxes are small in comparison to the liquid water pool in the xylem, but they determine the isotopic composition of the thin rind of water that exchanges.

Recall that the model compared three opposing ideas about how this rind should behave. First (model assumption 3.1), we assumed that it would simply mix into the much larger volume of xylem water that surrounds it. Next (model assumption 3.2), we assumed that the thin rind would enrich with time, reaching a steady-state isotopic composition given by the Craig-Gordon equation. Finally (model assumption 3.3), we assumed enrichment of the thin rind to the Craig-Gordon value but also a constant recharge of new xylem water into the rind. We found that the mixing rate needed to equal or exceed 35% of Craig-Gordon rind water with the remainder as unenriched xylem water. We used this value for our assessments of assumption 3.3 in all the work that follows.

The different assumptions are compared to model results in **Figures 6A–D**. When model assumption 3.1 (equilibrium with xylem water) was thus parameterized, the resulting value was

−25.6 ‰; this compares well with the equilibrium value of −25.7 ‰. If the flow rate is defined by the CRDAS pump (40 mL/min, or 0.000028 mol s^{-1}, at the far left of **Figure 6A**), then the steady-state with mixing water isotopic compositions was similar to the equilibrium value. Even if the flow were increased by ten-fold, the resulting steady-state prediction would still agree reasonably well. The Craig-Gordon steady-state value (model assumption 3.2) was quite different, but varied little, across the range of flow rates.

As tree diameter increased, the model predicted that water vapor concentration approaches saturation and the $\delta^{18}O$ of water vapor approaches equilibrium with the xylem water. Already at diameter 0.05 m, the steady-state with mixing agrees with the equilibrium with xylem water (**Figure 6B**). Again, model assumption 3.2 (Craig-Gordon steady state) is nearly constant, but quite different from the other two assumptions.

We also used the model to test the influence of the relative humidity of the air entering the borehole (**Figure 6C**). The Craig-Gordon model (assumption 3.2) was the only one that predicted a difference in the isotopic composition of the vapor, decreasing the predicted $\delta^{18}O$ linearly as the inlet humidity increased.

As noted above, model case 3.3 allowed for mixing of the unenriched xylem water with the evaporating water at borehole surface, where the latter was described by the Craig-Gordon equation. The x-axis in **Figure 6D** is a proportional mixing rate between the xylem water and the evaporating water. In the absence of mixing, the Craig-Gordon steady state (assumption 3.2) applies. But as the mixing rate increased, the water vapor from the mixing assumption (3.3) approached equilibrium with the unenriched xylem water (assumption 3.1). As noted above, in our modeling we used a value of 0.35. This was the lowest rate that yielded a value consistent with the empirical data, which approached equilibrium with the unenriched xylem water (**Figures 3**, **5**). However, any value higher than 0.35 would yield the same result.

DISCUSSION

We present the results of two experiments and a modeling exercise that show the isotopic composition of xylem water can be continuously monitored with a borehole through the stem. Under these conditions, the borehole water vapor predicted the isotopic composition of the liquid water in the xylem. This was true of both natural abundance and labeled water sources. Moreover, the label arrived at the boreholes approximately when it was expected. Sap flux in Scots pine (the cut-stem experiment) is reported to occur at about 1 meter per 12-h day (Tor-ngern et al., 2017). Because the height of the borehole above the cut end of the stem was 0.40 m, theory suggests that the label should have arrived in 4.8 h. Thus, the prediction was also well matched by the observations. This means that the method was able to detect the shift in xylem water approximately when it was expected to arrive. Sap flow was measured in the intact root experiment and, as noted above, it matched the arrival times very well.

The model shows that the borehole water vapor pool approaches equilibrium with the xylem water under suitable conditions, including the ones we measured. We also show that the method should work up to rather high flow rates, in small stems, and in the presence or absence of incoming water vapor. If there were problems, they would likely be detected as a failure to reach water vapor saturation at stem temperature.

Condensation and Water Scrubbing

The high relative humidity required by this method leads to practical concerns about condensation in the borehole and in the lines leading to the analyzer. This would create memory effects due to the condensed water, delaying the arrival of the isotopic signal from the xylem to the analyzer. This is one weakness of the borehole technique; condensation must be considered in the sampling design and frequent checks are needed to ensure that the sample lines are dry. However, this has been recognized as a main issue in any online water isotope measurement approach (e.g., Volkmann and Weiler, 2014; Gaj et al., 2016). We addressed this problem in the Umeå experiment by manually attaching a dry air supply to the lines every morning and evaporating the condensate. In the Freiburg experiment, an automated system provided dry air to the sample lines at intervals, clearing the lines of any condensate that might have formed. In addition, the sample lines were heated (Volkmann et al., 2016). The success of these approaches is reflected in the rapid response to changes in the xylem water supply, which matched predictions based on sap flow in both experiments. A second weakness of the approach is the risk of drawing liquid water into the CRDS. A mesh or filter can be used to protect against this. Ideally, the mesh would be small enough to block flow in the tube, stopping the water at the filter (**Figure 2**).

It may seem obvious that scrubbing the water out of the inlet air should improve the data. There would then be no need to make assumptions about the mixing of incoming water vapor and evaporated xylem water mixing. Any water in the exiting airstream would necessarily have come from the xylem, especially in the presence of positive pressure (Volkmann et al., 2016). The disadvantage is that the scrubbing of water vapor requires the replacement of chemical traps, or power to run a drying tower. Our model case 3.3 suggests that such precautions are unnecessary given the apparent mixing with xylem water (**Figure 6C**). The model results are confirmed by the match to empirical data even in the absence of water scrubbing (**Figure 3**).

$\delta^{18}O$ Discrepancies

Data from the Freiburg experiment showed an offset of up to 4 ‰ in $\delta^{18}O$ (for the time after the labeling pulse) relative to source water values in one of the boreholes. Interestingly, the borehole was more depleted than the source water, almost the same offset as found by Volkmann et al. (2016) in their equilibration probe experiments. No such discrepancy was observed in the Sweden data. The discrepancy observed in the Freiburg experiment can likely be attributed to non-equilibrium conditions caused by the shorter exchange path (smaller stem diameter) and was only observed in the upper of the two boreholes. Volkmann et al. (2016) speculated that their discrepancy was due to organic contamination of the water vapor, which interferes with the wavelengths used to determine the isotopic composition. They

suggested that these interferents can be accounted for in post-processing. In the presented experiments, we did not find a major influence of contamination by organic compounds; otherwise source and measured isotopic compositions would not have matched (see West et al., 2010, 2011). We argue here that the Volkmann et al. (2016) offset might be due to non-equilibrium conditions as well.

One other possible explanation for the $\delta^{18}O$ discrepancy in the intact-root experiment, but not the cut-stem experiment, is that the roots fractionate against ^{18}O during water uptake. Such fractionation was detected in mangroves (Lin and Sternberg, 1993) and a range of woody xerophytes (Ellsworth and Williams, 2007), but it was detected for $\delta^{2}H$ and not $\delta^{18}O$. This is opposite the pattern we observed, where the discrepancy was in $\delta^{18}O$, not $\delta^{2}H$. We therefore think that fractionation upon root uptake is not responsible for the observed discrepancy.

Location of Equilibration

What is the actual surface area equilibrated? The model (**Figure 6B**) assumes that the entire surface area of the borehole is available for equilibration. However, a core of heartwood at the center of a tree stem is often dry. If it is dry, its thickness should be removed from the calculated area. This may be a significant loss in some stems, e.g., oak trees. If it is not dry, as when the heartwood is partially decayed, its isotopic composition may be different from the sapwood. In fact, such differences have seldom been observed when the heartwood has been checked. However, if the heartwood signal were different, it might carry through into the outlet airstream, especially if the sapwood is thin (Turner et al., 2000).

This leads to the question of which part of the stem actually controls the final isotopic composition. Given the rapid equilibration and slow airflow in our experiment, it would seem that the final composition would be determined in the last few cm before the airstream is carried out of the tree. We used the pipe-fitting threads on Swagelok fitting to attach tubing to the boreholes. These fittings were turned approximately two cm into the tree. The outer portion was bark, which should be excluded from the xylem equilibration. However, the inner portion entered the sapwood and blocked contact between the borehole airspace and the outermost sapwood. This would also reduce the borehole surface area and might, if the sapwood were narrow, prevent equilibration. Sapwood thickness varies greatly amongst species (Marshall and Waring, 1986; Turner et al., 2000; Quiñonez-Piñón and Valeo, 2017), but it was thick in our pines—nearly to the center (as also observed by Torngern et al., 2017). The good match of source to measured water isotopic composition suggests that in the present case this was not an issue. Furthermore, the model predicts that equilibration occurs even over distances as short as 0.05 m (**Figure 6B**). On the other hand, the data from the upper borehole in the Freiburg experiments recommend caution when using stems less than 10 cm in diameter if the flow rate is 80 mL min^{-1} or more. In summary, the design of a stem borehole study needs to consider sapwood thickness depending on the species-of-interest and its growing conditions.

Pitch and Cavitation

The borehole creates a significant wound in the stem, especially if it is as large as the ones we used (6 and 10 mm diameter in Umeå and Freiburg, respectively). The model suggests that the diameter has no effect on the equilibration, but pines tend to produce pitch around wounds in the stem, which might close the hole. Before data collection, we washed the boreholes repeatedly with acetone hoping that it would remove the pitch and kill the cells that would otherwise produce more. This appeared to keep the boreholes open, but there was still some pitch appearing on the borehole walls. We presume that these wall deposits might further decrease the effective area available for equilibration. This problem should be reduced in most other genera of trees in comparison to the chosen pines because this species is known to produce large amounts of pitch. One might ask if the combination of boring and acetone will not damage the tree. It must have some effect, but there has been no sign of damage in the growth or gas-exchange of five 30-cm diameter Scots pine trees treated similarly in 2014.

Another concern is the extent of cavitation in xylem cells near the borehole wall. Because the xylem functions under tension, cavitation must occur at least in the cells that were cut by the drill, and probably several cells deeper (Pfautsch, 2016; Wiedemann et al., 2016). In addition, there is a compartment formed around the wound, primarily to prevent microbial invasion (Morris et al., 2016). Constant evaporation in the borehole could dry up its surface if cavitation or compartmentation blocked the supply of water from the cavitated xylem vessels or tracheids. We could not detect any trend in the relative humidity within the borehole that would have indicated drying of the borehole. It is possible that even if the cell lumens are cavitated, water continued to diffuse through the cell walls toward the borehole wall. Continued wetting of the borehole surface was the reasoning behind model assumption 3.3, where borehole surface water tends toward isotopic equilibrium with xylem water because it is constantly renewed and mixed with the water evaporating at Craig-Gordon steady state. However, it seems that the wounding and its repair should eventually lead to isolation of the borehole water supply from the flowing xylem water, limiting how long a borehole can be used. We saw no evidence that we approached this limit in our experiments.

Model Assumptions

The model was written such that it made three different assumptions about the evaporating water at the surface of the borehole. Model assumption 3.1 stated that the water vapor would equilibrate isotopically with xylem water in each segment of the borehole, and then be passed inward to equilibrate over the next segment, until the airstream left the borehole. This was based on the presumption that the xylem water pool is so much bigger than the borehole vapor pool that it would overwhelm the vapor signal on its passage through the stem. Note that this formulation contradicts the Craig-Gordon model (3.2) however, because the latter simply mixes water derived from the incoming water vapor with xylem water, disallowing any change in the borehole water vapor as it passes from one segment to the next. In contrast, model assumption 3.3 supposed that there is some mixing of the evaporating water at the borehole surface with the unenriched

xylem water nearby. The mixing was set at different rates, from 0 to 1 per time step, and the model was then run as normal. This model drove the isotopic composition of the borehole vapor rapidly to equilibrium with the unenriched xylem sap if at least 35% of the borehole surface water was replaced by unenriched xylem water (**Figure 6D**). This could happen, for example, if 35% of the borehole was exposed to unenriched xylem water and the remainder was at Craig-Gordon steady state. We think it is likely that the mixing occurred due to diffusion toward and away from the evaporation/condensation sites, especially after the borehole humidity had reached saturation.

Continuous measurements of the isotopic composition of xylem sap describe an important middle ground between soil and leaves. Both surface soils and leaves undergo rapid fluctuations in isotopic composition. It is possible to predict their influence on transpiration, but it is difficult. Soils vary due to precipitation events and subsequent evaporation from the surface (Dubbert et al., 2013). Transpiration varies over the course of a day as the leaf water pools are enriched and then depleted by exchange with the atmosphere (Dubbert et al., 2014). The isotopic composition of xylem sap changes more slowly. It provides a direct integrated measure of the isotopic composition of water uptake from all potential water sources (Brinkmann et al., 2018, but see, e.g., Vargas et al., 2017). A continuous monitoring of xylem water isotopes might therefore enable to directly detect changes in water sourcing (e.g. during droughts), identify groundwater use of vegetation (compare Beyer et al., 2018) or investigate hydraulic redistribution. Likewise, the rapid diurnal fluctuations in the isotopic composition of transpired water necessarily converge, when integrated over a day, on the isotopic composition of the water flowing up the xylem (Dubbert et al., 2014). Thus, many of the complexities of leaf transpiration disappear in the xylem-sap data. What remains is the isotopic composition of the daily sum of root water uptake and hence transpiration.

Note that the model is based on a simple description of flow in the borehole, where a central core of moving air flows through a volume of still air. Within the still volume, water vapor diffuses to and from the borehole wall to and from the moving airstream. The model could be made more realistic and experimental tests of the flow conditions in the borehole could be conducted. We argue that the model is sufficient for the current purpose. That argument is supported by the agreement of the modeled and measured data.

CONCLUSIONS

This study proves the potential utility of the stem borehole equilibration. The model leads us to suggest that the physics should be general, but it will of course be necessary to test the method in other species and other conditions. For example, angiosperm species with ring-porous wood, such as oak, might behave differently than the tracheid-bearing wood of pines. Comparisons to angiosperm species with and without tyloses and with varying hydraulic conductance would also be useful. The method appears to be accurate enough to measure the passage of small changes in natural abundance through the stems, for example after a precipitation event. In addition, we note that we were able to follow the passage of an isotopic label through tree stems. This might provide useful checks of *in situ* sap flow rates and a means of observing spatial patterns of water uptake in trees. *In situ* isotope methods offer an immense potential for describing and understanding the dynamic character of natural systems, which has been recognized by the scientific community as an urgent issue (e.g., Sprenger et al., 2016; Brantley et al., 2017; Penna et al., 2018). Combined data sets of depth-dependent soil water isotopes and xylem (transpiration) water isotopes will improve our understanding of ecosystems under changing environmental conditions and address several of the current shortcomings of traditional methods.

DATA AVAILABILITY STATEMENT

The datasets generated for this study are available on request to the corresponding author.

AUTHOR CONTRIBUTIONS

JM designed and conducted experiment 1. MB, MD, and KK designed and conducted experiment 2. MC wrote the model. All contributed to the writing.

FUNDING

JM was supported by the Knut and Alice Wallenberg Foundation (#2015.0047). MC was supported by a grant overseen by the French National Research Agency (ANR) as part of the Investissements d'Avenir program, LabEx ARBRE (ANR-11-LABX-0002-01), and by funding from the ERA-NET Sumforest project ForRISK, funded in France through ANR (Grant No. ANR-16-SUMF-0001-01). Sumforest was funded by the European Union under Grant Agreement No. 606803. MB was supported by MC was supported by the Volkswagen Foundation [A122505 (ref. 92889)].

ACKNOWLEDGMENTS

We thank Tomas Lundmark of the Department of Forest Ecology and Management, SLU, and the Svartbergert Field station, SLU for his partial support of JM, his purchase of the Picarro, and the provision of housing. Thomas Hörnlund, also of the Svartberget Field Station, provided logistical help in the cut-stem experiments. In addition, JM was partially supported by the Knut and Alice Wallenberg Foundation (2015.0047, Physiological Branch-Points with Ecosystem Consequences.). MC was supported by a grant overseen by the French National Research Agency (ANR) as part of the Investissements d'Avenir program, LabEx ARBRE (ANR-11-LABX-0002-01), and by funding from the ERA-NET Sumforest project ForRISK, funded in France through ANR (Grant No. ANR-16-SUMF-0001-01). Sumforest was funded by the European Union under Grant Agreement No. 606803. MB was supported by the Volkswagenstiftung under contract number A122505

(ref. 92889). We also thank Malkin Gerchow, University of Braunschweig, for technical support. We also thank Angelika Kübert, Ruth Magh, and Adrian Dahlmann for technical and scientific support, all at the Institute of Ecosystem Physiology in Freiburg. We also thank Christiane Werner for provision of infrastructure and general support during the Freiburg experiment. KK was supported in part by DFG project number is: DU1688/1-1.

REFERENCES

Barbeta, A., Jones, S. P., Clavé, L., Wingate, L., Gimeno, T. E., Fréjaville, B., et al. (2018). Hydrogen isotope fractionation affects the identification and quantification of tree water sources in a riparian forest. *Hydrol. Earth Syst. Sci. Dis.* 23, 1–29. doi: 10.5194/hess-2018-402

Barbeta, A., Jones, S. P., Clavé, L., Wingate, L., Gimeno, T. E., Fréjaville, B., et al. (2019). Unexplained hydrogen isotope offsets complicate the identification and quantification of tree water sources in a riparian forest. *Hydrol. Earth Syst. Sci.* 23, 2129–2146. doi: 10.5194/hess-23-2129-2019

Barr, A. G., Black, T. A., Hogg, E. H., Griffis, T. J., Morgenstern, K., Kljun, N., et al. (2007). Climatic controls on the carbon and water balances of a Boreal Aspen forest, 1994–2003. *Glob. Change Biol.* 13, 561–576. doi: 10.1111/j.1365-2486.2006.01220.x

Beyer, M., Hamutoko, J. T., Wanke, H., Gaj, M., and Koeniger, P. (2018). Examination of deep root water uptake using anomalies of soil water stable isotopes, depth-controlled isotopic labeling and mixing models. *J. Hydrol.* 566, 122–136. doi: 10.1016/j.jhydrol.2018.08.060

Beyer, M., Koeniger, P., Gaj, M., Hamutoko, J. T., Wanke, H., Himmelsbach, T. (2016). A deuterium-based labeling technique for the investigation of rooting depths, water uptake dynamics and unsaturated zone water transport in semiarid environments. *J. Hydrol.* 533(Suppl.C), 627–43. doi: 10.1016/j.jhydrol.2015.12.037

Brantley, S. L., Eissenstat, D. M., Marshall, J. A., Godsey, S. E., Balogh-Brunstad, Z., Karwan, D. L., et al. (2017). Reviews and syntheses: on the roles trees play in building and plumbing the critical zone. *Biogeosciences* 14, 5115–5142. doi: 10.5194/bg-14-5115-2017

Brinkmann, N., Seeger, S., Weiler, M., Buchmann, N., Eugster, W., and Kahmen, A. (2018). Employing stable isotopes to determine the residence times of soil water and the temporal origin of water taken up by *Fagus sylvatica* and *Picea abies* in a temperate forest. *New Phytol.* 219, 1300–1313. doi: 10.1111/nph.15255

Busch, D. E., Ingraham, N. L., and Smith, S. D. (1992). Water uptake in woody riparian phreatophytes of the Southwestern United States: a stable isotope study. *Ecol. Appl.* 2, 450–459. doi: 10.2307/1941880

Craig, H., and Gordon, L. I. (1965). "Deuterium and oxygen-18 variations in the ocean and the marine atmosphere," in *Stable Isotopes in Oceanographic Studies and Palaeotemperatures*, ed E. Tongiorgi (Pisa: Lab. Geologia Nucleare), 9–130.

Cuntz, M., Ogée, J., Farquhar, G. D., Peylin, P., and Cernusak, L. A. (2007). Modelling advection and diffusion of water isotopologues in leaves. *Plant Cell Environ.* 30, 892–909. doi: 10.1111/j.1365-3040.2007.01676.x

Dongmann, G., Nürnberg, H. W., Förstel, H., and Wagener, K. (1974). On the enrichment of H218O in the leaves of transpiring plants. *Rad. Environ. Biophys.* 11, 41–52. doi: 10.1007/BF01323099

Dubbert, M., Cuntz, M., Piayda, A., Maguás, C., and Werner, C. (2013). Partitioning evapotranspiration—testing the craig and gordon model with field measurements of oxygen isotope ratios of evaporative fluxes. *J. Hydrol.* 496, 142–153. doi: 10.1016/j.jhydrol.2013.05.033

Dubbert, M., Cuntz, M., Piayda, A., Maguás, C., and Werner, C. (2014). Oxygen isotope signatures of transpired water vapor: the role of isotopic non-steady-state transpiration under natural conditions. *New Phytologist* 203, 1242–1252. doi: 10.1111/nph.12878

Dubbert, M., and Werner, C. (2019). Water fluxes mediated by vegetation: emerging isotopic insights at the soil and atmosphere interfaces. *New Phytologist* 221, 1754–1763. doi: 10.1111/nph.15547

Ellsworth, P. Z., and Williams, D. G. (2007). Hydrogen isotope fractionation during water uptake by woody xerophytes. *Plant Soil* 291, 93–107. doi: 10.1007/s11104-006-9177-1

Evaristo, J., Jasechko, S., and McDonnell, J. J. (2015). Global separation of plant transpiration from groundwater and streamflow. *Nature* 525, 91–94. doi: 10.1038/nature14983

Farquhar, G. D., Cernusak, L. A., and Barnes, B. (2007). Heavy water fractionation during transpiration. *Plant Physiol.* 143, 11–18. doi: 10.1104/pp.106.093278

Flanagan, L. B., Ehleringer, J. R., and Marshall, J. D. (1992). Differential uptake of summer precipitation among co-occurring trees and shrubs in a pinyon-juniper woodland. *Plant Cell Environ.* 15, 831–836.

Gaj, M., Beyer, M., Koeniger, P., Wanke, H., Hamutoko, J., and Himmelsbach, T. (2016). *In situ* unsaturated zone water stable isotope (^{2}H and ^{18}O) measurements in semi-arid environments: a soil water balance. *Hydrol. Earth Syst. Sci.* 20, 715–731. doi: 10.5194/hess-20-715-2016

Gaj, M., Kaufhold, S., Koeniger, P., Beyer, M., Weiler, M., and Himmelsbach, T. (2017). Mineral mediated isotope fractionation of soil water. *Rapid Commun. Mass Spectr.* 31, 269–280. doi: 10.1002/rcm.7787

Granier, A. (1987). Evaluation of Transpiration in a Douglas-Fir Stand by Means of Sap Flow Measurements. *Tree Physiol.* 3, 309–20. doi: 10.1093/treephys/3.4.309

Haverd, V., Cuntz, M., Griffith, D., Keitel, C., Tadros, C., and Twining, J. (2011). Measured deuterium in water vapour concentration does not improve the constraint on the partitioning of evapotranspiration in a tall forest canopy, as estimated using a soil vegetation atmosphere transfer model. *Agri. Forest Meteorol.* 151, 645–654. doi: 10.1016/j.agrformet.2011.02.005

Herbstritt, B., Gralher, B., and Weiler, M. (2012). Continuous *in situ* measurements of stable isotopes in liquid water. *Water Resourc. Res.* 48:W03601. doi: 10.1029/2011WR011369

Hogg, E. H., Black, A. T., den Hartog, G., Neumann, H. H., Zimmermann, R., Hurdle, P. A., et al. (1997). A comparison of sap flow and eddy fluxes of water vapor from a boreal deciduous forest. *J. Geophys. Res.* 102, 28929–28937. doi: 10.1029/96JD03881

Jarvis, P. G., and McNaughton, K. G. (1986). "Stomatal control of transpiration: scaling up from leaf to region," in *Advances in Ecological Research*, eds A. MacFadyen and E. D. Ford (London: Academic Press), 1–49. doi: 10.1016/S0065-2504(08)60119-1

Jasechko, S., Sharp, Z. D., Gibson, J. J., Birks, S. J., Yi, Y., and Fawcett, P. J. (2013). Terrestrial water fluxes dominated by transpiration. *Nature* 496, 347–350. doi: 10.1038/nature11983

Koeniger, P., Marshall, J. D., Link, T., and Mulch, A. (2011). An inexpensive, fast, and reliable method for vacuum extraction of soil and plant water for stable isotope analyses by mass spectrometry. *Rapid Commun. Mass Spectr.* 25, 3041–3048. doi: 10.1002/rcm.5198

Kulmatiski, A., Beard, K. H., Verweij, R. J. T., and February, E. C. (2010). A depth-controlled tracer technique measures vertical, horizontal and temporal patterns of water use by trees and grasses in a subtropical Savanna. *New Phytologist* 188, 199–209. doi: 10.1111/j.1469-8137.2010.03338.x

Lin, G., and Sternberg, L. S. L. (1993). "Hydrogen isotopic fractionation by plant roots during water uptake in coastal wetland plants," in *Stable Isotopes and Plant Carbon- Water Relations*, eds J. R. Ehleringer, A. E. Hall, and G. D. Farquhar (San Diego, CA: Academic Press), 497–510.

Majoube, M. (1971). Fractionnement en oxygene 18 et en deuterium entre l'eau et sa vapeur. *J. Chimie Phys.* 68, 1423–1436.

Marshall, J. D., and Waring, R. H. (1986). Comparison of methods of estimating leaf-area index in old-growth douglas-fir. *Ecology* 67, 975–79.

Martín-Gómez, P., Barbeta, A., Voltas, J., Peñuelas, J., Dennis, K., Palacio, S., et al. (2015). Isotope-ratio infrared spectroscopy: a reliable tool for the investigation of plant-water sources? *New Phytologist* 207, 914–927. doi: 10.1111/nph.13376

Moreira, M. Z., da Sternberg, L. S. L., and Nepstad, D. C. (2000). Vertical patterns of soil water uptake by plants in a primary forest and an abandoned pasture in the Eastern Amazon: an isotopic approach. *Plant Soil* 222, 95–107. doi: 10.1023/A:1004773217189

Morris, H., Brodersen, C., Schwarze, F. W. M. R., and Jansen, S. (2016). The parenchyma of secondary xylem and its critical role in tree defense against fungal decay in relation to the CODIT model. *Front Plant Sci.* 7:e1665. doi: 10.3389/fpls.2016.01665

Murray, F. W. (1966). *On the Computation of Saturation Vapor Pressure*. Santa Monica: The RAND Corporation.

Ogée, J., Cuntz, M., Peylin, P., and Bariac, T. (2007). Non-steady-state, non-uniform transpiration rate and leaf anatomy effects on the progressive stable isotope enrichment of leaf water along monocot leaves. *Plant Cell Environ.* 30, 367–387. doi: 10.1111/j.1365-3040.2006.01621.x

Orlowski, N., Frede, H. G., Brüggemann, N., and Breuer, L. (2013). Validation and application of a cryogenic vacuum extraction system for soil and plant water extraction for isotope analysis. *J. Sensors Sensor Syst.* 2, 179–193. doi: 10.5194/jsss-2-179-2013

Orlowski, N., Pratt, D. L., and McDonnell, J. J. (2016). Intercomparison of soil pore water extraction methods for stable isotope analysis. *Hydrol. Proces.* 30, 3434–3449. doi: 10.1002/hyp.10870

Penna, D., Hopp, L., Scandellari, F., Scott Allen, T., Benettin, P., Beyer, M., et al. (2018). Ideas and perspectives: tracing terrestrial ecosystem water fluxes using hydrogen and oxygen stable isotopes—challenges and opportunities from an interdisciplinary perspective. *Biogeosciences* 15, 6399–6415. doi: 10.5194/bg-15-6399-2018

Pfautsch, S. (2016). Hydraulic anatomy and function of trees—basics and critical developments. *Curr. Forestry Rep.* 2, 236–248. doi: 10.1007/s40725-016-0046-8

Poca, M., Coomans, O., Urcelay, C., Zeballos, S. R., Bodé, S., and Boeckx, P. (2019). Isotope fractionation during root water uptake by acacia caven is enhanced by Arbuscular Mycorrhizas. *Plant Soil.* 441, 485–97. doi: 10.1007/s11104-019-04139-1

Poyatos, R., Granda, V., Molowny-Horas, R., Mencuccini, M., Steppe, K., and Martínez-Vilalta, J. (2016). SAPFLUXNET: towards a global database of sap flow measurements. *Tree Physiol.* 36, 1449–1455. doi: 10.1093/treephys/tpw110

Priyadarshini, K. V. R., Prins, H. H., T., de Bie, S., Heitkönig, I. M., A., et al. (2016). Seasonality of hydraulic redistribution by trees to grasses and changes in their water-source use that change tree-grass interactions. *Ecohydrology* 9, 218–228. doi: 10.1002/eco.1624

Quiñonez-Piñón, R. M., and Valeo, C. (2017). Allometry of sapwood depth in five boreal trees. *Forests* 8:457. doi: 10.3390/f8110457

Rothfuss, Y., and Javaux, M. (2016). Isotopic approaches to quantifying root water uptake and redistribution: a review and comparison of methods. *Biogeosci. Dis.* 14, 2199–2224. doi: 10.5194/bg-2016-410

Rothfuss, Y., Vereecken, H., and Brüggemann, N. (2013). Monitoring water stable isotopic composition in soils using gas-permeable tubing and infrared laser absorption spectroscopy. *Water Resourc. Res.* 49, 3747–3755. doi: 10.1002/wrcr.20311

Schulze, E. -D., Mooney, H., A., Sala, O., E., Jobbagy, E., et al. (1996). Rooting depth, water availability, and vegetation cover along an aridity gradient in patagonia. *Oecologia* 108, 503–511. doi: 10.1007/BF00333727

Simonin, K. A., Roddy, A. B., Link, P., Apodaca, R., Kevin Tu, P., Hu, J., et al. (2013). Isotopic composition of transpiration and rates of change in leaf water isotopologue storage in response to environmental variables. *Plant Cell Environ.* 36, 2190–2206. doi: 10.1111/pce.12129

Soderberg, K., Stephen Good, P., Wang, L., and Caylor, K. (2012). Stable isotopes of water vapor in the vadose zone: a review of measurement and modeling techniques. *Vadose Zone J.* 11:165. doi: 10.2136/vzj2011.0165

Sprenger, M., Leistert, H., Gimbel, K., and Weiler, M. (2016). Illuminating hydrological processes at the soil-vegetation-atmosphere interface with water stable isotopes. *Rev. Geophys.* 54, 674–704. doi: 10.1002/2015RG000515

Tor-ngern, P., Oren, R., Oishi, A. C., Uebelherr, J. M., Palmroth, S., Tarvainen, L., et al. (2017). Ecophysiological variation of transpiration of pine forests: synthesis of new and published results. *Ecol. Appl.* 27, 118–133. doi: 10.1002/eap.1423

Turner, D. P., Acker, S. A., Means, J. E., and Garman, S. L. (2000). Assessing alternative allometric algorithms for estimating leaf area of Douglas-fir trees and stands. *For. Ecol. Manage.* 126, 61–76. doi: 10.1016/S0378-1127(99)00083-3

Vargas, A. I., Schaffer, B., Yuhong, L., and da Silveira Lobo Sternberg, L. (2017). Testing plant use of mobile vs immobile soil water sources using stable isotope experiments. *New Phytologist* 215, 582–594. doi: 10.1111/nph.14616

Volkmann, T. H. M., Kühnhammer, K., Herbstritt, B., Gessler, A., and Weiler, M. (2016). A method for *in situ* monitoring of the isotope composition of tree xylem water using laser spectroscopy. *Plant Cell Environ.* 39, 2055–2063. doi: 10.1111/pce.12725

Volkmann, T. H. M., and Weiler, M. (2014). Continual *in situ* monitoring of pore water stable isotopes in the subsurface. *Hydrol Earth Syst Sci.* 18, 1819–1833. doi: 10.5194/hess-18-1819-2014

von Caemmerer, S., and Farquhar, G. D. (1981). Some relationships between the biochemistry of photosynthesis and the gas exchange of leaves *Planta* 153, 376–387. doi: 10.1007/BF00384257

Wershaw, R. L., Friedman, I., Heller, S. J., and Frank, P. A. (1966). "Hydrogen isotopic fractionation of water passing through trees," in *Advances in Organic Geochemistry, International Series of Monographs on Earth Sciences*, eds, G. D. Hobson, G. C. Speers, D. E. Inderson (New York, NY: Pergamon Press), 55–67.

West, A. G., Goldsmith, G., R., Brooks, P. D., and Dawson, T. E. (2010). Discrepancies between isotope ratio infrared spectroscopy and isotope ratio mass spectrometry for the stable isotope analysis of plant and soil waters. *Rapid Commun. Mass Spectr.* 24, 1948–1954. doi: 10.1002/rcm.4597

West, A. G., Goldsmith, G., R., Matimati, I., and Dawson, T., E. (2011). Spectral analysis software improves confidence in plant and soil water stable isotope analyses performed by Isotope Ratio Infrared Spectroscopy (IRIS). *Rapid Commun. Mass Spectr.* 25, 2268–2274. doi: 10.1002/rcm.5126

White, J. W. C., Cook, E. R., Lawrence, J. R., and Wallace, B. S. (1985). The DH ratios of sap in trees: implications for water sources and tree ring DH ratios. *Geochim Cosmochim Acta* 49, 237–246. doi: 10.1016/0016-7037(85)90207-8

Wiedemann, A., Marañón-Jiménez, S., Rebmann, C., Herbst, M., and Cuntz, M. (2016). An empirical study of the wound effect on sap flux density measured with thermal dissipation probes. *Tree Physiol.* 36, 1471–1484. doi: 10.1093/treephys/tpw071

Yakir, D., and da Sternberg, L. S. L. (2000). The use of stable isotopes to study ecosystem gas exchange. *Oecologia* 123, 297–311. doi: 10.1007/s004420051016

Conflict of Interest: The authors declare that the research was conducted in the absence of any commercial or financial relationships that could be construed as a potential conflict of interest.

frontiers in Plant Science

ORIGINAL RESEARCH
published: 29 May 2020
doi: 10.3389/fpls.2020.00695

Surface Density of the Spongy and Palisade Parenchyma Layers of Leaves Extracted From Wideband Ultrasonic Resonance Spectra

T. E. G. Alvarez-Arenas[1], D. Sancho-Knapik[2,3], J. J. Peguero-Pina[2,3] and Eustaquio Gil-Pelegrín[2]*

[1] *Instituto de Tecnologías Físicas y de la Información (ITEFI), Spanish National Research Council (CSIC), Madrid, Spain,*
[2] *Unidad de Recursos Forestales, Centro de Investigación y Tecnología Agroalimentaria de Aragón (CITA), Zaragoza, Spain,*
[3] *Instituto Agroalimentario de Aragón – IA2 (CITA-Universidad de Zaragoza), Zaragoza, Spain*

The wide band and air-coupled ultrasonic resonant spectroscopy together with a modified Simulated Annealing metaheuristic algorithm and a 1D layered acoustic-model are used to resolve the structure of plant leaves. In particular, this paper focuses on the extraction of the surface density of the different layers of tissue in leaves having a relatively simple structure. There are three main reasons to select the surface density as the focus of this study: (i) it is a parameter directly extracted by the proposed technique and it requires no further processing, (ii) it is relevant in order to study the dynamic of the water within the different tissues of the leaves and also to study the differential development of the different tissues, and (iii) unlike other parameters provided by this technique (like resonant frequency, impedance, ultrasonic elastic modulus, or ultrasonic damping), this parameter can be easier to understand as it is a direct measure of mass per unit surface. The selection of leaves with a simple structure is justified by the convenience of avoiding an unnecessary complication of the data extraction step. In this work, the technique was applied to determine the surface density of the palisade and spongy parenchyma layers of tissue of *Ligustrum lucidum*, *Vitis vinifera,* and *Viburnum tinus* leaves. The first species was used to study the variation of the surface density at full turgor with the thickness of the leaf, while the two other species were used to study the variation of the surface densities with the variation in the leaf relative water content. Consistency of the results with other conventional measurements (like overall surface density, and cross-section optical and cryo-SEM images) is discussed. The results obtained reveal the potential of this technique; moreover, the technique presents the additional advantage that can be applied *in-vivo* as it is completely non-invasive, non-destructive, fast, and equipment required is portable.

Keywords: ultrasound, air-coupled ultrasound, resonant spectroscopy, plant leaves, layered plant tissue, leaf's parenchyma layers

OPEN ACCESS

Edited by:
Cristina Maria Máguas, University of Lisbon, Portugal

Reviewed by:
Juan Jose Rios, Center for Edaphology and Applied Biology of Segura, Spanish National Research Council, Spain
Yangmin X. Kim, Division of Soil and Fertilizer, National Institute of Agricultural Sciences, South Korea

****Correspondence:***
T. E. G. Alvarez-Arenas
t.gomez@csic.es

Specialty section:
This article was submitted to Technical Advances in Plant Science, a section of the journal Frontiers in Plant Science

Received: *29 November 2019*
Accepted: *04 May 2020*
Published: *29 May 2020*

Citation:
Alvarez-Arenas TEG, Sancho-Knapik D, Peguero-Pina JJ and Gil-Pelegrín E (2020) Surface Density of the Spongy and Palisade Parenchyma Layers of Leaves Extracted From Wideband Ultrasonic Resonance Spectra. Front. Plant Sci. 11:695. doi: 10.3389/fpls.2020.00695

INTRODUCTION

The wide-band, air-coupled ultrasonic resonant spectroscopy method has been presented by Álvarez-Arenas et al. (2018). This method is an extension of the air-coupled ultrasonic resonant spectroscopy method presented in Álvarez-Arenas et al. (2009); Sancho-Knapik et al. (2010, 2012, 2013a) that has been widely used for different applications (Farinas and Alvarez-Arenas, 2014;

Farinas et al., 2014) where the determination of leaves water content attracted most of the interest: (Álvarez-Arenas et al., 2016; Sancho-Knapik et al., 2016; Farinas et al., 2019).

This ultrasonic technique is one of the methods available to measure physical properties of plant leaves. Other techniques are based on the measurement of dielectrical properties (Repo, 1988; Zhang and Willison, 1993; Chuah et al., 1995; Mizukami et al., 2006), the leaf response to pressure (Zimmermann et al., 2008; Rueger et al., 2011), and the leaf response to microwaves (Martínez et al., 1995; Menzel et al., 2009; Sancho-Knapik et al., 2013b). The main features of the ultrasonic method is that it is completely contactless, non-invasive, and non-destructive and that it can be applied *in-vivo*. In addition, the novel wide band ultrasonic technique present the unique feature that it can obtain information about the different layers in the leaves, also in a completely non-invasive and non-destructive way, which allows us to study not only the overall leaf properties and their variations, but also the differences between the main layers of tissue in the leaves and the differences in the variation of their properties (for example with the leaf development or with the modification of the leaf water content).

In a few words, the ultrasonic method consist on using a pair of air-coupled ultrasonic transducers (transmitter and receiver) whose frequency band is tuned to include the fundamental resonant frequency of the leaf thickness mode. The transmission coefficient spectra of the leaf around this fundamental resonant frequency is measured and leaf properties like thickness, density, impedance, elastic modulus, and ultrasonic damping are extracted from the solution of the inverse problem using a 1 dimensional model and assuming an effective medium approach to acoustically model the leaf. The use of this extremely simple model is justified by the following facts: (i) at the first thickness resonance the wavelength equals two times the thickness of the leaf, so it is much larger than the inner details of the leaf structure, (ii) the calculated spectra reproduce quite well the measured behavior, and (iii) the physical and physiological meaningfulness of the extracted parameters were confirmed by comparison of the extracted parameters with leaf properties obtained by conventional means (like total thickness, overall density, water potential, or turgor loss point).

By increasing the frequency it is possible to observe several orders of the leaf thickness resonances. However, those leaf spectra showing two or more resonances revealed a clear harmonic distortion. The effective medium approach used before, where the leaf is modeled as a homogeneous layer, is unable to provide a good fit into the measured spectra in these cases. This was not a fully unexpected result as the increase of the frequency implies a reduction of the wavelength, so the ultrasonic wave becomes more sensitive to the details of the leaf inner structure, especially to the layered structure. Álvarez-Arenas et al. (2018) shows that a simple layered model, where an effective acoustic model of the leaf is built using two layers (that mainly correspond to the spongy parenchyma -SP- and the palisade parenchyma -PP-), is able to explain or reproduce the measured spectra and that the extracted data (like impedance, resonant frequency, and elastic modulus) are consistent with direct measurements and with cross-section SEM observations of the leaf structure.

The two main challenges of the use of the wide-band technique are: (i) the solution of the inverse problem with two layers becomes intractable by conventional means and (ii) the difficulty of having efficient air-coupled ultrasonic transducers able to cover the required frequency range. For the former, a metaheuristic approach that consists on a modification of the Simulated Annealing algorithm was proposed for this application and successfully used in Álvarez-Arenas et al. (2018), for the later, the technology developed by CSIC to produce efficient air-coupled ultrasonic transducers with wide band response (Álvarez-Arenas et al., 2018) have been employed.

The first case of study shown in this work is the extraction of the surface densities of the PP and SP layers of tissue of *Ligustrum lucidum* leaves. For this case, leaves of different thickness (300–800 micron) have been used. Álvarez-Arenas et al. (2016, 2018) have shown that these leaves can be well measured with this technique and that the increase of the leaf thickness is mainly produced by an increase of the thickness of the PP layer. Therefore, this species provides a convenient case of study.

The second application of this technique presented here corresponds to the extraction of the surface densities of PP and SP layers in *Viburnum tinus* and *Vitis vinifera* leaves with different levels of water content, from full turgor down to the turgor loss point and beyond. As the loss of water will produce a decrease of the surface density, it is interesting to use this parameter to evaluate the water dynamic and use it as a proxy of relative water content (RWC). Moreover, the possibility to have measurements of different tissues of the leaf is extremely attractive as this information can be used to understand the different ways these tissues might cope with water deficit and how the whole leaf could manage these differences.

MATERIALS AND METHODS

Plant Material

Three plant species were used in this study: *Ligustrum lucidum* W.T. Aiton, *Viburnum tinus* L., and *V. vinifera* L. Plant material of these species was collected from the Real Jardin Botánico of Madrid (CSIC) following the next procedure. South exposure shoots from well-watered specimens were harvested early in the morning, introduced in sealed plastic bags together with wet filter paper to preserved leaf full turgor, and carried immediately to the laboratory in a portable cooler. Once in the lab, full-developed mature leaves without defects were selected and immediately used for the measurements. This procedure was repeated every single day when measurements were performed.

Concerning *L. lucidum*, 70 leaves with different thickness (from 250 to 800 microns) were measured throughout 5 days to study the influence of the thickness on the surface density of the different tissue layers. Each day, we selected 10 leaves for ultrasonic measurements and other four leaves to obtain the overall leaf surface and volumetric density and the images of the leaf cross sections. For *V. tinus*, a total of 56 leaves were measured throughout 8 days, selected in groups of 7 leaves per day (5 of them for ultrasonic and 2 for the other measurements). Finally,

for *V. vinifera*, we have measured 120 leaves throughout 20 days, selected in groups of six leaves per day (4 for ultrasonic and 2 for the other measurements).

Ultrasonic Methods

Two pairs of custom air-coupled transducers developed at CSIC (Alvarez-Arenas, 2004, 2017) were used to measure the transmission coefficient over a frequency band wide enough to observe, at least, two orders of the leaves thickness resonances. One pair with center frequency at 0.3 MHz (usable frequency range 0.15–0.5) and the other at 1.00 MHz (usable frequency range 0.5–1.6 MHz). Transducers (transmitter and receiver) were mounted on an *U*-shaped holder, that kept them (transmitter and receiver) in opposition and at a distance of 60 mm and 40 mm for the 0.3 MHz and the 1.0 MHz transducers, respectively. Aperture of the transducers is circular with diameter of 20 and 15 mm for the 0.3 and the 1.0 MHz, respectively. Area of the leaf were the ultrasonic measurements are performed is similar to transducer aperture. In addition, a polycarbonate cover wrapped around the *U*-shaped holder protects measurement area and provides a groove to introduce the leaves. This groove permits to properly place the leaf in between the transducers: at normal incidence and at the middle point. Images of this device can be seen in Álvarez-Arenas et al. (2016, 2018). Transmitter transducer is driven by a negative semicycle square wave, amplitude 400 V provided by an Olympus pulser/receiver (PR5077). The received signal in the receiver transducer is connected to the receiver stage of the PR5077, where it is amplified (0 dB for the reference signal: no leaf between transducers, and 40 dB for the measured signal through the leaves), and then sent to a digital oscilloscope Tektronix 5054. The oscilloscope is triggered by the synchronism signal provided by the PR5077. The oscilloscope digitizes the signal, averages it 100 times and sends it to a PC to extract fast Fourier transform (FFT).

First, the signal at R× without any leaf between the transducers and at 0 dB gain is acquired and FFT extracted. This is used as calibration or reference value. Then the leaf is placed in between the transducers, gain set to 40 dB and the measurement repeated.

Viburnum tinus leaves and *L. lucidum* leaves were measured at two points in the wider part of the leaf, at both sides of the midrib and trying to avoid it. *V. vinifera* leaves were measured at three different locations matching main interveinal areas.

Leaf Dehydratation Measurements

Viburnum tinus and *V. vinifera* leaves were left to dry at room conditions. Ultrasonic measurements were repeated every 5 min during 4 h. At each step, leaves were weighed (M). The first measurement corresponds to full turgor condition (M^{FT}). After ultrasonic measurements were finished, leaves were placed in an oven at 80°C for 48 h. After this, leaves were weighed again to obtain the leaf dry mass (M^{dry}).

Figure 1 shows some pictures of one leaf of *V. tinus* and *V. vinifera* at different values of RWC. This figure shows that the deformation of the leaves do not compromise the integrity of the ultrasonic measurement as the flatness of the measured areas remains rather unchanged.

Relative water content at state "i" was obtained from:

$$RWC^i = \frac{M^i - M^{dry}}{M^{FT} - M^{dry}} \tag{1}$$

It is of interest to show the close relationship between RWC and the surface density measurements. It can be easily derived:

$$RWC^i = \frac{\rho_S^i \varepsilon^i - \rho_S^{dry} \varepsilon^{dry}}{\rho_S^{FT} - \rho_S^{dry} \varepsilon^{dry}} \tag{2}$$

where ρ_S^i is the leaf surface density at state "i" and $\varepsilon^i = S^i/S^{FT}$, where S is the leaf surface, so ε^i is the leaf lateral shrinkage, that

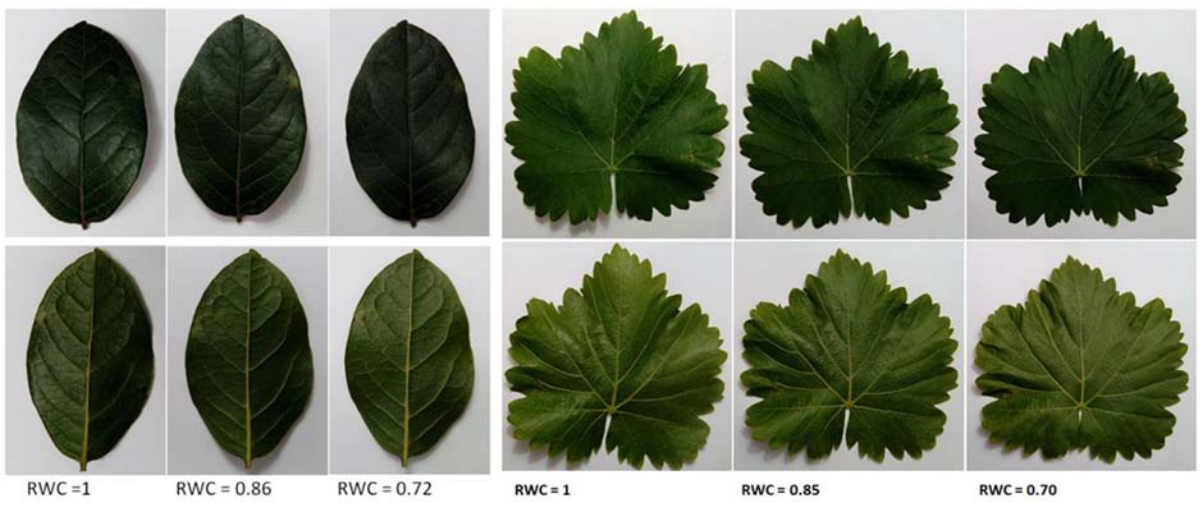

FIGURE 1 | Pictures of leaves of *Viburnum tinus* (left) and *Vitis vinifera* (right) at different values of RWC. The adaxial part of the leaf is showed up, while the abaxial is showed down.

is $\varepsilon \leq 1$. In the case that leaf lateral shrinkage can be considered negligible ($\varepsilon = 1$), then Eq. 2 reduces to:

$$RWC = \frac{\rho_S - \rho_S^{dry}}{\rho_S^{FT} - \rho_S^{dry}} \tag{3}$$

which is completely analogous to Eq. 1.

Leaf Thickness, Leaf Density, and Anatomical Images

Before each of the ultrasonic measurements, leaf thickness was measured using a micrometer. To obtain overall leaf surface density and volumetric density (ρ_S and ρ, respectively) two circles of 15 mm diameter were cut from each leaf by using a punch holder. Excised disks were weighed and thickness measured using a micrometer at 5 different locations to get an average value.

Both optical and cryo-SEM images of the leaves cross section were obtained for the three species at full turgor. In addition, cryo-SEM images of *V. tinus* leaves at different levels of water potential, measured by using a pressure chamber, were also obtained. Optical images of the leaf cross section were obtained by cutting the leaves into two cross-sections (0.2–0.3 mm apart) with a scalpel and the aid of a dissecting microscope. Then, a camera coupled to a light microscope was used to capture the leaf cross-sections which were later analyzed using ImageJ to obtain the total leaf thickness and the thicknesses of both palisade and spongy parenchyma. The purpose of obtaining cross-section images of the studied leaves was two-fold:

1. To show that the acoustic two-layers model for the leaves is a sensible one and to identify what is the relationship between the layers in the acoustic model and the actual layers of tissue in the leaves.
2. To get some insight into the modifications of these layers with leaf thickness (*L. lucidum*) and with water content (*V. tinus*), so that it is possible to infer some information about what modification can be expected in the surface density of the different layers.

Leaf Parameters Extraction From the Measured Spectra: Solution of the Inverse Problem

All measured ultrasonic transmission coefficients of the studied leaves contain, at least, two orders of the leaf thickness resonances. This response can be theoretically calculated using a layered model for the leaf. The required parameters to compute the leaf transmission coefficients are the impedance of the medium where measurements are preformed (air in this case) and:

$$f_{res}^i,\ Z^i,\ (\alpha_0 t)^i,\ n^i;\quad i = 1, 2, \ldots N \tag{4}$$

where:

N is the total number of layers in the acoustic model of the leaf, the superscript i denotes the number of layer, f_{res}^i is the resonant frequency of layer i, defined as v/t (v = ultrasound velocity and t = layer thickness), Z^i the complex acoustic impedance $\left(Z_R + jZ_i\right)$, α_0^i the ultrasonic attenuation coefficient and the parameter n^i describes the variation of the attenuation coefficient of the ith layer with the frequency as a power law:

$$\alpha = \alpha_0 \left(\frac{f}{f_0}\right)^n \tag{5}$$

Actually, Z_R and Z_i are not independent parameters, as it can be shown that:

$$Z_i = \frac{Z_R}{f_{res}\ \alpha t} \tag{6}$$

The estimation of the deviation of the calculated transmission coefficient: $TC[f_{res}^i,\ Z^i,\ (\alpha t)^i,\ n^i]$ compared to the measured one: TC^{exp} is obtained using the L2 norm. The search for the set of parameters in Eq. 4 that minimize this deviation is performed using a modified Simulated Annealing algorithm and the procedure explained in Álvarez-Arenas et al. (2018).

Therefore, there are a number of parameters to be determined (dimension of the space of search) equal to $4 \times N$. The solution of this problem for one layer can be found with conventional techniques (refs), but for two layers, the number of parameters is eight and it becomes necessary to use a metaheuristic approach.

The selection of the number of layers to be used in the acoustic model for the leaf is selected, as explained in Álvarez-Arenas et al. (2018) on the basis of the following features:

1. Information in the measured spectra. For example, the number of resonances observed in the spectra. If there is only one (the first one) the measurement does not contain enough information to obtain more than four parameters. Moreover, a one-layer model has always been able to provide a good fitting.
2. Capability of the model to reproduce the measured response and the Occam's razor principle. That is, if a one-layer leaf model is able to reproduce the observed behavior, this model is then preferred over the two-layers model and so on.
3. Compatibility between the acoustic model of the leaf and the actual leaf structure.

The algorithm is run five times for each case in order to have an estimation of the accurateness of the solution, to check for the existence of multiple solutions and to detect the presence of local minima.

The real part of the acoustic impedance (Z_R) is given by: $Z_R = \rho.v$ where ρ is the density of the medium and v the ultrasound velocity. Hence, it is clear that the surface density of the i-layer is then given by:

$$\rho_S^i = \frac{Z_R^i}{f_{res}^i} = \rho^i t^i \tag{7}$$

Another interesting feature of ρ_S^i is that:

$$\sum_{i=1}^{N} \rho_S^i = \rho_S \tag{8}$$

where ρ_S is the leaf overall surface density that can be easily obtained by conventional means, so Eq. 8 can be used to validate the values of ρ_S^i obtained with the ultrasonic technique.

RESULTS

Cross-Section Images

Previous analysis of cryo-SEM images of the cross-section of *L. lucidum* leaves were shown in Álvarez-Arenas et al. (2018). These images support the proposed acoustic layered model of these leaves, the use of two layers in the model, and the fact that leaf thickness increase is achieved by the thickening of the palisade parenchyma layer. Obtained thickness of the PP and SP layers in *L. lucidum* leaves are shown in **Figure 2**.

This layered structure of the leaves is also present in *V. tinus* leaves as it can be clearly seen in the cryo-SEM images (**Figure 3A**). For *V. vinifera* there are numerous evidences in the literature (see, for example, Alonso et al., 2011; Monteiro et al., 2013; Navarro et al., 2019). The two layer approach for the layer acoustic model is fully supported by the features observed in these images. This is because ultrasonic waves are only sensitive to variations of the acoustic impedance in the leaf. As the acoustic impedance is the result of the multiplication of the volumetric density and the ultrasound velocity, it is clear that the major acoustic differentiation within the leaf comes from the fact that the porosity in the SP layer is much larger and cell shape more rounded, hence, both density and ultrasound velocity in this layer must be much smaller. Additionally, cryo-SEM images also show a reduction in the PP thickness of *V. tinus* leaves toward lower values of water potential (**Figure 3**).

Measured Resonance Spectra and Calculated Ones Assuming a Two-Layers Model and the Leaf Parameters Obtained From the Solution of the Inverse Problem

Examples of the measured spectra of *V. tinus* and *V. vinifera* leaves at different conditions (water content) and the calculated ones using the values extracted from the solution of the inverse problem using the Simulated Annealing algorithm are shown in **Figures 4**, **5**. For *L. lucidum* leaves, measured and calculated spectra for different leaf thicknesses are shown in Álvarez-Arenas et al. (2018), and are, therefore, not repeated here. These results illustrate the main features of the measured spectra, their variation when leaves are modified and the goodness of the fittings. This later feature also reveals the capability of the proposed model to reproduce the actual leaf ultrasonic response.

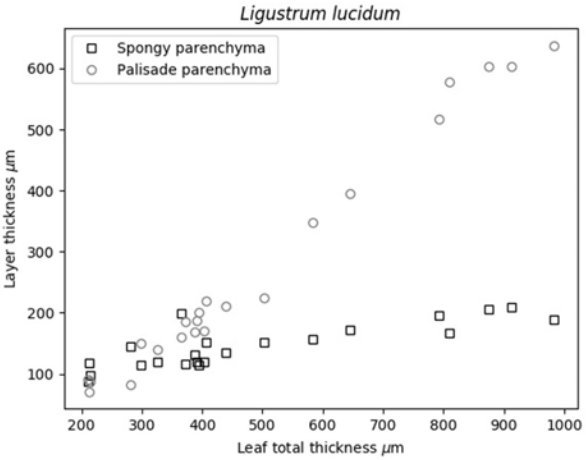

FIGURE 2 | Variation in the thickness of the PP and SP layers with the total leaf thickness.

Variation of the Mass Per Unit Area in the PP and SM Layers of the Leaf With the Total Leaf Thickness: *L. lucidum*

Figure 6 shows the variation in the surface density of the PP and SP layers versus leaf thickness extracted from the ultrasonic measurements, the calculated overall surface density (from Eq. 8) and the value of the overall surface density obtained from the excised leaf circles using the circle surface and mass.

Variation of the Mass Per Unit Area in the PP and SM Layers of the Leaf With the Leaf RWC: *V. tinus* and *V. vinifera*

Figures 7, **8** show the variation in the surface density of the PP and SP layers and of the whole leaf with RWC for the *V. vinifera* and the *V. tinus* leaves.

DISCUSSION

This work shows that resonant ultrasonic transmission coefficient in the frequency range 0.15–1.6 MHz measured using air-coupled ultrasound at normal incidence in *V. vinifera* and *V. tinus* leaves present, at least, two orders of resonances and that the measured magnitude and phase spectra can be well reproduced theoretically using a 1D two-layered model. Moreover, a modified simulated annealing algorithm (Álvarez-Arenas et al., 2018) has proven to be efficient to solve the inverse problem and to extract the parameters of the layers by achieving and excellent fitting of the calculated spectra into the measured ones (**Figures 4**, **5**, see Álvarez-Arenas et al., 2018 for *L. lucidum* results).

Cross-section images of the leaves suggest that the two layers in the acoustic leaf model correspond to the Palisade parenchyma + adaxial epidermis and the Spongy parenchyma + abaxial epidermis, as the major acoustic differentiation within the leaves is produced by both the larger porosity and the more rounded cell shape in the SP layer and the fact that there is a clear boundary between PP and SP layers. It can be worthwhile to remind that the acoustic differentiation between two tissues (two materials in general) is produced by the difference in the acoustic impedances. As the acoustic impedance is the product of density and ultrasound velocity, and ultrasound velocity depends on elastic modulus and density, then any difference in elastic modulus or density will contribute to variations in the acoustic impedance.

Focus of the paper is set on the surface density of these two layers extracted from the measured resonant spectra by the proposed modified Simulated Annealing algorithm and the 1D layered model for the leaves. As surface density is a measure

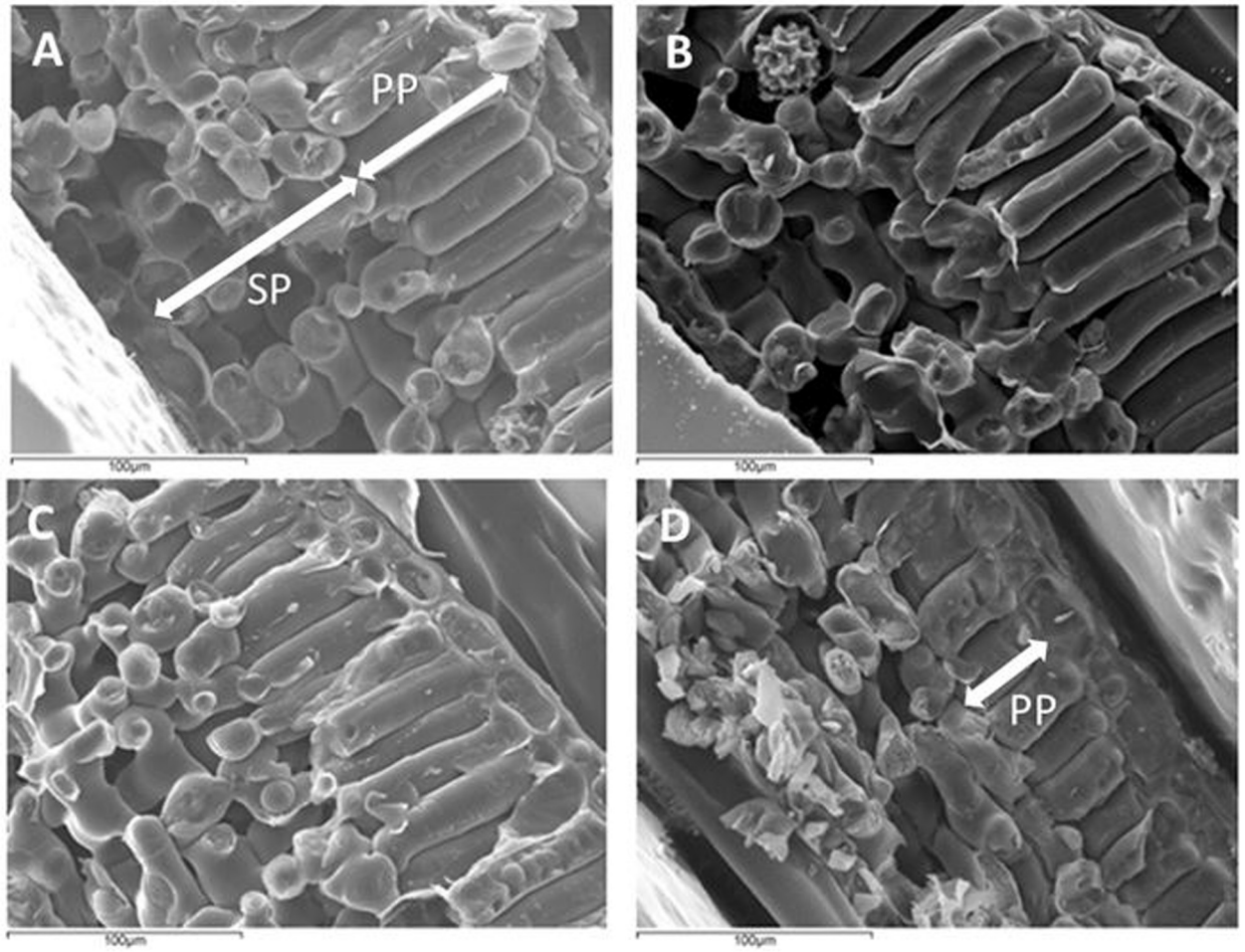

FIGURE 3 | Cryo-SEM images of *Viburnum tinus* leaves cross section at full turgor **(A)** and at water potential of: –2.0 **(B)**, -2.6 **(C)** and -3.5 **(D)** MPa. SP: spongy parenchyma. PP: palisade parenchyma. Notice the reduction in PP thickness between **A** and **D**.

of mass per area, this parameter can provide direct information about the variation of the water content or the biomass in the different tissues in the leaf. In addition, from the extracted surface density of the two layers in the leaf it is possible to obtain the total leaf surface density (Eq. 8), and this result can be compared with direct measurements obtained from excised circles from the leaves, and the measurement of area and mass. This can be used as an independent verification the obtained parameters.

Therefore, in all cases a direct comparison between total leaf surface density obtained by a conventional mean and extracted from the resonance spectra have been shown. Results appear in **Figures 6–8** for *L. lucidum*, *V. vinifera* and *V. tinus*, respectively. In all cases, the achieved agreement between both (overall) surface densities estimations is within the experimental error. This is a first verification of the correctness of the leaf parameters obtained by the proposed approach.

Álvarez-Arenas et al. (2018) showed that *L. lucidum* leaves present the interesting feature that the leaf thickness increase is, mainly, produced by the increase of the thickness of the PP layer. Measurements in this work (**Figure 2**) verify and quantify this feature. This is of interest as this permit us to anticipate that variation in surface density of PP and SP layers with total leaf thickness, must behave in a similar way compared with the variation in the thicknesses of each layer.

Figure 6 shows the surface density of the PP and the SP layers of *L. lucidum* leaves extracted from the resonance spectra. In this case, leaves of different thickness, all of them at full turgor, have been measured. In all cases, the surface density is larger for the PP layer than for the SM layer, which is an expected result due to the fact that the thickness of the PP layer is always larger, or at least equal, and the porosity of the SM layer is higher. As expected from data in **Figure 1** and cryoSEM images shown in Álvarez-Arenas et al. (2018) the increase of the surface density of the PP layer is more pronounced than the SM layer when the leaf thickness increases. This is a second verification of the correctness of the leaf parameters obtained by the proposed approach.

Figure 7 shows the surface density of the PP and the SP layers of *V. vinifera* leaves extracted from the resonance spectra. In this case, leaves at different values of RWC from 1 to 0.75 have been

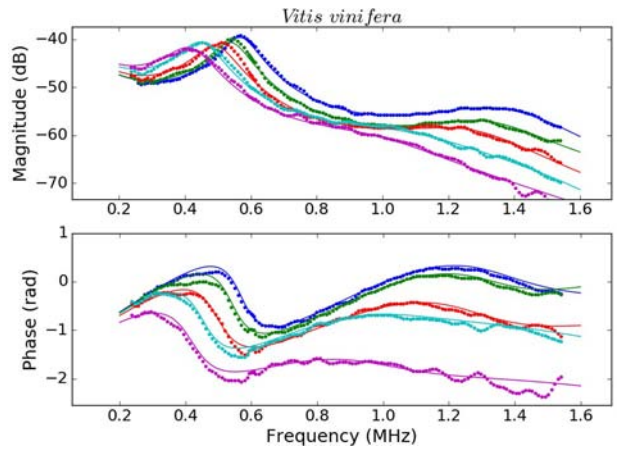

FIGURE 4 | Measured (dots) and calculated (solid line) magnitude (top) and phase spectra (bottom) of *V. vinifera* leaves at different values of RWC 1 (blue), 0.96 (green), 0.93 (red), 0.87 (cyan), and 0.82 (magenta).

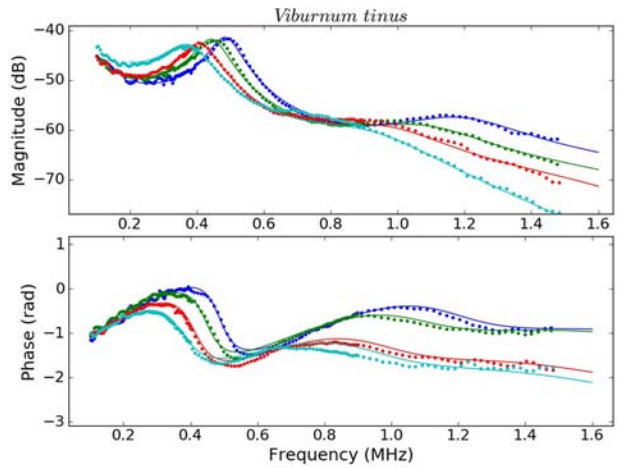

FIGURE 5 | Measured (dots) and calculated (solid line) magnitude (top) and phase spectra (bottom) of *V. tinus* leaves at different values of RWC: 1.00 (blue), 0.96 (green), 0.91 (red), and 0.85 (cyan).

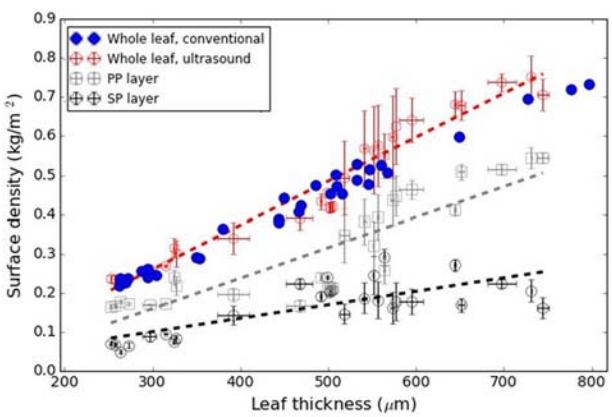

FIGURE 6 | *L. lucidum*: Surface density of the PP and SP layers (from the ultrasonic technique) and overall surface density from Eq. 8 and direct measurements. Dashed lines represent a trend line just for visualization purposes.

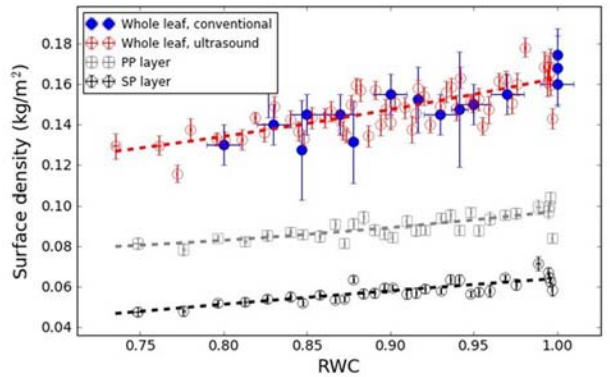

FIGURE 7 | Surface density of the PP and SP layers and of the whole leaf versus RWC for the *V. vinifera* leaves. Dashed lines represent a trend line just for visualization purposes.

measured. In all cases, the surface density is larger for the PP layer than for the SP layer, which is an expected result due to the fact that the thicknesses of PP and SP layers are similar and the porosity of the SP layer is larger. In addition, the results show that the decrease of the surface density of both layers when the leaves dehydrate is similar, so both follow a similar trend. This suggests that the loss of water in both layers is similar.

Figure 8 shows the surface density of the PP and the SP layers of *V. tinus* leaves extracted from the resonance spectra. In this case, leaves at different values of RWC from 1 to 0.60 have been measured. At full turgor, the surface density is larger for the PP layer than for the SM layer, which is an expected result given the features observed in cross-section images shown in **Figure 3A**: thickness of both layers is similar, but porosity of the SP layer is much higher. When the leaves loss water, and unlike in *V. vinifera*, the reduction of the surface density is quite different in both layers. Although between RWC 1.0 and 0.95 there are no big differences, for RWC < 0.94, the decrease in the surface density of the PP layer is much more pronounced. Eventually, surface density of both layers becomes similar for RWC < 0.85. CryoSEM images of the cross-section of *V. tinus* at different values of water potential were obtained, with the aim to provide further evidences for the reason for this behavior. Some of these images are shown in **Figure 3**. At high values of RWC, images show a slimming of the cells of the PP layer while at low RWC values a dramatic contraction of these cells along the direction normal to the leaf plane is observed. This implies a significant PP-cell volume reduction and, hence, a proportional loss of water. On the contrary, loss of cell volume in the SP layer is not so evident. It is clear that there is a reduction of the thickness of the SM layer, but thanks to the larger porosity of this layer, cell flattening is clear, but loss of cell volume (and hence of water) is not so evident as in the PP layer.

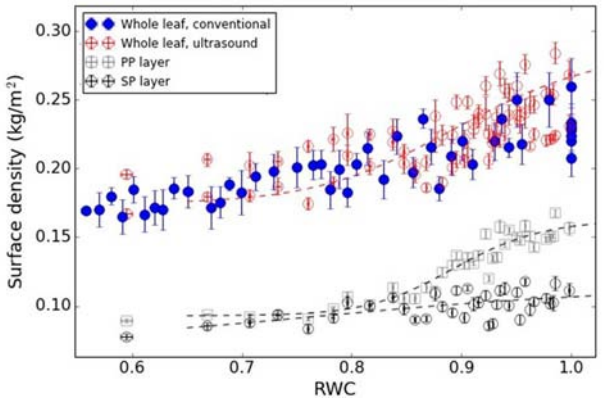

FIGURE 8 | Surface density of the PP and SP layers and of the whole leaf versus RWC for the *V. tinus* leaves. Dashed lines represent a trend line just for visualization purposes (using a logistic function).

CONCLUSION

The two-layered model of *L. lucidum, V. tinus* and *V. vinifera* provides a reasonable leaf model approach based on its ability to reproduce all features observed in the ultrasonic leaf resonances and that its consistency with actual leaf structure as revealed by the cryoSEM images. Moreover, comparison of the extracted leaf parameters obtained from this two-layered model and the ultrasonic measurements with data and evidences obtained by alternative methods permit to validate this approach. In particular, overall leaf surface density obtained by the ultrasonic method and from direct measurements agree within the experimental error range. In addition, an indirect verification of the correctness of the approach is provided by the fact that the observed variation of the extracted surface density of the layers of the *L. lucidum* with total leaf thickness are consistent with direct observations of the variation in the thicknesses of each layer.

In *V. vinifera* and *V. tinus*, the technique was used to extract the surface density of each layer for different values of the RWC. These two species present a quite different behavior. While in *V. vinifera* the surface density of both leaf layers decrease is a similar way as RWC decrease, the variation in the surface density of the layers of the *V. tinus* leaves is quite different. While the behavior of the *V. vinifera* leaves is closer to the classical analysis of water relations in leaves where the leaf is considered as a whole, the behavior of *V tinus* leaves shows a clear differential loss of water between the two layers. This unexpected feature is supported by evidences shown in cryoSEM images that show a much larger cell volume loss in the PP than in the SP due to the different cell shape and the presence of a large open porosity in the later.

This differential loss of water in the PP and the SP layers of *V. tinus* leaves pointed out by the ultrasonic technique here presented raise some fundamental questions about how can water potential in different parts of the leaf evolve in a differential way, how equilibrium is reached and what are the mechanisms that make this possible. Loss of water volume in the cells should induce a lower (more negative) osmotic potential (Sanders and Arndt, 2012). The larger volume drop in the cells of PP layer than in the SP layer should, in the absence of any other water potential components, produce a flux of water from the SP layer to the PP layer to recover the equilibrium. It is well documented that plant cells can actively change their osmotic potential by accumulating solutes, in the so-called osmotic adjustment (Boyer et al., 2008; Sanders and Arndt, 2012; Sancho-Knapik et al., 2016). In this situation, a way to compensate for the decrease in water potential in PP due to water loss would be an equivalent increase in solute accumulation (see Hare et al., 1998), but only in SP. While this solute accumulation has been described in photosynthetically active plants in diurnal (Sancho-Knapik et al., 2016) or seasonal cycles (Callister et al., 2008), under the experimental conditions of our measurements it is very unlikely that the equilibrium between PP and SP is restored in this way.

Alternatively, it could be possible that the turgor potential in the PP and SP layers follows a differential evolution so that the equilibrium of water potential between PP and SP is, in this way, kept. In fact, the finding of differences in turgor in different tissues within the same leaf has been described. Fricke (1996) reported such differences between the mesophyll and leaf epidermis as the consequence of "turgor-dependant processes." Oertli (1986) reported negative turgor pressure in living leaf cells, against previous theoretical assumptions (Tyree, 1976). This fact has been recently revisited (Ding et al., 2014; Yang et al., 2017), and the implications of the ability of living cells to develop negative turgor in the context of water relations of plants under dry conditions has been discussed (Gil-Pelegrín et al., 2017). Assuming differences in the response of cells in SP than in PP, with the development of extra negative potential due to different wall properties in the former may allow reaching equilibrium between both tissues, even with drastic changes in volume (and solute concentration) in PP as compared to SP.

Nevertheless, how the decrease of turgor potential in the cells of the PP layer can be smaller is not clear as the PP-cell volume reduction (and hence the loss of tension in the cell wall) is quite large. These features will be the subject of a future research. In particular, the ultrasonic technique permit to obtain elastic modulus of the PP and SP layers that could provide some insight into the differential evolution of the turgor potential and pressure chamber measurements permit to determine overall leaf water potential.

In summary, this work present a wideband ultrasonic resonant technique for plant leaves that permit to extract the surface density of PP and SP layers of tissue, the technique reveals the capability of the procedure to show the differential growth of thee tissues (*L. lucidum*) and the variation of the mass per area when the leaves loss water (in *V. tinus* and *V. vinifera*). In the particular case of *V. tinus* an unexpected differential evolution of the surface density in PP and SP layers is observed that will be the subject of a future research. This fact reveals the possibilities of the proposed technique that is completely non-destructive and non-invasive and can also be applied *in-vivo*.

DATA AVAILABILITY STATEMENT

The datasets generated for this study are available on request to the corresponding author.

AUTHOR CONTRIBUTIONS

All authors listed have made a substantial, direct and intellectual contribution to the work, and approved it for publication.

FUNDING

This research was funded by Instituto Nacional de Investigación y Tecnología Agraria y Alimentaria (INIA) grant no. RTA2015-00054-C02-01 and by Gobierno de Aragón H09_20R research group. Research of DS-K is supported by a DOC INIA-CCAA contract co-funded by INIA and European Social Fund and by the Spanish State Research Agency and European Regional Development Fund (ERDF/FEDER), grant no. DPI2016−78876−R.

REFERENCES

Alonso, V., Boso, S., Santiago, J. L., Gago, P., Rodriguez, M. I., and Martinez, M. C. (2011). Leaf thickness and structure of *Vitis vinifera* L. cv Albariño clones and its possible relation with susceptibility to downy mildew (*Plasmopara viticola*) infection. *J. Int. Sci. Vigne Vin* 45, 161–169.

Alvarez-Arenas, T. E. G. (2004). Acoustic impedance matching of piezoelectric transducers to the air. *IEEE Trans. Ultrason. Ferroelectr. Freq. Control.* 51, 624–633. doi: 10.1109/tuffc.2004.1320834

Alvarez-Arenas, T. E. G. (2017). "Air-coupled ultrasonic transducers," in *Ultrasound in Food Processing. Recent Advamces*, eds M. Villamiel, A. Montilla, J. V. García-Pérez, J. A. Cárcel, J. Benedito (Hoboken, NJ: Wiley).

Álvarez-Arenas, T. E. G., Gil-Pelegrin, E., Ealo Cuello, J., Fariñas, M. D., Sancho-Knapik, D., Collazos-Burbano, D. A., et al. (2016). Ultrasonic sensing of plant water needs for agriculture. *Sensors* 16, 1–20. doi: 10.3390/s16071089

Álvarez-Arenas, T. E. G., Sancho-Knapik, D., Peguero-Pina, J. J., and Gil-Pelegriìn, E. (2009). Noncontact and noninvasive study of plant leaves using air-coupled ultrasounds. *Appl. Phys. Lett.* 95:193702. doi: 10.1063/1.3263138

Álvarez-Arenas, T. E. G., Sancho-Knapik, D., Peguero-Pina, J. J., Gómez-Arroyo, A., and Gil-Pelegrín, E. (2018). Non-contact ultrasonic resonant spectroscopy resolves the elastic properties of layered plant tissues. *Appl. Phys. Lett.* 113:253704. doi: 10.1063/1.5064517

Boyer, J. S., James, R. A., Munns, R., and Passioura, J. (2008). Osmotic adjustment leads to anomalously low estimates of relative water content in wheat and barley. *Funct. Plant Biol.* 35, 1172–1182. doi: 10.1071/FP08157

Callister, A. N., Arndt, S. K., Ades, P. K., Mechant, A., Rowell, D., and Adams, M. A. (2008). Leaf osmotic potential of Eucalyptus hybrids responds differently to freezing and drought, with little clonal variation. *Tree Physiol.* 28, 1297–1304. doi: 10.1093/treephys/28.8.1297

Chuah, H. T., Lee, K. Y., and Lau, T. W. (1995). Dielectric constants of rubber and oil palm leaf samples at X-band. *IEEE Trans. Geosci. Remote Sens.* 33, 221–223. doi: 10.1109/36.368205

Ding, Y., Zhang, Y., Zheng, Q.-S., and Tyree, M. T. (2014). Pressure–volume curves: revisiting the impact of negative turgor during cell collapse by literature review and simulations of cell micromechanics. *New Phytol.* 203, 378–387. doi: 10.1111/nph.12829

Farinas, M. D., and Alvarez-Arenas, T. E. G. (2014). Ultrasonic assessment of the elastic functional design of component tissues of phormium tenax leaves. *J. Mech. Behav. Biomed. Mater.* 39, 304–315. doi: 10.1016/j.jmbbm.2014.07.018

Farinas, M. D., Jimenez-Carretero, D., Sancho-Knapik, D., Peguero-Pina, J. J., Gil-Pelegrin, E., and Alvarez-Arenas, T. E. G. (2019). Instantaneous and non-destructive relative water content estimation from deep learning applied to resonant ultrasonic spectra of plant leaves. *Plant Methods* 15:128. doi: 10.1186/s13007-019-0511-z

Farinas, M. D., Sancho Knapik, D., Peguero Pina, J. J., Gil Pelegrin, E., and Alvarez-Arenas, T. E. G. (2014). Monitoring plant response to environmental stimuli by ultrasonic sensing of the leaves. *Ultrasound Med. Biol.* 40, 2183–2194. doi: 10.1016/j.ultrasmedbio.2014.04.004

Fricke, W. (1996). Cell turgor, osmotic pressure and water potential in the upper epidermis of barley leaves in relation to cell location and in response to NaCI and air humidity. *J. Exp. Bot.* 48, 45–45.

Gil-Pelegrín, E., Saz, M. Á, Cuadrat, J. M., Peguero-Pina, J. J., and Sancho-Knapik, D. (2017). "Oaks under mediterranean-type climates: functional response to summer aridity," in *Oaks Physiological Ecology. Exploring the Functional Diversity of Genus Quercus L. Tree Physiology*, Vol. 7, eds E. Gil-Pelegrín, J. Peguero-Pina, and D. Sancho-Knapik (Cham: Springer), 137–193.

Hare, P. D., Cress, W. A., and Van Staden, J. (1998). Dissecting the roles of osmolyte accumulation during stress. *Plant Cell Environ.* 21, 535–553. doi: 10.1046/j.1365-3040.1998.00309.x

Martínez, M., Artacho, J. M., Forníes-Marquina, J. M., Letosa, J., García-Gracia, M., and Gil, E. (1995). Dielectric behaviour by T.D.R. of the water status in a vegetal leaf. *OHD Biennial Colloquium Digest* 13:520.

Menzel, M. I., Tittmann, S., Bühler, J., Preis, S., Wolters, N., Jahnke, S., et al. (2009). Non-invasive determination of plant biomass with microwave resonators. *Plant Cell Environ.* 32, 368–379. doi: 10.1111/j.1365-3040.2009.01931.x

Mizukami, Y., Sawai, Y., and Yamaguchi, Y. (2006). Moisture content measurement of tea leaves by electrical impedance and capacitance. *Biosyst. Eng.* 93, 293–299. doi: 10.1016/j.biosystemseng.2005.12.009

Monteiro, A., Teixeira, G., and Lopes, C. M. (2013). Comparative leaf micromorphoanatomy of *Vitis vinifera* SSP. vinifera (Vitaceae) red cultivars. *Ciência Téc. Vitiv.* 28, 19–28.

Navarro, B. L., Rodrigues, J. P., Appezzato, B., and Bellato, M. (2019). Histopathology of *Phakopsora euvitis* on *Vitis vinifera*. *Eur. J. Plant Pathol.* 154, 1185–1193. doi: 10.1007/s10658-019-01719-w

Oertli, J. J. (1986). The effect of cell size on cell collapse under negative turgor pressure. *J. Plant Physiol.* 124, 365–370. doi: 10.1016/s0176-1617(86)80048-7

Repo, T. (1988). Physical and physiological aspect of impedance measurement in plants. *Silva Fennica* 22, 181–193.

Rueger, S., Ehrenberger, W., and Zimmermann, U. (2011). The leaf patch clamp pressure probe: a new tool for irrigation scheduling and deeper insight into olive drought stress physiology. *Acta Hortic.* 888, 223–230. doi: 10.17660/ActaHortic.2011.888.25

Sancho-Knapik, D., Alvarez-Arenas, T. E. G., Peguero-Pina, J. J., and Gil-Pelegrín, E. (2010). Air-coupled broadband ultrasonic spectroscopy as a new non-invasive and non-contact method for the determination of leaf water status. *J. Exp. Bot.* 61, 1385–1391. doi: 10.1093/jxb/erq001

Sancho-Knapik, D., Calás, H., Peguero-pina, J. J., Ramos Fernandez, A., Gil-Pelegrín, E., and Alvarez-Arenas, T. E. G. (2012). Air-coupled ultrasonic resonant spectroscopy for the Study of the relationship between plant leaves' elasticity and their water content. *IEEE Trans. Ultrason. Freq. Control.* 59, 319–325. doi: 10.1109/tuffc.2012.2194

Sancho-Knapik, D., Medrano, H., Peguero-Pina, J. J., Mencuccini, M., Fariñas, M. D., Alvarez-Arenas, T. E. G., et al. (2016). The application of leaf ultrasonic resonance to *Vitis vinifera* L. suggests the existence of a diurnal osmotic adjustment subjected to photosynthesis. *Front. Plant Sci.* 7:1601. doi: 10.3389/fpls.2016.01601

Sancho-Knapik, D., Peguero-Pina, J. J., Fariñas, M. D., Alvarez-Arenas, T. E. G., and Gil-Pelegrín, E. (2013a). Ultrasonic spectroscopy allows a rapid determination of the relative water content at the turgor loss point: a comparison with pressure-volume curves in 13 woody species. *Tree Physiol.* 33, 695–700. doi: 10.1093/treephys/tpt052

Sancho-Knapik, D., Peguero-Pina, J. J., Medrano, H., Fariñas, M. D., Álvarez-Arenas, T. E. G., and Gil-Pelegrín, E. (2013b). The reflectivity in the S-band

and the broadband ultrasonic spectroscopy as new tools for the study of water relations in *Vitis vinifera* L. *Physiol. Plant* 148, 512–521. doi: 10.1111/ppl.12007

Sanders, G. J., and Arndt, S. K. (2012). "Osmotic adjustment under drought conditions," in *Plant Responses to Drought Stress*, ed. R. Aroca (Berlin: Springer), 199–229. doi: 10.1007/978-3-642-32653-0_8

Tyree, M. T. (1976). Negative turgor pressure in plant cells: fact or fallacy? *Can. J. Bot.* 54, 2738–2746. doi: 10.1139/b76-294

Yang, D. J., Li, Y., Ding, M. T., and Tyree, R. (2017). Experimental evidence for negative turgor pressure in small leaf cells of *Robinia pseudoacacia* L versus large cells of Metasequoia glyptostroboides Hu et W.C. Cheng. 2. Höfler diagrams below the volume of zero turgor and the theoretical implication for pressure-volume curves of living cells. *Plant Cell Environ.* 40, 340–350. doi: 10.1111/pce.12860

Zhang, M. I. N., and Willison, J. H. M. (1993). Electrical impedance analysis in plant tissues. *J. Exp. Bot.* 44, 1369–1375. doi: 10.1093/jxb/44.8.1369

Zimmermann, D., Reuss, R., Westhoff, M., Gessner, P., Bauer, W. D., Bamberg, E., et al. (2008). A novel, non-invasive, online-monitoring, versatile and easy plant-based probe for measuring leaf water status. *J. Exp. Bot.* 59, 3157–3167. doi: 10.1093/jxb/ern171

Conflict of Interest: The authors declare that the research was conducted in the absence of any commercial or financial relationships that could be construed as a potential conflict of interest.

frontiers in Plant Science

ORIGINAL RESEARCH
published: 05 June 2020
doi: 10.3389/fpls.2020.00758

The Response of Water Dynamics to Long-Term High Vapor Pressure Deficit Is Mediated by Anatomical Adaptations in Plants

Qingjie Du[1,2†], Xiaocong Jiao[1†], Xiaoming Song[1], Jiayu Zhang[1], Ping Bai[1], Juping Ding[1] and Jianming Li[1]*

[1] College of Horticulture, Northwest A&F University, Yangling, China, [2] College of Horticulture, Henan Agricultural University, Zhengzhou, China

Vapor pressure deficit (VPD) is the driver of water movement in plants. However, little is known about how anatomical adaptations determine the acclimation of plant water dynamics to elevated VPD, especially at the whole plant level. Here, we examined the responses of transpiration, stomatal conductance (g_s), hydraulic partitioning, and anatomical traits in two tomato cultivars (Jinpeng and Zhongza) to long-term high (2.2–2.6 kPa) and low (1.1–1.5 kPa) VPD. Compared to plants growing under low VPD, no variation in g_s was found for Jinpeng under high VPD conditions; however, high VPD induced an increase in whole plant hydraulic conductance (K_{plant}), which was responsible for the maintenance of high transpiration. In contrast, transpiration was not influenced by high VPD in Zhongza, which was primarily attributed to a coordinated decline in g_s and K_{plant}. The changes in g_s were closely related to stomatal density and size. Furthermore, high VPD altered hydraulic partitioning among the leaf, stem, and root for both cultivars via adjustments in anatomy. The increase in lumen area of vessels in veins and large roots in Jinpeng under high VPD conditions improved water transport efficiency in the leaf and root, thus resulting in a high K_{plant}. However, the decreased K_{plant} for Zhongza under high VPD was the result of a decline of water transport efficiency in the leaf that was caused by a reduction in vein density. Overall, we concluded that the tradeoff in anatomical acclimations among plant tissues results in different water relations in plants under high VPD conditions.

Keywords: anatomical acclimations, hydraulics, stomatal conductance, transpiration, vapor pressure deficit

OPEN ACCESS

Edited by:
Juan Pedro Ferrio, Fundacion Agencia Aragonesa para la Investigacion y el Desarrollo, Spain

Reviewed by:
Dimitrios Fanourakis, Technological Educational Institute of Crete, Greece
Gerardo Tapia, Institute of Agricultural Research, Chile

***Correspondence:**
Jianming Li
lijianming66@163.com

† These authors have contributed equally to this work

Specialty section:
This article was submitted to Technical Advances in Plant Science, a section of the journal Frontiers in Plant Science

Received: *14 January 2020*
Accepted: *12 May 2020*
Published: *05 June 2020*

Citation:
Du Q, Jiao X, Song X, Zhang J, Bai P, Ding J and Li J (2020) The Response of Water Dynamics to Long-Term High Vapor Pressure Deficit Is Mediated by Anatomical Adaptations in Plants. Front. Plant Sci. 11:758. doi: 10.3389/fpls.2020.00758

INTRODUCTION

The process of water movement through soil–plant–atmosphere continuum (SPAC) is driven by atmospheric evaporative demand which can be expressed as vapor pressure deficit (VPD). Although the optimal VPD for most greenhouse crops is below 1.5 kPa (Shamshiri et al., 2016), high VPD (>2 kPa) is currently observed in greenhouses, especially during summer (Lu et al., 2015; Zhang et al., 2018). For plants grown under high VPD conditions, a central question is how they regulate transpiration (Carins Murphy et al., 2014; Allen et al., 2015; Grossiord et al., 2017). In a plant, water absorbed through the roots is transported to leaves through the xylem, finally lost via

stomata by diffusion. Hence, the regulation of transpiration may occur at whole plant levels. However, the responses of physiological and anatomical traits that could influence transpiration remain largely unknown at whole plant levels during high VPD condition.

Most of the water loss by a plant occurs through stomatal apertures (Macková et al., 2013). Moreover, cuticular pathway is found to be important in regulating water loss when stomatal closure takes place (Fanourakis et al., 2013, 2019). Under steady state conditions and in the vapor phase, the transpiration rate (E) is defined mathematically as a function of stomatal conductance (g_s) and VPD. Although the regulation of transpiration depends on the response of g_s to VPD during the vapor phase, the efficiency of the hydraulic system determines the amount of liquid water lost to evaporation for any given soil water condition. Using an analogy of Ohm's law, E can be expressed as the product of hydraulic conductance and water potential gradient in liquid flux. Many studies have proposed a hydraulic feedback loop to interpret the dynamic link between the liquid and gas phases (Buckley, 2005; Domec et al., 2009; Simonin et al., 2015). Thus, a coordination may exist between g_s and whole plant hydraulic conductance (K_{plant}) with respect to water transport across the soil–plant–atmosphere continuum.

To deal with long-term environmental fluctuation, plants have evolved high plasticity in carbon allocation (Freschet et al., 2018). The changes in carbon investment generally trigger adjustments in anatomical traits involved in plant water dynamics, which occur at multiple places in the plant including stomatal and xylem tissues (Sperry et al., 1998; de Boer et al., 2016; Dewar et al., 2018). Previous studies demonstrates stomatal density decreased to prevent excessive water loss under high VPD in tomato (Lu et al., 2015; Du et al., 2019), rose (Fanourakis et al., 2012), and fava bean (Aliniaeifard et al., 2014). However, few stomata mean a reduction in the maximum potential carbon acquisition. Alternatively, plants resort to an efficient hydraulic system to withstand excessive evaporative demand. Despite a high carbon investment to xylem, these adjustments contribute to maintain carbon acquirement. Thus, a tradeoff between water loss and carbon acquirement would exist during the acclimation process of plants to high VPD. Additionally, the hydraulic system in plants shows a strong hydraulic segmentation (Cruiziat et al., 2002; Sperry and Love, 2015). Although the dynamics of hydraulic conductance of leaves, stems, and roots have been well-documented in response to soil water deficit (Domec et al., 2009; Torres-Ruiz et al., 2015), the adjustment of hydraulic structure to long-term high VPD has been poorly investigated. Therefore, systematic knowledge about acclimation at the whole plant level is critical to determining the responses of plants to high VPD and is necessary to understand the tradeoff between carbon investment in regulating water dynamics and carbon acquirement.

Tomato (*Solanum lycopersicum* L.) is one of the most important agricultural plants in the world. High VPD induces contrasting responses in plant water status among tomato cultivars (Zhang et al., 2018; Du et al., 2019). In the present study, two tomato cultivars, Jingpeng and Zhongza, were selected on the basis that they exhibit different responses to altered VPD (Du et al., 2019). The responses of water dynamics and anatomical traits were measured on these two cultivars after exposure to long-term high and low VPD. We hypothesized that (1) for plants with high water loss under high VPD, K_{plant} would increase with unaffected g_s; (2) for plants with relatively low water loss under high VPD, K_{plant} and g_s would synchronously decline; and (3) acclimation in terms of water dynamics is related to anatomical changes at multiple places in plants.

MATERIALS AND METHODS

Plant Material and Growth Conditions

Seeds of Jinpeng and Zhongza were germinated and grown in plastic pots [15 cm × 10 cm (diameter × height); 1 plant/pot] containing a mixed peat-perlite substrate. The seedlings were kept in a walk-in growth chamber. The light in the chambers was given daily for 14 h at a photon flux density of 300 μmol m^{-2} s^{-1}. The temperature was 28–30°C day/19–20°C night. Relative humidity was regulated between 64–70% day/77–82% night using an ultrasonic humidifier (KAJ-9.0B, Kawasima Appliance Co., Ltd., Changzhou, China) and dehumidifier (DH-702B, Chuanjing Electric Co., Ltd., Hangzhou, China). Consequently, the VPD was 1.1–1.5 kPa day/0.4–0.5 kPa night. After 5 weeks, 30 of the healthiest plants were divided into two random groups of 15 for each cultivar. For low VPD treatment, the plants were kept on previous humidity conditions. A high VPD was performed by setting 36–42% relative humidity during the day (VPD 2.2–2.6 kPa). Plants were grown for 30 d and kept well-watered during the entire growth period. New fully expanded leaves were used for measurements.

Transpiration and Stomatal Conductance

To determine transpiration at the canopy level (E_{canopy}) during the photoperiod, pots were covered with plastic film and aluminum foil on the day before measurement. After at least 2 h of acclimation in the photoperiod, five pots were weighed 2 and 8 h after turning on the lights. E_{canopy} was calculated by differences in weight divided by the total leaf area. Canopy stomatal conductance (g_s-*canopy*) was determined according to a simplified inversion of the Penman–Monteith model (Monteith and Unsworth, 1990):

$$g_{s-canopy} = \frac{RT_a \rho E_{canopy}}{VPD},$$

where R is the universal gas constant adjusted for water vapor (0.46 m^3 kPa K^{-1} kg^{-1}), T_a is air temperature (K), and ρ is the density of water (998 kg m^{-3}).

Leaf level transpiration (E_{leaf}) and stomatal conductance (g_{s-leaf}) were measured with a plant porometer (Yaxin-1301, Yaxin Liyi Technology Co., Ltd., Beijing, China). After at least 2 h of acclimation in the photoperiod, five leaves from different plants for each treatment and cultivar were used for measurements. VPD, light, and the temperature of the cuvette were kept at ambient levels.

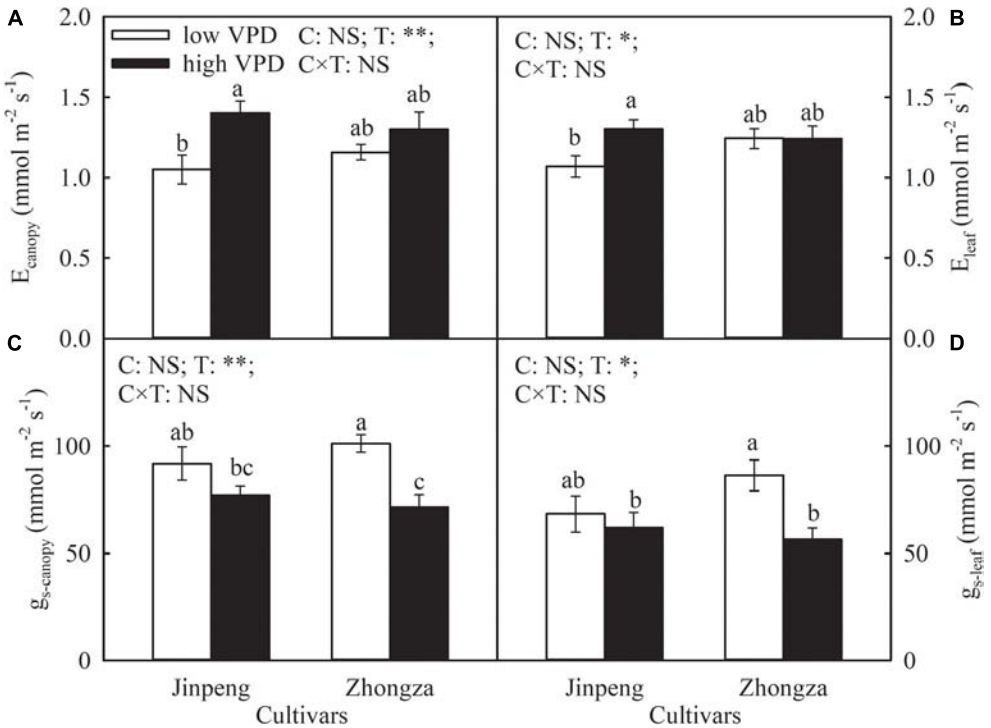

FIGURE 1 | Transpiration rate at the canopy (E_{canopy}) **(A)** and leaf level (E_{leaf}) **(B)**, stomatal conductance at the canopy (g_s-*canopy*) **(C)** and leaf level (g_s-*leaf*) **(D)** for two tomato cultivars, Jinpeng and Zhongza, grown under low (1.1–1.5 kPa) and high (2.2–2.6 kPa) VPD. Data are means ± standard error (n = 5 plants). Different letters denote statistically significant differences (Duncan's test, $P < 0.05$). Two-way ANOVA was used to estimate the effect of cultivar (C), treatment (T), and their interaction (C × T) (**$P < 0.01$; *$P < 0.05$; NS, not significant).

TABLE 1 | Stomatal density (SD) and area (SA) for two tomato cultivars, Jinpeng and Zhongza, grown under low (1.1–1.5 kPa) and high (2.2–2.6 kPa) VPD.

Cultivars	Treatments	$SD_{adaxial}$ (mm^{-2})	$SD_{abaxial}$ (mm^{-2})	SD (mm^{-2})	$SA_{adaxial}$ (μm^2)	$SA_{abaxial}$ (μm^2)	SA (μm^2)
Jinpeng	Low VPD	53.83 ± 3.29 a	132.66 ± 4.67 b	186.49 ± 6.86 ab	277.46 ± 9.92 ab	294.56 ± 11.74 b	286.74 ± 10.74 b
	High VPD	52.91 ± 4.12 a	125.95 ± 2.71 b	178.81 ± 4.45 bc	265.60 ± 8.20 b	300.01 ± 10.42 b	282.83 ± 8.21 b
Zhongza	Low VPD	51.46 ± 3.64 a	150.59 ± 4.87 a	202.05 ± 4.94 a	296.21 ± 9.27 a	378.95 ± 18.90 a	337.58 ± 6.53 a
	High VPD	38.01 ± 2.03 b	130.75 ± 4.26 b	168.76 ± 5.54 c	285.99 ± 5.66 ab	247.21 ± 19.28 c	266.60 ± 11.63 b
Cultivar		*	*	NS	*	NS	NS
Treatment		*	**	**	NS	**	**
Cultivar × Treatment		NS	NS	*	NS	**	**

Data are given for the abaxial and adaxial sides of the leaves. Leaf integrated values for the whole leaf are also given: $SD = SD_{adaxial} + SD_{abaxial}$, $SA = (SA_{adaxial} + SA_{abaxial})/2$. Data are means ± standard error (n = 5 plants). Different letters within the same column denote statistically significant differences (Duncan's test, $P < 0.05$). Two-way ANOVA was used to estimate the effect of cultivar, treatment, and their interaction ($P < 0.05$; **$P < 0.01$; NS, not significant).*

Hydraulic Conductance

Hydraulic conductance of the leaf (K_{leaf}), stem (K_{stem}), and root (K_{root}) and K_{plant} were calculated according to Domec et al. (2009). Briefly,

$$K_{plant} = \frac{E_{leaf}}{\Psi_{soil} - \Psi_{leaf}},$$

$$K_{leaf} = \frac{E_{leaf}}{\Psi_{stem-up} - \Psi_{leaf}},$$

$$K_{stem} = \frac{E_{leaf}}{\Psi_{stem-base} - \Psi_{stem-up}},$$

$$\frac{1}{K_{root}} = \frac{1}{K_{plant}} - \frac{1}{K_{leaf}} - \frac{1}{K_{stem}},$$

where Ψ_{soil} is the soil water potential measured with a PSYPRO Water Potential System (PSYPRO; Wescor, Inc., Logan, UT, United States), Ψ_{leaf} is the water potential of the leaf used for gas exchange measurement (transpiring leaf), Ψ_{stem}-*up* is the stem water potential in the upper crown section, and $\Psi_{stem-base}$ is the stem water potential at the stem base. Ψ_{stem} was estimated from the leaf water potential of a non-transpiring leaf (achieved by covering with plastic film and aluminum foil the night before measurement) (Richter, 1997; Zsögön et al., 2015). The

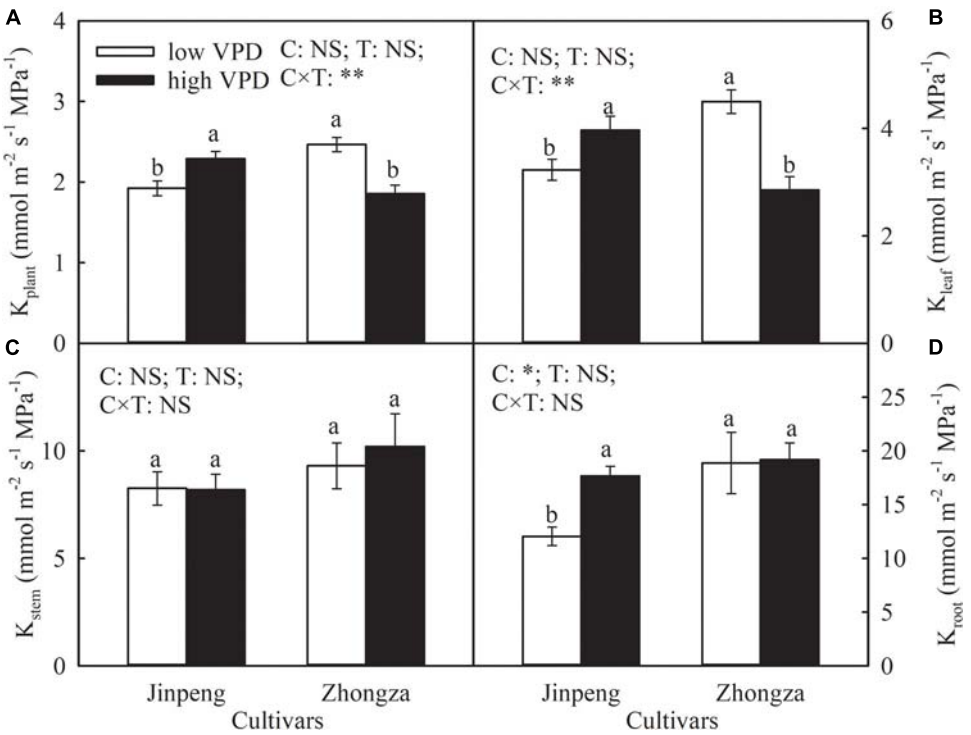

FIGURE 2 | Hydraulic conductance of whole plant (K_{plant}) **(A)**, leaf (K_{leaf}) **(B)**, stem (K_{stem}) **(C)**, and root (K_{root}) **(D)** for two tomato cultivars, Jinpeng and Zhongza, grown under low (1.1–1.5 kPa) and high (2.2–2.6 kPa) VPD. Data are means ± standard error (n = 5 plants). Different letters denote statistically significant differences (Duncan's test, $P < 0.05$). Two-way ANOVA was used to estimate the effect of cultivar (C), treatment (T), and their interaction (C × T) (**$P < 0.01$; *$P < 0.05$; NS, not significant).

leaf adjacent to the transpiring leaf was used for Ψ_{stem}-*up* and the first true leaf was used for Ψ_{stem}-*base*. Measurements of Ψ_{leaf}, Ψ_{stem}-*up*, and $\Psi_{stem\text{-}base}$ were performed on the same five plants used for gas exchange measurements with a pressure chamber (PMS, Corvallis, OR, United States). After measurement of hydraulic conductance, the plants were used for morphological observation.

Stomatal Characteristics

Stomatal morphological characteristics were determined using the impression method as described by Xu and Zhou (2008). Briefly, epidermis was smeared with nail varnish in the mid-area between the midrib and lateral margin, avoiding midrib and secondary veins (Fanourakis et al., 2015b). Then, the thin film (approximately 5 mm × 5 mm) was peeled off from the leaf surface and mounted on a glass slide. All stomatal characteristics were measured on both the adaxial and abaxial sides of the leaf. For determining stomatal density (SD), five images per sampling area were taken at a magnification of 200× with a light microscope (BX50, Olympus, Tokyo, Japan). Stomatal area (SA) was measured on at least 20 stomata per sampling area at a magnification of 400× with ImageJ software (National Institutes of Health, Bethesda, MD, United States). SA was defined as the combined area of pore and a pair of guard cells following Savvides et al. (2012).

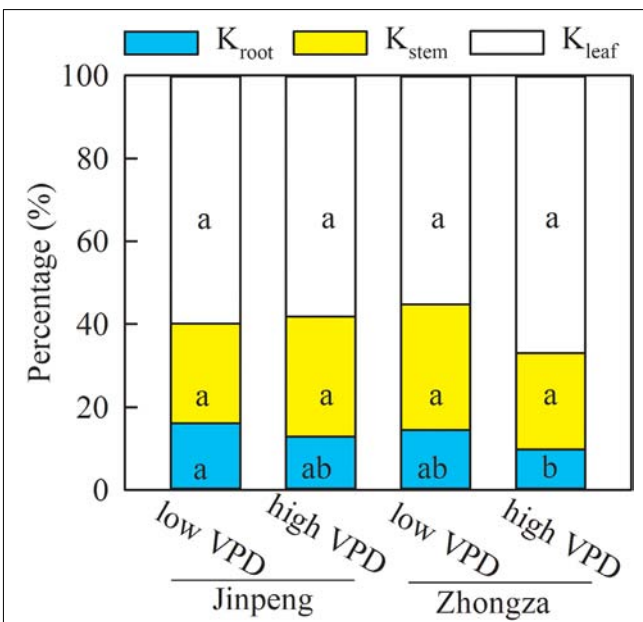

FIGURE 3 | Percentage contributions of leaf (K_{leaf}), stem (K_{stem}), and root (K_{root}) hydraulic conductance to whole plant hydraulic conductance for two tomato cultivars, Jinpeng and Zhongza, grown under low (1.1–1.5 kPa) and high (2.2–2.6 kPa) VPD. Different letters denote statistically significant differences (Duncan's test, $P < 0.05$).

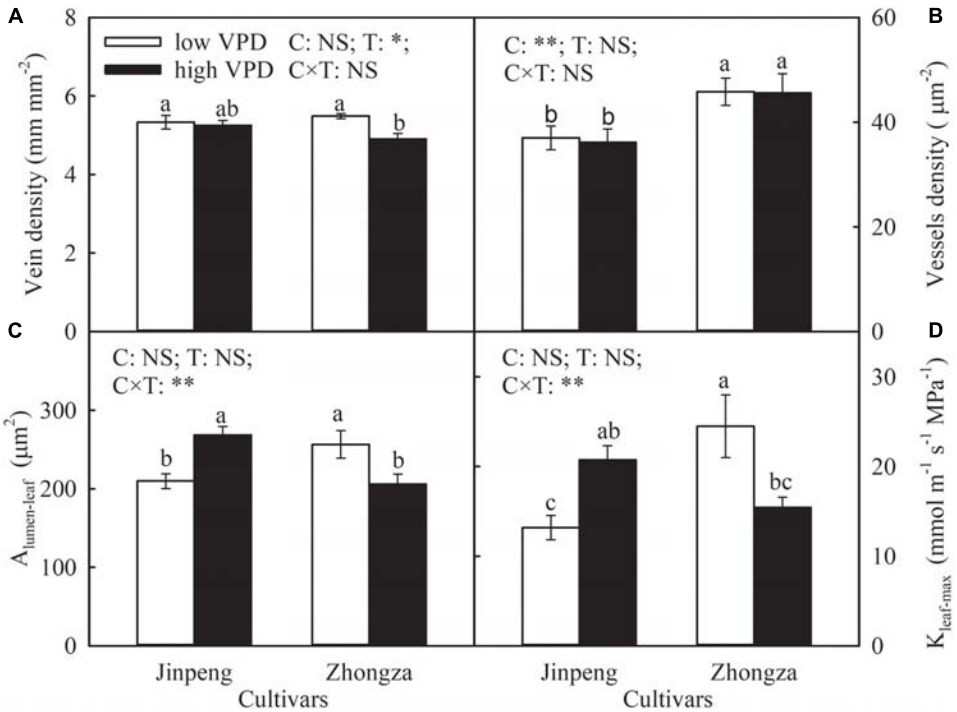

FIGURE 4 | Vein density **(A)**, vessel density **(B)**, lumen area of vessels in leaf vein (A_{lumen}-*leaf*) **(C)**, and maximum theoretical leaf vein axial hydraulic conductivity (K_{leaf}-*max*) **(D)** for two tomato cultivars, Jinpeng and Zhongza, grown under low (1.1–1.5 kPa) and high (2.2–2.6 kPa) VPD. Data are means ± standard error (n = 5 plants). Different letters denote statistically significant differences (Duncan's test, $P < 0.05$). Two-way ANOVA was used to estimate the effect of cultivar (C), treatment (T), and their interaction (C × T) (**$P < 0.01$; *$P < 0.05$; NS, not significant).

Vein and Stem Anatomical Traits

To evaluate leaf vein traits, leaflets were detached from the leaves used for Ψ_{leaf} measurements. Cleared leaflets were scanned to estimate the length of the midrib and secondary vein as well as the leaf area. Veins with an order higher than secondary were measured on 1-cm^2 leaf pieces from the center of each leaf at a magnification of 40× according to Kono et al. (1982). Briefly, the lamina was boiled in 70% ethanol to remove pigment. After washing with distilled water, samples were transferred to boiling 85% lactic acid for 20 min and then spread out flat on a slide for observation. The vein density was calculated as the ratio of total vein length to the analyzed area.

To assess the xylem composition in veins, segments (0.3 cm in length) were cut from the petiole immediately below the lamina insertion point. This section was selected because it was connected to the midrib and water entering the leaflet would have to pass through this part. The middle of the plant was sampled to estimated xylem composition in the stem. After fixing in a mixture of formaldehyde, acetic acid, and alcohol for 24 h, the sample material was dehydrated in a graded ethanol-xylene series and infiltrated with paraffin. Then 12-μm thick sections were made using a rotary microtome, stained with safranin and fast green, and mounted on slides with a cover slip (Berlyn and Miksche, 1976). The cross-sectional area of the petiole and total number of vessels in the petiole were measured at magnifications of 40× and 100×, respectively. Vessel density was defined as the number of vessels per unit area. The lumen area of vessels in the leaf vein (A_{lumen}-*leaf*) and stem (A_{lumen}-*stem*), and wall thickness of vessels in the stem (T_w-*stem*), were estimated at a magnification of 400× with ImageJ (at least three different field-of-view regions). The lumen diameter of each vessel was calculated from its lumen area, assuming a circular shape. The maximum theoretical leaf vein axial hydraulic conductivity (K_{leaf}-*max*) was estimated as follows (North et al., 2013):

$$K_{leaf-max} = \sum_{i}^{N} \frac{\pi d_i^4}{128\eta},$$

where N is total number of vessels in the petiole, d_i is the lumen diameter of each vessel, and η is the viscosity of water, further normalized by leaf area (Sack and Frole, 2006).

Root Morphological Characteristics

After measurement of hydraulic conductance, roots were detached from the plant and carefully washed. The cleaned samples were scanned and analyzed with WinRhizo software (WinRhizo, Regent Ltd., Canada).

Growth Analyses

Five plants per treatment were selected to measure plant biomass and total leaf area. The aboveground and underground dry biomass of plant was determined after drying to a constant

weight at 80°C. The net assimilation rate (NAR) was calculated as follows:

$$NAR = \frac{W_2 - W_1}{T_2 - T_1} \times \frac{lnL_2 - lnL_1}{L_2 - L_1},$$

where W_1 and W_2 are total dry weights of the whole plant at times T_1 and T_2; L_1 and L_2 are total leaf areas of the whole plant at times T_1 and T_2.

Statistical Analysis

All statistical analyses were performed using SPSS 19.0 (IBM Corp., Armonk, NY, United States). One-way ANOVA was used to test differences between mean values (Duncan's test). Two-way ANOVA was used to determine the main effects of cultivar, treatment, and their interactions.

RESULTS

Transpiration and Stomatal Conductance

The effects of VPD on E_{canopy} and E_{leaf} were similar and cultivar specific (**Figure 1**). The E_{canopy} and E_{leaf} of Jinpeng significantly increased under high VPD compared to low VPD. On the contrary, in Zhongza, these measures were both unaffected by VPD treatment. Under high VPD, g_s-*canopy* and g_s-*leaf* decreased by 29 and 35%, respectively, in Zhongza relative to low VPD whereas VPD had no influence on either g_s-*canopy* or g_s-*leaf* in Jinpeng.

Stomatal Characteristics

No significant differences in SD or SA for either the adaxial or abaxial sides of the leaf were found between low and high VPD in Jinpeng (**Table 1**). For Zhongza, high VPD significantly decreased SD on both sides and SA on the adaxial side only. Moreover, the integrated values of SD and SA for the whole leaf also declined under high VPD compared to low VPD in Zhongza.

Plant Hydraulic Conductance

Compared to low VPD, K_{plant} and K_{leaf} in Jinpeng significantly increased but in Zhongza declined by 24 and 36%, respectively, under high VPD (**Figure 2**). No difference in K_{stem} was noted between low and high VPD conditions for either cultivar. K_{root} increased by 46% in Jingpeng under high VPD but was similar under low and high VPD in Zhongza.

Relative contributions were analyzed to discern the role of K_{leaf}, K_{stem}, and K_{root} in the observed changes in K_{plant} (**Figure 3**). The percentages of K_{leaf}, K_{stem}, and K_{root} that made up K_{plant} were similar between low and high VPD in both Jinpeng and Zhongza. K_{leaf} accounted for 56–66% of the changes in K_{plant}, followed by K_{stem} (26%) and K_{root} (13%).

Leaf Vein Traits

Vein density was not affected by VPD treatment in Jinpeng, but declined in Zhongza under high VPD compared to low VPD (**Figure 4**). For both cultivars, high VPD had no influence on vessel density in leaf veins. Under high VPD, A_{lumen}-*leaf* and K_{leaf}-*max* increased by 28 and 57%, respectively, in Jinpeng but decreased by 20 and 37%, respectively, in Zhongza.

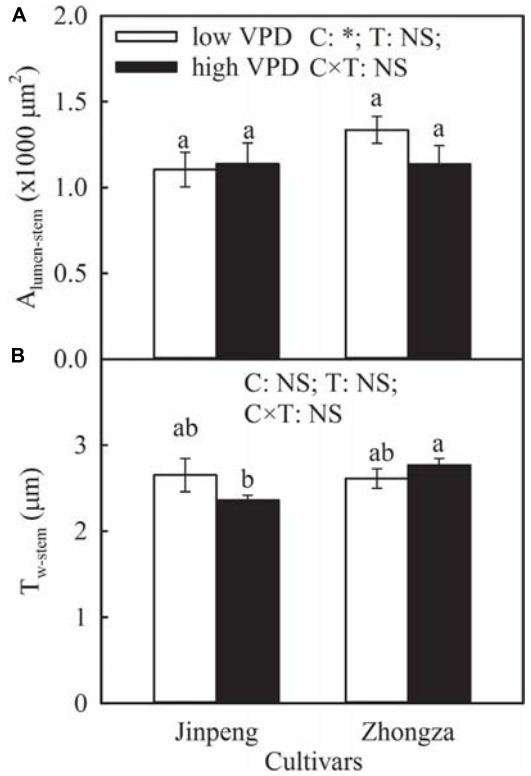

FIGURE 5 | Lumen area (A_{lumen}-*stem*) **(A)** and wall thickness (T_w-*stem*) **(B)** of vessels in stem for two tomato cultivars, Jinpeng and Zhongza, grown under low (1.1–1.5 kPa) and high (2.2–2.6 kPa) VPD. Data are means ± standard error (n = 5 plants). Different letters denote statistically significant differences (Duncan's test, $P < 0.05$). Two-way ANOVA was used to estimate the effect of cultivar (C), treatment (T), and their interaction (C × T) (*$P < 0.05$; NS, not significant).

Stem and Root Morphological Characteristics

A_{lumen}-*stem* and T_w-*stem* was not significantly different between low and high VPD in either Jinpeng or Zhongza (**Figure 5**). Under high VPD, Jinpeng roots had 57, 33, and 17% higher volume, surface area, and average diameter, respectively, than under low VPD (**Table 2**). No differences in root volume, surface area, or average diameter were found in Zhongza between low and high VPD. Root total length was similar under low and high VPD in both cultivars.

Growth Analyses

Aboveground dry weight, total dry weight and NAR was similar under high and low VPD in Jinpeng, but these parameters were significantly lower under high VPD than low VPD in Zhongza (**Table 3**). Although no statistical differences in underground dry weight were found between low and high VPD for both cultivars, it increased by 14% in Jinpeng and decreased by 7% in Zhongza under high VPD.

TABLE 2 | Root volume, surface area, average diameter, and total length for two tomato cultivars, Jinpeng and Zhongza, grown under low (1.1–1.5 kPa) and high (2.2–2.6 kPa) VPD.

Cultivars	Treatments	Root volume (cm^3)	Root surface area (cm^2)	Root average diameter (mm)	Root total length (cm)
Jinpeng	Low VPD	0.86 ± 0.08 b	87.44 ± 7.17 b	0.39 ± 0.01 b	708.52 ± 49.62 ab
	High VPD	1.35 ± 0.11 a	116.07 ± 6.50 a	0.46 ± 0.02 a	798.41 ± 50.90 a
Zhongza	Low VPD	1.36 ± 0.14 a	104.25 ± 8.73 ab	0.51 ± 0.03 a	653.36 ± 34.47 b
	High VPD	1.37 ± 0.12 a	103.50 ± 6.99 ab	0.48 ± 0.02 a	721.20 ± 53.97 ab
Cultivar		*	NS	**	NS
Treatment		*	NS	NS	NS
Cultivar × Treatment		NS	NS	*	NS

Data are means ± standard error (n = 5 plants). Different letters within the same column denote statistically significant differences (Duncan's test, $P < 0.05$). Two-way ANOVA was used to estimate the effect of cultivar, treatment, and their interaction ($P < 0.05$; **$P < 0.01$; NS, not significant).*

TABLE 3 | Aboveground dry weight, underground dry weight, total dry weight, and net assimilation rate (NAR) for two tomato cultivars, Jinpeng and Zhongza, grown under low (1.1–1.5 kPa) and high (2.2–2.6 kPa) VPD.

Cultivars	Treatments	Aboveground dry weight (g)	Underground dry weight (g)	Total dry weight (g)	NAR ($g\ m^{-2}\ d^{-1}$)
Jinpeng	Low VPD	1.577 ± 0.079 a	0.119 ± 0.008 a	1.696 ± 0.084 a	2.580 ± 0.147 a
	High VPD	1.482 ± 0.058 a	0.135 ± 0.009 a	1.617 ± 0.063 a	2.357 ± 0.059 ab
Zhongza	Low VPD	1.451 ± 0.105 a	0.123 ± 0.014 a	1.574 ± 0.119 a	2.253 ± 0.078 b
	High VPD	1.177 ± 0.086 b	0.115 ± 0.021 a	1.292 ± 0.106 b	1.847 ± 0.093 c
Cultivar		*	NS	*	**
Treatment		*	NS	NS	**
Cultivar × Treatment		NS	NS	NS	NS

Data are means ± standard error (n = 5 plants). Different letters within the same column denote statistically significant differences (Duncan's test, $P < 0.05$). Two-way ANOVA was used to estimate the effect of cultivar, treatment, and their interaction ($P < 0.05$; **$P < 0.01$; NS, not significant).*

DISCUSSION

In the soil–plant–atmosphere continuum, VPD is the driving force for water flow. High VPD induced a higher E in Jinpeng than low VPD, but E was not affected by VPD treatment in Zhongza, suggesting cultivar differences in water dynamic responses to long-term high VPD (**Figure 1**). Acclimation of water transport pathways for liquid and vapor phases to high VPD may separately or simultaneously occur in plants, leading to a new homeostatic state (Brodribb and Holbrook, 2006; Domec et al., 2009; Simonin et al., 2015; Fernandes-Silva et al., 2016). In the vapor phase, evaporation from the mesophyll surface to the substomatal cavity is enhanced with increasing VPD. The reduced g_s in Zhongza under high VPD prevents excessive vapor diffusion out of the leaf while E is proportional to changes in VPD due to unchanged g_s in Jinpeng. Additionally, water supply determines how much water can evaporate from the plant. For liquid flow moving through the plant, water supply depends on the K_{plant} for given soil moisture conditions. In Jinpeng, the increased E under high VPD would been maintained by a high K_{plant} (**Supplementary Figure S1**). The coupling between K_{plant} and E enables leaves to minimize variation in plant water status (Simonin et al., 2015). However, the coordination between K_{plant} and E is disrupted in Zhongza. The reduced K_{plant} suggests a limited water supply in Zhongza under high VPD. Thus, E for Zhongza growing under high VPD is kept at the same level as for low VPD conditions to maintain the balance between water supply and loss.

g_s is tightly linked to plant water status (Bunce, 2006; Ripullone et al., 2007). According to the hydraulic feedback hypothesis, a hydraulic feedback loop can describe the mechanism driving the relationship between g_s and K_{plant} (Buckley, 2005; Brodribb and Jordan, 2011; Savvides et al., 2012; Simonin et al., 2015). The absence of change in g_s and the increase in K_{plant} demonstrated by Jinpeng growing under high VPD suggest that adequate water supply prevents leaf dehydration and therefore the stomata remain open. This acclimation would maximize carbon acquisition under high VPD, which was confirmed by the similar plant biomass and NAR under high and low VPD in Jinpeng (**Table 3**). In contrast, a coordinated declines in K_{plant} and g_s were noted in Zhongza under high VPD (**Supplementary Figure S2**). Low water transport efficiency has been regarded as the initial cause of water stress symptoms (Fanourakis et al., 2012). Plants are prone to close stomata due to reductions in leaf turgor when subjected to water stress (Martins et al., 2016; Rodriguez-Dominguez et al., 2016). Thus, g_s in Zhongza decreases under high VPD to minimize water loss in plants despite limiting carbon acquisition (**Table 3**). However, the coordination between g_s and K_{plant} would also play a role in maintaining the integrity of xylem water transport and reducing the risk of hydraulic failure (Galmés et al., 2013; Liu et al., 2015; Salmon et al., 2015; Du et al., 2018).

Alternatively, the responses of g_s to long-term high VPD could be driven by changes in stomatal size and density (Fanourakis et al., 2013; Lu et al., 2015). Franks and Beerling (2009) showed mathematically that g_s is positively related to stomatal density

and size based on the physics of diffusion through pores. Stomatal size and density decreased in Zhongza under high VPD but no active acclimation to high VPD occurred in Jinpeng. Thus, the reductions in stomatal density and size under high VPD are at least partially responsible for the decline in g_s (**Table 1** and **Supplementary Figure S2**). This adjustment in stomatal morphology helps plants avoid the risk of excessive water loss under conditions of high evaporative demand. Furthermore, morphological differences in stomata were more evident in the abaxial epidermis for Zhongza. Fanourakis et al. (2015a) also confirmed that operating g_s was mostly situated on the abaxial surface. For plants, the regulation of g_s is more effective by changing abaxial stomatal morphology because a broader distribution of stomata in abaxial epidermis.

Due to hydraulic segmentation in the plant water transport system, the hydraulic resistance of the whole plant is partitioned into its functional components related to leaves, stems, and roots (Cruiziat et al., 2002; Sperry and Love, 2015). Our study showed that K_{leaf} determines approximately 60% of the changes in K_{plant} (**Figure 3**). Moreover, a synchronized increase in K_{plant} and K_{leaf} was found for Jinpeng whereas a coordinated decrease in K_{plant} and K_{leaf} occurred for Zhongza under high VPD (**Figure 2**). Thus, K_{plant} was mostly dominated by K_{leaf}, which is consistent with previous studies even though leaves constitute less than 3% of the pathway for water flow through the whole plant (Sack et al., 2003; Domec et al., 2009; Tabassum et al., 2016).

During water movement in the leaf, leaf vein structural characteristics are a substantial constraint on K_{leaf} (Sack and Holbrook, 2006; Carins Murphy et al., 2014; Xiong et al., 2017). The decline in vein density of Zhongza under high VPD means not only a reduction in the surface area for the exchange of xylem water with surrounding tissue but an increase in distance for water movement from the xylem into mesophyll cells (Roth-Nebelsick et al., 2001; Sack and Frole, 2006), therefore resulting in a decrease in K_{leaf}. Additionally, A_{lumen}-*leaf* also declined in Zhongza under high VPD (**Figure 4** and **Supplementary Figure S3**). A small vessel diameter in general corresponds to a high resistance for water transport, but it can withstand very low negative pressure without generating an embolism (Pittermann and Sperry, 2003). In contrast, Jinpeng showed a unaffected leaf vein density and synchronized increases in A_{lumen}-*leaf* and E under high VPD (**Figure 4** and **Supplementary Figure S3**), suggesting that large vessel diameter plays a critical role in improving K_{leaf} and maintaining E.

Interestingly, high VPD treatment also resulted in an increase in K_{root} and a concurrent increase in root volume, surface area, and average diameter for Jinpeng whereas no acclimations of K_{root} and root morphology were observed in Zhongza (**Table 2** and **Supplementary Figure S4**). Meanwhile, the large root was tightly related to high E. Modifications in root morphology would improve hydraulic properties at the soil-root interface, promoting water uptake and transport (Steudle, 2000; Domec et al., 2009). However, this active acclimation in root and leaf veins is likely to occur in plants that can maintain a high carbon acquirement because of a high carbon investment. Plants with closed stomata under high VPD would prefer to reduce the investment to aboveground according to the multiple limitation hypothesis (Farrior et al., 2013; Sellin et al., 2015). This may explain the different changes in plant biomass and NAR between Jinpeng and Zhongza under high VPD (**Table 3**). In the present study, no changes in K_{stem}, A_{lumen}-*stem* and T_w-*stem* were found under high VPD in either cultivar (**Figure 5**). Thus, the major role in regulating K_{plant} under high VPD is attributed to the leaf and root, as previously reported for several tree species (Domec et al., 2009; Torres-Ruiz et al., 2015).

CONCLUSION

The present study indicates that different hydraulic regulation strategies are responsible for the discrepancies found in terms of water dynamics in the cultivars studied. Furthermore, the main results of the present study reinforce the idea that the responses of water dynamics to high VPD depend on acclimation at the whole plant level, particularly at the stomatal, leaf and root levels. High carbon investment in the hydraulic architecture of leaves and roots warrants a sufficient water supply to meet the requirement of water loss, maintaining g_s. In contrast, plants are prone to triggering a simultaneous decrease in g_s and K_{leaf} to prevent excessive water loss when environmental factors have a negative effect on the leaf hydraulic system. Therefore, high VPD treatment would impose a tradeoff between the water and carbon economy of the plant.

DATA AVAILABILITY STATEMENT

The datasets generated for this study are available on request to the corresponding author.

AUTHOR CONTRIBUTIONS

QD, XJ, and JL conceived and designed the experiments. QD, XS, JZ, PB, and JD performed the experiments. QD and XJ analyzed the data and wrote this manuscript. JL contributed extensively to its finalization.

FUNDING

This work was financially supported by the China Agriculture Research System (CARS-23-C05), Project of Science and Technology Plan in Qinghai (2018-NK-123), and Project of Scientific and Technical Innovation Demonstration for Vegetable Industry in Qinghai (QNKP-2018-03-01).

SUPPLEMENTARY MATERIAL

The Supplementary Material for this article can be found online at: https://www.frontiersin.org/articles/10.3389/fpls.2020.00758/full#supplementary-material

REFERENCES

Aliniaeifard, S., Matamoros, P. M., and van Meeteren, U. (2014). Stomatal malfunctioning under low VPD conditions: induced by alterations in stomatal morphology and leaf anatomy or in the ABA signaling? *Physiol. Plant.* 152, 688–699. doi: 10.1111/ppl.12216

Allen, C. D., Breshears, D. D., and McDowell, N. G. (2015). On underestimation of global vulnerability to tree mortality and forest die-off from hotter drought in the Anthropocene. *Ecosphere* 6, 129. doi: 10.1890/es15-00203.1

Berlyn, G. P., and Miksche, J. P. (1976). *Botanical Microtechnique and Cytochemistry. The*. Ames, IA: Iowa State University Press.

Brodribb, T. J., and Holbrook, N. M. (2006). Declining hydraulic efficiency as transpiring leaves desiccate: two types of response. *Plant Cell Environ.* 29, 2205–2215. doi: 10.1111/j.1365-3040.2006.01594.x

Brodribb, T. J., and Jordan, G. J. (2011). Water supply and demand remain balanced during leaf acclimation of Nothofagus cunninghamii trees. *New Phytol.* 192, 437–448. doi: 10.1111/j.1469-8137.2011.03795.x

Buckley, T. N. (2005). The control of stomata by water balance. *New Phytol.* 168, 275–292. doi: 10.1111/j.1469-8137.2005.01543.x

Bunce, J. A. (2006). How do leaf hydraulics limit stomatal conductance at high water vapour pressure deficits? *Plant Cell Environ.* 29, 1644–1650. doi: 10.1111/j.1365-3040.2006.01541.x

Carins Murphy, M. R., Jordan, G. J., and Brodribb, T. J. (2014). Acclimation to humidity modifies the link between leaf size and the density of veins and stomata. *Plant Cell Environ.* 37, 124–131. doi: 10.1111/pce.12136

Cruiziat, P., Cochard, H., and Ameglio, T. (2002). Hydraulic architecture of trees: main concepts and results. *Ann. For. Sci.* 59, 723–752. doi: 10.1051/forest:2002060

de Boer, H. J., Price, C. A., Wagner-Cremer, F., Dekker, S. C., Franks, P. J., and Veneklaas, E. J. (2016). Optimal allocation of leaf epidermal area for gas exchange. *New Phytol.* 210, 1219–1228. doi: 10.1111/nph.13929

Dewar, R., Mauranen, A., Makela, A., Holtta, T., Medlyn, B., and Vesala, T. (2018). New insights into the covariation of stomatal, mesophyll and hydraulic conductances from optimization models incorporating nonstomatal limitations to photosynthesis. *New Phytol.* 217, 571–585. doi: 10.1111/nph.14848

Domec, J. C., Noormets, A., King, J. S., Sun, G., McNulty, S. G., Gavazzi, M. J., et al. (2009). Decoupling the influence of leaf and root hydraulic conductances on stomatal conductance and its sensitivity to vapour pressure deficit as soil dries in a drained loblolly pine plantation. *Plant Cell Environ.* 32, 980–991. doi: 10.1111/j.1365-3040.2009.01981.x

Du, Q. J., Liu, T., Jiao, X. C., Song, X. M., Zhang, J. Y., and Li, J. M. (2019). Leaf anatomical adaptations have central roles in photosynthetic acclimation to humidity. *J. Exp. Bot.* 70, 4949–4962. doi: 10.1093/jxb/erz238

Du, Q. J., Xing, G. M., Jiao, X. C., Song, X. M., and Li, J. M. (2018). Stomatal responses to long-term high vapor pressure deficits mediated most limitation of photosynthesis in tomatoes. *Acta Physiol. Plant.* 40, 149. doi: 10.1007/s11738-018-2723-7

Fanourakis, D., Carvalho, S. M. P., Almeida, D. P. F., van Kooten, O., van Doorn, W. G., and Heuvelink, E. (2012). Postharvest water relations in cut rose cultivars with contrasting sensitivity to high relative air humidity during growth. *Postharvest Biol. Technol.* 64, 64–73. doi: 10.1016/j.postharvbio.2011.09.016

Fanourakis, D., Heuvelink, E., and Carvalho, S. M. P. (2013). A comprehensive analysis of the physiological and anatomical components involved in higher water loss rates after leaf development at high humidity. *J. Plant Physiol.* 170, 890–898. doi: 10.1016/j.jplph.2013.01.013

Fanourakis, D., Giday, H., Milla, R., Pieruschka, R., Kjaer, K. H., Bolger, M., et al. (2015a). Pore size regulates operating stomatal conductance, while stomatal densities drive the partitioning of conductance between leaf sides. *Ann. Bot.* 115, 555–565. doi: 10.1093/aob/mcu247

Fanourakis, D., Heuvelink, E., and Carvalho, S. M. P. (2015b). Spatial heterogeneity in stomatal features during leaf elongation: an analysis using Rosa hybrida. *Funct. Plant Biol.* 42, 737–745. doi: 10.1071/FP15008

Fanourakis, D., Hyldgaard, B., Giday, H., Aulik, I., Bouranis, D., Körner, O., et al. (2019). Stomatal anatomy and closing ability is affected by supplementary light intensity in rose (Rosa hybrida L.). *Hortic. Sci.* 46, 81–89. doi: 10.17221/144/2017-HORTSCI

Farrior, C. E., Tilman, D., Dybzinski, R., Reich, P. B., Levin, S. A., and Pacala, S. W. (2013). Resource limitation in a competitive context determines complex plant responses to experimental resource additions. *Ecology* 94, 2505–2517. doi: 10.1890/12-1548.1

Fernandes-Silva, A. A., López-Bernal, Á, Ferreira, T. C., and Villalobos, F. J. (2016). Leaf water relations and gas exchange response to water deficit of olive (cv. Cobrançosa) in field grown conditions in Portugal. *Plant Soil* 402, 191–209. doi: 10.1007/s11104-015-2786-9

Franks, P. J., and Beerling, D. J. (2009). Maximum leaf conductance driven by CO2 effects on stomatal size and density over geologic time. *Proc. Natl. Acad. Sci. U.S.A.* 106, 10343–10347. doi: 10.1073/pnas.0904209106

Freschet, G. T., Violle, C., Bourget, M. Y., Scherer-Lorenzen, M., and Fort, F. (2018). Allocation, morphology, physiology, architecture: the multiple facets of plant above- and below-ground responses to resource stress. *New Phytol.* 219, 1338–1352. doi: 10.1111/nph.15225

Galmés, J., Ochogavía, J. M., Gago, J., Roldán, E. J., Cifre, J., and Conesa, M. À (2013). Leaf responses to drought stress in Mediterranean accessions of *Solanum lycopersicum*: anatomical adaptations in relation to gas exchange parameters. *Plant Cell Environ.* 36, 920–935. doi: 10.1111/pce.12022

Grossiord, C., Sevanto, S., Borrego, I., Chan, A. M., Collins, A. D., Dickman, L. T., et al. (2017). Tree water dynamics in a drying and warming world. *Plant Cell Environ.* 40, 1861–1873. doi: 10.1111/pce.12991

Kono, Y., Nakata, K., and Tatsumi, J. (1982). Observations of cross veins of the second foliage leaf blade in the rice plant by use of a revised method for clearing leaves. *Jap. J. Crop Sci.* 51, 445–454. doi: 10.1626/jcs.51.445

Liu, Y. Y., Song, J., Wang, M., Li, N., Niu, C. Y., and Hao, G. Y. (2015). Coordination of xylem hydraulics and stomatal regulation in keeping the integrity of xylem water transport in shoots of two compound-leaved tree species. *Tree Physiol.* 35, 1333–1342. doi: 10.1093/treephys/tpv061

Lu, N., Nukaya, T., Kamimura, T., Zhang, D., Kurimoto, I., Takagaki, M., et al. (2015). Control of vapor pressure deficit (VPD) in greenhouse enhanced tomato growth and productivity during the winter season. *Sci. Hortic.* 197, 17–23. doi: 10.1016/j.scienta.2015.11.001

Macková, J., Vašková, M., Macek, P., Hronková, M., Schreiber, L., and Šantrůček, J. (2013). Plant response to drought stress simulated by ABA application: changes in chemical composition of cuticular waxes. *Environ. Exp. Bot.* 86, 70–75. doi: 10.1016/j.envexpbot.2010.06.005

Martins, S. C. V., McAdam, S. A. M., Deans, R. M., DaMatta, F. M., and Brodribb, T. J. (2016). Stomatal dynamics are limited by leaf hydraulics in ferns and conifers: results from simultaneous measurements of liquid and vapour fluxes in leaves. *Plant Cell Environ.* 39, 694–705. doi: 10.1111/pce.12668

Monteith, J., and Unsworth, M. (1990). *Principles of Environmental Physics*, 2nd Edn. London: Edward Arnold.

North, G. B., Lynch, F. H., Maharaj, F. D. R., Phillips, C. A., and Woodside, W. T. (2013). Leaf hydraulic conductance for a tank bromeliad: axial and radial pathways for moving and conserving water. *Front. Plant Sci.* 4:78. doi: 10.3389/fpls.2013.00078

Pittermann, J., and Sperry, J. (2003). Tracheid diameter is the key trait determining the extent of freezing-induced embolism in conifers. *Tree Physiol.* 23, 907–914. doi: 10.1093/treephys/23.13.907

Richter, H. (1997). Water relations of plants in the field: some comments on the measurement of selected parameters. *J. Exp. Bot.* 48, 1–7. doi: 10.1093/jxb/48.1.1

Ripullone, F., Guerrieri, M. R., Nole, A., Magnani, F., and Borghetti, M. (2007). Stomatal conductance and leaf water potential responses to hydraulic conductance variation in Pinus pinaster seedlings. *Trees* 21, 371–378. doi: 10.1007/s00468-007-0130-6

Rodriguez-Dominguez, C. M., Buckley, T. N., Egea, G., de Cires, A., Hernandez-Santana, V., Martorell, S., et al. (2016). Most stomatal closure in woody species under moderate drought can be explained by stomatal responses to leaf turgor. *Plant Cell Environ.* 39, 2014–2026. doi: 10.1111/pce.12774

Roth-Nebelsick, A., Uhl, D., Mosbrugger, V., and Kerp, H. (2001). Evolution and function of leaf venation architecture: a review. *Ann. Bot.* 87, 553–566. doi: 10.1006/anbo.2001.1391

Sack, L., Cowan, P. D., Jaikumar, N., and Holbrook, N. M. (2003). The 'hydrology' of leaves: co-ordination of structure and function in temperate woody species. *Plant Cell Environ.* 26, 1343–1356. doi: 10.1046/j.0016-8025.2003.01058.x

Sack, L., and Frole, K. (2006). Leaf structural diversity is related to hydraulic capacity in tropical rain forest trees. *Ecology* 87, 483–491. doi: 10.1890/05-0710

Sack, L., and Holbrook, N. M. (2006). Leaf hydraulics. *Annu. Rev. Plant Biol.* 57, 361–381. doi: 10.1146/annurev.arplant.56.032604.144141

Salmon, Y., Torres-Ruiz, J. M., Poyatos, R., Martinez-Vilalta, J., Meir, P., Cochard, H., et al. (2015). Balancing the risks of hydraulic failure and carbon starvation: a twig scale analysis in declining Scots pine. *Plant Cell Environ.* 38, 2575–2588. doi: 10.1111/pce.12572

Savvides, A., Fanourakis, D., and van Ieperen, W. (2012). Co-ordination of hydraulic and stomatal conductances across light qualities in cucumber leaves. *J. Exp. Bot.* 63, 1135–1143. doi: 10.1093/jxb/err348

Sellin, A., Rosenvald, K., Õunapuu-Pikas, E., Tullus, A., Ostonen, I., and Lõhmus, K. (2015). Elevated air humidity affects hydraulic traits and tree size but not biomass allocation in young silver birches (*Betula pendula*). *Fronti. Plant Sci.* 6:860. doi: 10.3389/fpls.2015.00860

Shamshiri, R., Che Man, H., Zakaria, A., Van Beveren, P., Wan Ismail, W. I., and Ahmad, D. (2016). Membership function model for defining optimality of vapor pressure deficit in closed-field cultivation of tomato. *Acta Hortic.* 1152, 281–290. doi: 10.17660/actahortic.2017.1152.38

Simonin, K. A., Burns, E., Choat, B., Barbour, M. M., Dawson, T. E., and Franks, P. J. (2015). Increasing leaf hydraulic conductance with transpiration rate minimizes the water potential drawdown from stem to leaf. *J. Exp. Bot.* 66, 1303–1315. doi: 10.1093/jxb/eru481

Sperry, J. S., Adler, F. R., Campbell, G. S., and Comstock, J. P. (1998). Limitation of plant water use by rhizosphere and xylem conductance: results from a model. *Plant Cell Environ.* 21, 347–359. doi: 10.1046/j.1365-3040.1998.00287.x

Sperry, J. S., and Love, D. M. (2015). What plant hydraulics can tell us about responses to climate-change droughts. *New Phytol.* 207, 14–27. doi: 10.1111/nph.13354

Steudle, E. (2000). Water uptake by plant roots: an integration of views. *Plant Soil* 226, 45–56. doi: 10.1023/a:1026439226716

Tabassum, M. A., Zhu, G., Hafeez, A., Wahid, M. A., Shaban, M., and Li, Y. (2016). Influence of leaf vein density and thickness on hydraulic conductance and photosynthesis in rice (*Oryza sativa* L.) *during water stress*. *Sci. Rep.* 6:36894. doi: 10.1038/srep36894

Torres-Ruiz, J. M., Diaz-Espejo, A., Perez-Martin, A., and Hernandez-Santana, V. (2015). Role of hydraulic and chemical signals in leaves, stems and roots in the stomatal behaviour of olive trees under water stress and recovery conditions. *Tree Physiol.* 35, 415–424. doi: 10.1093/treephys/tpu055

Xiong, D. L., Flexas, J., Yu, T. T., Peng, S. B., and Huang, J. L. (2017). Leaf anatomy mediates coordination of leaf hydraulic conductance and mesophyll conductance to CO2 in *Oryza*. *New Phytol.* 213, 572–583. doi: 10.1111/nph.14186

Xu, Z. Z., and Zhou, G. S. (2008). Responses of leaf stomatal density to water status and its relationship with photosynthesis in a grass. *J. Exp. Bot.* 59, 3317–3325. doi: 10.1093/jxb/ern185

Zhang, D. L., Jiao, X. C., Du, Q. J., Song, X. M., and Li, J. M. (2018). Reducing the excessive evaporative demand improved photosynthesis capacity at low costs of irrigation via regulating water driving force and moderating plant water stress of two tomato cultivars. *Agric. Water Manag.* 199, 22–33. doi: 10.1016/j.agwat.2017.11.014

Zsögön, A., Alves Negrini, A. C., Peres, L. E. P., Nguyen, H. T., and Ball, M. C. (2015). A mutation that eliminates bundle sheath extensions reduces leaf hydraulic conductance, stomatal conductance and assimilation rates in tomato (*Solanum lycopersicum*). *New Phytol.* 205, 618–626. doi: 10.1111/nph.13084

Conflict of Interest: The authors declare that the research was conducted in the absence of any commercial or financial relationships that could be construed as a potential conflict of interest.

Advantages of publishing in Frontiers

OPEN ACCESS
Articles are free to read for greatest visibility and readership

FAST PUBLICATION
Around 90 days from submission to decision

HIGH QUALITY PEER-REVIEW
Rigorous, collaborative, and constructive peer-review

TRANSPARENT PEER-REVIEW
Editors and reviewers acknowledged by name on published articles

Frontiers
Avenue du Tribunal-Fédéral 34
1005 Lausanne | Switzerland

Visit us: www.frontiersin.org
Contact us: info@frontiersin.org | +41 21 510 17 00

REPRODUCIBILITY OF RESEARCH
Support open data and methods to enhance research reproducibility

DIGITAL PUBLISHING
Articles designed for optimal readership across devices

FOLLOW US
@frontiersin

IMPACT METRICS
Advanced article metrics track visibility across digital media

EXTENSIVE PROMOTION
Marketing and promotion of impactful research

LOOP RESEARCH NETWORK
Our network increases your article's readership